VYSOKÁ ŠKOLA CHEMICKO-TECHNOLOGCIKÁ V PRAZE

FAKULTA CHEMICKÉ TECHNOLOGIE

ANORGANICKÉ BIOMATERIÁLY A JEJICH HODNOCENÍ *IN VITRO*

Habilitační práce

Dr. Ing. Dana Rohanová

Ústav skla a keramiky

Praha, 2017

Prohlašuji, že jsem předloženou habilitační práci „Anorganické materiály a jejich hodnocení *in vitro*“ vypracovala samostatně s uvedením všech použitých literárních pramenů. Byla jsem seznámena s tím, že se na moji práci vztahují práva a povinnosti vyplývající ze zákona č. 121/2000 Sb., o právu autorském, o právech souvisejících s právem autorským a o změně některých zákonů (autorský zákon). Souhlasím se zveřejněním své práce podle zákona č. 111/1998 Sb., o vysokých školách, ve znění pozdějších předpisů.

V Praze, dne 11. srpna 2017 Dr. Ing Dana Rohanová

Poděkování

Moje poděkování patří kolegům z Laboratoře Chemie skla, Ústavu skla a keramiky, především pak (nejen kolegyni) **Ing. Dianě Horkavcové, PhD**., za její obětavost, pracovitost a trpělivost. **Dr. RNDr. Petrovi Bezdičkovi** z Ústavu anorganické chemie, AV ČR děkuji za precizní provedení a vyhodnocení XRD analýz. Za věcné diskuse a konzultace jsem vděčná **prof. Ing. Janu Hlaváčovi, DrSc. a prof. Ing. Aleši Helebrantovi, CSc.** Druhá tématika, kterou se zabývám víc než 10 let, ale zde nyní není prezentována mi přinesla do života další milou a pracovitou kolegyni **PhDr. Hedviku Sedláčkovou, CSc.** Ráda bych také poděkovala **mým nejbližším**, kteří – když doma sednu k PC a „upadnu do pracovního módu“ - nechají maminku v klidu pracovat a fungují samostatně.

Souhrn

Předložená habilitační práce je souborem dvanácti prací, které se zabývají problematikou biomateriálů. Komentář k pracím jsem rozdělila do dvou částí. V první části prezentuji přípravu bioaktivního povrchu pomocí fosforečnanů vápenatých na bioinertních kovech (Ti a jeho slitiny) a ve druhé části se zabývám chováním bioaktivních a resorbovatelných materiálů v průběhu testů *in vitro* a jejich vypovídací hodnotou.

V dentální chirurgii a ortopedii se využívají inertní kovové implantáty, které je nutné na některých místech opracovat tak, aby s kostí vytvořily pevnou chemickou vazbu. Nově připravená vrstva musí splňovat přísné požadavky lékařů i samotných výrobců. Má dobře reagovat s krevní plazmou, nesmí měnit rozměr implantátu a musí mít dobrou adhezi k podkladu. Námi připravená vrstva amorfního fosforečnanu vápenatého (ACP) o tloušťce řádově desítek nanometrů je propojená se substrátem nejenom mechanicky ale i chemicky. Připravili jsme ji na površích Ti a Ti slitin tryskáním částicemi Al_2O_3 (mechanická úprava) a chemickými úpravami (leptáním v HCl a následně v NaOH). Takto připravené povrchy Ti a Ti slitin byly poté exponovány v roztocích přesycených vůči fosforečnanům vápenatým za pomoci ultrazvukové lázně. Postup přípravy ACP na površích Ti a Ti slitin byl doladěn pro účely sériové výroby (užitný vzor) a nyní je v patentovém řízení.

Druhá část publikací se věnuje *in vitro* testům materiálů v SBF (Simulated Body Fluid) při teplotě 36,5^{o}C za statických, dynamických i staticko-dynamických podmínek testu. Ukázalo se, že pufr TRIS (ISO norma 23317) není inertní vůči skelným a sklokeramickým materiálům (např. apatit-wollastonitová sklokeramika). S Ca^{2+} ionty tvoří rozpustnou komplexní sloučeninu a předpokládáme i jeho chelatační efekt. Tvorba komplexních sloučenin významně urychluje rozpouštění skelného či sklokeramického materiálu, což následně iniciuje vznik krystalického hydroxyapatitu (HAp[1]) na povrchu materiálu. Výsledky testů pro tyto vysoce reaktivní materiály tak mohou být falešně pozitivní.

Další práce jsou zaměřené na hledání vhodnějšího pufračního systému (např. pufr HEPES, roztok DMEM) a podmínek *in vitro* testu, jako je například vhodné nastavení poměru povrchu testovaného materiálů a objemu testovací kapaliny (S/V = poměr plochy vzorku k objemu SBF).

[1] v textu i v publikacích používáme zkratku HAp pro hydroxyapatit vytvořený z roztoku SBF při testu *in vitro* a zkratku HA používáme pro implantační materiál

OBSAH

1. ÚVOD

Biomateriály jsou syntetické či přírodní materiály, které se používají v lékařských aplikacích k opravě nebo k náhradě části lidské tkáně nebo orgánu poškozeným nemocí či úrazem. Jsou schopné vytvářet mezifázi s biologickým systémem za účelem vývoje, fixace nebo náhrady jakékoliv tkáně, orgánu nebo funkce v organizmu. Biomateriál nesmí být toxický a nesmí zapříčinit žádné poškození, ať už na úrovni buněčné nebo na úrovni celého systému. Biomateriál je vždy navržen na základě potřeby specifické aplikace a jelikož je určen k interakci s živým organismem, hlavním požadavkem je biokompatibilita[2]. Biokompatibilita materiálu je definována jako schopnost materiálu vhodně fungovat s tkání hostitele.

Tvrdé, neboli kostní tkáně, tvořené apatitem - $Ca_{10}(PO_4)_6(OH)_2$ se lidském těle nachází v mnoha pozicích. Materiály, které je mohou nahradit, musí splňovat různorodé požadavky jak mechanické tak chemické povahy. Materiály určené k náhradám tkání můžeme tedy rozdělit podle:

a) interakce v živém organizmu
b) typu materiálu

a) Interakce materiálů v živém organismu

1. *Resorbovatelné materiály* v průběhu času degradují a postupně jsou nahrazovány přírodní tkání hostitele. Základní otázkou je rychlost biologického a fyzikálního rozkladu, které musí být v rovnováze s mírou regenerace kosti. Mezi materiály degradovatelné v živém organismu patří β-trikalciumfosfát (β-TCP), kopolymer kyselin polyglykolové a polymléčné.

2. *Bioaktivní materiály* produkují specifickou biologickou odpověď a tvoří interfaciální vazbu s přilehlou tkání. Indukují tvorbu kostní tkáně na povrchu implantátu a vytváří kontinuální přechod živé tkáně na povrch implantátu. Tímto procesem dojde k ukotvení implantátu bez zapouzdření materiálu měkkou tkání. Mezi materiály tvořící chemickou vazbu s tkanivem patří např. hydroxyapatit (HA), bioaktivní sklokeramika nebo biosklo (Bioglass®).

3. *Inertní materiály* nevytváří chemickou ani biologickou vazbu s kostní tkání. Reakce organismu na bioinertní materiál je zapouzdření daného materiálu vazivovou tkání, kdy tloušťka závisí na stavu implantátu a okolní tkáně. Proto jsou bioinertní materiály aplikovány

[2] Williams D.F.: On the mechanisms of biocompatibility. Biomaterials. 29(20): 2941-2953, 2008.

v oblastech, kde jsou mechanicky fixovány pomocí šroubů, hřebů, případně kostního cementu. Další možností fixace je úprava jejich povrchu tak, aby se na něm vytvořila bioaktivní vrstva. Mezi bioinertní materiály patří hlavně kovy (titan a jeho slitiny), korozivzdorné slitiny (Co-Cr) a keramika na bázi Al_2O_3, ZrO_2.

b) Typy biomateriálů

1. ***Polymery*** mohou být použity jako náhrady měkkých i tvrdých tkání a tvoří největší skupinu biomateriálů. Jsou vyuužívány pro transport a uvolňování léčiv. Polymery mohou být přírodní (kolagen, alginát sodný, celulózy) nebo syntetické (silikonová pryž, PMMA, polyvinylchlorid).

2. ***Kovy*** (Ti a jeho slitiny, korozivzdorné oceli a Co-Cr slitiny) jsou využívány jako implantáty ve stomatologii a ortopedické chirurgii díky svým vynikajícím mechanickým vlastnostem (pevnost). Jednou z nejběžnějších aplikací titanu a jeho slitin je umělý kyčelní kloub, který se skládá z kloubního ložiska (femorální hlavice a jamka) a dříku (obr. 1). Dále jsou běžně používány pro náhrady kolenního kloubu nebe jako implantáty ve stomatologii

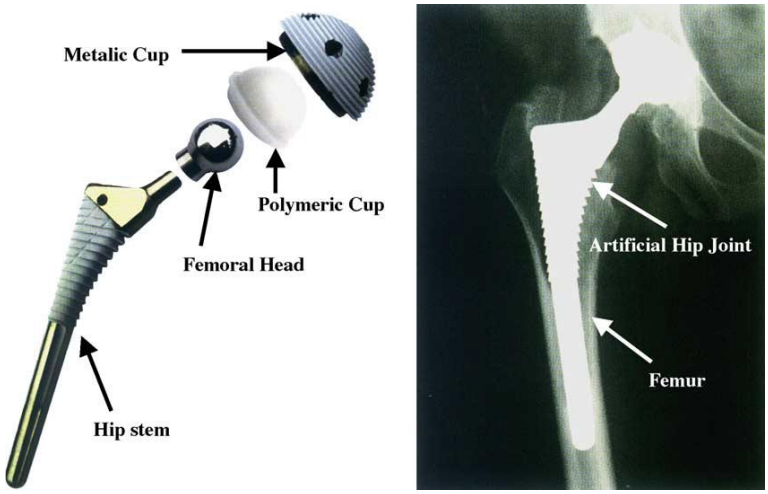

Obr. 1: Umělý kyčelní kloub

3. ***Keramika*** se používá hlavně k výplním a regeneraci tvrdých tkání, a to zejména v nenosných aplikacích nebo jako bioaktivní povlak na kovové implantáty. Nejpoužívanějším keramickým biomateriálem je keramika na bázi fosforečnanů vápenatých (Ca-P keramika), dále oxidu hlinitého (Al_2O_3) a oxidu zirkoničitého (ZrO_4).

4. ***Sklo*** se využívá tam, kde nejsou vysoké nároky na pevnost, ale je nutná interakce s tělními tekutinami pro vytvoření pevného spoje kost – implantát[3]. Bioaktivní skla jsou amorfní materiály na silikátové bázi, které jsou biokompatibilní s živým organizmem. Vážou se na kost a mohou dokonce stimulovat její růst, zatímco samy se rozpouštějí nebo resorbují. Proto mají potenciál obnovit nemocné či poškozené kostní tkáně (kostní regenerace). Bioaktivní sklo vynalezené prof. L.L. Henchem o složení 46.1 mol% SiO_2, 24.4 mol% Na_2O, 26.9 mol% CaO and 2.6 mol% P_2O_5 je známé pod obchodním názvem 45S5 Bioglass®[4].

4.1 ***Sklokeramika*** má lepší mechanické vlastnosti než sklo. Připravuje se ze skel řízenou krystalizací při přesně nastaveném teplotním režimu. Řízenou krystalizací se ve sklech vyvolá růst krystalických fází jako jsou apatit a wollastonit (sklokeramika typu A-W ($MgO–CaO–SiO_2–P_2O_5$) nebo apatit a flogopit (sklokeramika Bioverit® (výchozí složení $Na_2O–MgO–CaO–Al_2O_3–SiO_2–P_2O_5–F$)).

5. ***Kompozity*** – *kost* sama o sobě představuje kompozitní materiál (je to nanokompozit) s unikátními mechanickými vlastnostmi. Nanostruktura je tvořena fibrilami kolagenu typu I, ve kterých jsou vestavěny hydroxyapatitové krystaly[5]. Synteticky připravené kompozitní materiály vhodně spojují vlastnosti obou materiálů (kov-polymer nebo kov-(Ca-P) keramika) [1]) a ideální je také propojení kovu s materiály na bázi skla či sklokeramiky..

Obr. 2: Schéma šroubového závitu Ti dentální náhrady s bioaktivní vrstvou Ca-P keramiky[6]

[3] Hench L.L., et al.: Bonding mechanisms at the interface of ceramic prosthetic materials. Journal of Biomedical Materials Research 5 (6): 117-141, 1971.
[4] Jones JR.: 12 Bioactive glasses, in Bioceramics and their Clinical Applications, ed. Kokubo T., Woodhead publishing, p. 266-283, 2008.
[5] Nudelman F., Sommerdijk N.A.J.M.: Biomineralization as an inspiration for materials Chemistry. Angewandte Chemie International Edition. 51 (27): 6582-6596, 2012.
[6] Liu X., Chu P.K., Ding C.: Surface modification of titanium, titanium alloys and related materials for biomedical applications. Materials Science and Engineering. R: reports 47(3-4): 49-121, 2004.

5.1. Propojení vlastností obou skupin materiálů do kompozitního implantátu (části totální endoprotézy nebo dentální náhrady (viz.obr.2) se dá docílit **nanesením nebo vysrážením vápenato-fosforečných vrstev (Ca-P)** na povrch kovového substrátu[7] těmato metodami:[8]

- Plazmové nanášeni
- Magnetronové naprašování
- Elektro-sprejová metoda
- Sol-gel metoda
- Biomimetická metoda a prekalcifikace (srážení Ca-P) z roztoků

5.1.1. *Biomimetická metoda a prekalcifikace povrchu*

Tyto metody se jeví jako jedny z nejslibnějších, protože jsou to jednoduché, levné a účinné cesty pro přípravu Ca-P vrstvy. Zjednodušeně je postup tvorby Ca-P vrstvy na povrchu inertního kovu shrnutý do těchto kroků: povrch kovu se upraví mechanickou (tryskání) a chemickou cestou (úpravami v HCl nebo NaOH)[9], následovanými tzv. prekalcifikací (precipitací fosforečnanů vápenatých (Ca-P) z přesycených roztoků).

Příprava dobře interagující, bioaktivní Ca-P vrstvy na povrchu kovových materiálů (Ti a Ti6Al4V slitina) s dokonalou adhezí byla předmětem bakalářských a diplomových prací mých studentů a vyústila do tvorby užitného vzoru a podaného patentu. Připravená amorfní Ca-P vrstva (ACP) má odhadovanou tloušťku v řádu desítek nm, takže nijak neovlivňuje finální rozměr implantátu a adheze je zaručena chemickou vazbou přímo s povrchem Ti nebo jeho slitin (EPMA). Při srovnávacích testech *in vitro* v SBF se ukázalo, že tvorba HAp se iniciuje okamžitě po vložení implantátu do roztoku. Vzhledem k amorfnímu charakteru vrstvy není předpoklad, že by byla pro buňky cytotoxická.

Druhá část prací je věnována **roztoku SBF (Simulated Body Fluid)** a uspořádání testu dle ISO normy. Testy *in vitro* předchází testům *in vivo* a mají za cíl „vytřídit“ nadějné

[7] Narayanan R, et al.: Calcium-phosphate based coatings on titanium and its alloys. J. of Biomedical materials Research 7 (3) 1-23, 1973.
[8] Best S.M., Porter A.E., Thien E.S., et al: Bioceramics, Past, present and for the future. J. Europ. Ceram. Soc. 28; 1319-1327,2008.
[9] Jonášová L., et al.: Biomimetic apatite formation on chemically treated titanium. Biomaterials 25 (7) 1187-1194, 2004.

biomateriály od materiálů nereaktivních. Výhodou *in vitro* testů je jednoduchost, kontrolovatelnost a relativně nízká cena. Jejich zavedení do praxe rapidně snížilo využití zvířat pro účely testů.

***In vitro* testy v simulované tělní tekutině SBF** se využívají pro testování materiálů prakticky od doby, kdy bylo prof. Henchem[10] vyvinuté sklo Bioglass® (od počátku 70tých let 20tého století). **ISO norma 23317**[11] (Implants for surgery – *In vitro* evaluation for apatite-forming ability of implant materials) sestavená na základě prací prof. Kokuba[12] je založená na expozici materiálu v SBF (**Simulated Body Fluid**). Testovací roztok SBF obsahuje pouze anorganickou část krevní plazmy s některými odchylkami oproti reálné krevní plazmě (viz. Tab.1). K udržení pH tohoto modelového roztoku se využívá pufr TRIS - tris (hydroxymethyl) aminomethan.

Tab. 1: Složení SBF a anorganické části lidské krevní plazmy [mmol.dm^{-3}]

	Na^+	K^+	Ca^{2+}	Mg^{2+}	Cl^-	$(HCO_3)^-$	$(HPO_4)^{2-}$	$(SO_4)^{2-}$
Plasma	142,0	3,6-5,5	2,1-2,6	1,0	95-107	27,0	1,0	0,7-1,5
SBF	142,0	5,0	2,5	1,0	126,0	4,2	1,0	1,0

Obecně je přijímán názor, že tvorba apatitu na povrchu biomateriálů v průběhu expozice v simulované tělní tekutině je důkazem biologické aktivity materiálu[13]. ISO norma tedy stanovuje jako nejdůležitější ukazatel budoucí možné bioaktivity materiálu tvorbu hydroxyapatitu (HAp) na povrchu testovaného materiálu. Změny koncentrace Ca^{2+} a $(PO_4)^{3-}$ iontů ve výluzích se obecně nesledují, přičemž tyto výborně odráží reaktivitu testovaného materiálu (rychlost odčerpávání biogenních iontů z SBF, rozpouštění materiálu a kinetiku tvorby nové vrstvy) a pomáhají nastavit podmínky budoucího *in vitro* testu (např. poměr S/V a délku trvaní testu) tak, abychom pochopili chování materiálu hlavně v kritické periodě na počátku expozice.

[10] Hench L.L.: Bioceramics, J Am. Cer. Soc. 81 (7) 1705-1728, 1998.
[11] ISO 23317(2014) Implants for surgery – In vitro evaluation for apatite-forming ability of implant materials, Geneva, Switzerland, 13 p.
[12] Kokubo T., Takadama H.: How useful is SBF in predicting in vivo bone bioactivity. Biomaterials 27 (15): 2907-2915, 2006.
[13] Kokubo T., Takadama H.: How useful is SBF in predicting *in vivo* bone bioactivity, Biomaterials 27 (15): 2907-2915, 2006.

Kinetika rozpouštění skleného nebo sklokeramického materiálu v SBF je, podle výsledků testů, silně ovlivněna přítomností pufru TRIS. Ale i zde můžeme uplatnit obecně platný mechanizmus rozpouštění skelného materiálu. Iniciačním dějem je difuze alkalických iontů (zde Na^+ a Ca^{2+}) z krystalické fáze materiálu do roztoku výměnou za H^+ $(H_3O)^+$ ionty, což vede k rozpouštění materiálu a okamžité precipitaci nových fází (hydroxyapatit (HAp), amorfní fosforečnany vápenaté (ACP) nebo křemičitany vápenaté (CS)).

To, že pufr TRIS ovlivňuje výsledky *in vitro* testů, ukázaly testy A-W sklokeramiky v mé disertační práci vedené prof. Hlaváčem. Druhým klíčovým bodem bylo setkání s profesorem Boccaccinim na Imperial College London a diskuse na téma „nosiče" bioaktivních vlastností ve sklokeramickém *scaffoldu*, inspirované články skupiny prof. Henche[14]. Naše testy ukázaly, že pufr TRIS mění pohled také na sklokeramické materiály s krystalickou fázi *combeit* $Na_2O.2CaO.3SiO_2$ - připravený na Imperial College London z bioaktivního skla Bioglass®).

V publikacích jsme dále diskutovali tato zjištění:

1. pufr TRIS není inertní při testech vysoce reaktivních anorganických materiálů a napomáhá krystalizaci HAp
2. podmínky doporučené ISO normou vyhovují pouze omezené části testovaných materiálů (jiné S/V vyžadují celistvé vzorky a jiné vzorky ve formě granulí (HA nebo β-TCP) nebo také vysoce reaktivní materiály jako je sklo nebo sklokeramika.

Články věnované tématu *in vitro* testů mají velký ohlas a je patrné, že jsme inspirovali mnoho dalších vědců k zamyšlení se nad způsobem testování reaktivity materiálů (neboli možné bioaktivity). Cílem dalších prací v této tématice je nalezení vhodnějšího, inertního pufrovacího systému a nastavení podmínek *in vitro* testu tak, aby vyhovovaly danému účelu a materiálu. Dalším cílem je studium interakce TRIS-Ca a potvrzení chelatačních vlastností TRISu.

[14] Filho O.P., La Torre G.P, Hench L.L: Effect of crystallization on apatite-layer formation of bioactive glass 45S5. Journal of Biomedical Materials Research, 30; 509-514, 1996.

2. KOMENTÁŘ K PŘEDLOŽENÝM PUBLIKACÍM

2.1. Ca-P vrstvy připravené na Ti nebo Ti slitině a jejich reaktivita *in vitro*

Cílem práce **[1]** bylo na povrchu slitiny Ti-6Al-4V vytvořit celistvou vrstvu fosforečnanu vápenatého a optimalizovat podmínky tzv. prekalcifikace z přesycených roztoků SCS1 až 3 s rozdílnou koncentrací Ca^{2+} a $(PO_4)^{3-}$ iontů. Slitina byla před samotným povlakováním chemicky upravena pomocí HF, což se později ukázalo jako ne zcela vhodný způsob z důvodu poměrně masivního rozpouštění slitiny – hlavně uvolňování Al a V. Úprava povrchu pomocí NaOH (10 M roztok) je však pro biomimetické úpravy nezbytná, protože se na povrchu vytvoří amorfní fáze titaničitanu (dle XRD - sodného), který nejenomže enormně zvětšuje povrch, ale zvyšuje i pH samotného povrchu (pH měřeno dotykovou skleněnou elektrodou). Nejvhodnějším pro prekalcifikaci se jevil roztok SCS2 (4 $mmol.dm^{-3}$ Na^{+}, 5 $mmol.dm^{-3}$ Ca^{2+} a 2,5 $mmol.dm^{-3}$ $(PO_4)^{3-}$). Prekalcifikační roztok je silně přesycený vůči fosforečnanům vápenatým (Ca-P) a poměrně rychle se ochuzuje o biogenní prvky v důsledku jejich precipitace. Proto musí být připravován vždy čerstvý. Mechanicky a chemicky upravený kovový substrát má na povrchu zvýšené pH a nové fáze přednostně precipitují právě na něm. Vzniklé vrstvy fosforečnanu vápenatého (OCP) o tloušťce až 50 μm byly podrobeny testům *in vitro* v SBF. Při srovnání s povrchem bez této vrstvy se jednoznačně potvrdilo, že prekalcifikace urychluje precipitaci HAp z roztoku SBF.

Na předchozí práci navazuje práce **[2]**, ve které jsme problematickou kyselinu fluorovodíkovou nahradili HCl. Struktura povrchu slitiny po leptání pomocí HCl byla mnohem jemnější, povrch se mnohonásobně zvětšil (až 1000x oproti původnímu – měřeno BET), a navíc nedocházelo k tak enormnímu úbytku materiálu slitiny. Pomocí XRD bylo zjištěno, že nově vznikající fáze z prekalcifikačního roztoku byly fosforečnany vápenaté: okta kalcium fosfát OCP ($Ca_8H_2(PO_4)_6.5H_2O$) a brushit ($CaHPO_4.2H_2O$). Testy v SBF probíhaly na rozdíl od předchozích testů za dynamických podmínek, tj. s permanentní cirkulací čerstvého SBF. Průtok roztoku byl odhadnutý a nastavený na 48 $ml.den^{-1}$. Precipitací HAp se potvrdil pozitivní efekt tzv. prekalcifikace povrchu, čím se předpokládá také zkrácení doby vhojování dentálního nebo ortopedického implantátu.

V dalších testech se ukázalo, že tvorba krystalické fáze OCP s deskovitými krystalky tloušťce vrstvy až 10 a více μm na povrchu Ti nebo jejich slitin negativně ovlivnila cytotoxicitu

(životaschopnost buněčných řad). Proto jsme se zaměřili na přípravu amorfní Ca-P vrstvy **[3]**. Série testů vyústila do vytvoření Užitného vzoru č.28285 **[4]**, ve kterém jsou uvedeny specifikace tvorby vrstvy amorfních fosforečnanů vápenatých (ACP) na površích kovových implantátů. Z důvodů probíhajícího patentového řízení nebyla tato problematika široce publikována. Avšak nadále v této oblasti pracuji a společně s Ústavem kovových materiálů a korozního inženýrství připravujeme další způsoby přípravy bioaktivních povrchů (tentokrát nanášení vrstev skelných a sklokeramických materiálů s bioaktivními vlastnostmi) na porézních Ti slitinách (TiSi5). Roztok SBF pufrovaný TRISem ve výše uvedených případech slouží k relativnímu srovnání připravených vrstev. Testy *in vivo* sice rozdíl od ne-prekalcifikovaných vzorků nepotvrdily, ovšem testované implantáty byly vyjmuté z kostí psů až po dvouměsíční expozici. Námi navržené úpravy povrchu by měly fungovat hlavně v prvních hodinách po implantaci, kde by prekalcifikovaný povrch měl okamžitě iniciovat tvorbu nového HAp (osseointegrace) a zabránit tak nebezpečnému zapouzdření implantátu měkkými tkáněmi. Obohacení povrchu bioinertního kovového substrátu o biogenní prvky má jednoznačně pozitivní efekt na indukci vzniku pevné vazby implantát – kost.

2.2. Resorpce fosforečnanů a síranů vápenatých v SBF

Pro posouzení resorpce a bio-reaktivity synteticky připravených fosforečnanů vápenatých (HA, β-TCP – dle angl. tri-kalcium fosfát) ve formě granulí jsou testy *in vitro* nezbytné. Ve následujících pracích bylo oproti ISO normě nutné upravit jak poměr S/V, tak uspořádání testu. Je zřejmé, že smyslem *in vitro* testů by mělo být nejenom konstatování, že se vytvořila nová fáze HAp, ale také detailní sledování procesu z analýz výluhů SBF (analýzy Ca^{2+} (AAS) a $(PO_4)^{3-}$ spektrofotometrie) a vlastností vznikající fáze (pomocí XRD, SEM/EDS a BET). Tyto výsledky je poté možné využít pro sledování kinetiky tvorby HAp. Testy resorpce průmyslově připravených fosforečnanů vápenatých (β-TCP a HA) **[5]** ve formě granulí v podmínkách podobných v živém organizmu simulované dynamickým testem – kontinuálním průtokem SBF a poměrně dlouhou dobu testu – 14 dní, měly ukázat, do jaké míry se tyto materiály opravdu transformují (resorbují do nově vytvořené HAp fáze). Ideálně by se synteticky připravené materiály měly organizmem postupně kompletně resorbovat. Jak se ukázalo v práci **[5],** oba materiály jsou v prostředí SBF vysoce reaktivní a jejich reaktivita závisí nejen na povaze testovaného fosforečnanu vápenatého (β-TCP nebo HA), ale logicky na jejich granulometrii (tedy velikosti povrchu) a na „zaplnění“ testovací cely (byla zaplněná z ¼ objemu (1/4 V) nebo

zcela vyplněná testovaným materiálem (1V)). Zde jsme sledovali vznik HAp fáze z odčerpávání Ca^{2+} a $(PO_4)^{3-}$ iontů z roztoku SBF i finální hmotnosti vytvořené vrstvy. Ukázalo se, že rychlost odčerpávání $(PO_4)^{3-}$ iontů a z něj vypočtené teoretické množství vzniklého HAp (po dvoutýdenním dynamickém testu) byly ve velmi dobré korelaci s přírůstkem materiálu zjištěným vážením. Toto platilo pro oba materiály. Zajímavým zjištěním bylo, že pokud byly cely zcela vyplněné materiálem, proces tvorby nové fáze byl pomalejší, oproti zaplnění cely z ¼ objemu. Rychlostní konstanta pro vznik HAp byla cca dvojnásobná pro syntetický HA oproti β-TCP v obou případech zaplnění cely. Důvodem byl mnohem vyšší specifický povrch HA (cca 30 x vyšší). Nově vytvořená fáze HAp vznikala konstantní rychlostí. Ani po dvoutýdenní expozici nebyl proces tvorby HAp ukončen, otázkou ovšem zůstává, jestli se výchozí syntetické Ca-P materiály vůbec resorbovaly. Spíše se přikláníme k tomu, že okamžitá tvorba HAp fáze na povrchu částic vytvoří bariéru vůči dalšímu rozpouštění původního materiálu a brání tak (nebo zpomalí) jejich další resorpci. Pomocí XRD bohužel nebylo možné odlišit nově vytvořenou HAp fázi od původní z důvodu jejich identické struktury. Je pravděpodobné, že v prostředí reálné krevní plazmy (bez pufru TRIS) by materiály asi tak bouřlivě nereagovaly a zůstal by tak prostor na jejich pozvolné rozpouštění.

V další práci **[6]** jsme se zaměřili na reaktivitu synteticky připraveného a bovinního HA, které se nelišily chemicky ani krystalograficky, mírně odlišné byly specifické povrchy materiálů. Testované materiály reagovaly odlišně již na počátku *in vitro* testu. Z porovnání odčerpaných $(PO_4)^{3-}$ iontů a přírůstku hmotnosti pevné fáze se ukázalo, že u bovinního HA byly tyto výsledky v dokonalé shodě, tj. všechen odčerpaný fosfor se spotřeboval na tvorbu stechiometrického HAp. U syntetického HA od počátku expozice až do 28. dne mírně převažovalo množství HAp zjištěné vážením nad množstvím zjištěným z odčerpaných $(PO_4)^{3-}$ iontů. Zde se pravděpodobně tvořil amorfní, nestechiometrický fosforečnan vápenatý (ACP), což mohlo zkreslit výsledek při uvažované tvorbě stechiometrické fáze HAp. Tomu by nasvědčovala i odlišná krystalinita (SEM/EDS) vznikajícího HAp. Druhým možným vysvětlením zkreslení výsledku je intenzivnější rozpouštění syntetického HA do SBF, čímž se zdánlivě koncentrace $(PO_4)^{3-}$ iontů v roztoku navýšila (menší rozdíl koncentrace $(PO_4)^{3-}$ iontů oproti původní hodnotě). Toto podporuje i zjištění, že s delší dobou interakce s roztokem SBF reagovala pouze nově vznikající HAp fáze.

V článku **[7]** jsme studovali kompozitní materiály na bázi sádry (využívané jako kostní cement) a několik typů PVA (polyvinylalkohol) a jejich kopolymerů, které měly vylepšit mechanickou pevnost sádry. Vzorky sádry byly exponovány v roztocích standardního SBF (1 SBF) a roztoku

s navýšenou koncentrací biogenních složek (1,5 SBF). Ukázalo se, že přítomnost polymeru v sádře zvýšila mechanickou pevnost materiálu exponovaného v roztocích SBF. Sádra se silně rozpouštěla, čemuž nasvědčovala rostoucí koncentrace Ca^{2+} i $(SO_4)^{2-}$ iontů ve výluzích SBF. Na povrchu vzorků byly po 14-ti denní expozici detekovány apatitové krystalky velikosti 200 nm, které tvořily sférolity o velikosti cca 2 μm. U silně přesyceného roztoku 1,5 SBF pokrývaly celý povrch vzorků. Kompozit sádra – PVA polymer se zdá být výhodným propojením rozpustné fáze, která iniciuje vznik HAp a polymeru, který je nositelem pevnosti materiálu pro účely kostního cementu.

Výsledky prací **[5-7]** mohou být ovlivněné přítomností pufru TRIS v roztoku SBF. Je zřejmé, že okamžitá interakce materiálu s SBF, která se projevila významným poklesem Ca^{2+} i $(PO_4)^{3-}$ iontů v prvních hodinách testů může souviset s interakcí materiál-pufr TRIS, což je diskutováno v následujícím textu.

2.3. Vliv pufru TRIS na výsledky *in vitro* testů sklokeramických materiálů

Již při prvních testech sklokeramického materiálu (s obsahem krystalických fází apatit, wollastonit a whitlockit a zbytkové skelné fáze) *in vitro* v SBF se ukázalo, že sklokeramický materiál se za přítomnosti pufru TRIS silně rozpouští **[8]**. Toto je patrné ze změn koncentrace SiO_2, který postihuje rozpouštění materiálu. Podobné změny koncentrace byly zaznamenány i pro vápník, avšak Ca se zároveň i zpětně sráží. Hodnota pH ve výluzích vzrostla ze 7,5 při laboratorní teplotě na cca 8 v roztoku pufrovaném TRISem (na hodnotu 8,5 u roztoku SBF bez pufru). Navíc, pufr TRIS neudržel pH roztoku na požadované neutrální hodnotě. Výsledky testů ukázaly, že TRIS je komplexotvorné činidlo a s Ca^{2+} (i dalšími s kationty – např. Mg^{2+}) tvoří rozpustné komplexní sloučeniny. Zdálo se, Ca^{2+} vázaný do komplexní sloučeniny nebude k dispozici pro tvorbu HAp. Rychlost loužení iontů ze skelného a sklokeramického materiálu souvisí s pH roztoku a rychlost tvorby HAp je z termodynamického pohledu funkcí relativního přesycení $S = (1/K)^{1/18}$. Předpokládali jsme, že komplex TRIS-Ca sníží relativní přesycení vůči HAp na přibližně polovinu původní hodnoty čímž se zpomalí precipitace HAp. Tato domněnka pravděpodobně platí v případě statických *in vitro* testů a pokud se z testovaného materiálu neuvolňuje do roztoku Ca^{2+}. V roztoku SBF s koncentrací Ca^{2+} iontů (2,5 $mmol.dm^{-3}$) a TRIS s koncentrací 50 $mmol.dm^{-3}$ se vyváže pravděpodobně veškerý Ca^{2+} obsažený v SBF do rozpustného komplexu a stejné množství Ca^{2+} se do roztoku uvolňuje v prvních hodinách testu ze sklokeramického materiálu **[9-11]**.

V případě vzniku rozpustného komplexu je Ca^{2+} k dispozici pro tvorbu HAp nebo i jiné vápenaté fáze. Jak bylo diskutováno výše **[5-6]**, u *in vitro* testů HA a β-TCP keramiky za dynamických podmínek (s přísunem „čerstvého“ SBF), rychlost přírůstku hmoty nově vytvořené fáze HAp byla v souladu s rychlostí odčerpávání Ca^{2+} a $(PO_4)^{3-}$ iontů z roztoku.

Na výše uvedené výsledky navázala práce **[9]**, kde jsme pozorovali při statických *in vitro* testech sklokeramického materiálu připraveného ze skla Bioglass® (sklo s obsahem cca 45 hm% SiO_2 24,5 hm% Na_2O, 24,5 hm% CaO a 6 hm% P_2O_5 metodou „green body“) stejný efekt. Částice bioskla o velikosti do 5 μm byly smíchány s roztokem kyseliny poly (D-mléčné) a vzniklá suspenze byla nanesena na polyuretanový nosič. Nosič byl ve formě porézní pěny, což zabezpečilo vzniklému *scaffoldu* finální tvar. Vysušené vzorky byly vypáleny při teplotě 1100°C po dobu pěti hodin. Vznikla porézní struktura sklokeramického materiálu, tvořená hlavní krystalickou fází combeit ($Na_2O.2CaO.3SiO_2$) – deskovité krystalky, který obsahuje prakticky veškerý vápník a další minoritní krystalické fáze (odhadujeme max. 5 % materiálu) ve formě jehliček - buchwaldit ($NaCaPO_4$) a wollastonit ($CaO.SiO_2$). Zbytková skelná fáze naproti tomu obsahuje prakticky veškerý P. Byly provedeny jak statické *in vitro* testy bez výměny roztoku SBF, tak *in vitro* testy za dynamických podmínek s kontinuální výměnou kapaliny, které trvaly dva týdny. Při ověřování reaktivity v roztocích s pufrem TRIS (SBF+TRIS), bez pufru TRIS (SBF), ve vodě i v roztoku samotného pufru (TRIS) se potvrdilo, že přítomnost TRISu až dvojnásobně urychluje rozpouštění materiálu oproti roztokům bez pufru TRIS. Dále se ukázalo, že krystalická forma HAp se tvořila pouze v roztocích, kde byl přítomný TRIS. V roztoku SBF (bez TRIS) se tvořila pouze amorfní fáze fosforečnanu vápenatého (pravděpodobně nanočástice HAp). Zajímavé bylo, že i v roztoku H_2O+TRIS se vytvořilo malé, ale detekovatelné množství hydroxyapatitu z iontů, které byly uvolněné ze samotného materiálu. HAp tedy vznikl, i když přesycení celého objemu roztoku vůči HAp jistě nedosahovalo potřebné hodnoty. Úvahy o precipitaci nových fází je nutné vztáhnout k okolí jednotlivých částic, na kterých se pravděpodobně vytvoří difuzní vrstvička nehybné kapaliny s limitovanou tloušťkou. Vrstvička kapaliny obalující částice se pravděpodobně rychle přesytí vůči HAp. Vlivem TRISu se materiál dobře rozpouští a ionty Ca^{2+} i $(PO_4)^{3-}$ difundující z materiálu tuto vrstvu roztoku velmi rychle přesytí. Pokud TRIS vytvořil s Ca rozpustnou komplexní sloučeninu (a je pravděpodobně i chelatačním činidlem), nebránilo to tomu, aby Ca byl následně využitý pro precipitaci HAp. Zároveň se zvýší pH díky uvolňování iontů Na^+ (a systém TRIS-HCl není schopen tak velký nárůst koncentrace OH^- iontů pufrovat), což jsou ideální podmínky pro precipitaci HAp. Dále se ukázalo, že v samotné demineralizované vodě

se krystalické fáze scaffoldu téměř nerozpouštěly, ale naopak rozpustila se zbytková skelná pojivová fáze, což je křemičito-fosforečné sklo o složení 24,8 hm% SiO_2, 26,5 hm% P_2O_5 a 48,5 hm% Na_2O. Proto se scaffold v DEMI vodě zcela rozmělnil. Z práce vyplynulo, že pufr TRIS při testu reaktivního sklokeramického materiálu nedostatečně plnil úlohu pufrovacího činidla (pH ve všech případech strmě rostlo do alkalické oblasti) a navíc působil jako katalyzátor rozpouštění sklokeramického materiálu, což je v souladu se závěry předchozího článku **[8]**. Díky rychlému rozpouštění krystalické fáze scaffoldu se poruší rovnováha v metastabilním roztoku SBF a prakticky okamžitě se tvoří nová fáze HAp. Vzniká tak falešně pozitivní náhled na tento druh biomateriálů a predikce jejich bioaktivity.

2.4. Hledání vhodného pufrovacího systému pro *in vitro* testy

Zajímalo nás, jestli by se dala SBF nahradit jinou, komerčně dostupnou kapalinou, která není pufrována TRISem. Mnozí autoři využívají i další kapaliny typu Ringerův roztok nebo roztoky s organickou fází $HBSS^+$ a $HBSS^-$. My jsme pro test vybrali tzv. DMEM roztok (Dulbecco´s Modified Eagle´s Medium) bez přidaných pufrů TRIS nebo HEPES, který se běžně využívá pro růst tkáňových kultur **[10]**. Tento syntetický roztok se vyznačuje tím, že kromě anorganické části krevní plazmy obsahuje i její organickou část (aminokyseliny, proteiny). Roztok byl obohacen bovinním sérem a ošetřen antibiotiky. Celý experiment se musel vést ve sterilním režimu, což ho značně komplikovalo. Anorganická část roztoku měla nižší koncentraci Ca^{2+} iontů – pouze 1,9 $mmol.dm^{-3}$ oproti 2,5 $mmol.dm^{-3}$ v plazmě, a naopak velmi vysokou koncentraci HCO_3^- iontů (až 44 $mmol.dm^{-3}$), což téměř dvojnásobně převyšovalo hodnotu v lidské plazmě a 7x v standardním SBF. Pro pochopení funkce organické části roztoku DMEM jsme připravili roztok *I-solution*, který kopíroval anorganickou část DMEM a neobsahoval organické látky ani pufr TRIS. Testy jsme provedli na stejném materiálu, jako v předchozím případě – na sklokeramickém scaffoldu. Pro lepší pochopení tvorby nové HAp fáze jsme zvolili tzv. staticko-dynamický typ testu, kde jsme každý den vyměňovali roztok za čerstvý (50 $ml.den^{-1}$) – podobně jako byl nastaven průtok u dynamického testu. Staticko-dynamický test nám umožnil podrobně studovat nejenom změny koncentrace iontů v roztoku, ale i změny materiálu pomocí XRD, XRF, SEM/EDS nebo BET analýzy. I když rozpouštění materiálu probíhalo ve výše uvedených roztocích mírně odlišným mechanizmem (dle výsledků analýz výluhů) na povrchu scaffodlu se netvořil hydroxyapatit (HAp) ale uhličitan vápenatý (kalcit). Toto zjištění dobře koresponduje s vyšší koncentrací HCO_3^- iontů. Další vznikající fází byl amorfní

fosforečnan vápenatý (zjištěno pomocí EDS – zvýšená koncentrace Ca a P na povrchu materiálu). Organická část plazmy tedy nepotlačuje precipitaci nových fází, jak se domnívali někteří autoři[15], ale je možné, že nově vzniklé fáze, které precipitují na povrchu materiálu, omezují překotné rozpouštění sklokeramiky. Opět se potvrdilo, že nepřítomnost pufru TRIS vedla ke vzniku pouze amorfní Ca-P fáze (ACP). Zajímavý byl pokus s využitím albumínu v práci **[8]**, kde se koncentrace Ca ve výluhu měnila stejným způsobem, jako tomu bylo v roztoku SBF+TRIS. V případě DMEM se tento trend ovšem nepotvrdil.

Pro běžné *in vitro* testy je roztok DMEM nevhodný, proto jsme se rozhodli prozkoumat možnosti dalších pufrů **[11]**. Do skupiny tzv. Goodsových pufrů patří i aminokyselina (2-[4-(2-hydroxyethyl)piperazin-1-yl]ethansulfonic acid) zkráceně HEPES. Tento pufr se také využívá v mikrobiologických laboratořích pro udržení neutrálního prostředí roztoků pro pěstování tkáňových kultur. Testy byly opět provedeny na sklokeramickém scaffoldu (detaily jsou uvedeny v článku **[9]**) za staticko-dynamických podmínek a porovnali jsme dva roztoky: SBF, kde jsme nahradili pufr TRIS pufrem HEPES (SBF+HEPES) a roztok samotného pufru (D+HEPES). Nastavení vhodné koncentrace samotného pufru předcházela série testů, ze kterých jsme se rozhodli pro koncentraci 37,5 $mmol.dm^{-3}$ v obou roztocích. Výsledky ukázaly, že pufr HEPES se také silně podílí na rozpouštění *scaffoldu* ihned od začátku experimentu. Již první hodiny (8 hod) po expozici se koncentrace vápenatých iontů ve výluhu zdvojnásobila oproti původní hodnotě v SBF a v samotném roztoku HEPESu dosáhla hodnot kolem 130 $mg.dm^{-3}$. Tyto změny byly doprovázené i růstem pH, až k hodnotám kolem 7,9 a to v obou případech. Druhý a třetí den koncentrace iontů ve výluzích, stejně jako pH klesly na hodnoty blízké původním. Při analýze materiálu jsme zaznamenali, že i obsah Na_2O klesl z 24,5 hm% na 1 hm%. Z materiálu se tedy vyloužily prakticky veškeré alkalické složky (CaO i Na_2O) a zároveň se začal tvořit HAp. Na konci testu, po 11. dni byl materiál scaffoldu prakticky resorbován a fáze HAp s amorfním fosforečnanem vápenatým (ACP) tvořila 80 % materiálu. Zbytek byl tvořen SiO_2 sítí. Podobný mechanizmus byl sledován i v samotném roztoku pufru, kde fáze HAp fáze tvořila 40 % hmoty. Pufr HEPES, stejně jako TRIS bezpochyby ovlivňují kinetiku rozpouštění sklokeramického materiálu a tím i výsledek *in vitro* testu. Prozkoumali jsme i další možné pufrovací systémy ze série Goodsových pufrů (TES, BES a MOPS) a je zřejmé, že i tyto rozpouštění sklokeramického, ale i skelných materiálů urychlují, ale ne

[15] Theodorou O.M., Goudouri E., Kontonasaki X., et al.: Comparative bioactivity study of 45S56 and 58S bioglasses in organic and inorganic environment. Bioceramics, edit. Kim S. 2009,22, 391-394.

v takové intenzitě jako TRIS a HEPES. Zde se ukázal taky další zajímavý efekt – a to souvislost kinetiky rozpouštění a krystalinity (velikosti, tvaru) vznikající fáze.

2.5. Hodnocení testů in vitro

Zjištění, že pufr TRIS mění pohled na sklokeramické materiály ve falešně pozitivním smyslu nás přivedlo k úvahám o smyslu *in vitro* testů a jejich uspořádání **[12]**. Dnes bychom se měli při zjišťování reaktivity (ne bioaktivity – ta se dá zjistit pouze *in vivo* testy) materiálů řídit ISO normou 23317 (2014). Jak je v celé práci patrné, pokud bychom ji chtěli pro naše testy striktně dodržet, některé důležité informace by nám zůstaly skryté. Použití pufru TRIS pro testy skel a sklokeramických materiálů je diskutabilní, ale i samotný roztok SBF, který má reprezentovat anorganickou část krevní plazmy má až 5 x sníženou koncentraci HCO_3^- iontů, nebo naopak velmi vysokou koncentraci Cl^-. Připravili jsme roztok SBF se správnou koncentrací HCO_3^- iontů a ukázalo se, že koncentrace těchto iontů ovlivňuje kinetiku rozpouštění *scaffoldu*. Vliv na krystalinitu vznikající fáze publikovali Helebrant et al.[16] a Müller et al.[17]. Dalším požadavkem je omezení tvaru testovaného materiálu na kompaktní hranol. Tvar hranolu je nemožné dodržet například při testech granulovaných materiálů. Ve snaze vytvořit z nich hranol, bychom změnili vlastnosti testovaného materiálu, a navíc získali data, která by nám nepodala pravý obraz o jeho chování při samotné aplikaci. S tím samozřejmě souvisí i poměr S/V (plocha vzorku/objem SBF). Tento poměr je v normě nastaven na hodnotu 0.1 cm^{-1}, což znamená, že objem kapaliny (v ml) by měl být desetinásobkem plochy vzorku (v cm^2). V případě jemnozrnných materiálů (např. bovinní HA), který má specifický povrch cca 95 m^2 na 1 g vzorku bychom museli použít úctyhodných 950 m^3 roztoku nebo pro 100 ml SBF použít pouze 10 µg vzorku. ISO norma se omezuje na tzv. statické testy – tedy testy bez výměny kapaliny po dobu 28 dní. Díky analýzám výluhů (které nejsou v normě doporučeny) jsme zjistili, že reaktivnější materiály odčerpají biogenní prvky na tvorbu HAp již v řádech hodin a další expozice v roztoku již nemá smysl. Nám se osvědčily dynamické nebo statická-dynamické testy s každodenní výměnou kapaliny. Staticko-dynamické testy navíc umožňují analyzovat jak výluhy, tak materiál a sledovat i vznik nové fáze na povrchu materiálu v každé fázi testu. Vznik hydroxyapatitu (HAp) na povrchu matriálu je dalším ze sporných požadavků. *In vitro* test materiálů určených k náhradám kostních tkání je soustředěn na vznik krystalické

[16] A.Helebrant, L. Jonášová, L. Šanda, The influence of Simulated body fluid composition on carbonated hydroxyapatite formation, Ceramics-Silikáty 46 (1): 9-14, 2001.
[17] L. Müller, F.A. Müller, Preparation of SBF with different HCO_3^- content and its influence on the composition of biomimetic apatites, Acta Biomaterialia 2; 181-189, 2006.

formy HAp. Tento požadavek může být zavádějící i díky používanému pufru TRIS. Mnohem důležitější se jeví sledování chování materiálu v průběhu celé interakce se simulovanou tělní tekutinou. Dovede nás to k pochopení jednotlivých dějů či mechanizmů, získáme i detailní přehled o kinetice procesu. Navíc, v případě látek, které nejsou živému organizmu přirozené (dopování skel prvky jako Nb nebo Cu a další) by bylo vhodné zjistit kinetiku jejich uvolňování z materiálu, vliv množství uvolněné složky na okamžitou možnou toxicitu a nejenom, jestli se na testovaném materiálu vytvoří vrstva HAp.

ZÁVĚR

Nejdůležitější výsledky v oboru biomateriálů a *in vitro* testů je možné shrnout do těchto bodů:

1. do aplikačního stádia (užitný vzor a patentové řízení) byla připravena precipitace vrstvy amorfního fosforečnanu vápenatého s bioaktivním chováním na Ti nebo Ti slitinách
2. byla zjištěno, že úplná resorpce syntetického a bovinního HA nebo β-TCP není možná, následkem rychle se tvořícího HAp na jejich povrchu (v přítomnosti pufru TRIS)
3. byl potvrzen vliv pufru TRIS na kinetiku rozpouštění sklokeramického scaffoldu (i na sklo) následkem tvorby rozpustného komplexu s Ca^{2+} ionty
4. bylo zjištěno, že krystalická forma HAp vzniká pouze v přítomnosti pufru TRIS
5. pufr HEPES (i další z Goodsových pufrů) vykazuje stejné chování jako TRIS, není tedy vhodnou náhradou pufru TRIS v SBF
6. organická část krevní plazmy v modelové kapalině DMEM nepotlačuje růst nové fáze
7. za zvýšené koncentrace HCO_3^- iontů se v DMEM (i SBF) přednostně tvoří kalcit ($CaCO_3$)

Z uvedených výsledků plyne, že je nutná revize ISO normy 23317 a nový přístup (použití jiné pufrovací soustavy a variabilní nastavení podmínek *in vitro* testu) k testování reaktivity anorganických biomateriálů.

SEZNAM PŘEDLOŽENÝCH PRACÍ V OBORU BIOMATERIÁLŮ

[1] Horváthová R., Rohanová D., Helebrant A.: The calcium phosphate formation on Ti alloy by precalcification proces under static conditions, Ceramics – Silikáty 50 (3): 153-158, 2006.

[2] Rohanová D., Helebrant A., Haufová P., Brázda L., Bezdička P.: A Resorbable Surface Formed on Ti Alloy Material, Key Engineering Materials Vols. 361-363; 701-704, 2008.

[3] Rohanová D., Touš M., Helebrant A., Strnad J.: Amorphous Calcium Phosphate Layer Prepared Ultrasonically on Titanium, Bioceramics 22, pp 253-256, 2009.

[4] Nežiková A., Kolafová M., Strnad J., Strnad Z., Rohanová D., Helebrant A.: Nitrokostní implantát s bioaktivní povrchovou úpravou, Lasak s.r.o. Praha 9, CZ, VŠCHT Praha. z 11.6.2015, Užitný vzor pod číslem: 28285.

[5] Horkavcová D., Zítková K., Rohanová D., Helebrant A., Cílová Z.: The resorption of β-TCP and HA materials under conditions similar to those in living organisms. Ceramics-Silikáty 54 (4): 398-404, 2010.

[6] Horkavcová D., Rohanová D., Kuncová L., Zítková K., Zlámalová Cílová Z, Helebrant A.: Comparison of reactivity of synthetic and bovine hydroxyapatite *in vitro* under dynamic Conditions. Ceramics-Silikáty 58 (1): 70-78, 2014.

[7] El-Maghraby H.F., Gedeon O., Rohanová D., Greish Y.E.: Compressive strength and preliminary in vitro evaluation of gypsum and gypsum-polymer composites in protein-free SBF at 37^{o}C. Ceramics International 36; 1561-1569, 2010.

[8] Hlaváč J., Rohanová D., Helebrant A.: The effect of TRIS-buffer on the leaching behaviour of bioactive glass-ceramics. Ceramics- Silikáty 38 (3-4): 119-122, 1994.

[9] Rohanová D., Boccaccini A.R., Yunos D.M., Horkavcová D., Březovská I., Helebrant A.: TRIS buffer in simulated body fluid distorts the assessment of glass-ceramic scaffold bioactivity. Acta Biomaterialia 7; 2623-2630, 2011.

[10] Rohanová D., Boccaccini A.R., Horkavcová D., Bozděchová P., Bezdička P., Častorálová M.: Is non-buffered DMEM solution a suitable medium for in vitro bioactivity test? Journal of Materials Chemistry B 2; 5068-5076, 2014.

[11] Rohanová D., Horkavcová D., Paidere L., Boccaccini A.R., Bozděchová P., Bezdička P.: Interaction of HEPES buffer with glass-ceramic scaffold: Can HEPES replace TRIS in SBF? Journal of Biomedical Materials Research Part B, DOI:10.1002/jbm.b.33818, 2017 in print.

[12] Rohanová D., Horkavcová D., Helebrant A., Boccaccini A.R.: Assessment of *in vitro* testing approaches for bioactive inorganic materials. Journal of Non-Crystalline Solids 432; 53-59, 2016.

Práce **[1]**

Horváthová R., Rohanová D., Helebrant A.: The calcium phosphate formation on Ti alloy by precalcification proces under static conditions, Ceramics – Silikáty 50 (3): 153-158, 2006.

Podíl: 50%: návrh experimentu, analýzy výluhů, zpracování výsledků a příprava publikace

THE CALCIUM PHOSPHATE FORMATION ON TI ALLOY BY PRECALCIFICATION PROCESS UNDER STATIC CONDITIONS

RENÁTA HORVÁTHOVÁ, DANA ROHANOVÁ, ALEŠ HELEBRANT

Department of Glass and Ceramics, Institute of Chemical Technology, Prague
Technická 5, 166 28, Prague, Czech Republic

E-mail: renata.horvathova@vscht.cz

Submitted January 17, 2006; accepted May, 30, 2006

Keywords: Precalcification, Calcium phosphate, Titanium alloy (Ti-6Al-4V), Hydroxyapatite, Biomimetic process

The aim of this paper was to study the influence of precalcification process on the nucleation as well as growth of calcium-phosphates crystals (Ca-P) on the surface of Ti alloy. Ti alloy was precalcified by the calcification solutions (SCS1-3) with different content of Ca^{2+} and $(PO_4)^{3-}$ ions and compared with the non-precalcified sample. The results of Ca^{2+} and $(PO_4)^{3-}$ analysis indicate that precalcification step accelerates the consumption of both Ca^{2+} and $(PO_4)^{3-}$ ions from simulated body fluid (SBF) solution. The deposition of Ca-P phase was completed approximately 6 days earlier when compared it with the non-treated samples. Analytical measurements as well as the surface observation enable to find optimal calcification solution marked as SCS2 containing (mmol/dm^3) 4.0 Na^+, 5.0 Ca^{2+}, 10.0 Cl^-, 2.5 $H_2PO_4^-$ and 1.5 HCO_3^-. The influence of S/V ratio (surface area / volume of soaking media) changes on the nucleation and thickness of Ca-P layer formed in the SCS2 solution has been studied in the second part of this work. It was found out that 4 days immersion in SCS2 solution at S/V ratios at 0.1 and 0.5 cm^{-1}, respectively, is enough time for complete deposition by Ca-P phase on the alloy surface. The changes of the S/V ratio allow adjusting the thickness of Ca-P layer on the surface.

INTRODUCTION

Materials based on calcium-phosphate, such as hydroxyapatite, have been shown to enhance bone apposition to orthopedic implants; they do not form fibrous tissues, but instead an extremely thin, epitaxial bonding layer with existing bone. These materials have an excellent bioactive behavior but due to their low mechanical properties they are mostly used as coatings on implant surfaces of substrates such as Ti6Al4V and other medical alloys [1]. Biomimetic coating processes overcome many of the shortcomings of conventional vapor phase coating techniques and are designed to mimic biomineralization processes based on using of the calcification solutions [2-4]. Uniform coatings can be applied to any surface that has access to an aqueous solution. The process involves controlled crystal nucleation and growth. All surfaces within a porous implant can be uniformly coated without dogging or filling the implant.

Titanium materials have been used successfully in orthopedic and dental surgery due to their good mechanical properties for many years. However, in order to successful bonding to hard tissue the Ti alloy surface has to be treated before applying by strong acid and base (HF or HCl and NaOH) at the first step. After this chemical treatment a thin TiO_2 gel-like layer with presence of Na^+ ion is formed on the alloy surface. Presence of this layer gives bioactive properties to Ti [5-6]. Chemical analysis of the supersaturated solutions with the time of exposure of tested materials confirmed continuous but very slow consumption of Ca^{2+} as well as $(PO_4)^{3-}$ ions [7]. The objective of this work was to choice the more advantageous supersaturated calcification solutions (SCS1-3) and the second part of work was focused on calcium-phosphate growth in SCS2 solution depending on *S*/*V* ratio (surface area / volume of soaking media). The quality of calcium-phosphate layer depends on the concentration and ratio of both Ca^{2+} and $(PO_4)^{3-}$ as well as the presence of $NaHCO_3$ in the role of buffer in SCS. Subsequent in vitro testing in SBF indicated an acceleration of new calcium-phosphate forming (probably hydroxyapatite).

EXPERIMENTAL

Chemical treatment: The Ti6Al4V alloy surfaces with the dimension of 10×10×0.7 mm (figure 1) were etched in HF (1:10) for 1 min, 5-times washed by demineralized water. Pre-treatment continued by soaking in 10M NaOH solution at 60°C for 24 hours with subsequent (5-times) gentle rinsing by demineralized water (figure 2).

Precalcification: The samples were precalcified in supersaturated calcification solutions (SCS1-3) (table 1). The Ti alloy samples were soaked in SCS solutions under static condition at 37°C for 7 days at S/V = 0.5 cm^{-1} (S = sample surface (cm^2), V = volume of soaking solution (cm^3)).

Table 1. The ion concentration of the SCS solutions (mmol/dm^3).

solution	Na^+	Ca^{2+}	Cl^-	$H_2PO_4^-$	HCO_3^-
SCS1	6.5	5.0	10.0	5.0	1.5
SCS2	4.0	5.0	10.0	2.5	1.5
SCS3	4.0	10.0	20.0	2.5	1.5

Exposition in SBF: The effect of Ti alloy pre-treatment and precalcification on calcium phosphate formation was examined in simulated body fluid (SBF) which simulates inorganic part of human blood plasma (table 2). The SBF solution was prepared by dissolving reagent grade KCl, NaCl, $NaHCO_3$, $MgSO_4$, $CaCl_2$ a KH_2PO_4 into demineralized water and buffered at *pH* = 7.3 with TRIS [tris(hydroxymethyl)aminomethan] and HCl at 37°C. The samples were exposed into SBF solution under static conditions in a biological thermostat at 37°C. The sample without precalcification was soaked in SBF at $S/V = 0.5$ cm^{-1} for 14-20 days and precalcified ones at $S/V = 0.5$ cm^{-1} for 7-14 days.

Analytical measurement: Sample-solution interactions were quantified on the basis of solution analysis. To evaluate the ability and rate of Ca-P formation, the concentration of phosphates and calcium ions in the solution were performed by spectrophotometric measurement and atomic absorption spectroscopy (AAS), respectively.

The analysis of Ca^{2+} ions concentration were performed at $\lambda = 442$ nm by AAS. The KCl releasing buffer with concentration of 4000 ppm was added to each sample. The $(PO_4)^{3-}$ analyses were performed by spectrophotometric method. The analysis was based on determination of phosphate ions on the yellow form at 460 nm. Reproducibility of results was 5-10 %. Error bars in time dependences represent maximum difference for 2 independent measurements.

pH measurement: Value of *pH* was measured at 25°C by glass electrode.

Analysis of sample surface: Ti alloy surfaces after chemical treatment and exposure in precalcification and subsequently in SBF solution were observed by scanning electron microscope Hitachi S4700 (SEM-EDS) and by optical microscopy using image analysis with software LUCIA. The thickness of the calcium-phosphate layers was observed on the cross section of the samples fixed in resin and subsequently polished by 3 μm grains of diamond paste. WAXS-GI XRD methods confirmed crystal character of newly formed layers.

RESULTS AND DISCUSSION

Figure 2 shows the morphology of Ti alloy surface changed by chemical treatment. Leaching of titanium alloy in NaOH results in the formation of a hydrated titanium oxide gel layer containing alkali ions in its surface. This interlayer has thickness up to 5 μm. EDS analyses detected small amount of Na^+ ions in the surface (table 3). The amorphous character of TiO_2 layer was confirmed by WAXS-GI XRD method.

Table 2. The ion concentrations of SBF compare to inorganic part of blood plasma (mmol/dm^{-3}).

	Na^+	K^+	Ca^{2+}	Mg^{2+}	Cl^-	HCO_3^-	HPO_4^{2-}	SO_4^{2-}
plasma	142.0	3.6-5.5	2.1-2.6	1.0	95.0-107.0	27.0	0.7-1.5	1.0
SBF	142.0	5.0	2.5	1.0	131.0	5.0	1.0	1.0

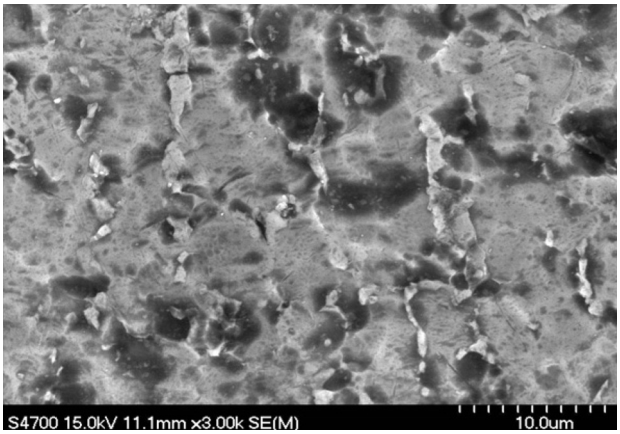

Figure 1. SEM micrograph of Ti alloy original surface.

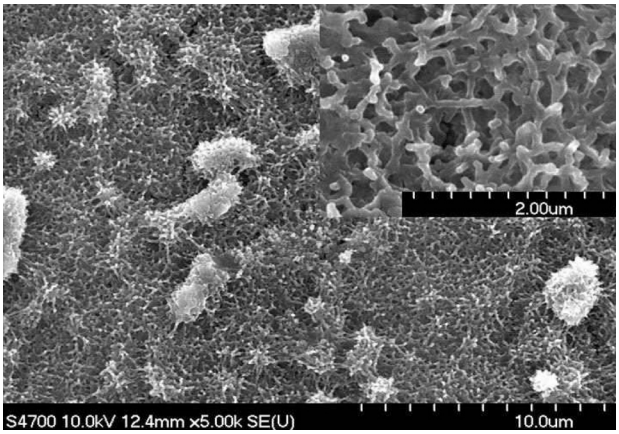

Figure 2. SEM micrograph of Ti surface after treatment in HF, NaOH (detail of the structure in the corner).

Table 3. Chemical composition of the surface before and after chemical treatment.

Method of analyses	Surface treatment	Ti (at.%)	Al (at.%)	V (at.%)	Ti/Al	Ti/V	Al/V	Na (at.%)
SEM-EDS	before	83.5	12.1	4.4	6.9	19.0	2.8	-
SEM-EDS	HF, NaOH	30.0	1.7	0.9	18.2	34.9	1.9	5.5

Analysis of the SCS1-3 solutions after precalcification process

Results of SCS1-3 solutions were published and discussed in [7]. The significant decrease of the Ca^{2+} and $(PO_4)^{3-}$ ions was detected already after the first day of the exposure in SCS1-2 solutions. The ions consumption stopped after the 4th day of the exposition. We can assume that the nucleation period of the Ca-P precipitation started in the first minutes of the samples exposition and Ca-P phase formed continuously till the solution is supersaturated to precipitated calcium-phosphate. The solution named SCS3 was unstable and calcium-phosphates precipitated before exposition of the Ti-alloy sample.

In vitro test (exposition in SBF solution)

In vitro test compares results of the precalcified samples with the non-precalcified sample in SBF solution. Analysis confirmed that precalcified samples (figures 3b-d) had absorbed Ca^{2+} and $(PO_4)^{3-}$ ions immediately after immersion till the 7th day of exposition in SBF. In the case of the non-precalcified sample (figure 3a) this phenomenon had occurred on the 6th day after immersion and finished till the 14th day. The residual concentration of the both ions was about 40-50 mg/dm^3 and subsequently the Ca-P precipitation stopped.

Analysis of SBF solutions after exposure of Ti alloy samples had only informative character (figures 3a-d). In spite of this fact, there is evident phenomenon - shortening of incubation period of forming Ca-P if the samples were precalcified.

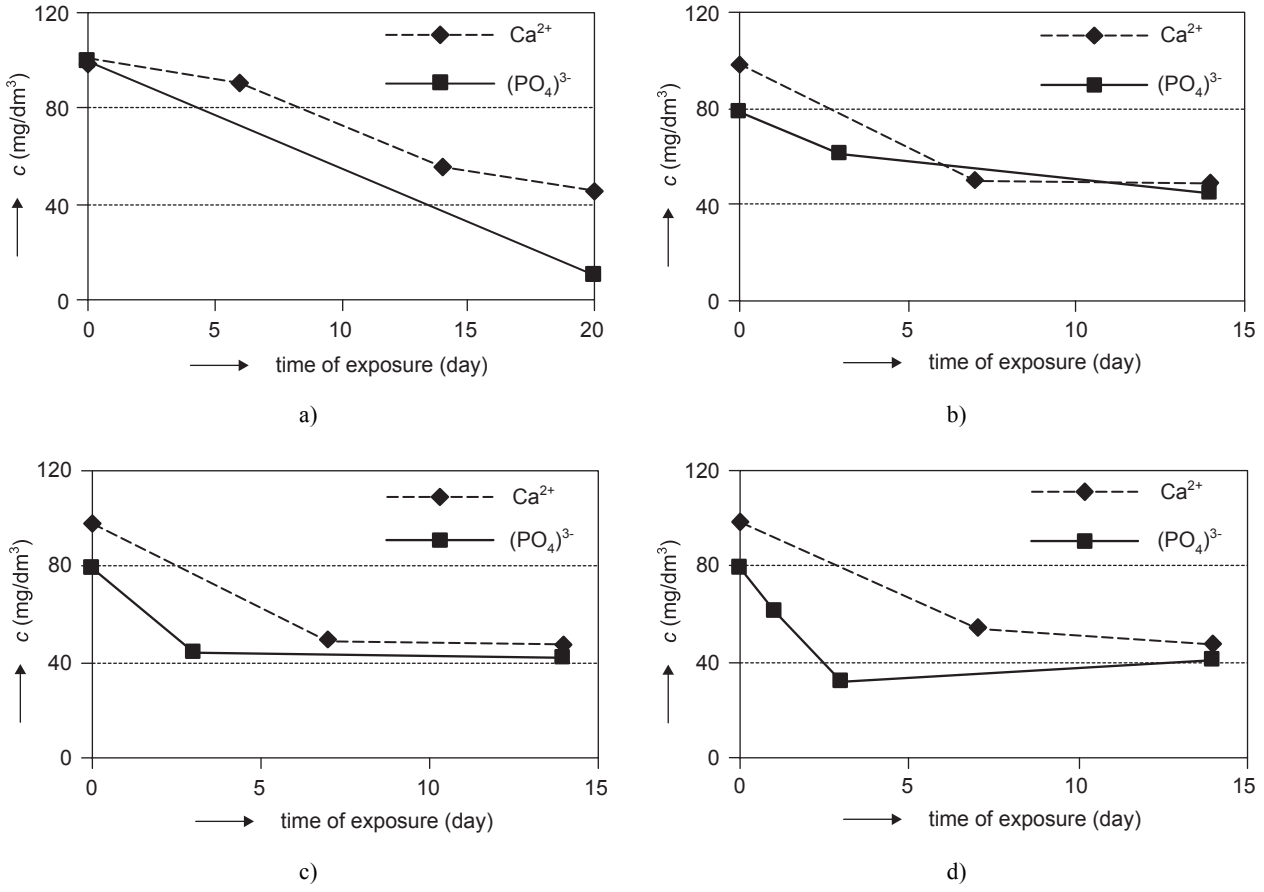

Figure 3. Time dependence of Ca^{2+} and $(PO4)^{3-}$ concentrations a) of the non-precalcified sample in SBF (20 days) and precalcified ones in b) SCS1 (7 days), c) SCS2 (7 days), d) SCS3 (7 days) solutions with subsequent exposure in SBF (14 days).

Study of Ca-P layer on the surface after exposure in SBF

The quality and thickness of the formed layers seems different (figures 4-5). Ca-P spherulites formed on non-precalcified surface are distributed non-homogenously on the sample surface containing of Ca-P layer (figure 4). This fact was confirmed by SEM-EDS [8]. However, only 7 days of exposition in SBF in the case of precalcified sample (SCS2) is enough time for complete covering of the sample surface by homogenous Ca-P layer (figure 5). This layer shows the crystalline character. Needle-like crystals are spherically seated.

Thickness of the Ca-P layer was approximately 5 μm after 20 days in the case of non-precalcified sample and 13 μm on the precalcified surface after 14 days in SBF, respectively (both under static conditions). Studying of the layers by optical microscopy after immersion in SBF confirmed that precalcification treatment had positive influence on the Ca-P growth. The analytical measurement (figures 3a-d) confirmed the layer observations (figures 4-5).

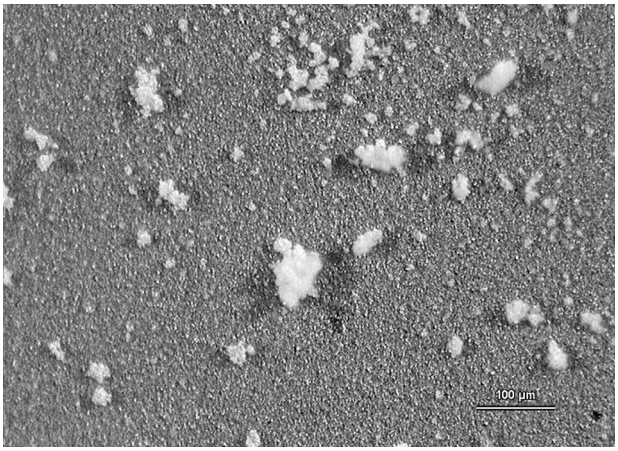

Figure 4. Optical micrograph of the surface of non-precalcified sample after soaking in SBF (20 days).

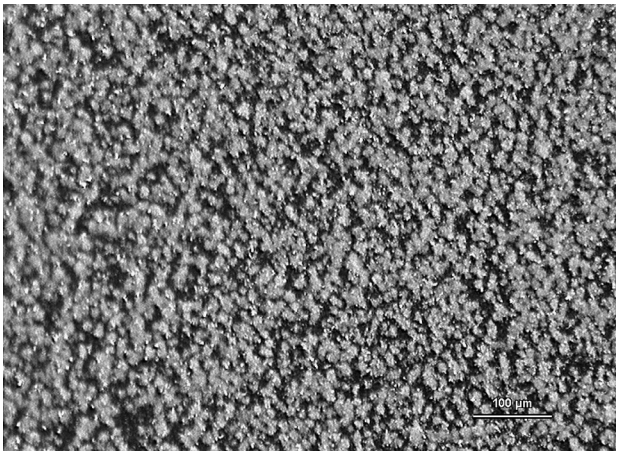

Figure 5. Optical micrograph of the precalcified surface in SCS2 (7 days) with subsequent exposure to SBF (7 days).

It has been concluded that using SCS2 solutions can help to precipitate of the Ca-P phase in SBF solution. Consequently, the Ti alloy surface with nucleated Ca-P phase is good base for next growth of crystalline Ca-P phase in SBF as well as human plasma solutions.

The effect of *S*/*V* ratio on the thickness and quality of Ca-P layer

The SCS2 solution was chosen as the base for the precalcification process with the aim to study the influence of *S*/*V* ratio on nucleation and growth of Ca-P layer. Ti alloy samples were immersed in SCS2 solution under static condition at 37°C for 7 days and at S/V = 0.1; 0.3 and 0.5 cm^{-1}.

Results of precalcification analysis for various aspect of the *S*/*V*

The results of analysis confirmed (figures 6a-c), that the ions consumption with time of exposure have analogous trend for each *S*/*V* ratio in SCS2 solution. The absorption of ions was stopped on the range of about 160-170 mg/dm^3 for Ca^{2+} and 140-150 mg/dm^3 for $(PO_4)^{3-}$ after the 4th day of exposure in SCS2 solution independent on *S*/*V* ratio. Measurement of *pH* value confirmed that *pH* decreased continuously from 6.4 to 5.8 in all cases. It means that SCS2 solution had become under saturated to Ca-P which is formed on the surface on the 4th or 7th day, respectively. The optimum time for Ca-P phase formation seems to be the 4th day of exposure, when the Ca/P molar ratios (calculated from consumed amount of ions) achieved 1.72; 1.81 and 1.67 (1.67 is the theoretical value for hydroxyapatite) for *S*/*V* 0.1; 0.3 and 0.5 cm^{-1}, respectively (figure 6d).

Study of the Ca-P layers (thickness and morphology) after precalcification process by optical microscopy

Ti alloy surfaces are completely covered by fine grain minerals of Ca-P phase at *S*/*V* = 0.1 cm^{-1} as well as 0.5 cm^{-1} (figure 7). Differences are in thickness and probably quality of this layer. The thicknesses continuously grow from 25 μm (*S*/*V* = 0.5 cm^{-1}) to 50 μm (*S*/*V* = 0.1 cm^{-1}). Figures 7 and 8 demonstrate the thickness of the layer (cross section) on surface after the 7th days of exposure at *S*/*V* = 0.1 and 0.3 cm^{-1}, respectively. Spherulites formed in SCS2 solution at *S*/*V* = 0.3 cm^{-1} do not covered of the sample surface completely. The diameter of these spherulites is approximately of 30 μm (figure 8).

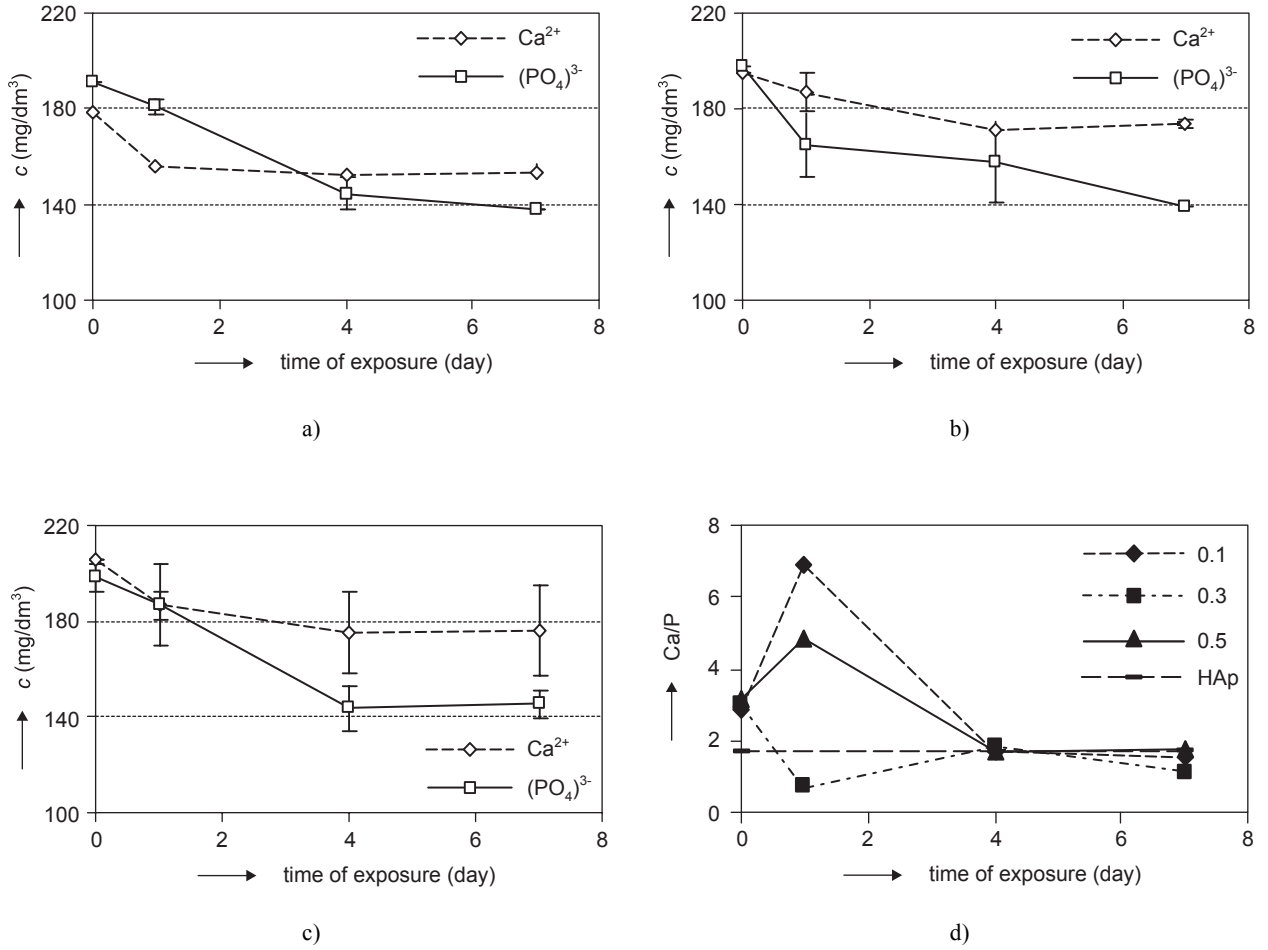

Figure 6. Time dependence of changes in Ca^{2+} and $(PO_4)^{3-}$ concentration after exposition in SCS2 solution - a) S/V = 0.1 cm^{-1}, b) S/V = 0.3 cm^{-1}, c) S/V = 0.5 cm^{-1}, d) calculated Ca/P molar ratio of consumed ions under various S/V.

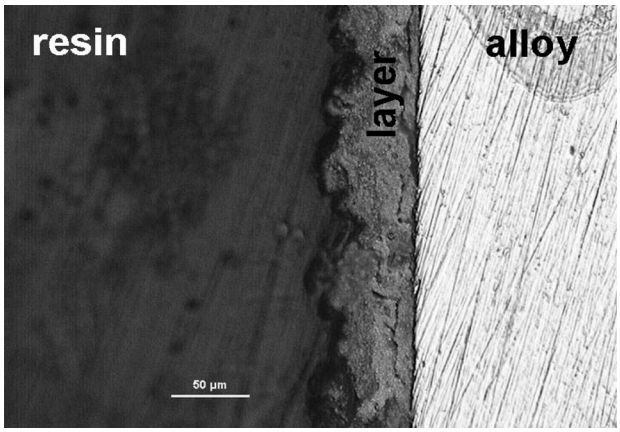

Figure 7. Optical micrograph, cross section of the layer formed in SCS2.

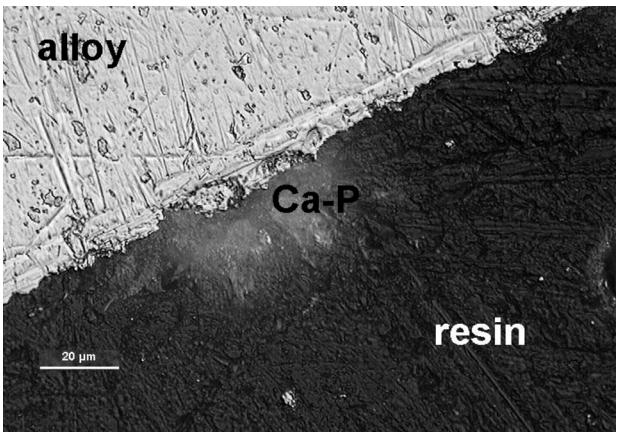

Figure 8. Optical micrograph, cross section of the spherulit.

CONCLUSION

1) Precalcification process has significant influence on shortening of incubation period of Ca-P precipitation in SBF, resulting Ca-P layer is twice thicker compared to the non-precalcified samples.
2) The thickness of the Ca-P layer nucleated by precalcification depends on *S*/*V* ratio and can be predicted.
3) Precalcification process is finished where the solution became under saturated for formation of Ca-P and in our experiments it was on the 4th day, consequently static conditions for in vitro testing are not satisfying because of quick consumption of Ca^{2+} and $(PO_4)^{3-}$ ions as well as decrease of *pH* value in supersaturated solutions.

Acknowledgement

This study was partially supported by Ministry of Education of the Czech Republic (research programme MSM 6046137302).

References

1. Hlaváč J.: Ceramics - Silikáty *43*, 133 (1999).
2. Li F., Feng Q. L., Cui F. Z., Li H. D., Schubert H.: Surf.Coat.Technol. *154*, 88 (2002).
3. Skrčená A., Gerhard H., Helebrant A.: Poster Glastechnische Tagung 79, DGG, Deutsche Glastechnische Ges. e.V., Würzburg, 23.-25. May 2005.
4. Baker K. C., Anderson M. A., Oehlke S. A., Astashkina A. I., Haikio D. C., Drelich J., Donahue S. W.: Mat.Sci.Eng. *C* (in press).
5. Wei M., Kim H.-M., Kokubo T., Evans J. H.: Mater. Sci.Eng. *C 20*, 125 (2002).
6. Jonášová L., Müller A. F., Helebrant A., Strnad J., Greil P.: Biomaterials *25*, 1187 (2004).
7. Horváthová R., Rohanová D., Calvez P., Helebrant A.: Sklář a keramik *55C*, 25 (2005).
8. Horváthová R., Brázda L., Rohanová D., Helebrant A. in: *Príprava keramických materiálov*, p. 18-19, Ed. Kuffa T., Plešingerová B., HF TU, Košice 2005.

PŘÍPRAVA KALCIUMFOSFÁTU NA Ti SLITINĚ PREKALCIFIKAČNÍM PROCESEM ZA STATICKÝCH PODMÍNEK

RENÁTA HORVÁTHOVÁ, DANA ROHANOVÁ, ALEŠ HELEBRANT

Ústav skla a keramiky,
Vysoká škola chemicko-technologická v Praze
Technická 5, 166 28 Praha 6

Bioaktivním materiálem v souvislosti s náhradami kostní tkáně rozumíme materiál, který je schopen za dostatečně krátkou dobu vytvořit s kostní tkání pevnou vazbu. Titanové materiály (Ti6Al4V) využívané k ortopedickým nebo dentálním náhradám jsou materiály inertní. Chemickou úpravou jejich povrchu pomocí silných kyselin a zásad se docílí pokrytí povrchu tenkou vrstvičkou TiO_2 gelu. Následně několikadenní expozicí v přesycených roztocích označených SCS1-3 (vysoký obsah Ca^{2+} a $(PO_4)^{3-}$ iontů a vhodné pH) se na povrchu gelu nukleuje a sráží dostatečně silná vrstva kalcium-fosfátu. Přítomnost této rozpustné kalcium-fosfátové vrstvičky následně urychlil cca o 6 dnů proces tvorby kalcium-fosfátu při in vitro testech v statickém uspořádání. Prekalcifikace tak může urychlit proces vyhojování. Druhá část práce byla zaměřena na vliv poměru *S*/*V* (plochy vzorku ku objemu kapaliny (SCS2)). Z měření koncentrace iontů Ca^{2+} a $(PO_4)^{3-}$ vyplynulo, že největší změny se v prekalcifikačním roztoku odehrávají 1. den po vložení vzorku a prakticky ukončují do 4. dne od začátku expozice. Roztok přestává být přesycen vůči kalciumfosfátu, který se na povrchu vysrážel odčerpáním Ca^{2+} i $(PO_4)^{3-}$ iontů a snížením jeho pH. Tloušťka i velikost vzniklých jehlicovitých krystalků sféroliticky uspořádaných je závislá na poměru *S*/*V*. Odčerpané množství Ca i P a jejich poměr se již po 4. dnu blíží teoretickému poměru v HAp. Z naměřených dat také vyplývá, že k testování bioaktivních materiálů je vhodnější tzv. dynamické uspořádání testu, kde bude zaručen přívod čerstvého roztoku SBF (simulated body fluid) po celou dobu testování materiálu.

Práce **[2]**

Rohanová D., Helebrant A., Haufová P., Brázda L., Bezdička P.: A Resorbable Surface Formed on Ti Alloy Material, Key Engineering Materials Vols. 361-363; 701-704, 2008.

Podíl: 50%: návrh a realizace experimentu, analýzy výluhů, zpracování výsledků a příprava publikace

Key Engineering Materials Vols. 361-363 (2008) pp. 701-704
online at http://www.scientific.net

A Resorbable Surface Formed on Ti Alloy Material

D. Rohanová[1,a], A. Helebrant, P. Haufová, L. Brázda, P. Bezdička[2]

[1] Institute of Chemical Technology, Prague, Department of Glass and Ceramics, Technická 5, 166 28 Prague 6, Czech Republic
[2] Institute of Inorganic Chemistry, Academy of Sciences of the Czech Republic, v.v.i., 250 68 Husinec - Řež, Czech Republic

[a]dana.rohanova@vscht.cz

Keywords: Ti alloy, resorbable surface, precalcification

Abstract. This paper performs a new way of a resorbable surface on Ti alloy preparation. Precalcification of a chemically treated Ti or Ti alloy surface by a **s**upersaturated **c**alcification **s**olution - SCS2 (high content of Ca^{2+} as well as $(PO_4)^{3-}$ ions) allows to short of an induction period in SBF solution (practically immediate reaction stats a hydroxyapatite precipitation). Soluble octacalcium phosphate ($Ca_8H_2(PO_4)_6$. $5H_2O$ was detected by RTG on the surface after calcification. Presumption is: a healing time of the calcified Ti alloy could be shortened.

Introduction

Ti alloy regarded its excellent mechanical properties as biomaterial for bones and teeth implants. Naturally it is an inert material in body environment and so it has to be mechanically and chemically treated before implantation to achieve a good roughness and reactivity. Bioactive surface on Ti alloy can be prepared by subsequent etching and leaching in HCl and NaOH according to Kokubo and Jonášová procedure [1, 2]. Formed porous TiO_2 gel contains Na^+ ions coming from a previous treatment. A surface enhanced pH value (near 8) ensures a calcium phosphate preferential precipitation directly on the Ti alloy sample. The aim of our study was to increase the surface bioactivity by two-step process, when etching of the surface was followed by exposition in SCS2 (supersaturated calcifying solution) [3, 4] in order to prepare resorbable calcium phosphate layer.

Materials and Methods

Chemical treatment. The Ti6Al4V alloy samples with the diameter of 9 mm x1 mm were etched in HCl (concentrated) for 90 min and 4-times washed by demineralized water. Pre-treatment continued by soaking in 10M solution of NaOH at 60 °C for 24 hours with subsequent (5-times) gentle rinsing by demineralized water .
Calcification. The samples were calcified in supersaturated calcifying solutions (SCS2) (table 1). The Ti samples were soaked in SCS2 solutions under static condition at 20°C for 3, 6, 24 and 72 hours at S/V = 0.1 cm^{-1} (S = sample surface [cm^2], V = volume of soaking solution [cm^3]).

Table 1. Composition of the SCS2 solution ($mmol.dm^{-3}$).

solution	Na^+	Ca^{2+}	Cl^-	$H_2PO_4^-$	HCO_3^-	Ca/P
SCS2	4.0	5.0	10.0	2.5	1.5	2

Test of bioactivity in SBF (simulated body fluid) under static and dynamic conditions. The effect of Ti alloy pre-treatment and precalcification on HAp formation was examined in simulated body fluid (SBF) which simulates inorganic part of human blood plasma (table 2). The SBF solution was prepared by dissolving reagent grade KCl, NaCl, $NaHCO_3$, $MgSO_4$, $CaCl_2$ a KH_2PO_4 into demineralized water and buffered at pH = 7.3 with TRIS [tris(hydroxymethyl)aminomethane] and HCl at 37°C. The samples were exposed into SBF under static (S/V = 0.1 cm^{-1}) and dynamic conditions with flow 48ml SBF per day (S/F= 0.2 cm^{-1}). The cells with samples were placed into a biological thermostat at 37°C. The continual flow of the SBF solution was maintained by a peristaltic volume pump. The total time of testing was 7 days in both cases.

Table 2. The ion concentrations in SBF ($mmol.dm^{-3}$).

	Na^+	K^+	Ca^{2+}	Mg^{2+}	Cl^-	HCO_3^-	HPO_4^{2-}	SO_4^{2-}
SBF	142.0	5.0	2.5	1.0	131.0	5.0	1.0	1.0

Analytical measurement in solutions. To evaluate the ability and rate of Ca-P formation, the concentration of phosphates and calcium ions in the solution were determined by spectrophotometry and atomic absorption spectroscopy (AAS), respectively.
The analysis of Ca^{2+} ions concentration were performed at λ = 442 nm by AAS. The KCl releasing buffer with concentration of 4000 ppm was added to each sample. The $(PO_4)^{3-}$ analyses were performed by spectrophotometry method. The analysis was based on determination of phosphate ions on the blue form at 830 nm. Reproducibility of results was 5-10 %. Error bars in time dependences represent maximum difference for 2 independent measurements.
pH value measurement. Value of pH was measured at 25°C by the glass electrode and pH on the sample surface by the glass electrode with a plate diaphragm
Optical microscopy of sample surface. Ti surfaces after chemical treatment and SCS2 or/and subsequently in SBF solution were observed by optical microscopy using image analysis with software Lucia. The calcium-phosphate layers were observed on the samples cross section fixed in resin.
XRD microanalysis. Diffraction patterns were collected with a PANalytical X´Pert PRO diffractometer equipped with a conventional X-ray tube (Co K_α radiation, 40 kV, 30 mA, point focus) and a multichannel detector X'Celerator with an anti-scatter shield. X-ray patterns were measured in the range of 4 to 100° 2 Θ with step of 0.0167° and 1050 s counting per step. In this case we used the conventional Bragg-Brentano geometry with 0.02 rad Soller slit, 0.25° divergence slit, 0.5° anti-scatter slit, and 10 mm mask in the incident beam, 5.0 mm anti-scatter slit, 0.02 rad Soller slit and Fe beta-filter in the diffracted beam. XRD patterns were not pre-treated before interpretation as no background correction was-needed.

Results and discussion

Mechanical treatment of the Ti alloy surface enhanced the adhesion properties of formed surface. Acid etching by HCl make up a fine surface porosity and following leaching in NaOH solution increased pH value (up to 8) on the sample surface. Higher pH value ensures preferential precipitation of calcium phosphate on the Ti alloy surface However HAp layer precipitated in SBF did not cover surface completely (non-calcified sample).
Using precalcification by soaking the samples in fresh SCS2 solution, octacalcium phosphate ($Ca_8H_2(PO_4)_6.5H_2O$ - OCP) precipitated as a main phase on Ti surface. Octacalcium phosphate formed the needle like crystals shaped spherically into rosettes after 1 day exposition in SCS2. Also the big plate crystals of dicalcium phosphate ($CaHPO_4.\ 2H_2O$ - DCPD) were detected using XRD diffraction in 7 days old solutions. (Figure 1 and 2).

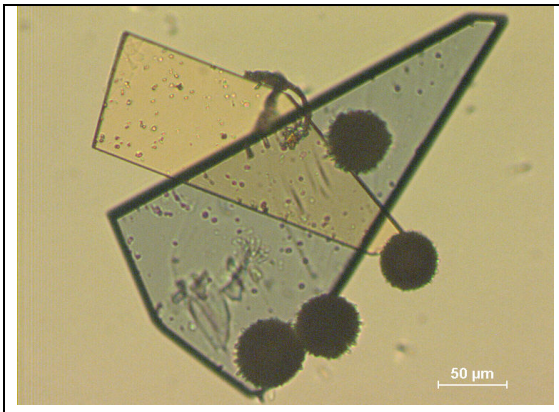

Figure 1. Ca/P phases formed in SCS2 solution

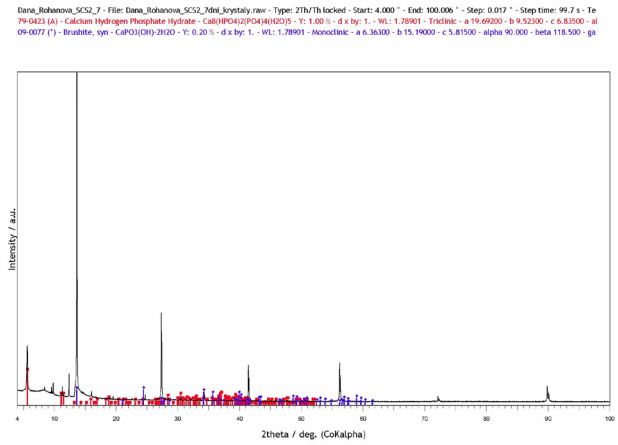

Figure 2. XRD analysis of crystals formed in SCS2 (OCP and DCPD)

Properties (crystalinity, thickness...) of newly formed Ca/P phases depended on the arrangement of the precalcification step. Thickness of a new layer depends on S/V ratio (surface of sample/ volume of solution) as well as duration of calcification process. Calcium phosphate has not visibly precipitated on the surface at short time exposition (3 hours). However shortly exposed surface in the SCS2 reacts similarly to the surfaces visibly covered by the Ca/P amorphous or crystal phases in SBF. Calcium and phosphate ions were soaked into a porous gel like TiO_2 layer probably. The longer exposition time (6 and 24) shows precipitation of an amorphous phase on the sample surface. Crystallization of Ca/P phase starts 24 hours after immersion into SCS2 solution Figure 3. Both static and dynamic in vitro tests showed that the HA phase was precipitated on the calcified surfaces immediately after immersion into SBF contrary to non-calcified sample (0 h SCS) (figure 4).

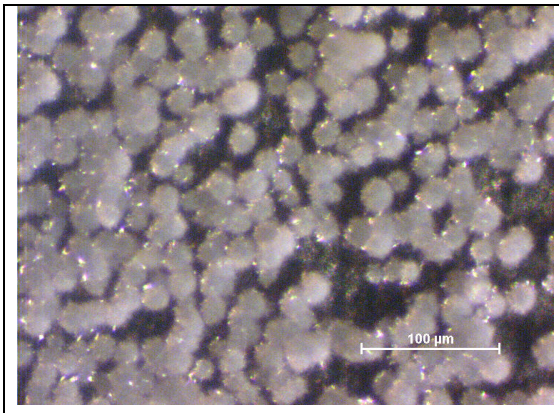

Figure 3. The OCP on Ti alloy surface formed in SCS2 solution after 24 exposition

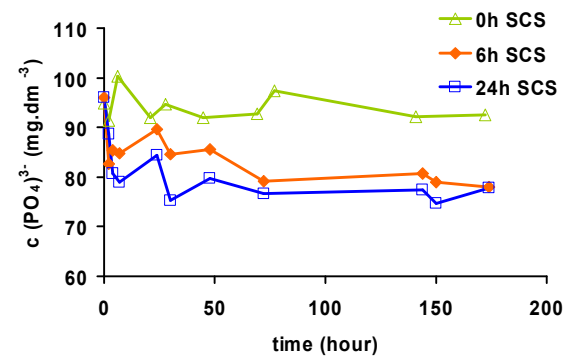

Figure 4. The PO_4 ions outflow from SBF solution indicates the HAp precipitation (dynamic condition)

Already very short-time exposition in SCS2 solution (a several hours) ensure shortening of initial time of HAp precipitation compared to the non-calcified samples. This fact could positively affect healing time of implanted Ti alloy. Toxicity of precalcified sample will be tested on living cell (ex vivo test) in future.

Conclusions

1. Inert surface of Ti can be convert to bioactive or resorbable by precalcification in SCS2 solution;
2. soluble octacalcium phosphate (OCP) as dominant phase is formed on the surface;
3. Presumption: using SCS2 solution could shorten the healing time

Acknowledgement

This study was supported by Ministry of Education and by Ministry of Industry and Trade as parts of the projects MSM 6046137302 and 2A-1TP1/063.

References

1. L. Jonášová, F.A.Müller, et al. (2004) Biomaterials 25:1187-94.
2. T.Kokubo, et al. (2003) Biomaterials 24:2161-75.
3. F.F.Li, Q.L.Feng, et al. (2002) Surface and Coatings Technol. 154: 88 – 93.
4. D.Rohanova et al.: Precalcification as a method of optimization of bioactive surfaces, poster on 8th.Oto Schott Col. (2006) Jena

Práce **[3]**

Rohanová D., Touš M., Helebrant A., Strnad J.: Amorphous Calcium Phosphate Layer Prepared Ultrasonically on Titanium, Bioceramics 22, p. 253-256, 2009.

Podíl: 60%: návrh a realizace experimentu, analýzy výluhů, vyhodnocení výsledků, zpracování publikace

Bioceramics 22 (2009) pp253-256
www.bioceramics22.com

Amorphous Calcium Phosphate Layer Prepared Ultrasonically on Titanium

Dana Rohanová[1], Milan Touš[1], Aleš Helebrant[1], Jakub Strnad[2]

[1]Department of Glass and Ceramics, Institute of Chemical Technology, Prague, Technická 5, 166 28 Praha 6
[2]LASAK spol. s.r.o. Papírenská 25, 160 00 Praha 6
dana.rohanova@vscht.cz

Keywords: Hydroxyapatite, Titanium, Amorphous Calcium Phosphate, SCS2, Ultrasonic bath

Abstract An inert titanium surface was treated with the so-called BIO treatment (developed by the company Lasak, s.r.o.), i.e. its surface area was increased by mechanical and chemical treatment with blasting and exposure to HCl and NaOH. The treated surface was provided with thin layers of calcium phosphate OCP (octacalcium phosphate) or ACP (amorphous calcium phosphate) by means of precalcification under static conditions (using an oversaturated SCS2 solution). In vitro tests in SBF (Simulated Body Fluid) under dynamic conditions have shown that precalcified OCP layers have the ability to induce development of HAp (hydroxyapatite) on the surface much faster than BIO surfaces without such layers. OCP crystals develop during 24 hours of precalcification (under static conditions in SCS2 (Supersaturated Calcifying Solution) and they are up to 20 μm thick. The layers are well adhesive but cytotoxicity tests have shown that a bioactive layer prepared in this manner is slightly toxic. Therefore a very thin interlayer was prepared from SCS2 ultrasonically. The amorphous calcium phosphate prepared in this manner is incorporated directly into the TiO_2 gel and thus does not increase implant´s dimension. During in *vitro* tests in SBF under dynamic conditions the layer induces growth of HAp at the same rate as the thicker layer of OCP crystals, while the thinner layer is not toxic.

Introduction

In order to ensure bioactive behaviour of an otherwise inert material – titanium (Ti) or its alloy (Ti6Al4V) it is necessary to increase its reactive surface as much as possible (by creating layers of TiO_2 gel). The so-called BIO treatment, i.e. mechanical treatment (blasting) and chemical treatment (etching in HCl and NaOH), increase the surface area up to 1000 times [1]. The principle of bioactivity of many glass- and ceramics-based materials consist in their ability to release biogenic elements Ca and P (the basic building units of HAp) into their proximity. Hydroxyapatite precipitation starts on the implant surface immediately after a local increase of HAp supersaturation on the surface of the material. Therefore it is desirable to create a resorbable interlayer of calcium phosphate on the surface of an inert implant, which in body fluids dissolves easier than HAp as such. The prepared interlayer shall meet not only high requirements for adhesion to the substrate but also requirements for dimensional stability of the implant. One of the simple and cheap methods to prepare bioactive (resorbable) interlayers is a method of surface precalcification [2, 3]. In earlier works published by our laboratory we used mechanically and chemically treated surfaces to prepare OCP layers by precalcification from SCS2 solution. OCP forms little tabular crystals arranged in spherulites and it is a convenient precursor for nucleation and crystallization of HAp [4]. If placed freely into SCS2 solution a layer of OCP or ACP (shorter exposure) spontaneously precipitates on the sample surface within several hours. The objective of the submitted work was to prepare a

layer of calcium phosphate on a Ti substrate surface, whose bioactivity was to be comparable with that of OCP layer, but without significantly changing the implant dimensions, and whose preparation was to be reproducible. Therefore we used an ultrasonic bath for the precalcification, as the ultrasonic waves support incorporation of elements (Ca and P) into the previously prepared TiO_2 gel (BIO treatment).The ability of the layer (identified as **1 SCS - UTZ**) to induce formation of HAp was tested with an *in vitro* test in SBF under dynamic conditions (which simulate the conditions in a living organism better) and its behaviour was compared with (ACP and OCP) layers prepared under static conditions for periods of 6 or 24 hours in SCS2 (identified as **6 SCS** and **24 SCS**). The reference sample was a BIO treated Ti (**0 SCS**). The prepared layers were tested for cytotoxicity. The cytotoxicity *in vitro* tests are conducted on live cells (mice) and they represent the next level of evaluation for the potential application of tested samples.

Materials and Methods

Ti in form of disc 9 mm (or 15 mm diameter x 1 mm height, with BIO surface treatment, made by Lasak Ltd was used. The Ti surface was sandblasted with 250 μm Al_2O_3 particles and treated with HCl and then with NaOH (4M solution) , i.e. the so-called **BIO** treatment. The sample was identified as **0 SCS**.

Precalcified Ti surface with BIO treatment was exposed for 6 hours (sample **6 SCS)** or 24 hours (sample **24 SCS)** to a SCS2 solution at a laboratory temperature. Another sample was prepared by means of exposure to SCS2 solution for one hour in an ultrasonic bath (sample **1 SCS - UTZ).** The S/V ratio was in all cases $0.1 cm^{-1}$, while the sample area was calculated from geometric dimension of the Ti disc. The composition of SCS2 is shown in Table 1

Table 1: Supersaturated Calcifying Solution (SCS2) designed by Li et al. [3]

SCS2	Na^+	Ca^{2+}	Cl^-	$H_2PO_4^-$	HCO_3^-
$mmol.l^{-1}$	4. 0	5. 0	10. 0	2. 5	1. 5

Experimental methods

Simulated body fluid (SBF) was buffered with TRIS (tris (hydroxyethyl) aminomethane), pH 7.4 at 37°C under dynamic conditions (with a continual flow of fresh SBF solution).

Table 2: Ion concentrations of corrected SBF ($mmol.dm^{-3}$) [5].

	Na^+	K^+	Ca^{2+}	Mg^{2+}	Cl^-	HCO_3^-	HPO_4^{2-}	SO_4^{2-}
SBF	142.0	5. 0	2. 5	1. 5	148. 0	4. 2	1. 0	0.5

The testing conditions were as follows:

Temperature: 37 +/- 0.5°C

Duration: 10 days

Flow rate of the solution: 48ml/day

Testing cell volume: 5.5 ml or 15 ml (cm^3)

The parameters related to the samples are as follows: The surface area of Ti (9 mm or 15 mm in diameter) in testing cell was 9 cm^2 (without the BIO treatment effect).

Analytical methods

The concentration of **Ca** was measured at λ = 442 nm by AAS. KCl was added to each sample as a releasing buffer in the concentration of 4000 ppm. Acetylene and N_2O were used as a carrier gas. **$(PO_4)^{3-}$ ions** concentration was measured with spectrophotometry. The analysis was based on the determination of the concentration of phosphate ions at λ = 830 nm.

Weight increases were monitored both after precalcification and after *in vitro* tests in SBF by weighing on analytical scales Mettler Toledo AG 204.

SEM/EDS – the samples were examined with an electro raster microscope Hitachi S 4700 with energy-dispersive spectroscopy. The acceleration voltage of the primary electrons was 15 kV and the working distance was 11.9 mm.

X-ray microdiffraction: Microdiffraction experiments were conducted on PANalytical X´PertPRO equipped with CoKalfa X-ray tube (voltage 40 kV, current 30 mA) and semi-conductor detector X´Celerator. The measurements were performed in the Institute of Inorganic Chemistry of the Czech Academy of Science in Řež u Prahy.

The cytotoxicity test monitored toxic effects of extracts from the solid material on a cell line of mice fibroblasts NIH 3T3 or Balb/c 3T3 in the cell culture under EN ISO 10933 and 7405. The cytotoxicity tests were performed in the Laboratory of Cell Cultures at the Medical Faculty of the Palacký University in Olomouc. The tests were contracted by the company Lasak, s.r.o.

Results and Discussion

BIO treated samples were precalcified for 6 and 24 hours under static test conditions (without stirring or agitation). An amorphous layer of Ca-P (ACP) developed on the surface of the sample **6 SCS**. After 24 hours of precalcification (**24 SCS**) the X-Ray micro diffraction method detected crystals of OCP on the **Ti** surface and, as a minority phase, also DCPD (brushite). The thickness of the layer was 20 μm [6]. The appearance of small tabular OCP crystals arranged into spherulites is well visible in Figure 1 showing an SEM image. Precalcification in an ultrasonic bath for one hour produced a layer of amorphous nature or nanocrystalline particles of amorphous calcium phosphate (ACP) (Figure 2), which has been also confirmed by X-ray microdiffraction.

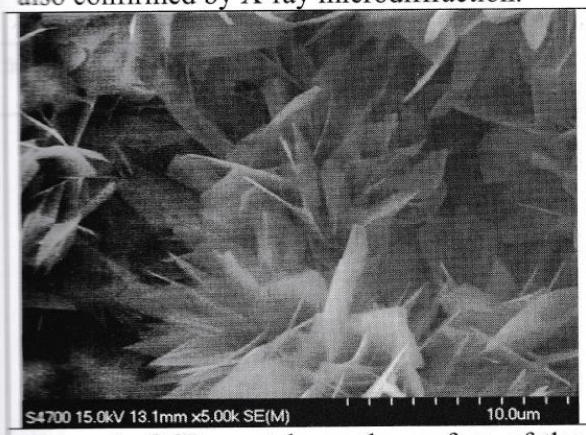

Figure 1: OCP crystals on the surface of the **24 SCS** sample after precalcification, measured by SEM

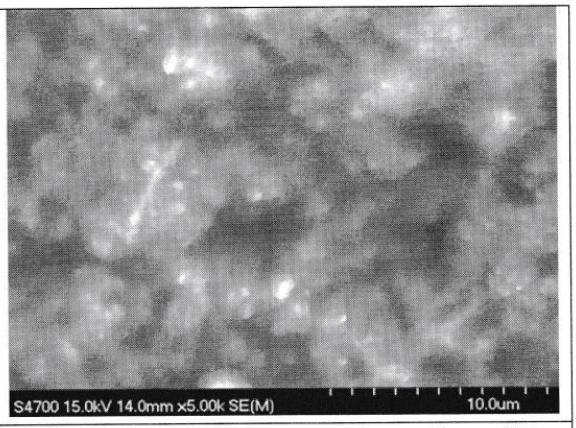

Figure 2.: An ACP layer on the surface of the **1 SCS – UTZ** sample after precalcification (SEM)

Tests of reproducibility of precalcification were performed by weighing of the samples before and after the precalcification process. The weight increases were used to calculate the rate of the precalcification process. The results indicate that the precalcification solution SCS2 gets quickly exhausted and the rate of Ca-P formation on the surface decreases with longer precalcification times (Table 3). The table also indicates the total quantity of the Ca-P phase formed by precalcification under the specified conditions.

Table 3: Quantities of the Ca-P phase formed by precalcification and growth rates of the Ca-P phase on Ti samples

Sample	Increase Ca-P ($mg.cm^{-2}$)	Rate ($mg.cm^{-2}.hour^{-1}$)
1 SCS-UTZ	0.0312	0.0312
6 SCS	0.1633	0.0272
24 SCS	0.2990	0.0125

The prepared layers were tested using *in vitro* cytotoxicity and dynamic tests (continual flow of fresh SBF solution) and a BIO- treated Ti surface was used as a reference sample (identified as **0 SCS**).

The cytotoxicity tests suggested a slight toxicity of the crystalline layer (OCP) developed on the sample **24 SCS**. On the contrary, the amorphous layer created by means of an ultrasonic bath (**1 SCS-UTZ**) was evaluated as non-toxic.

Analyses of Ca and $(PO_4)^{3-}$ in effluents (Figures 3 and 4) have shown that the amorphous layer, spontaneously developed after six hours in SCS2 (**6 SCS**), behaves differently from the amorphous layer developed ultrasonically (**1 SCS-UTZ**). The dissolving rate of the amorphous layer on **6 SCS** at the beginning of its exposure (increase of concentration of Ca and $(PO_4)^{3-}$ above the original levels in SBF) is higher than the rate of HAp formation. On the contrary, the samples **24 SCS** and **1 SCS-UTZ** indicate that both the surfaces induce HAp formation immediately and at the same rates, although the nature of the two layers is totally different (crystalline OCP versus amorphous layer).

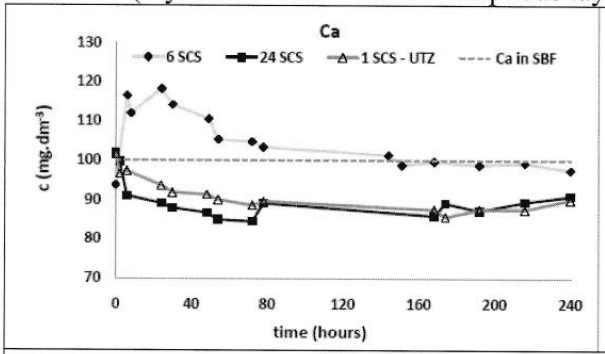

Figure 3: Concentration of Ca in the effluent-dynamic test in SBF

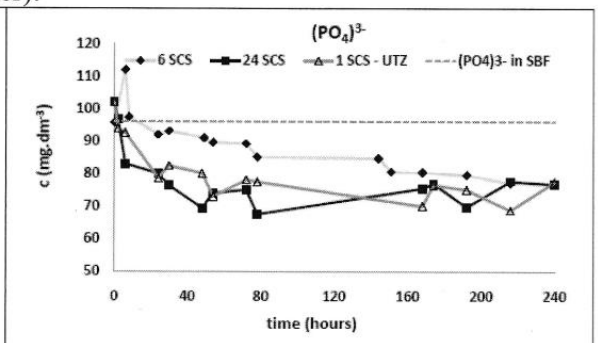

Figure 4: Concentration of $(PO_4)^{3-}$ in the effluent - dynamic test in vitro in SBF

This fact has been confirmed also by the weight increase of HAp found after the dynamic in vitro test and the subsequently calculated rate of Ca-P phase formation per day. The calculated rate of HAp formation on the Ti sample with a BIO-treated surface (**0 SCS**) was 0.0134 $mg.cm^{-2}.day^{-1}$. For samples **6 SCS**, **24 SCS** and **1 SCS-UTZ** the rates of HAp formation were ten times higher (0.1301, 0.1148 and 0.111 $mg.cm^{-2}.day^{-1}$ respectively). A higher increase of HAp on the **6 SCS** sample is probably due to a higher quantity of amorphous Ca-P phase developed after precalcification (see Table 3).

Conclusions

A layer of amorphous calcium phosphate has been created ultrasonically, with the following characteristics:

a/ the layer was incorporated into the TiO_2 gel layer, it did not alter the sample dimensions

b/ the ultrasonically prepared amorphous layer (**1 SCS-UTZ**) was different from the amorphous layer on the sample **6 SCS**

c/ the preparation of bioactive layers on Ti surfaces by precalcification in an ultrasonic bath was simple and reproducible

d/ during *in vitro* tests (in SBF) of **1 SCS-UTZ** the layer demonstrated the same behaviour as the crystalline OCP layer 20 μm thick (**24 SCS**)

References

[1] D. Rohanová, D.M. Yunos et al: Poster on: Ceramics, Cells and Tissues, 12th Seminar, Faenza, Italy, May 2009.

[2] B. Feng, J. Y. Chen: Biomaterials, 23 (2002) p 173-179

[3] F. Li, Q. L. Feng, F.Z. Cui et al: Surface and Coating Technology, 154 (2002) p 88 - 93

[4] D. Rohanová, A. Helebrant et al: Key Engineering Materials, 361 – 363 (2008) p 701- 703

[5] T. Kokubo, H. Takadama: Biomaterials 27 (2006) 2907 - 2915

[6] D.Rohanová, J. Strnad et al: poster on 8th WBC, Amsterdam, the Netherlands, May 2008.

Acknowledgements This work was supported by the grant MSM 604 613 7302

Práce **[4]**

Nežiková A., Kolafová M., Strnad J., Strnad Z., Rohanová D., Helebrant A.: Nitrokostní implantát s bioaktivní povrchovou úpravou, Lasak s.r.o. Praha 9, CZ, VŠCHT Praha. z 11.6.2015. Užitný vzor pod číslem: 28285.

Podíl: 30%: vývoj metodiky, laboratorní práce, vyhodnocení analýz a odladění metody pro provozní účely

ČESKÁ REPUBLIKA
ÚŘAD PRŮMYSLOVÉHO VLASTNICTVÍ

OSVĚDČENÍ

O ZÁPISU UŽITNÉHO VZORU

Josef Kratochvíl
předseda
Úřadu průmyslového vlastnictví

Úřad průmyslového vlastnictví

zapsal podle § 11 odst. 1 zákona č. 478/1992 Sb., v platném znění, do rejstříku

UŽITNÝ VZOR

číslo

28285

na technické řešení uvedené v přiloženém popisu.

ÚŘAD PRŮMYSLOVÉHO VLASTNICTVÍ

V Praze dne 11.6.2015

Za správnost:

Ing. Jan Mrva
vedoucí oddělení rejstříků

Číslo zápisu: **28285** Datum zápisu: 11.06.2015

Číslo přihlášky: **2015-30767** Datum přihlášení: 20.02.2015

MPT:

A 61 C 8/00	(2006.01)
A 61 F 2/02	(2006.01)
A 61 F 2/30	(2006.01)
A 61 F 2/44	(2006.01)

Název: Nitrokostní implantát s bioaktivní povrchovou úpravou

Majitel: LASAK s.r.o., Praha 9 - Hloubětín
Vysoká škola chemicko- technologická v Praze, Praha 6

Původce: Ing. Alžběta Nežiková, Hostivice
Ing. Martina Kolafová, Praha 3
Ing. Jakub Strnad, Ph.D., Říčany
doc. Ing. Zdeněk Strnad, CSc., Praha 6
Ing. Dana Rohanová, Ph.D., Unhošť
prof. Ing. Aleš Helebrant, CSc., Pětihosty

ŽITNÝ VZOR

(11) Číslo dokumentu:

28 285

(13) Druh dokumentu: **U1**

(51) Int. Cl.:

A61C 8/00	(2006.01)
A61F 2/02	(2006.01)
A61F 2/30	(2006.01)
A61F 2/44	(2006.01)

(21) Číslo přihlášky: **2015-30767**
(22) Přihlášeno: **20.02.2015**
(47) Zapsáno: **11.06.2015**

(73) Majitel:
LASAK s.r.o., Praha 9 - Hloubětín, CZ
Vysoká škola chemicko- technologická v Praze, Praha 6, CZ

(72) Původce:
Ing. Alžběta Nežiková, Hostivice, CZ
Ing. Martina Kolafová, Praha 3, CZ
Ing. Jakub Strnad, Ph.D., Říčany, CZ
doc. Ing. Zdeněk Strnad, CSc., Praha 6, CZ
Ing. Dana Rohanová, Ph.D., Unhošť, CZ
prof. Ing. Aleš Helebrant, CSc., Pětihosty, CZ

(74) Zástupce:
Ing. Marie Smrčková, patentový zástupce, Ing. Marie Smrčková, Velflíkova 10, 160 00 Praha 6

(54) Název užitného vzoru:
Nitrokostní implantát s bioaktivní povrchovou úpravou

Nitro kostní implantát s bioaktivní povrchovou úpravou

Oblast techniky

Technické řešení se týká nitrokostního implantátu s bioaktivní povrchovou úpravou substrátu na bázi titanu. Povrchová úprava představuje povrchovou bioaktivní vrstvu s osseokondukčními vlastnostmi.

Dosavadní stav techniky

Pro náhradu kostní tkáně je známa řada materiálů, zejména ze skupiny kovových materiálů, plastických polymerních látek, keramických materiálů a jejich kompozitů. Použitelnost jednotlivých materiálů pro implantace do živého organismu záleží na jejich vlastnostech, zejména na tkáňové biokompatibilitě, enzymatické a hydrolytické stabilitě, chemických, fyzikálních, mechanických a dalších vlastnostech.

Biokompatibilita každého implantátu je určována především vzájemnou interakcí mezi tkání hostitele a implantátem. Organismus se snaží každé cizí těleso izolovat od okolní tkáně, vytváří kolem něj demarkační vazivový obal a snaží se jej z těla vyloučit. Tloušťka stěny pouzdra kolem implantátu indikuje snášenlivost implantátu s tkání. Tenká stěna pouzdra charakterizuje dobrou snášenlivost materiálu, silná signalizuje vysoký stupeň odmítavé reakce. Samozřejmým požadavkem na kompatibilní látky je, že nesmí působit toxicky, vyvolávat tkáňové nekrózy a zánětlivé reakce.

Vývoj materiálů pro kostní náhrady vede jednoznačně od materiálů biotolerantních (např., ocel) přes bioinertní (např., korund, titan) k materiálům bioaktivním (např., kalcium-fosfátová keramika, bioaktivní titan), které doznávají širokého uplatnění v klinické praxi. Tvorba více nebo méně silného vazivového pouzdra, které se vytváří mezi bioinertním povrchem implantátu a tkáni přináší nemalé obtíže při fixaci implantátů v organizmu. Zejména při zatížení takto vhojeného implantátu může docházet ke vzniku nežádoucích lokálních napětí na rozhraní kosti a implantátu, což může vést až k jeho vyloučení. Bioaktivní materiály naproti tomu jsou schopny vytvářet s tkání pevnou vazbu bez intermediální vazivové vrstvy, což přispívá k rovnoměrnému rozložení napětí v kostním lůžku u zatíženého implantátu. Významnou charakteristikou bioaktivních materiálů je jejich schopnost vytvářet na svém povrchu tenké vrstvy obohacené o vápník a fosfor, které jsou výsledkem interakce mezi implantátem a tělní tekutinou. Tato vrstva, z počátku amorfní, se s časem mění na polykrystalickou vrstvu apatitových aglomerátů chemicky a krystalograficky totožných s kostním apatitem. Je předpokládáno, že takto vzniklá apatitová vrstva má klíčovou úlohu při vzniku vazby povrchu implantátu s živou kostní tkání [1].

Pro hodnocení bioaktivity implantačních materiálů se používají testy *in vitro*, kdy se sleduje schopnost materiálu indukovat precipitaci hydroxyapatitu na jeho povrchu při jeho expozici v roztoku modelujícím tělní tekutinu (SBF, Simulated Body Fluid). Test se provádí podle platné mezinárodní normy ISO 23317 [2].

Další často používaná metoda *in vivo* pro stanovení bioaktivity spočívá ve stanovení podílu přímého kontaktu nově vytvořené kostní tkáně k celkovému povrchu implantátu (BIC% Bone Implant Contact) při jeho implantaci na zvířecím modelu v závislosti na době [3].

Bioaktivita může být také vyjádřena jako bioaktivní index $I_b=100/t_{(BIC=50\%)}$ [d^{-1}], kde t je počet dní, kdy přímý kontakt nově vytvořené kostní tkáně dosáhne padesáti procent celkového povrchu implantátu.

Bioaktivita křemičitých skel, případně gelů, v závislosti na složení, může být také odhadnuta na základě zjednodušené strukturní představy polymerního charakteru těchto materiálů ($O°+O''=20'$) [4] a pro první přiblížení pomocí Stevelsových strukturálních parametrů Y a X [5], které vyjadřují střední počet můstkových ($O°$) a nemůstkových (O') kyslíků na jeden polyedr zesítěné struktury. Strukturní parametry $Y(O°)=2Z-2R$ a $X(O')=2R-Z$ jsou určeny z molárního složeni skla, kde Z je střední počet všech kyslíků na polyedr, a R je poměr celkového počtu kyslíků k celkovému počtu síťotvořičů. Z kladné korelace mezi bioaktivitou (I_b) a středním

počtem nemůstkových kyslíků (O´) pro sodnovápenatokřemičitá skla byly určeny hodnoty X(O´) >1,5 a Y(O°)<2,5, kdy skla začínají jevit bioaktivitu, která roste se snižujícím se poměrem $SiO_2/(CaO+Na_2O)$ a rovnováha O°+O´´ - 2O´ je posunuta ve prospěch nemůstkových kyslíků (O´).

Titan, v současné době často používaný biomateriál s vynikajícími mechanickými vlastnostmi, se však na rozdíl od bioaktivních materiálů jeví v interakci s kostní tkání jako bioinertní materiál, který za běžných podmínek nevytváří přímou vazbu s kostí, jako je tomu u bioaktivních materiálů. Při nedokonalé kongruenci mezi kostním lůžkem a titanovým implantátem nebo při nízké primární stabilitě implantátu dochází k vmezeření vazivové tkáně v důsledku nízkých osseokondukčních vlastností, a tím k obtížnějšímu, méně kvalitnímu a déle trvajícímu vhojení implantátu.

Proto je povrch titanových implantátů upravován nanášením *bioaktivních povlaků*, nejčastěji vysokoteplotními postupy jako je nanášení hydroxyapatitu (HA, $Ca_{10}(PO_4)_6(OH)_2$), plazmou. Nevýhody tohoto postupu spočívají v tom, že takto vytvořená vrstva apatitu nevykazuje vždy dostatečnou stabilitu mechanickou či chemickou, je nehomogenní složením i morfologicky a v tělním prostředí se často resorbuje, zejména v kyselém prostředí při zánětu tkáně, případně dochází k delaminaci povrchové vrstvy. Všechny tyto nedostatky zamezují zejména dlouhodobému, pevnému ukotvení implantátu v kosti [6], [7], [8], [9].

Dále jsou známy *nízkoteplotní postupy nanášení bioaktivních vápenatofosforečnanových povlaků* jako jsou například postupy chemické depozice a biomimetické metody, metody sol-gel, nebo metody elektro-depozice. Tyto metody nanášeni bioaktivních vápenato-fosforečnanových povlaků jsou však charakteristické tím, že vytvářejí diskrétní kalcium-fosfátovou vrstvu na povrchu titanového substrátu (aditivní metoda), což přináší obdobné nevýhody, jaké pozorujeme u povrchových vrstev, vytvářených plazmatickým nanášením z hlediska jejich nestability, limitované přilnavosti k titanovému substrátu, nejednotností povlaku a někdy i náročnosti a nákladnosti surovin a zařízení pro průmyslovou výrobu.

Biomimetické metody jsou relativně jednoduché procesy nevyžadující žádné speciální vybavení či vysokoteplotní zpracování. Pro přípravu povlaků lze použít roztok SBF (simulated body fluid), který je součástí normy ISO 23317:2012 [2] pro hodnocení bioaktivity materiálů *in vitro* [10]. Případně je možné využít roztoky, u nichž je koncentrace SBF nebo některých jejích komponent upravena z důvodů urychlení depozice [11], [12]. I přes zvyšování koncentrace iontů v roztoku SBF je depozice povlaků časově náročná. Je to dáno také tím, že roztok SBF obsahuje Mg^{2+} a HCO_3^- ionty, které působí jako inhibitory krystalového růstu [12], [13]. Nedostatečná rychlost tvorby vrstev v prostředí SBF je jednou z vážných nevýhod metody.

V patentu US 6,344,061 [14] byly k vytvoření vrstvy vápenato-fosforečnanové fáze použity kalcifikační roztoky, jako je Hanksův vyvážený solný roztok HBSS (Hanks' balanced salt solution) nebo rychlý kalcifikační roztok FCS (fast calcification solution), příp. FCS s přídavkem bovinního sérového albuminu. V prostředí roztoku HBSS se na povrchu broušených a leštěných titanových slitin během 16-denní expozice vytvořila amorfní vrstva apatitového typu, jejíž morfologie se měnila v závislosti na použitém materiálu i aplikované povrchové úpravě. Pomocí rastrovací elektronové mikroskopie (SEM) byla tloušťka vrstvy stanovena na 5 μm, podle XPS (rentgenové fotoelektronové spektroskopie) 90 nm. Analýza povrchu pomocí elektronové spektroskopie pro chemickou analýzu (ESCA, příp. XPS) odhalila pozvolný přechod definované vápenato-fosforečnanové vrstvy v intermediární vrstvu TiO_2 na povrchu titanové slitiny.

Li et al. [15] použili k prekalcifikaci titanu přesycené kalcifikační roztoky SCS1-3 (Supersaturated calcification solution). Prekalcifikace byla prováděna ve třepačce při teplotě 37°C po dobu 24 hodin. V případě vzorků prekalcifikovaných v roztoku SCS3 se na substrátu během expozice vytvořila uniformní *30-40 μm* silná vrstva hydroxyapatitu. Vrstva vytvořená v SCS1 obsahovala vedle hydroxyapatitu v menší míře i brushit DCPD (dikalcium fosfát dihydrát) $CaHPO_4.2H_2O$. V případě roztoku SCS2 byl povrch pokryt jednotlivými globulemi hydroxyapatitu.

Rohanová et al. [16] exponovala v SCS2 titan, na kterém byla vytvořena gelová vrstva TiO_2 leptáním v HCl a následně v NaOH. V prvních hodinách se Ca^{2+} a PO_4^{3-} ionty inkorporovaly do

gelové vrstvy, po šesti hodinách na povrchu byla patrná amorfní vrstva. Jeden den po expozici byl na povrchu nalezen oktakalcium fosfát (OCP, $Ca_8(HPO_4)_2(PO_4)_4.5H_2O$) ve formě jehlicovitých krystalků orientovaných do růžic a několik velkých krystalů DCPD. Prekalcifikace vedla ke značnému zkrácení doby precipitace hydroxyapatitu v SBF, při následných testech však byla zjištěna lehká *cytotoxicita připravených vrstev*.

Dalším známým způsobem pro nanášení povlaků na titan je metoda sol-gel [17], [18]. Sol je koloidní suspenze, vzniklá smícháním alkoxidů kovů s alkoholem a vodou v přítomnosti kyselého či bazického katalyzátoru. Po odpaření rozpouštědel a kondenzaci hydrolyzovaných molekul vzniká gel, který je následně sušen. Takto získaný povlak je značně porézní, často amorfní se slabou přilnavostí. Musí být proto podroben následné teplotní úpravě, čímž dochází ke zhutnění, krystalizaci a zlepšeni adheze vrstvy, avšak tato tepelná úprava značně zvyšuje riziko vzniku trhlin. Některé vstupní suroviny (alkoxidy kovů) jsou nákladné. Tato metoda je časově poměrně náročná, a velmi citlivá na podmínky nanášení, neboť i malá změna může způsobit odchýlení od očekávaného výsledku.

Vápenato-fosforečnanové povlaky lze také nanášet elektrolytickou depozicí či elektroforézou. V prvním případě se jedná o proces, který představuje nanášení vápenato-fosforečnanových povlaků z roztoku elektrolytu s obsahem Ca^{2+} a $(PO_4)^{3-}$ iontů [19], [20], [21], v druhém případě je povlak nanášen ze suspenze (nejčastěji HA). Zásadním rozdílem, vyplývajícím ze způsobu přípravy, je tloušťka vytvořených povlaků. V případě elektroforézy se může jednat až o stovky mikrometrů [22], a takto silné vrstvy vyžadují následné slinování při vysokých teplotách, které zvyšuje riziko vzniku trhlin.

Je popsána úprava povrchu titanových implantátů [24], která se provádí tak, že opískovaný nebo strojně opracovaný povrch se moří 20 až 150 minut při teplotě 30 až 60 °C v inertní atmosféře kyselinou chlorovodíkovou, s výhodou 35 až 37 % hmotn., nebo sírovou, s výhodou 3 až 4 $mmol.l^{-1}$. Tento povrch se následně leptá 1 až 24 hodin při teplotě 40 až 70 °C ve vodném roztoku hydroxidu alkalického kovu, s výhodou 1 až 10 $mmol.l^{-1}$ hydroxidem sodným. Takto chemicky opracovaný povrch se poté louží pod ultrazvukem v deionizované vodě při teplotě 18 až 40 °C po dobu 2 až 40 minut. Výhodou tohoto řešení je dosažení texturovaného a hydratovaného submikroporézního povrchu titanových implantátů. Nevýhodou řešení může být, že inkorporace iontů Ca a P do nárokované povrchové struktury titanových implantátů probíhá až v tělním prostředí, v němž lze předpokládat, že dochází k adsorpci proteinů, která může zpomalit až utlumit transport a inkorporaci Ca a P iontů do této povrchové struktury, čímž může být zpomalen proces tvorby přímého spojení implantátu s kostí.

Podstata technického řešení

Uvedené nevýhody se odstraní nebo podstatně omezí nitrokostním implantátem podle tohoto technického řešení, jehož podstata spočívá v tom, že nitrokostní implantát je připravitelný po mechanickém opracování povrchu neporézního bioinertního substrátu na bázi titanu mořením v nejméně jedné anorganické kyselině v inertní atmosféře a následným leptáním ve vodném roztoku nejméně jednoho hydroxidu alkalického kovu pro získání hydrofilní, porézní, nanostrukturované, výchozí vrstvy, která je podrobena kalcifikaci pro získání hydrofilní, porézní, nanostrukturované, bioaktivní konečné vrstvy s inkorporovánými vápenatými a fosforečnanovými ionty, případně s jejich krystalickým a/nebo amorfním vápenato-fosforečnanovým depozitem. Tloušťka konečné vrstvy nepřesahuje tloušťku výchozí vrstvy. Výchozí i konečná vrstva vykazují velikost měrného povrchu minimálně 80 mm^2/mm^2 a úhel smáčení menší než 90°, s výhodou 45°.

Hlavní výhodou tohoto technického řešení je získání bioaktivního materiálu s mechanicky a chemicky upraveným bioaktivním povrchem substrátu na bázi titanu s vysokou velikostí měrného povrchu a příznivým úhlem smáčení konečné vrstvy. Nitrokostní implantát je chirurgicky implantovatelný do živé kostní tkáně. Vysoký měrný povrch konečné vrstvy zvyšuje plochu kontaktu mezi nitrokostním implantátem a okolní tkání, což napomáhá zajištění primární stability po implantaci a zvyšuje plochu pro interakci s tělními tekutinami a buňkami. Vysoká smáčivost konečné vrstvy umožňuje dobrý kontakt s tělními tekutinami. Měrný povrch konečné vrstvy

může dosahovat i vyšší hodnoty než nárokované, např. i 200 mm^2 na 1 mm^2, případně se tato hodnota běžně pohybuje kolem 500 až 800 mm^2/mm^2 i výše. Čím vyšší je tato hodnota měrného povrchu konečné vrstvy, tím lze očekávat její vyšší mikroporozitu a tím i příznivější prorůstání tkáně při její aplikaci. Nitro kostní implantát s povrchovou úpravou vykazuje velmi příznivé bioaktivní a osseokondukční vlastnosti, což urychluje vhojení implantátu a zajišťuje vznik stabilního a funkčního rozhraní mezi povrchem implantátu a kostním lůžkem. Získání konečné vrstvy podle tohoto technického řešení je časově i finančně nenáročné a lze ho aplikovat i na složité tvary implantabilních prostředků, zejména v těch indikacích, kde dochází k vysokému mechanickému zatížení nebo aplikovaný klinický postup vyžaduje urychlené vhojení implantátu a jeho časnou fixaci v kostním loži.

Výchozí/ konečnou vrstvu v tomto řešení je myšlena, nikoliv pevná vrstva s jasným a daným rozhraním mezi povrchovou výchozí/konečnou vrstvou a substrátem. Výchozí/ konečnou vrstva v tomto řešení je vrstva, která nemá ostré rozhraní na povrchu se substrátem, ale má pozvolný přechod mezi neporézním a nehydrofilním substrátem na bázi titanu, a mezi převážně hydrofilní, mikroporézní výchozí /konečnou vrstvu nanostrukturovaného charakteru. Výchozí/ konečná vrstva pozvolna přechází do substrátu a je v podstatě součástí jeho povrchu, což vyplývá i z povahy chemického zpracování substrátu. Výchozí/konečná vrstva jsou porézní, přičemž jejich porozita klesá směrem do hloubky, až přechází k neporéznímu kovovému substrátu na bázi titanu. Tloušťka výchozí/konečné vrstvy je řádově přibližně v nanometrech či jednotkách mikronů.

Mechanickým opracováním se získá makrostrukturovaný povrch substrátu na bázi titanu, čímž se získá povrch o vhodném reliéfu a roztečích, jednotlivých nerovností, který je vhodný pro další chemické úpravy ve dvou základních technologických krocích. Prvním krokem chemické úpravy je získání nanostrukturované výchozí vrstvy ve formě titaničitanového gelu na substrátu na bázi titanu. Druhým krokem chemické úpravy je získání porézního hydrofilního a nanostrukturovaného konečného povrchu se zvýšenými bioaktivními vlastnostmi. Prvním krokem chemické úpravy je nejprve moření makrostrukturovaného povrchu substrátu na bázi titanu v nejméně jedné anorganické kyselině a následné leptání v hydroxidu alkalického kovu, čímž dochází ke vzniku výchozí vrstvy titaničitanového gelu, obsahující ionty alkalického kovu dle druhu užitého louhu alkalického kovu. Jedním z principů tohoto technického řešení je, aby většina iontů alkalického kovu, jako jsou v tomto případě s výhodou sodné ionty, byla nahrazena ionty vápenatými. Ve druhém kroku chemické úpravy je získaný výchozí povrch podroben kalcifikaci, při níž je získána konečná vrstva obsahující vápenaté a fosforečnanové ionty, případně s jejich krystalickým a/nebo amorfním vápenato-fosforečnanovým depozitem. Získaný konečný povrch je bioaktivní, což je prokazováno nejčastěji tvorbou uhličitanového apatitu, k jehož tvorbě dochází vlivem hydratovaných gelů TiO_2 na povrchové konečné vrstvě při testech v prostředí simulované tělní tekutiny. Ti-OH skupiny hydratovaných titaničitých gelů u bioaktivního titanu, jsou považovány za nukleační centra pro precipitaci uhličitanového apatitu. Je předpokládáno, že zvýšení bioaktivity je dosahováno inkorporací vápenatých iontů do struktury zesítěných gelů TiO_2 snížením stupně polymerace a růstem koncentrace nemůstkových kyslíků O', které generují nukleační centra pro precipitaci uhličitanového apatitu. Vápenaté a fosforečnanové ionty jsou v nanostrukturované, porézní povrchové konečné vrstvě chemicky vázány. A jelikož nevytváří diskrétní vápenato-fosforečnanovou vrstvu, nedochází k fragmentaci či lokální degradaci, jako je tomu u jiných metod depozice vápenato-fosforečnanových povlaků.

Je výhodné, když zdrojem pro moření mechanicky opracovaného substrátu na bázi titanu kyselinou je kyselina chlorovodíková o koncentraci 35 až 37 % hmotn. nebo kyselina sírová o koncentraci 3 až 4 $mmol.l^{-1}$. Kyselina chlorovodíková nebo sírová jsou běžné kyseliny, snadno dostupné a finančně dostupné a ekologicky neškodlivé, pokud se dodržuje technologický postup. Je možno užít i jiných kyselin, např. kyseliny fluorovodíkové nebo i směsi kyselin.

Dále je výhodné, když zdrojem pro následné leptání je vodný roztok hydroxidu sodného o koncentraci 1 až 10 $mmol.l^{-1}$. Hydroxid sodný je též běžný chemický prostředek. Je možno využít i hydroxidu draselného.

Pro postupnou kalcifikaci výchozí vrstvy je výhodné, když zdrojem vápenatých iontů je roztok chloridu vápenatého o koncentraci 20 až 800 mmol.l^{-1}a zdrojem fosforečnanových iontů zředěná kyselina fosforečná o koncentraci 0,23 až 100 mmol.l^{-1} nebo vodný roztok dihydrogenfosforečnanu sodného o koncentraci 1 až 100 mmol.l^{-1}.

Pro kalcifikaci může být zdrojem vápenatých a fosforečnanových iontů přesycený kalcifikační roztok o iontovém složení: 4 až 5 mmol.l^{-1} Na^+; 4 až 6 mmol.l^{-1} Ca^{2+}; 9 až 11 mmol.l^{-1} Cl^-; 1,5 až 3,5 mmol.l^{-1} H_2PO_4 ; a 0,5 až 2,5 mmol.l^{-1} HCO_3^-. Také tyto použité chemické prostředky pro kalcifikaci jsou dostupné chemické prostředky, zvolené v optimální koncentraci pro daný účel. Substrátem na bázi titanu může být technicky čistý titan nebo jeho slitiny, které obsahují alespoň jeden prvek ze skupiny, zahrnující hliník, vanad, zirkonium, niob, hafnium, cín, železo a tantal.

Konečná vrstva může obsahovat jeden nebo více kationtů ze skupiny zahrnující H^+, Na^+, K^+ , Mg^{2+} a jeden nebo více aniontů ze skupiny zahrnující OH^-, Cl^-,$(CO_3)^{2-}$, $(SO_4)^{2-}$, NO_3^-, které doprovází použité chemické suroviny, a které lze v podstatě považovat za technické ekvivalenty nárokovaných chemikálií.

Pokud se kalcifikace se provádí v ultrazvukové lázni, probíhá intenzivněji. Od přebytečných chemikálií se konečná vrstva se oplachuje v ultrazvukové lázni, v deionizované vodě nebo v etanolu, nebo v deionizované vodě a poté v etanolu, nebo v etanolu a poté v deionizované vodě. Obvykle při teplotě okolí až 65 °C po dobu 2 až 80 minut.

Konečná vrstva se po omytí suší volně nebo při teplotě okolí až 125 °C.

Přehled obrázků na výkresech

Lepší porozumění různým aspektům tohoto technického řešení se získá v následném podrobném popisu některých neomezujících konkrétních příkladů provedení, s odkazem na připojené obrázky 1 až 4.2.

Provedení technického řešení, popsaném v příkladu 1, je blíže patrné z obr. 1 až 1.2, z nichž ukazuje

obr. 1: vývoj koncentrace vápníku a fosforu po jednotlivých technologických operacích;

obr. 1.1: SEM (rastrovací elektronovou mikroskopii) povrchu vzorku exponovaného v roztoku $CaCl_2$ a následně H_3PO_4; a

obr. 1.2: precipitáty hydroxyapatitu, vzniklé po 7-denní expozici v SBF (simulované tělní tekutině - simulated body fluid) na povrchu vzorku, exponovaného v roztoku $CaCl_2$ a následně H_3PO_4.

Provedení technického řešení dle přikladu 2 je osvětleno blíže na obr. 2.1 až 2.9, kde znázorňuje

obr. 2.1: SEM povrch vzorku s výchozí vrstvou;

obr. 2.2: SEM konečné vrstvy vzorku exponovaného v přesyceném kalcifikačním roztoku;

obr. 2.3: EDX analýzu (energiově disperzní spektroskopie) exponované konečné vrstvy vzorku v přesyceném kalcifikačním roztoku;

obr. 2.4: GD-OES hloubkový profil prvků (optická emisní spektroskopie s doutnavým výbojem) vzorku s výchozím povrchem;

obr. 2.5: GD-OES hloubkový profil prvků konečné vrstvy vzorku, exponované v přesyceném kalcifikačním roztoku;

obr. 2.6 ESCA (elektronová spektroskopie pro chemickou analýzu) spektra s výchozí vrstvou na obrázku dole a s konečnou vrstvou vzorku exponovaného v přesyceném kalcifikačním roztoku na obrázku nahoře;

obr. 2.7: SEM konečné vrstvy vzorku exponovaného v přesyceném roztoku po 7 dnech v SBF;

obr. 2.8: vývoj koncentrace Ca^{2+} iontů v roztoku SBF během testu bioaktivity vzorku s výchozí vrstvou a vzorku konečnou vrstvou, exponovaného v přesyceném kalcifikačním roztoku; a

obr. 2.9: vývoj koncentrace PO_4^{3-} iontů v roztoku SBF během testu bioaktivity vzorku s výchozí vrstvou a vzorku s konečnou vrstvou exponovaného v přesyceném kalcifikačním roztoku.

Provedení technického řešení dle příkladu 3 je patrné z

obr. 3: schematicky znázorňujícím příčný svislý řez zkušebních implantátů ve tvaru válečků implantovaných do tibií zkušebních psů plemene bígl;

Provedení technického řešení dle Příkladu 4 odkazuje na obr. 4.1 až 4.2, z nichž ukazuje

obr. 4.1 SEM konečné vrstvy vzorku z titanové slitiny exponovaného v roztoku $CaCl_2$ a následně H_3PO_4 ; a

obr. 4.2: EDX analýzu (energiově disperzní spektroskopie) konečné vrstvy vzorku z titanové slitiny exponovaného v roztoku $CaCl_2$ a následně H_3PO_4.

Příklady provedení technického řešení

Příklad 1

(Obr. 1 až 1.2)

Pro výrobu zubního nitrokostního implantátu byly vyrobeny z technicky čistého titanu (Grade 4) vzorky substrátu ve tvaru disků o průměru 8 mm a tloušťce 0,5 mm. Tyto disky byly mechanicky upraveny zdrsněním povrchu pískováním práškem korundu o střední velikosti zrn 200 až 250 μm při tlaku 600 až 700 kPa, čímž se získá makrostrukturovaný neporézní povrch substrátu o tloušťce řádově v mikrometrech či nanometrech, a se středními roztečemi nerovností řádově v nanometrech či mikrometrech, v desítkách μm. Následná chemická úprava povrchu disků byla provedena mořením v 37% kyselině chlorovodíkové, v inertní atmosféře argonu při teplotě 40 °C po dobu 130 minut. Povrch disků byl potom očištěn od zbytků kyseliny mytím v ultrazvukové lázni v deionizované vodě, následně omyt v ethanolu a poté sušen při teplotě 105 °C. Povrch vzorků byl dále leptán ve vodném 5 $mmol.l^{-1}$ roztoku hydroxidu sodného při teplotě 60 °C po dobu čtyř hodin. Touto mechanickou a následnou chemickou úpravou povrchu u všech vzorků bylo dosaženo nanostrukturované, porézní, hydrofilní výchozí vrstvy vzorku s měrným povrchem 504 mm^2/mm^2 a úhlem smáčení 27,2°.

Vzorky s výchozí vrstvou gelovité struktury byly po vyjmutí z NaOH ihned ponořeny do roztoku 0,45 $mmol.l^{-1}$ chloridu vápenatého při teplotě 60 °C po dobu 4 hodin, a následně myty dvakrát v deionizované vodě po dobu 4 minut v ultrazvukové lázni. Takto získané vzorky byly dále exponovány ve zředěné kyselině fosforečné 0,06 $mmol.l^{-1}$ při pokojové teplotě po dobu 1 minuty. Poté byly myty v ultrazvuku dvakrát v deionizované vodě po dobu 4 minut a poté 2 minuty v ethanolu a následně sušeny při teplotě 105 °C. Úpravou podle tohoto technického řešení byla získána konečná vrstva na substrátu z čistého titanu, u níž byl naměřen měrný povrch 420 mm^2/mm^2 a úhel smáčení 31°.

Výchozí/ konečnou vrstvou se rozumí vrstva bez ostrého rozhraní na povrchu se substrátem, která pozvolna přechází do substrátu a je v podstatě součástí jeho povrchu. Výchozí i konečná vrstva jsou porézní, jejich porozita klesá směrem do hloubky, až přechází k neporéznímu kovovému substrátu na bázi titanu. Tloušťka výchozí/konečné vrstvy je řádově přibližně v nanometrech či mikrometrech.

U výchozí vrstvy i konečné vrstvy substrátu byl měřen jejich měrný povrch a úhel smáčení.

Měrný povrch, vyjádřený v mm^2 a vztažený na 1 mm^2 plochy, byl měřen metodou BET (Braun-Emmett-Teller) na přístroji ASAP 2020 (Micromeritics). Metoda měření BET je založena na fyzikální adsorpci molekul plynu (Kr).

Úhel smáčení (neboli kontaktní úhel) je úhel, který svírá tečna k povrchu kapky (destilované vody), vedená v bodě styku kapky s rozhraním a vyjadřuje smáčivost materiálu. V případě, že je úhel smáčení <90°, lze povrch označit za hydrofilní (smáčivý).

Konečná vrstva pro nitrokostní implantát dle tohoto technického řešení byla analyzována pomocí rastrovací elektronové mikroskopie (SEM, Vega 11 LSU, Tescan) s analyzátorem energiově disperzní spektroskopie (EDX, Bruker). Kvantitativní vyhodnocení EDX analýzy provedené v jednotlivých technologických krocích přípravy konečné vrstvy vzorků podle tohoto technického řešení dokumentuje inkorporaci Ca a P v povrchové nanostrukturované vrstvě a jejich hydrolytickou stabilitu během mytí, jak je znázorněno na obr. 1. Na obr. 1.1 je znázorněna SEM konečné vrstvy vzorku dle tohoto technického řešení. Morfologie této konečné vrstvy a přítomnost vápníku a fosforu, zaznamenaná pomocí EDX analyzátoru indikuje, že Ca^{2+} a $(PO_4)^{3-}$ ionty, případně s jejich krystalickým a/nebo amorfním depozitem, jsou inkorporovány do výchozí nanostrukturované vrstvy, přičemž konečná vrstva nepřesahuje tloušťku nanostrukturované výchozí vrstvy. To znamená, že konečná vrstva představuje nanostrukturovanou výchozí vrstvu titaničitanového hydrogelu, v podstatě bez iontů, nebo s minimem iontů alkalického kovu (Na^+) a obohacenou o vápenaté a fosforečnanové ionty, případně s jejich depozitem. Bioaktivita konečné vrstvy vzorku dle tohoto technického řešení byla testována v roztoku SBF dle ISO 23317. Na obr. 1.2 je pomocí SEM znázorněna konečná vrstva dle vynálezu po 7 dnech expozice roztoku SBF. Během této doby se na povrchu vytvořila celistvá vrstva biologického hydroxyapatitu, indikující žádoucí bioaktivitu konečné vrstvy. Přitom pro srovnání, apatit na vzorku s výchozí vrstvou nebyl po 7 denní expozici v roztoku SBF prokázán.

Příklad 2

(Obr. 2.1 až 2.9)

Pro získání nitrokostního implantátu, vhodného jakožto zubní implantát nebo spinální implantát, byly vyrobeny z technicky čistého titanu (ISO 5832-2) vzorky ve tvaru disků o průměru 16 mm a výšce 1 mm. Vzorky byly mechanicky upraveny pískováním práškem korundu o střední velikosti zrn 180 až 250 μm při tlaku 600 až 650 kPa. Následně byl povrch vzorků chemicky upraven mořením v 35%ní kyselině chlorovodíkové, v inertní atmosféře argonu při teplotě 45 °C po dobu 100 minut. Povrch disků byl potom očištěn od zbytků kyseliny mytím v ultrazvukové lázni v deionizované vodě a poté v ethanolu. Následně byly vzorky sušeny při teplotě 105 °C po dobu 15 minut. Povrch vzorků byl dále leptán ve vodném 4 $mmol.l^{-1}$ roztoku hydroxidu sodného při teplotě 60 °C po dobu 4 hodin, a potom očištěn od zbytků NaOH mytím v deionizované vodě a etanolu v ultrazvukové lázni. Mechanickou a následnou chemickou úpravou povrchu u všech vzorků bylo dosaženo nanostrukturované, porésní, hydrofilní výchozí vrstvy na substrátu z čistého titanu s měrným povrchem 412 mm^2/mm^2 a úhlem smáčení 25°.

Titanové disky s gelovitou výchozí vrstvou titaničitanového hydrogelu byly dále exponovány v roztoku, přesyceném vůči vápenatým a fosforečnanovým iontům, o iontovém složení: 4 $mmol.l^{-1}$ Na^+; 5 $mmol.l^{-1}$ Ca^{2+}; 10 $mmol.l^{-1}$ Cl^-; 2,5 $mmol.l^{-1}$ $H_2PO_4^-$; a 1,5 $mmol.l^{-1}$ HCO_3^- [15] po dobu jedné hodiny v ultrazvukové lázni. Po ukončení expozice v tomto roztoku byly vzorky vyjmuty a omyty absolutním etanolem v ultrazvukové lázni po dobu osmi minut a sušeny při 60 °C. Touto úpravou dle tohoto technického řešení byla získána na titanovém substrátu konečná vrstva pro nitrokostní implantát, u níž byl naměřen měrný povrch 297 mm^2/mm^2 a úhel smáčení 40°.

Tato konečná vrstva vzorku může obsahovat v minimálním množství jakožto doprovodné prvky použitých chemikálií kationty, jako jsou např. H^+, Na^+, K^+ a Mg^{2+} a anionty, jako jsou např. OH^-, Cl^-, $(CO_3)^{2-}$, $(SO_4)^{2-}$, NO_3^-. Tyto doprovodné kationty či anionty v podstatě většinou splňují stejnou nebo obdobnou chemickou funkci a chemickou vazbu v konečné vrstvě jako použité chemikálie

Vzorky s konečnou vrstvou dle tohoto technického řešení byly charakterizovány metodami povrchové analýzy, SEM (Vega 11 LSU, Tescan) s EDX analyzátorem (Bruker), optickou emisní spektroskopií s doutnavým výbojem (GD-OES, GD-Profiler 2, HORIBA Jobin Yvon) a elektro-

novou spektroskopií pro chemickou analýzu (ESCA, ESCA Probe P, Omicron NanoTechnology). Bioaktivita byla testována v roztoku SBF dle ISO 23317 po dobu 7 dnů při teplotě 37 °C. Po testu bioaktivity byla konečná vrstva vzorků pozorována pomocí SEM. Za účelem sledování vývoje koncentrací vápenatých a fosforečnanových iontů byly v průběhu testu prováděny odběry roztoku SBF. Koncentrace vápníku byla stanovována metodou atomové absorpční spektrometrie (AAS, SpectrAA 330, Varian). Koncentrace fosforečnanů byla měřena UV spektrofotometrií (UV-1201, SHIMADZU). Jako reference byly vždy použity disky s výchozí vrstvou. Na konečné vrstvě dle tohoto technického řešení byl rovněž proveden test cytotoxicity formou extraktu. Testování bylo provedeno dle platné normy ČSN EN ISO 10993 (2009) a ČSN EN ISO 7405 (2009).

Na obr. 2.1 je zobrazena SEM analýza výchozí vrstvy. Na obr. 2.2 je znázorněna SEM analýza konečné vrstvy vzorku dle tohoto technického řešení. Ze srovnání je patrné, že expozicí v přesyceném kalcifikačním roztoku nedošlo k morfologickým změnám či k vytvoření silné vrstvy vápenato-fosforečnanové fáze na porésním povrchu. Přestože precipitáty vápenato-fosforečnanové fáze nebyly pozorovány, přítomnost vápníku a fosforu byla zaznamenána pomocí EDX analyzátoru, jak je znázorněno na obr. 2.3.

Ze srovnání hloubkových profilů GD-OES, a to konečné vrstvy vzorku dle tohoto technického řešení, jak je znázorněno na obr. 2.5, a výchozí vrstvy vzorku dle obr. 2.4, je zřejmé, že při expozici v přesyceném kalcifikačním roztoku došlo k výměně Na^+ iontů, vázaných ve výchozí vrstvě ve formě titaničitanu, za Ca^{2+} ionty z kalcifikačního roztoku.

Obr. 2.5 ukazuje metodou GD-OES měřený hloubkový profil prvků konečné vrstvy vzorku, exponovaného v přesyceném kalcifikačním roztoku. Vysoká intenzita signálu vápníku a fosforu v počátku odprašování a jejich plynulý pokles naznačují, že Ca_2^+ a $(PO_4)^{3-}$ ionty byly inkorporovány do nanostruktury titaničitanového hydrogelu výchozí vrstvy. Dokládá to i profil titanu s podobným průběhem jako v případě výchozí vrstvy, jak je znázorněno na obr. 2.4.

Inkorporace iontů do porésní struktury byla podpořena použitím ultrazvukové lázně pro úpravu konečné vrstvy dle tohoto technického řešení. Jako oplachové médium byl zvolen etanol, který nevymývá Ca_2^+ a $(PO_4)^{3-}$ ionty z povrchu, a zabraňuje vzniku krystalických vápenato-fosforečnanových precipitátů a stabilizuje amorfní vápenato-fosforečnanovou fázi [23]. Povrch byl charakterizován metodou ESCA, znázorněným na obr. 2.6. Měřena byla spektra z povrchu konečné vrstvy z hloubky 2 až 5 nm a po pěti minutách odprášení do hloubky 10 nm, z hloubky 12 až 15 nm. Na obou vzorcích byl detekován titan v oxidačním stavu IV+ již na povrchu. Vazebná energie vápníku na vzorku dle tohoto technického řešení odpovídala vápníku v oxidačním stavu II+ vázanému na kyslík. Rovněž byla potvrzena přítomnost fosforečnanových aniontů. Na rozdíl od výchozí vrstvy nebyl na konečné vrstvě vzorku dle vynálezu detekován sodík. Během úpravy dle tohoto technického řešení totiž došlo k výměně sodných iontů za vápenaté, což dokládá i analýza povrchů metodou GD-OES, jak je znázorněno na obr. 2.4.

Kvantitativní analýza jednotlivých prvků v atomových % metodou ESCA, provedená na povrchu a po odprášení povrchu, cca do hloubky 10 nm, z hloubky 12 až 15 nm pro výchozí povrch a pro konečný povrch nanostruktury vzorku, je přehledně znázorněna v následující Tabulce 1.

Tabulka 1 - Kvantitativní analýza prvků metodou ESCA provedená na povrchu a z hloubky 12 až 15 nm

	At. %					
Vzorek	C	O	Ti	Na	Ca	P
Výchozí vrstva z hloubky 2 – 5 nm	32,2	48,1	18,2	0,7	0,8	-
Výchozí vrstva z hloubky 12 - 15 nm	14,6	59,0	25,2	0,6	0,9	-
Konečná vrstva z hloubky 2 - 5 nm	24,5	49,9	4,0	-	12,6	9,0
Konečná vrstva z hloubky12 - 15 nm	5,0	58,9	12,8	-	15,6	7,7

Z kvantitativního vyhodnocení dat z ESCA je patrné, že po odprášení vrstvy asi 10 nm povrchu, z hloubky 12 až 15 nm, se zvýšil obsah titanu a mírně narostlo zastoupení vápníku, zatímco množství fosforu kleslo. Během úpravy dle tohoto technického řešení nejdříve došlo k uvolnění sodných iontů z nanostrukturované negativně nabitých Ti-OH skupin. Následně byly z kalcifikačního roztoku navázány kladné vápenaté ionty a po převládnutí pozitivního náboje na povrchové vrstvě došlo k navázání záporných fosforečnanových iontů. Výsledkem těchto elektrostatických interakcí byl vznik chemické vazby iontové povahy v této povrchové konečné vrstvě.

Bioaktivita konečné vrstvy vzorku dle tohoto technického řešení byla testována v roztoku SBF dle ISO 23317. Na obr. 2.7 je znázorněna SEM konečné vrstvy vzorku dle tohoto technického řešení po 7 dnech v SBF, a během této doby se na povrchu vytvořila celistvá vrstva hydroxyapatitu. Na obr. 2.8 je zobrazen vývoj koncentrací Ca_2^+ a $(PO_4)^{3-}$ iontů v roztoku simulované tělní tekutiny SBF. V roztoku SBF, ve kterém byl exponován vzorek s konečnou vrstvou dle tohoto technického řešení, došlo k poklesu koncentrace iontů spojenému s precipitací hydroxyapatitu. V případě vzorku s výchozí vrstvou koncentrace stanovovaných iontů v roztoku SBF oscilovala okolo výchozích hodnot.

Provedený test cytotoxicity potvrdil, že konečná vrstva vzorku dle tohoto technického řešení nevykazuje cytotoxické chování v celém rozsahu testovaných koncentraci.

Uvedený příklad ilustruje inkorporaci Ca^{2+} a $(PO_4)^{3-}$ iontů do amorfní struktury titaničitanového hydrogelu expozicí v přesyceném kalcifikačním roztoku v ultrazvukové lázni. Ca^{2+} a $(PO_4)^{3-}$ ionty jsou v konečné vrstvě vázány chemickou vazbou s iontovým charakterem, což bylo dokázáno pomocí ESCA a GD-OES. Morfologie titaničitanového hydrogelu zůstala po úpravě dle tohoto technického řešení zachována, a Ca^{2+} a $(PO_4)^{3-}$ ionty jsou vázány uvnitř, a přitom nevytvářejí navíc diskrétní vápenato-fosforečnanovou vrstvu na titaničitanové vrstvě hydrogelu.

Příklad 3

(Obr. 3)

Pro nitrokostní implantát podle tohoto technického řešení, vhodný zejména pro dentální či spinální aplikace, byl vyroben substrát, a to z technicky čistého titanu (ISO 5832-2). Bylo vyrobeno 32 ks zkušebních nitro kostních implantátů ve tvaru válečků o průměru 3,1 mm a výšce 6 mm, se dvěma drážkami po jejich obvodu o hloubce 0,6 mm a šířce 1 mm, jak je znázorněno na obr. 3. Zkušební implantáty byly mechanicky upraveny pískováním práškem korundu o střední velikosti zrn 100 až 250 μm při tlaku 600 až 700 kPa. Následná chemická úprava povrchu zkušebních implantátů byla provedena mořením v 37% kyselině chlorovodíkové, v inertní atmosféře argonu při teplotě 40 °C po dobu 90 minut. Povrch zkušebních implantátů byl potom očištěn od zbytků kyseliny mytím v ultrazvukové lázni napřed v deionizované vodě, poté v ethanolu a následně sušen při teplotě 120 °C. Zkušební implantáty byly dále leptány ve vodném 6 $mmol.l^{-1}$ roztoku hydroxidu sodného při teplotě 65 °C po dobu čtyř hodin, potom v ultrazvuku očištěny od zbytků NaOH mytím v deionizované vodě a následným oplachem v etanolu. Mechanickou a následnou chemickou úpravou všech 32 zkušebních implantátů bylo dosaženo nanostrukturované, porésní, hydrofilní výchozí vrstvy, která vykazovala měrný povrch 137,8 mm^2/mm^2 a úhel smáčení 28°.

16 ks zkušebních implantátů se získanou výchozí vrstvou gelovité struktury bylo dále exponováno v přesyceném kalcifikačním roztoku vápenatých a fosforečnanových iontů, a to o iontovém složení: 4 $mmol.l^{-1}$ Na^+; 5 $mmol.l^{-1}$ Ca^{2+}; 10 $mmol.l^{-1}$ Cl^-; 2,5 $mmol.l^{-1}$; $H_2PO_4^-$; a 1,5 $mmol.l^{-1}$ HCO^{3-} [15] po dobu 1 hodiny v ultrazvukové lázni. Po ukončení expozice v tomto kalcifikačním roztoku byly zkušební implantáty vyjmuty, poté v ultrazvukové lázni omyty absolutním etanolem po dobu 10 minut a vysušeny v sušárně při 65 °C. Touto úpravou bylo dosaženo konečné vrstvy s měrným povrchem 114 mm^2/mm^2 a úhlem smáčení 30°. Zbývajících 16 ks zkušebních implantátů s výchozí vrstvou bylo použito jako referenční vzorky při hodnocení bioaktivity a osseokondukčních vlastností na zvířecím modelu.

16 ks zkušebních implantátů s konečnou vrstvou dle tohoto technického řešení a 16 kusů referenčních zkušebních implantátů s výchozí vrstvou bylo zaimplantováno do tibií psů plemene bígl. Studie na zvířecím modelu byla povolena etickou komisí a Ústřední komisí na ochranu zvířat

proti týrání při Ministerstvu průmyslu a obchodu České republiky. Obr. 3 schematicky znázorňuje příčný svislý řez zkušebních nitrokostních implantátů ve tvaru válečků o průměru 3,1 mm s vyznačením drážek čárkovanou čárou o hloubce 0,6 mm a šířce 1 mm. V drážkách, vyznačených čárkovaně na obr. 3, byl vyhodnocován kontakt nově vytvořené tkáně s povrchem implantátu (BIC% kontakt mezi implantátem a kostí (bone-implant contact) v tibiích zkušebních psů plemene bígl.

Osseokondukční vlastnosti povrchů implantátů byly hodnoceny histomorfometrickým stanovením přímého kontaktu nově vytvořené kosti v drážce implantátů dle obr. 3, po 2 a 8 týdnech od implantace pomocí optické mikroskopie.

Přímý kontakt nově vytvořené kosti na povrchu implantátu (BIC% - bone implant contact) byl vytvořen na třiceti čtyřech procentech povrchu implantátů s konečnou vrstvou (BIC% = 34,4 ± 15,3) a na dvaceti sedmi procentech povrchu implantátů s referenční výchozí vrstvou (BIC% = 27,7 ± 14,7), v obou případech po dvou týdnech od implantace. Po osmi týdnech od implantace přímý kontakt nově vytvořené kosti s povrchem implantátů s konečnou vrstvou a referenčních implantátů s výchozí vrstvou nevykázal statisticky významný rozdíl. Pro implantáty s konečnou vrstvou byl zjištěn BIC% = 51,5 ± 25,8 a pro referenční implantáty s výchozí vrstvou BIC% = 47,8 ± 20. Výsledky dokumentují zvýšenou bioaktivitu a osseokondukční schopnost titanových implantátů s konečnou vrstvou, ve srovnání s referenčními implantáty s výchozí vrstvou, uplatňující se zejména v počátcích vhojování nitrokostního implantátu.

Příklad 4

(Obr. 4.1 až 4.3)

Pro nitrokostní implantát byly vyrobeny vzorky z titanové slitiny Ti6Al4V, a to disky o průměru 15 mm a výšce 1 mm. Tyto vzorky byly mechanicky upraveny pískováním práškem korundu o střední velikosti zrn 250 μm při tlaku 600 kPa. Následně byl povrch vzorků chemicky upraven mořením v 37 % kyselině chlorovodíkové, v inertní atmosféře argonu při teplotě 40 °C po dobu 130 minut. Disky byly potom očištěny od zbytků kyseliny mytím v ultrazvukové lázni v deionizované vodě, poté v ethanolu a následně sušeny při teplotě 105 °C. Disky byly dále leptány ve vodném 5 $mmol.l^{-1}$ roztoku hydroxidu sodného při teplotě 60 °C po dobu čtyř hodin. Touto mechanickou a následnou chemickou úpravou všech disků bylo u nich dosaženo gelovité, hydrofilní, nanostrukturované, porésní výchozí vrstvy s měrným povrchem 439 mm^2/mm^2 a úhlem smáčení 33°.

Vzorky s výchozí vrstvou byly po vyjmutí z NaOH ihned ponořeny do roztoku 0,45 M chloridu vápenatého při 60 °C po dobu 60 minut a poté lehce opláchnuty destilovanou vodou. Následně byly vzorky exponovány v ultrazvukové lázni ve zředěné kyselině fosforečné 0,38 $mmol.l^{-1}$ po dobu 2 minut. Potom byly vzorky myty v ultrazvuku, a to dvakrát v deionizované vodě po dobu 4 minut a následně 2 minut v ethanolu, a po vyjmutí byly vysušeny při teplotě 105 °C. Touto úpravou dle tohoto technického řešení byla získána na substrátu z titanové slitiny konečná vrstva s měrným povrchem 416 mm^2/mm^2 a úhlem smáčení 35°.

Získaná konečná vrstva byla analyzována pomocí rastrovací elektronové mikroskopie (SEM, Vega 11 LSU, Tescan) s EDX analyzátorem (Bruker). Morfologie konečné vrstvy je znázorněná na obr. 4.1. Přítomnost vápníku a fosforu byla zaznamenána pomocí EDX analyzátoru, jak je znázorněno na obr. 4.2, z něhož je zřejmé, že Ca^{2+} a $(PO_4)^{3-}$ ionty jsou inkorporovány do nanostrukturovaného titaničitanového hydrogelu a nedošlo k morfologickým změnám či k vytvoření silné vrstvy vápenato-fosforečnanové fáze.

Tento příklad ilustruje inkorporaci Ca^{2+} a $(PO_4)^{3-}$ iontů do výchozí vrstvy, kdy materiálem použitým pro zhotovení substrátu pro implantabilní prostředek je titanová slitina Ti6Al4V.

Předchozí popis se nutně netýká jen výhodných výsledků, kterých je možno dosáhnout nebo kterých je třeba dosáhnout použitím mechanického a chemického opracování povrchu substrátu pro nitrokostní implantáty podle popisu tohoto technického řešení, ale pouze ilustruje příkladné výhody, které mohou být možné v určitých konkrétních aplikacích.

Uvedené příkladná provedení nitrokostních implantátů, konkrétní popsané mechanické a chemické postupy, konkrétní chemikálie ve zvolených rozmezích, jsou pouze ilustrativní a nejsou omezující pro další možné alternativní příklady nitrokostních implantátů podle tohoto technického řešení, zde neuvedené, které je možno aplikovat v rozsahu patentových nároků tohoto technického řešení.

Průmyslová využitelnost

Nitrokostní implantáty s povrchovou úpravou podle tohoto technického řešení vykazují zvýšené bioaktivní a osseokondukční vlastnosti a jsou určeny pro výrobu dentálních, ortopedických, spinálních a jiných kostních implantátů.

Seznam zkratek a symbolů:

BIC kontakt mezi implantátem a kostí (bone-implant contact)

DCPD dihydrát hydrogenfosforecnanu vápenatého - brushit ($CaHPO_4.2H_2O$)

EDX energiově dispersní spektroskopie

ESCA elektronová spektroskopie pro chemickou analýzu

FCS rychlý kalcifikační roztok (Fast calcification solution)

GD-OES optická emisní spektroskopie s doutnavým výbojem

HA hydroxyapatit ($Ca_{10}(PO_4)_6(OH)_2$)

HBSS kalcifikační roztok (Hank's balanced salt solution - Hanksův vyvážený solný roztok)

Ib index bioaktivity

OCP oktakalcium fosfát ($Ca_8(HPO_4)_2(PO_4)4.5H_2O$)

SBF simulovaná tělní tekutina (Simulated body fluid)

SCS kalcifikační roztok (Supersaturated calcification solution)

SEM rastrovací elektronová mikroskopie

XPS rentgenová fotoelektronová spektroskopie

NÁROKY NA OCHRANU

1. Nitrokostní implantát s bioaktivní povrchovou úpravou substrátu na bázi titanu s bioaktivním nanostrukturovaným povrchem, majícím osseokondukční vlastnosti a obsahující vápenaté fosforečnany, je připravitelný po mechanickém zdrsnění povrchu substrátu do neporézní makrostrukturované vrstvy, poté mořením v nejméně jedné anorganické kyselině v inertní atmosféře a následným leptáním ve vodném roztoku nejméně jednoho alkalického kovu do získání hydrofilní, porézní, nanostrukturované, výchozí vrstvy, která je podrobena kalcifikaci do získání hydrofilní, porézní, nanostrukturované, bioaktivní konečné vrstvy s inkorporovanými vápenatými a fosforečnanovými ionty, případně s jejich krystalickým a/nebo amorfním vápenato-fosforečnanovým depozitem, a po nejméně jednom oplachování následným sušením, přičemž

- tloušťka konečné vrstvy nepřesahuje tloušťku výchozí vrstvy a
- výchozí i konečná vrstva vykazují velikost měrného povrchu minimálně 80 mm^2/mm^2,

úhel smáčení menší než 90°, s výhodou 45°

2. Nitrokostní implantát podle nároku 1, **vyznačující se tím**, že kyselinou pro moření je kyselina chlorovodíková o koncentraci 35 až 37 % hmotn. nebo kyselina sírová o koncentraci 3 až 4 $mmol.l^{-1}$.

3. Nitrokostní implantát podle nároku 1, **vyznačující se tím**, že alkalickým louhem pro leptání je vodný roztok hydroxidu sodného o koncentraci 1 až 10 $mmol.l^{-1}$.

4. Nitrokostní implantát podle nároku 1 až 3, **vyznačující se tím**, že pro postupnou kalcifikaci je zdrojem vápenatých iontů roztok chloridu vápenatého o koncentraci 20 až 800 $mmol.l^{-1}$ a zdrojem fosforečnanových iontů zředěná kyselina fosforečná o koncentraci 0,23 až 100 $mmol.l^{-1}$ nebo vodný roztok dihydrogenfosforečnanu sodného o koncentraci 1 až 100 $mmol.l^{-1}$.

5. Nitrokostní implantát podle nároku 1 až 3, **vyznačující se tím**, že pro kalcifikaci je zdrojem vápenatých a hořečnatých iontů přesycený kalcifikační roztok o iontovém složení:

až 5 $mmol.l^{-1}$ Na^+;

až 6 $mmol.l^{-1}$ Ca^{2+};

až 11 $mmol.l^{-1}$ Cl^-;

1,5 až 3,5 $mmol.l^{-1}$ $H_2PO_4^-$;

0,5 až 2,5 $mmol.l^{-1}$ HCO_3^-.

6. Nitrokostní implantát podle nároku 1, **vyznačující se tím**, že substrátem na bázi titanu je technický čistý titan nebo jeho slitiny, které obsahují alespoň jeden prvek ze skupiny, zahrnující hliník, vanad, zirkonium, niob, hafnium, cín, železo a tantal.

7. Nitrokostní implantát podle některého z nároků 1 až 4, **vyznačující se tím**, že konečná vrstva obsahuje jeden nebo více

kationtů ze skupiny zahrnující H^+, Na^+, K^+, Mg^{2+} a

aniontů ze skupiny zahrnující OH^-, Cl^-,$(CO_3)^{2-}$, $(SO_4)^{2-}$, NO_3^-.

8 výkresů

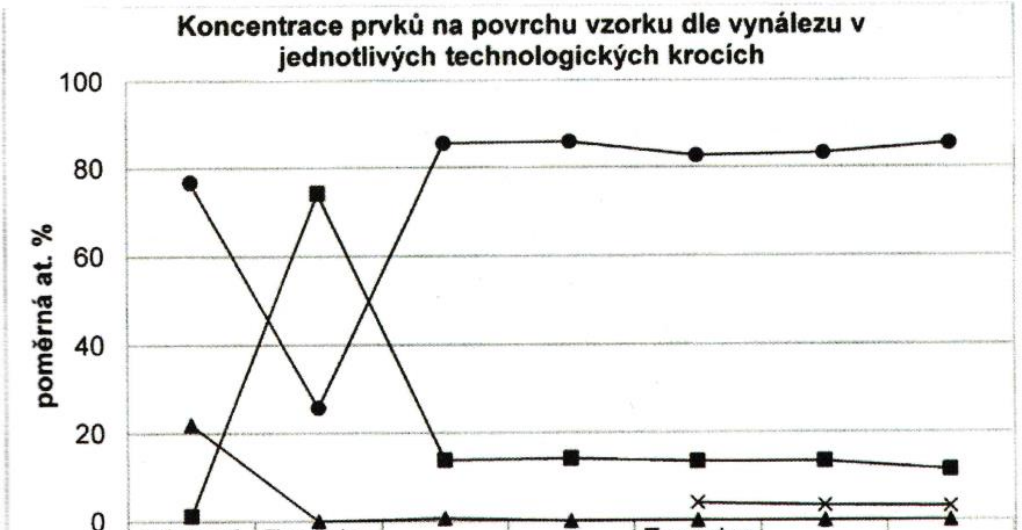

	Výchozí vrstva	Expozice v CaCl2	1. mytí	2.mytí	Expozice v H3PO4	1.mytí	2.mytí
Ca	1,25	74,29	13,78	14,08	13,37	13,41	11,42
P					3,97	3,36	3,10
Ti	76,85	25,71	85,59	85,92	82,66	83,24	85,48
Na	21,90	0,00	0,63	0,00	0,00	0,00	0,00

Obr. 1

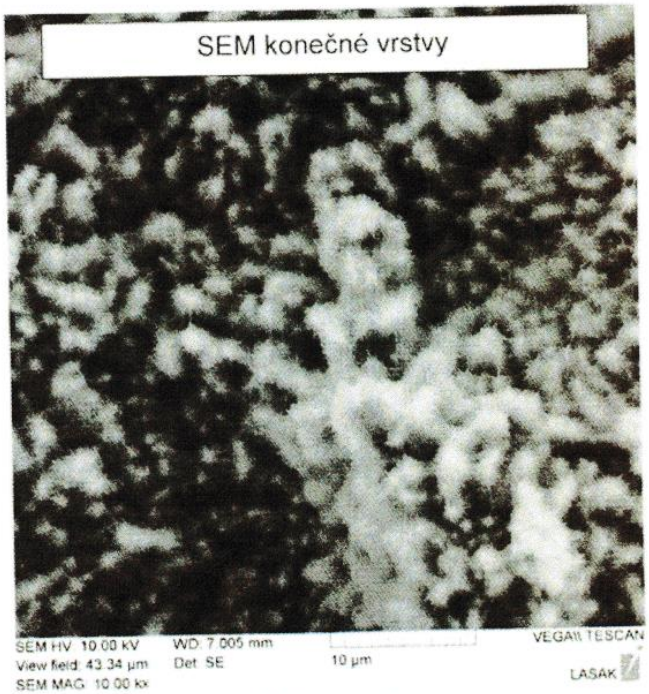
SEM konečné vrstvy
SEM HV: 10.00 kV
View field: 43.34 µm
SEM MAG: 10.00 kx
WD: 7.005 mm
Det: SE
10 µm
VEGA\\ TESCAN
LASAK

Obr. 1.1

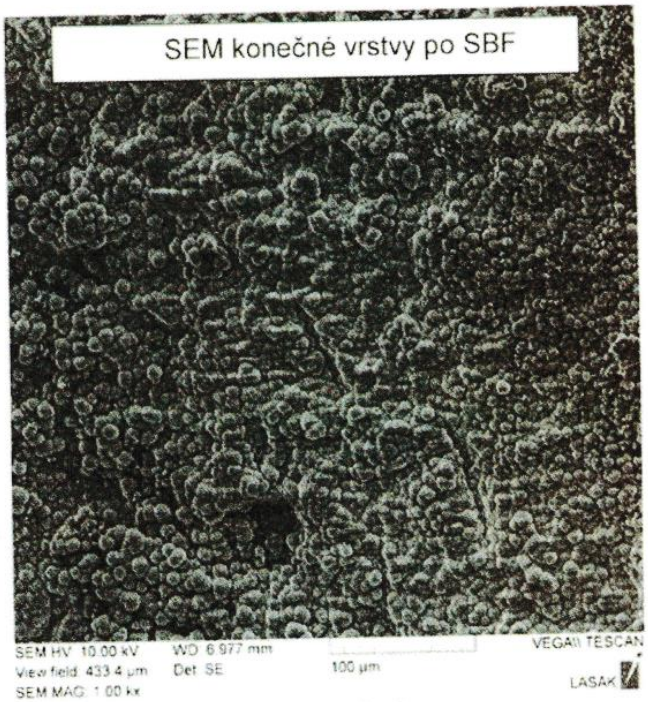
SEM konečné vrstvy po SBF
SEM HV: 10.00 kV
View field: 433.4 µm
SEM MAG: 1.00 kx
WD: 6.977 mm
Det: SE
100 µm
VEGA\\ TESCAN
LASAK

Obr. 1.2

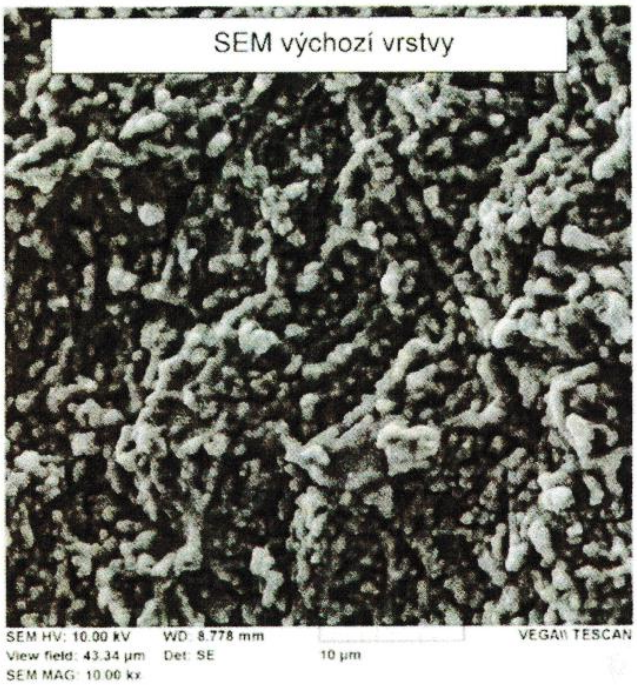
SEM výchozí vrstvy
SEM HV: 10.00 kV
WD: 8.778 mm
VEGA\\ TESCAN
View field: 43.34 µm
Det: SE
10 µm
SEM MAG: 10.00 kx

Obr. 2.1

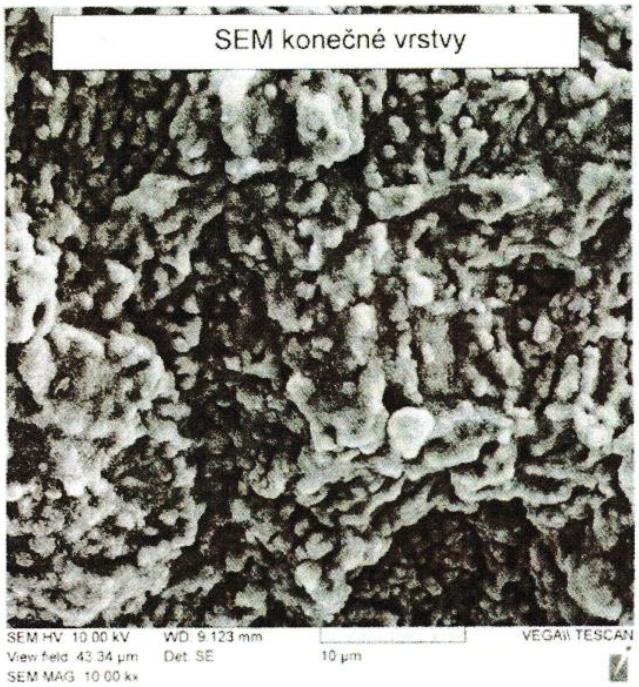
SEM konečné vrstvy
SEM HV: 10.00 kV
WD: 9.123 mm
VEGA\\ TESCAN
View field: 43.34 µm
Det: SE
10 µm
SEM MAG: 10.00 kx

Obr. 2.2

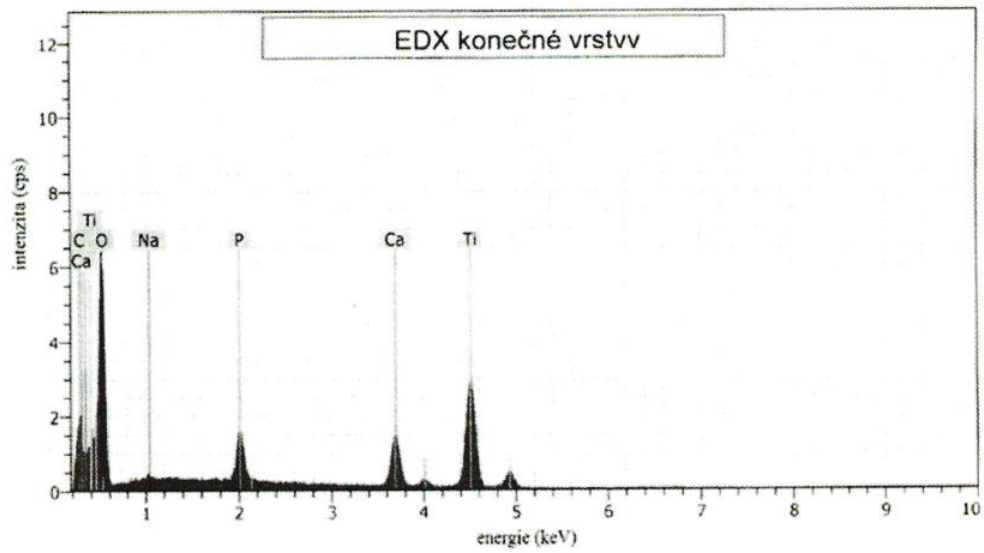
EDX konečné vrstvv
intenzita (cps)
energie (keV)
Ti
C O
Ca
Na
P
Ca
Ti

Obr. 2.3

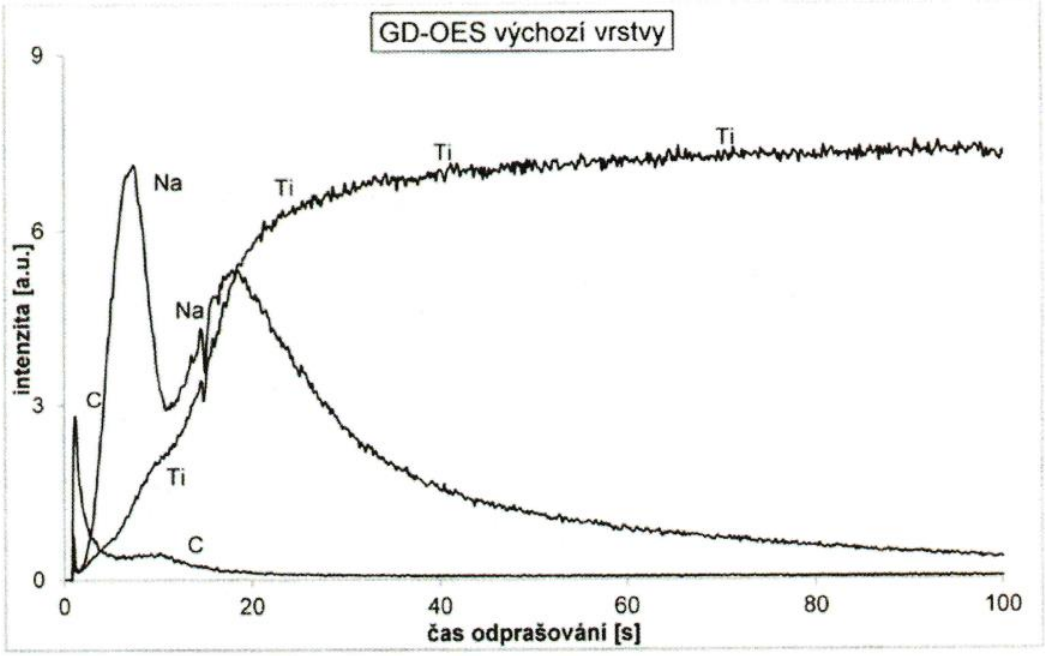
GD-OES výchozí vrstvy
intenzita [a.u.]
čas odprašování [s]
Na
Ti
Ti
Ti
Na
C
Ti
C

Obr. 2.4

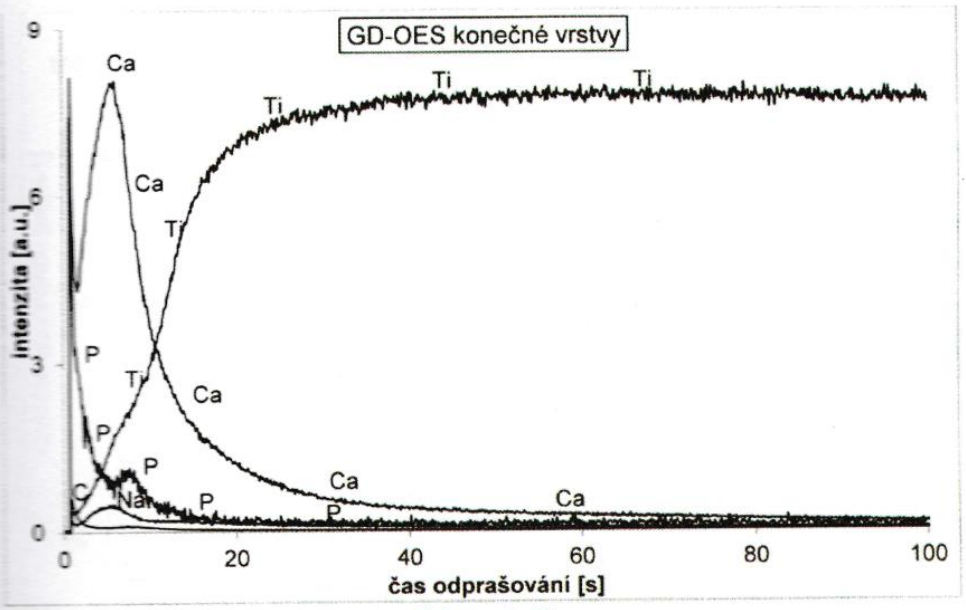
GD-OES konečné vrstvy
intenzita [a.u.]
čas odprašování [s]
Ca
Ti
P
C
Na
0
20
40
60
80
100

Obr. 2.5

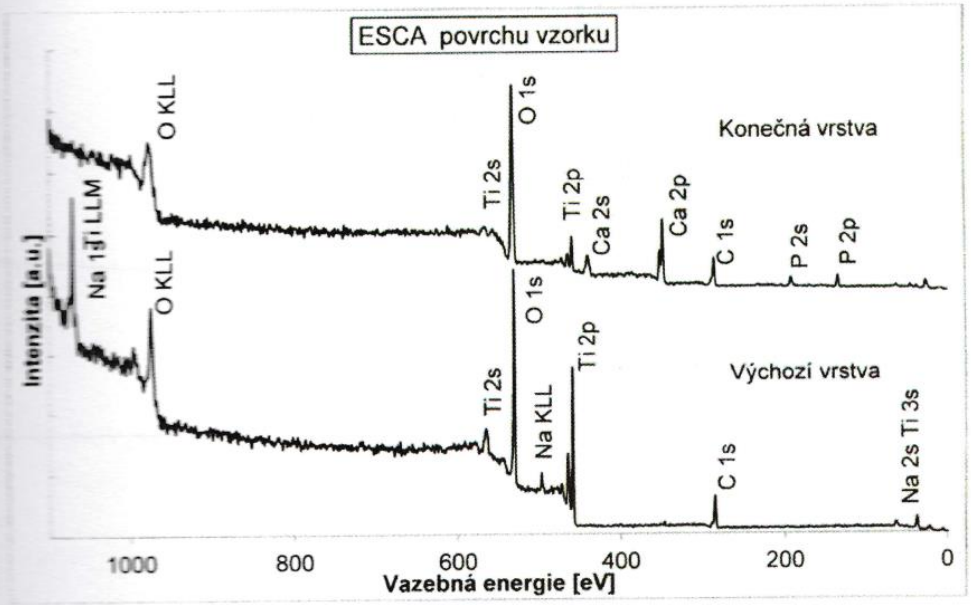
ESCA povrchu vzorku
Konečná vrstva
Výchozí vrstva
intenzita [a.u.]
Vazebná energie [eV]
O KLL
O 1s
Ti 2s
Ti 2p
Ca 2s
Ca 2p
C 1s
P 2s
P 2p
Na 1s
Ti LLM
Na KLL
Na 2s Ti 3s
1000
800
600
400
200
0

Obr. 2.6

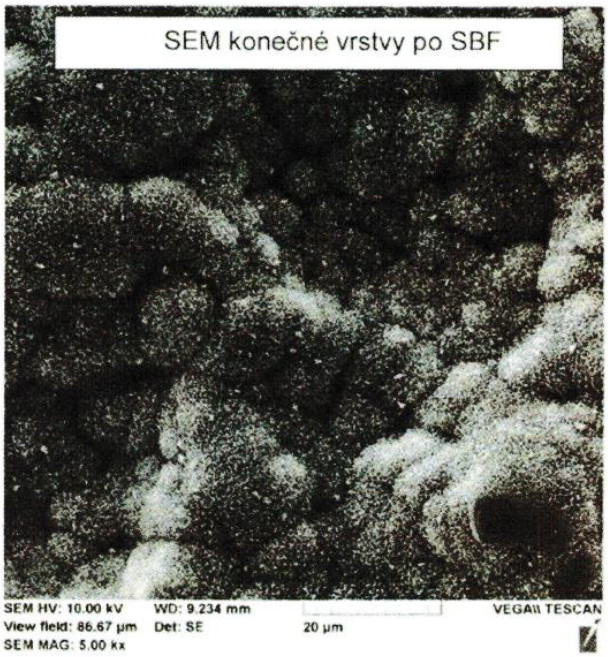
SEM konečné vrstvy po SBF
SEM HV: 10.00 kV
WD: 9.234 mm
VEGA\\ TESCAN
View field: 86.67 µm
Det: SE
20 µm
SEM MAG: 5.00 kx

Obr. 2.7

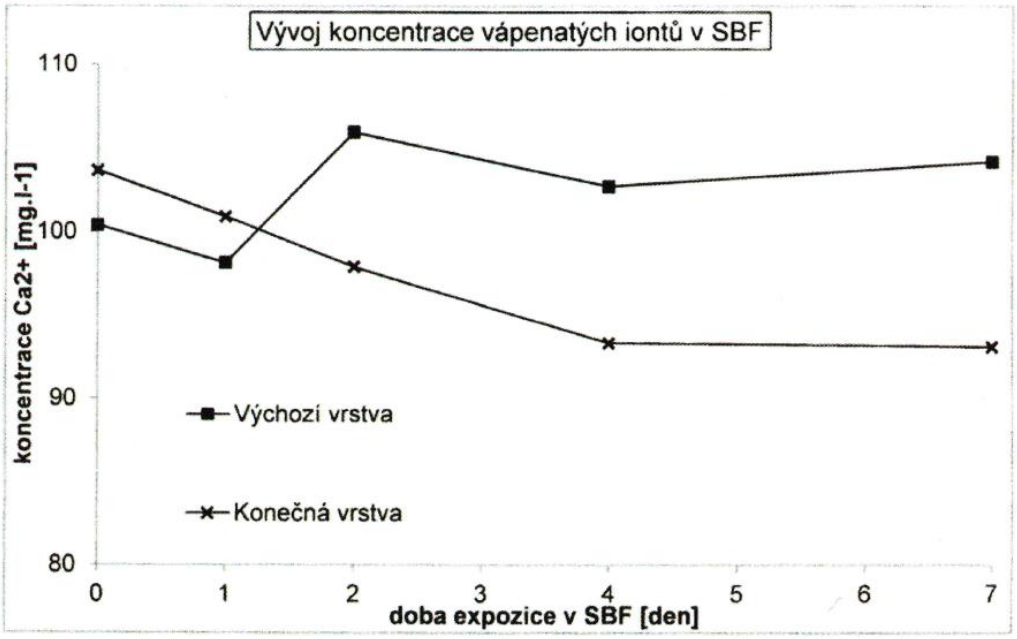
Vývoj koncentrace vápenatých iontů v SBF
koncentrace Ca2+ [mg.l-1]
110
100
90
80
0
1
2
3
4
5
6
7
doba expozice v SBF [den]
Výchozí vrstva
Konečná vrstva

Obr. 2.8

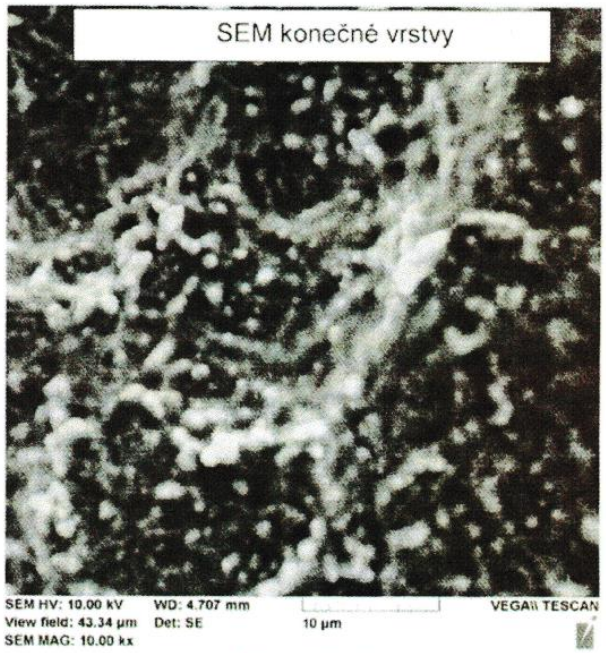

Obr. 4.1

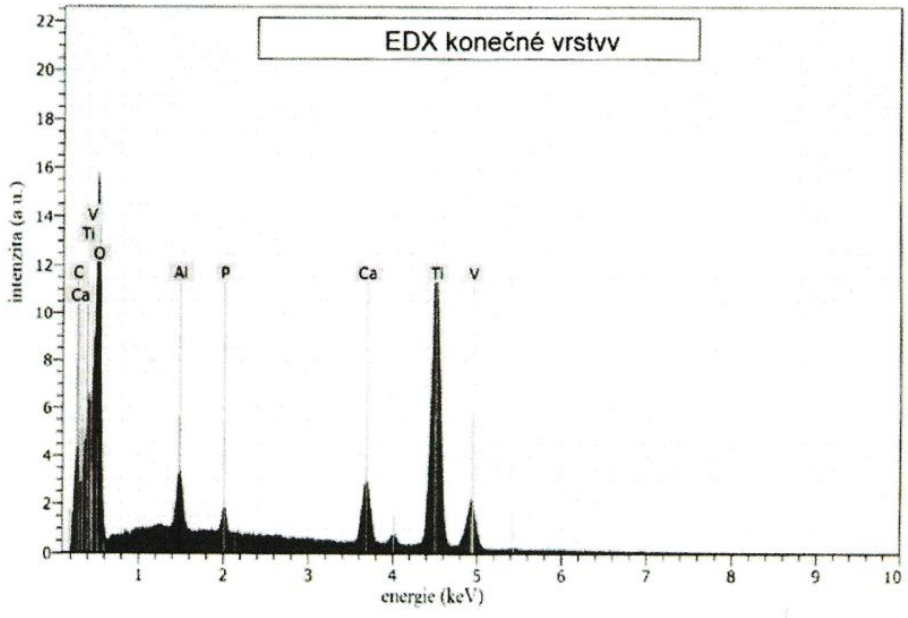

Obr. 4.2

Konec dokumentu

Práce **[5]**

Horkavcová D., Zítková K., Rohanová D., Helebrant A., Cílová Z.: The resorption of β-TCP and HA materials under conditions similar to those in living organisms. Ceramics-Silikáty 54 (4): 398-404, 2010.

Podíl: 30%: zpracování výsledků, příprava publikace

THE RESORPTION OF ß-TCP AND HA MATERIALS UNDER CONDITIONS SIMILAR TO THOSE IN LIVING ORGANISMS

DIANA HORKAVCOVÁ, KLÁRA ZÍTKOVÁ, DANA ROHANOVÁ, ALEŠ HELEBRANT, ZUZANA CÍLOVÁ

Department of Glass and Ceramics, Faculty of Chemical Technology,
Institute of Chemical Technology in Prague, Technická 5, 16628 Prague, Czech Republic

E-mail: diana.horkavcova@vscht.cz

Submitted August 27, 2010; accepted November 26, 2010

Keywords: Resorbable materials, β-Tricalcium Phosphate, Hydroxyapatite, *In vitro* test under dynamic conditions, Simulated body fluid

The submitted work examined kinetics of formation of a newly formed phase of hydroxyapatite (HAp) on two synthetically prepared bone regenerating materials: β-tricalcium phosphate (TCP) and porous hydroxyapatite (HA). In vitro tests with simulated body fluid (SBF) were performed under a continual flow of fresh SBF solution in partly and fully filled testing cells. It has been found out that in the case of testing cells partly filled (¼ of the volume) with TCP and porous HA the contact between the material and SBF was better and thus also the precipitation of the new phase HAp was faster. The BET method identified a ten times increase of the (originally very small) TCP surface in both cases of cell filling, which indicates precipitation of the HAp phase. For porous HA the newly formed phase (HAp) cannot have been identified with SEM/EDS or RTG diffraction as its character was the same as that of the tested material. However, the BET analysis demonstrated a decrease in the size of the specific area of the porous HA after its exposure in the SBF solutions in both test arrangements, which indicates covering of the material surface with a newly formed HAp phase. Precipitation of the new phase was also confirmed by the increased weight of tested porous HA. The tested materials were not completely covered with the new HAp phase after 13 days of testing and their surface thus remained accessible for further resorption.

INTRODUCTION

Hydroxyapatite (HA, $Ca_{10}(PO_4)_6(OH)_2$) is, in terms of its chemical composition, similar to the inorganic part of bone tissue. It has been used for regeneration of bone tissue in dental and maxillofacial surgery for defects resulting from bone resorption, extraction or removal of tumors, in treatment of periodontal defects, filling of bone defects in orthopedics, but also in neurosurgery, e.g. as a material filling the vertebral bodies or for replacement of intervertebral discs. Further, it has been applied in form of coatings on inert materials (Ti and its alloys) for the purposes of implants, where higher compression strength is required from the material (hip joint replacements, dental implants) [1-5]. The resorbable materials induce formation of new bone tissue by their dissolving, which results in supersaturation of the blood plasma in respect to hydroxyapatite that starts precipitating in that particular location [1,4]. The biodegradation is also affected by the size of particles and porosity of the material. The ability of interaction of a synthetically prepared HA therefore also depends on the method of its preparation - its sintering phase. It has been found out that kinetics of the formation of the bone apatite decreases with the growing sintering temperature of the synthetically prepared HA [6].

Apart from HA, other materials based on calcium phosphates have been tested for bone replacements. One of the most important is β-tricalcium phosphate (β-TCP, $Ca_3(PO_4)_2$) [7-9].

The initial tests for any material with anticipated clinical use are *in vitro* tests. *In vitro* tests put the materials in contact either with a simulated body fluid (SBF), simulating the inorganic part of blood plasma, or with other testing solutions (e.g. Ringer´s solution) [2, 6,7,9-11]. The resulting reactions include dissolution, precipitation and ion exchange accompanied by absorption and incorporation of biological molecules [7]. Two models have been proposed to explain dissolution of calcium phosphates: the first model is dissolution, where the phenomenon controlling the process is the transport of mass – diffusion model (the driving force is a concentration gradient in the Nernst diffusion equation), and the second model, in which the phenomenon controlling the process is the surface reaction (the driving force is the gradient of potentials

between the surfaces of apatite crystals and the solution). Kinetics of the dissolution depends on many parameters, particularly on the pH value, temperature, exposure time and saturation of the surrounding solution with calcium and phosphate ions [4,5,12]. In the first model the rate of dissolution is therefore controlled by transport of chemical reagents, while the other model uses the rate of the chemical reaction on the apatite surface as the limiting factor [5].

The knowledge of behavior of hydroxyapatite and β-tricalcium phosphate in contact with simulated body fluid is useful for methods of their application as bone tissue replacements. An important question is e.g. the granulometry and the best way of cavity filling with the resorbable material so that it transforms into the new bone tissue as much as possible. The question is whether the entire volume of the cavity should be filled in or only a part of it. It should be also considered which size of particles is the most suitable to ensure good reaction of the filing material with blood plasma so that the resorbable material is completely transformed into the new HAp phase.

The objective of the work was to monitor kinetics of HAp formation on surfaces of synthetically prepared resorbable materials. Porous hydroxyapatite (HA) and porous β-tricalcium phosphate (TCP) were exposed to SBF solution under dynamic conditions at two levels of filling of testing cells. In the first case one quarter of the cell volume was filled and in the second case the cell was filled in completely.

EXPERIMENTAL

The tested materials were prepared by Lasak spol. s.r.o. The first material - resorbable β-tricalcium phosphate (β-TCP, $Ca_3(PO_4)_2$), called Poresorb®-TCP was supplied in form of white granules (1-2 mm) with the specific weight 2 900-3 100 $kg.m^{-3}$ and it contained macro (100-200 μm) and micro (1-5 μm) pores. In the work it is identified as TCP. The second material was hydroxyapatite (HA, $Ca_{10}(PO_4)_6(OH)_2$), called OSSABASE®-HA and it was supplied in form of white granules (1-2 mm) with submicro pores and macro pores. In the work it is identified as HA. For verification of their bioactivity a model simulated body fluid (SBF) was used, which simulates the inorganic part of human blood plasma with the chemical composition shown in Table 1. The solution was prepared from the following reagents: KCl, NaCl, $NaHCO_3$, $MgSO_4$, $CaCl_2$, K_2HPO_4, the value pH = 7.45 and was buffered with a solution of (Tris-hydroxymethyl aminomethan) and HCl [13].

Table 1. Composition of the simulated body fluid (SBF) [13].

Solution	Ionic concentration (mmol l^{-1})							
	Na^+	K^+	Ca^{2+}	Mg^{2+}	Cl^-	HPO_4^{2-}	HCO_3^-	SO_4^{2-}
SBF	142.0	5.0	2.5	1.0	131	1.0	5.0	1.0

The first group of testing cells had one quarter of their volumes filled, for which 1g of TCP material was sufficient. In this work the cells are identified as ¼V TCP. The second group of testing cells contained 4g TCP each - identified as 1V TCP. Similarly, one group of testing cells had one quarter of their volumes filled with the 0.5g of the HA material and they were identified as ¼V HA and the second group of testing cells was filled completely with 1.83g HA each and identified as 1V HA. The volume of each testing cell was 5.5 ml. Throughout the test duration (13 days) a peristaltic pump was used to ensure continual flow of fresh SBF (50 ml per day). The temperature of SBF was maintained with a thermostat at 36.5 ± 0.5°C. In selected time intervals small portions of leachate were collected and analyzed for concentrations of calcium and $(PO_4)^{3-}$ ions and pH value. Experiments were conducted always in two parallel cells for both types of filling and materials.

Surfaces of the samples before and after the exposure were examined with the electron microscope HITACHI S-4700 with EDS analyzer with the accelerating voltage 15kV. RTG diffraction analysis was measured on the diffractometer PANalytical X´Pert PRO at the accelerating voltage 40kV. The specific surface of the granules before and after the exposure was determined with the BET method on the ASAP 2020 device made by Micromeritic, using Kr and N_2 gases. The concentration of calcium ions in the leachates was analyzed with atomic absorption spectrometry using VARIAN-Spectr AA 300. Atomization of samples was performed by means of acetylene-N_2O flame. The absorbance of Ca was measured at the wavelength of 422.7 nm. The content of phosphates was analyzed on the UV-VIS Spectrophotometer UV1601 at λ = 830 nm, in conformity with ČSN 830540. The pH value was measured with the inoLab pH-meter, with a combined glass electrode at the laboratory temperature.

RESULTS AND DISCUSSION

Material Poresorb®-TCP: porous β-Tricalcium Phosphate (TCP)

Measurements of weights of the material before and after the experiment (Tab. 2) have shown that the weight of TCP material increased for two types of cell filling (both ¼V TCP and 1V TCP).

The increase of weight of the TCP material was higher for partial filling of the cell with the sample (¼V TCP), up to two times (4%), in comparison with the completely filled cells (1V TCP) where the weight increased by 2%. This effect can be explained as follows: The smaller quantity of the material was washed with

SBF more evenly and thus better conditions were ensured for the development of a new (probably HAp) phase on the surface of TCP granules.

Table 2. Average* weights of the TCP material before and after its exposure to SBF.

Partly filled testing cell ¼V TCP			
Weight (g)		Increase	
Before	After	Δ (g)	Δ (%)
1.00	1.04	0.04	4
Completely filled testing cell 1V TCP			
Weight (g)		Increase	
Before	After	Δ (g)	Δ (%)
4.00	4.08	0.08	2

** The average value of weights of the materials for two parallel experiments*

The values of specific surface of the TCP material before and after the exposure were measured with the BET method and they are shown in Table 3.

Table 3. Specific surfaces of the TCP material before and after the exposure v solution SBF.

TCP	Specific surface (m^2g^{-1})
Original	0.15*
¼V TCP	1.79
1V TCP	1.35

** measured in Kr*

The results confirm a substantial increase of the surface of the TCP material after the exposure to the SBF solution for both types of filling. The specific surface in the partially filled cell (¼V TCP) increased in comparison with the original value up to twelve times. In the completely filled testing cell (1V TCP) the specific surface increased by the factor of nine.

The following images from the electron microscope show the surface of the TCP material before (Figure 1) and after (Figures 2, 3) its exposure to the SBF solution.

The images (Figures 2, 3) indicate that the surface of the TCP material was after 13 days of exposure to the SBF solution covered with small crystals of calcium phosphate - probably HAp. In the case of the partial filling of the testing cell (¼V TCP) we suppose a better contact of the material with the SBF solution, which has been confirmed by formation of plate-shaped nano-crystals of HAp. Nano-crystals are arranged into spherulites with the size of 5-10 μm (Figure 2). Spherulites are formed preferentially on convex locations, which are energetically more favorable for crystallization of the new phase. In the second case, when the testing cells were completely filled with the material (1V TCP), we suppose that the contact of the material with the SBF solution was imperfect. An image from SEM (Figure 3) demonstrates that only a small quantity of the new phase has developed and the crystals of calcium phosphate are distributed on the TCP surface very unevenly. The plate-shaped nano-crystals are again grouped into spherulites,

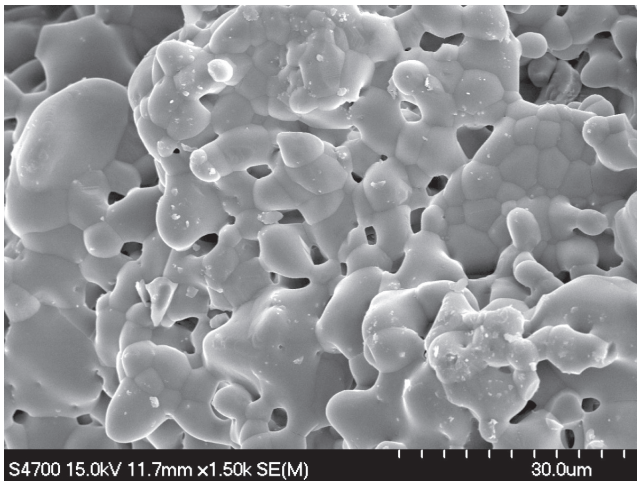

Figure 1. Surface of the original TCP material before the exposure.

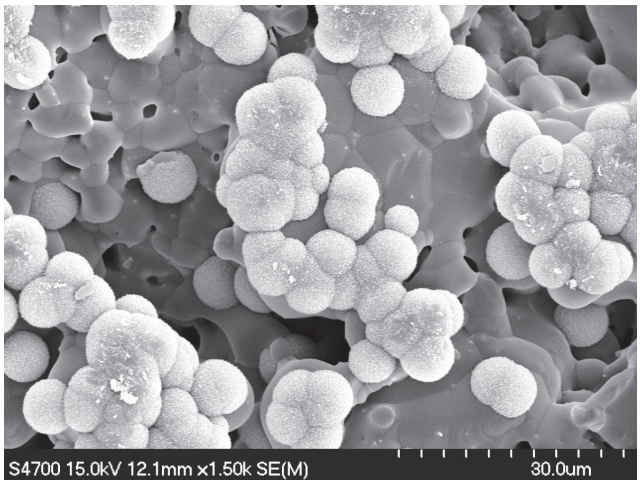

Figure 2. Surface of the material ¼V TCP (partly filled testing cell) after the exposure to SBF with the newly formed HAp phase.

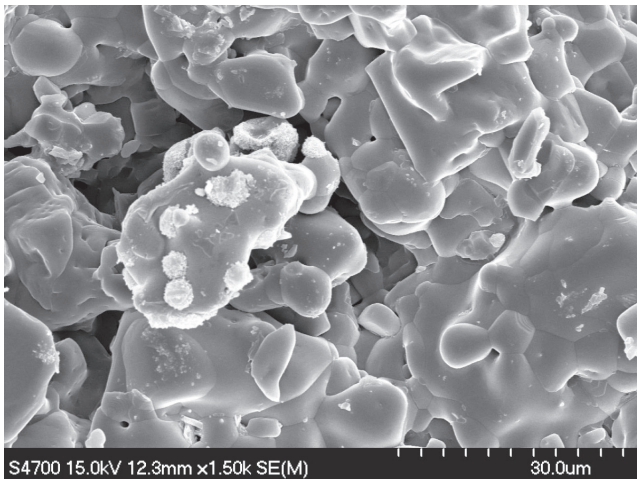

Figure 3. Surface of the 1V TCP material (completely filled testing cell) after the exposure to SBF.

which are much smaller (up to 5μm) than those formed in the case of partially filled testing cells. Also in this case the spherulites formed preferentially on convex locations.

EDS analyses of the surface of the TCP material after its exposure to SBF (¼V TCP and 1V TCP) have shown that the ratio Ca/P is not significantly different from that before the exposure.

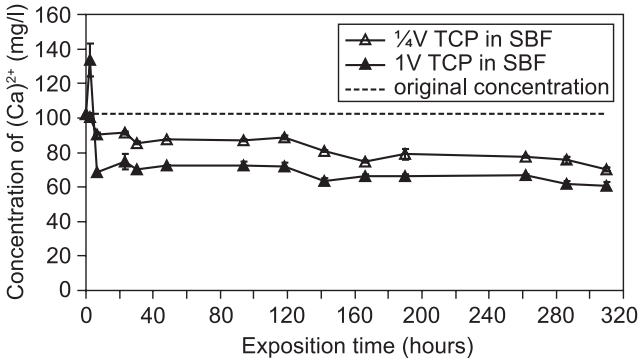

Figure 4. Concentration of calcium ions in the SBF solution for partial (¼V TCP) and complete (1V TCP) filling of the testing cells.

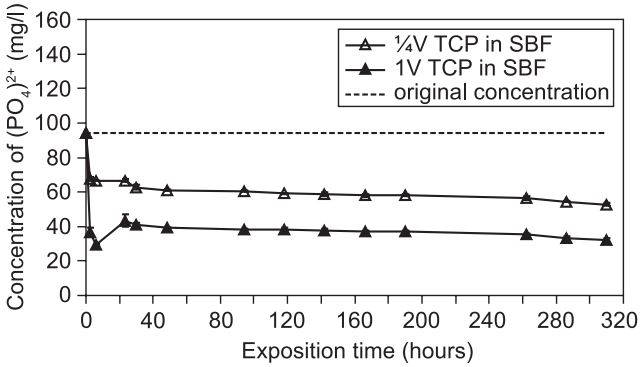

Figure 5. Concentrations of phosphate ions in the SBF solution for partial (¼V TCP) and complete (1V TCP) filling of the testing cells.

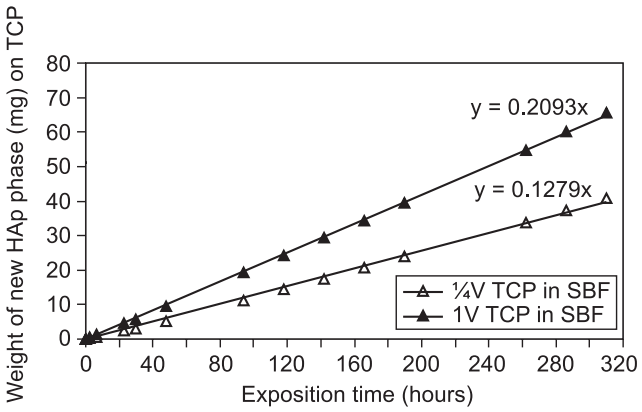

Figure 6. Weight increases of TCP calculated from decreases of concentration of $(PO_4)^{3-}$ ions for partial (¼V TCP) and complete (1V TCP) filling of the testing cells.

RTG difractograms of the TCP material (Ref. Code: 01-070-2065) after its exposure to the SBF solution (¼V TCP and 1V TCP) were not different from those of the original material. This has been probably due to the small quantity of the newly formed phase in comparison with the original material.

Figures 4 and 5 show the time dependence of Ca^{2+} and $(PO_4)^{3-}$ concentrations in SBF in the course of the material exposure for both types of filling (¼V TCP and 1V TCP). Figure 6 shows weight increases of TCP (i.e. the weight of the new HAp phase) in the course of the exposure, calculated from decreases of concentration of $(PO_4)^{3-}$ ions in the leachates.

Table 4 contains precipitation rates of the HAp phase on the TCP surface which were calculated from the actual weight increases and decreases of $(PO_4)^{3-}$ ions from the beginning of the exposure (equations (1)-(3)). A substantial decrease of the $(PO_4)^{3-}$ ions in the leachate from the beginning of the exposure (up to 2 hours) actually indicates immediate precipitation of the new HAp phase.

From the weight of the new phase:

$$R_{\mathrm{HAp}} = (m_{\mathrm{TCP(final)}} - m_{\mathrm{TCP(initial)}}) / t \qquad (1)$$

From the decrease of concentration of $(PO_4)^{3-}$ ions:

$$c_{(PO4)}{}^{3-} = k_{\mathrm{HAp}}\ t \qquad (2)$$

Relative rate of the precipitation:

$$R'_{\mathrm{HAp}} = R_{\mathrm{HAp}} / m_{\mathrm{TCP(initial)}} \qquad (3)$$

where R_{HAp} is the rate of formation of the new HAp phase, calculated from the increased weight; $m_{\mathrm{TCP(final, initial)}}$ are weights of TCP after and before the exposure, respectively; $c_{(PO4)}{}^{3-}$ is the concentration of phosphate ions in SBF leachates; k_{HAp} is a constant determined from the line slope (Fig. 6); R'_{HAp} is the rate of precipitation of the new HAp phase related to a unit of weight; t is the time of exposure.

Table 4. Rate of precipitation of the HAp phase on the surface for ¼V TCP and 1V TCP in SBF.

Filling of the cell with the TCP material	R_{HAp} (mg hour^{-1})	k_{HAp} (mg hour^{-1})	R'_{HAp} (mg hour^{-1}g^{-1})
¼V TCP - 1 g	0.129	0.128	0.129
1V TCP - 4 g	0.258	0.209	0.065

Analyses of SBF solutions (Figures 4 and 5) have suggested that the TCP material dissolves significantly from the very beginning of the test: the concentration of Ca^{2+} ions in the solution increases within 2 hours while the concentration of $(PO_4)^{3-}$ ions decreases. Those contrary trends suggest that after its exposure TCP dissolves immediately and this causes a substantial supersaturation of the SBF solution in respect to HAp and, at the same time, the new HAp phase precipitates from the SBF solution. Within a short period of time (within 24 hours

for both types of cell filling) a stable removal of Ca^{2+} and $(PO_4)^{3-}$ ions from the SBF solution occurred, i.e. a stable precipitation of HAp. The diagram indicates that in the partly filled cell (¼V TCP) the removal of Ca^{2+} and $(PO_4)^{3-}$ ions is less intense than in the completely filled cell (1V TCP). This phenomenon corresponds well with the overall quantity of the tested material inside the cell. The weight of the sample in a partly filled cell is one quarter of that in a completely filled cell (Tab. 2) and therefore the increase of a newly forming HAp phase is higher in the case of the partly filled cell (¼V TCP) than in the completely filled cell (1V TCP) (Tab. 4). The values of pH of the SBF solution for both types of filling did not differ significantly.

The diagram showing dependence of weight increases of the TCP material (Fig. 6) indicate that the weight increase during the 13 days of exposure to SBF is linear. The rate of formation of the new HAp phase is calculated from the beginning of the exposure. The relative rate of HAp precipitation in the partly filled cell (¼V TCP) is twice higher when compared to the completely filled cell (1V TCP). The results indicate the new apatite layer on the TCP material is formed more readily in the cell which was only partly filled with the material. However, a question remains whether the fast formation of HAp on the TCP surface is a desirable process from the viewpoint of its resorbability. If the surface is covered too fast the further resorption of the material may significantly slow down or stop completely.

Material OSSABASE®-HA: porous hydroxyapatite (HA)

The dynamic conditions, under which an interaction between porous hydroxyapatite and SBF was monitored, were the same as with the previous material. The weight of materials was determined before and after the experiment for two parallel measurements and it was found out that also in case of porous hydroxyapatite (HA) its weight after the experiments increased (Tab. 5). Similarly as with TCP**,** we observed a twice higher increase of the new phase in respect to the initial weight for the partially filled cell (¼V HA).

Table 5. Weight of HA before and after the exposure to SBF*.

Partly filled testing cell ¼V HA			
Weight (g)		Increase	
Before	After	Δ (g)	Δ (%)
0.5	0.6	0.1	20
Completely filled testing cell 1V HA			
Weight (g)		Increase	
Before	After	Δ (g)	Δ (%)
1.83	2.0	0.17	9.2

** The average value of weights of the materials for two parallel experiments*

Equally as with the previous material (TCP), this significant difference can be explained for the porous hydroxyapatite (HA) by a better contact of the SBF solution with the smaller quantity of the material.

The values of the specific surface of the porous hydroxyapatite before and after the exposure in the SBF solution were measured with the BET method and they are shown in Table 6.

Table 6. Specific surfaces of the porous HA before and after the exposure in the SBF solution.

HA	Specific surface ($m^2\ g^{-1}$)
Original	70.79
¼V TCP	61.34
1V TCP	67.05

The results indicate a decrease in the values of the specific surface after the exposure to the SBF solution for both test arrangements. A higher decrease (up to 13.4 %) was found for the material in a partly filled cell (¼V HA), which suggests formation of a bigger quantity of the new nano-crystalline HAp phase.

The following images from the electron microscope show the HA surface before (Figure 7) and after (Figures 8, 9) its exposure to the SBF solution.

The comparison of images from SEM have shown that the surface of the porous hydroxyapatite partly changed after its exposure. Figure 8 shows a strongly broken relief of the hydroxyapatite in the case of the partly filled cell (¼V HA). Rod-shaped crystals were found on the surface which formed bigger agglomerates (up to 4 μm). In the completely filled cell (1V HA) the quantity of agglomerates was lower (Figure 9).

The results from the EDS analysis did not show a significant difference in the composition of the hydroxyapatite surface before and after the exposure to the SBF solution.

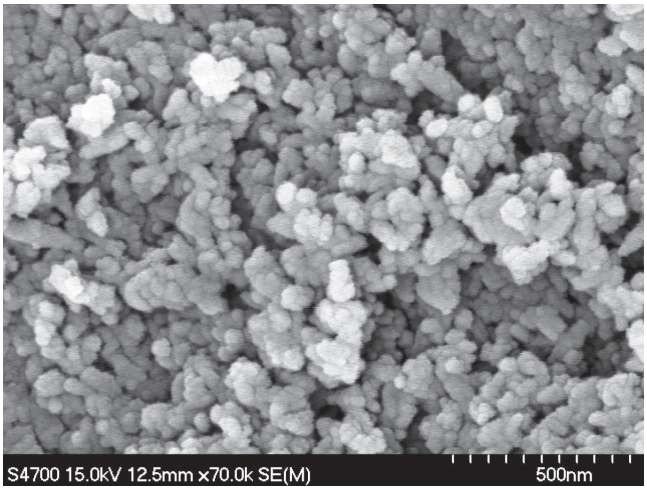

Figure 7. Surface of the original hydroxyapatite (HA) material before the exposure.

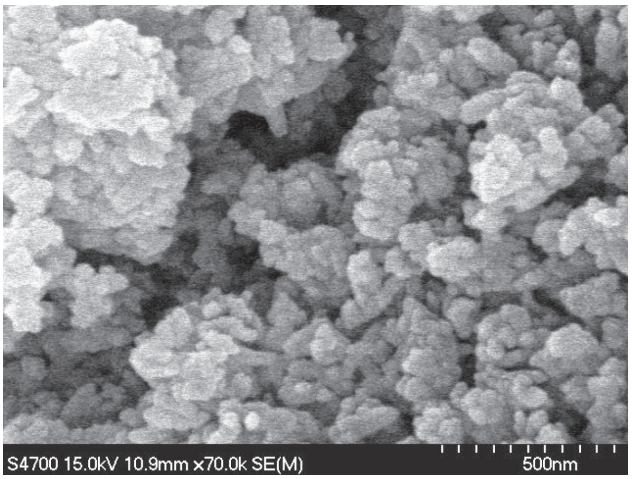

Figure 8. Surface of the ¼V HA material (from the partly filled testing cell) following the exposure to SBF.

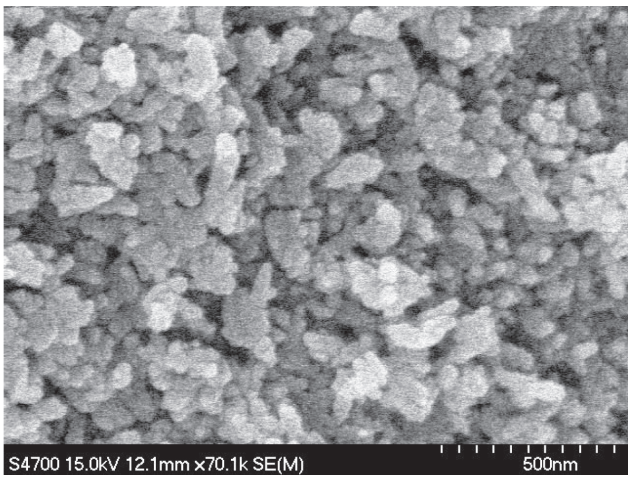

Figure 9. Surface of the material 1V HA (completely filled testing cell) after the exposure to SBF.

Again, the diffractogram ¼V HA was not different from the original hydroxyapatite (Ref. Code: 01-089-6439), which is logical considering the composition of the expected new phase - the hydroxyapatite. In the completely filled cell 1V HA a small difference was found in the stoichiometry of the newly formed HAp (Ref. Code: 01-089-6438) in comparison with the tested porous HA, which suggests formation of a defective HAp.

Figures 10 and 11 show of Ca^{2+} and $(PO_4)^{3-}$ concentrations in SBF during the exposure.

Figure 12 shows the linear dependence of the growth of weight of the tested porous hydroxyapatite in both test arrangements (¼V HA and 1V HA), calculated from the decrease of $(PO_4)^{3-}$ ions. Table 7 contains precipitation rates of the new phase (HAp) on the porous HA surface, as calculated from the slope of the lines for ¼V HA and 1V HA.

Figure 10 indicates that concentrations of calcium ions in SBF are similar at the beginning of the exposure for individual types of test arrangements, as it was in the case of TCP. For the partly filled cell (¼V HA) the concentration of Ca^{2+} decreased immediately from the very beginning which indicates that the precipitation of the new HAp phase from the SBF solution is faster in comparison with the dissolution of the porous phase HA. In the case of the completely filled cell (1V HA) the concentration of calcium ions increased at the beginning (within 24 hours) which suggests a massive dissolution of the HA material.

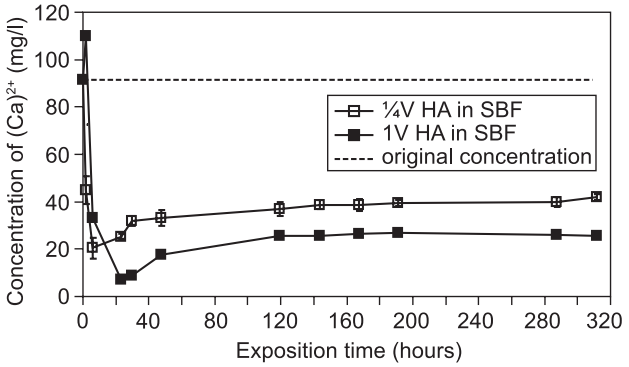

Figure 10. Concentrations of calcium ions in the SBF solution in the partially (¼V HA) and completely (1V HA) filled testing cells.

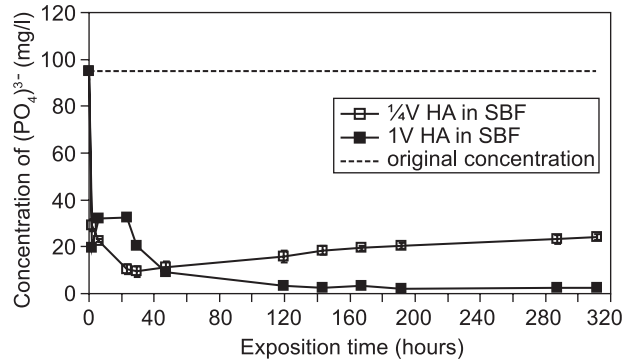

Figure 11. Concentrations of phosphate ions in the SBF solution in the partially (¼V HA) and completely (1V HA) filled testing cells.

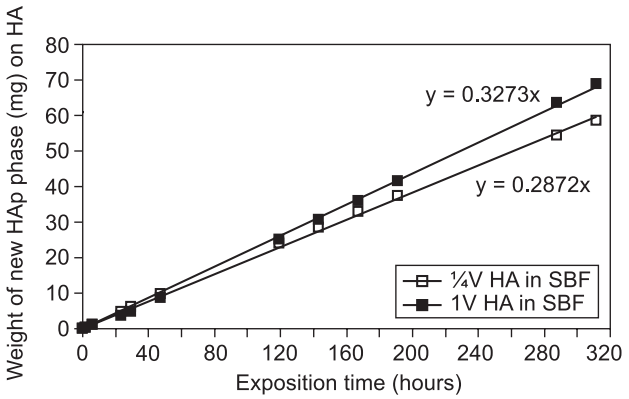

Figure 12. Weight increases of HA (i.e. new HAp phase) for partial (¼V HA) and complete (1V HA) filling of the testing cell.

In the case of $(PO_4)^{3-}$ ions (Figure 11) their concentrations at the beginning of the exposure decreased for both test arrangements. The decrease was more significant in the fully filled cell (1V HA) where the concentration of $(PO_4)^{3-}$ ions decreased substantially (from 95 mg l^{-1} to 19 mg l^{-1}). Subsequently, the removal of ions stabilized and practically all $(PO_4)^{3-}$ ions contained in SBF were continually removed. After approximately 60 hours the rates of ion removal and the precipitation of the new phase became stable in both test arrangements.

Relative precipitation rates (mg.hour^{-1}.g^{-1}) shown in Table 7 indicate a high reactivity of the HA surface with the simulated body fluid. A higher quantity of the precipitated HAp phase in [mg.hod^{-1}] in the case of the HA material has been achieved thanks to the enormously large specific surface of HA in comparison with TCP. The surface of HA per one gram is up to 470 times larger than that of TCP.

Table 4. Precipitation rates of the HAp phase on the surface for ¼V HA and 1V HA in SBF.

Filling of the cell with the HA material	R_{HAp} (mg hour^{-1})	k_{HAp} (mg hour^{-1})	R'_{HAp} (mg hour^{-1})
¼V HA - 0.5 g	0.320	0.287	0.640
1V HA - 1.83 g	0.545	0.328	0.174

** The symbols are explained in the section on TCP (Table 4)*

CONCLUSION

1. For both the HA and TCP materials it was found out that the precipitation of the new HAp phase is more intense in case of partial filling of the cell with the material (¼V**).**
2. The precipitation rate of new HAp phase allows to do a conclusion that the precipitation proceeds continually for both types of materials.
3. Analyses of Ca^{2+} and $(PO_4)^{3-}$ ions in SBF leachates for both materials clearly show that the processes of dissolution and precipitation of the new phase became stable after 24 hours of the exposure for TCP and after 60 hours of exposure for HA.
4. The tests have shown that the materials were not completely covered with the new (nearly insoluble) HAp phase after 13 days of the experiments and therefore the resorption process may continue.
5. Further experiments will seek to identify conditions for the maximum resorption of the materials, by extending the experiment duration or by changing the set-up conditions of the dynamic test.

Acknowledgement

This work has been supported by the Ministry of Schools, Youth and Physical Education within the research plan MSM 6046137302. We would like to thank to our colleague, Ing. Miloslav Lhotka, PhD, who measured surfaces of the materials with the BET method.

References

1. Best S.M., Porter A.E., Thian E.S., Huang J.: J. Eur. Ceram. Soc. *28*, 1319 (2008).
2. Queiroz A.C., Santos J.D., Monteiro F.J., Prado da Silva M.H.: Mater. Character. *50*, 197 (2003).
3. Zítková K.: Bachelor thesis, VSCHT, (2009).
4. Kwon S-H., Jun Y-K., Hong S-H., Kim H-E.: J. Eur. Ceram. Soc. *23*, 1039 (2003).
5. Dorozhkin S.V.: Prog. Cryst. Grow. Character. Mater. *45*, 45 (2002).
6. Kim H-M., Himeno T., Kokubo T., Nakamura T.: Biomaterials *26*, 4366 (2005).
7. Ducheyne P., Qiu Q.: Biomaterials *20*, 2287 (1999).
8. Porter A.E., Patel N., Skepper J.N., Best S.M., Bonfield W.: Biomaterials *24*, 4609 (2003).
9. Kohri M., Miki K., Waite D.E., Nakajima H., Okabe T.: Biomaterials *14*, 299 (1993).
10. Kokubo T., Takadama H.: Biomaterials *27*, 2907 (2006).
11. Leng Y., Chen J., Qu S.: Biomaterials *24*, 2125 (2003).
12. Bohner M., Lemaître J., Ring T.A.: J. Coll. Inter. Sci. *190*, 37 (1997).
13. Helebrant A., Jonášová L., Šanda L.: Ceramics - Silikáty *46*, 9 (2002).

Práce **[6]**

Horkavcová D., Rohanová D., Kuncová L., Zítková K., Zlámalová Cílová Z, Helebrant A.: Comparison of reactivity of synthetic and bovine hydroxyapatite *in vitro* under dynamic Conditions. Ceramics-Silikáty 58 (1): 70-78, 2014.

Podíl: 30%: zpracování výsledků, příprava publikace

COMPARISON OF REACTIVITY OF SYNTHETIC AND BOVINE HYDROXYAPATITE *IN VITRO* UNDER DYNAMIC CONDITIONS

#DIANA HORKAVCOVÁ, DANA ROHANOVÁ, LENKA KUNCOVÁ, KLÁRA ZÍTKOVÁ, ZUZANA ZLÁMALOVÁ CÍLOVÁ, ALEŠ HELEBRANT

Department of Glass and Ceramics, Institute of Chemical Technology, Technická 5, 166 28 Prague 6, Czech Republic

#E-mail: diana.horkavcova@vscht.cz

Submitted October 5, 2013; accepted March 4, 2014

Keywords: Hydroxyapatite, in vitro test, SBF

Hydroxyapatite materials prepared by two methods: synthetic (HA–S) and bovine (HA-B) granules were exposed to a long-term in vitro test under dynamic conditions. Testing cells, filled up to one fourth (¼V) of their volume with the tested material, were exposed to continuous flow of simulated body fluid (SBF) for 56 days. The objective of the experiment was to determine whether reactivity of the biomaterials (hydroxyapatites), prepared by different methods but identical in terms of their chemical and phase composition, in SBF were comparable. Analyses of the solutions proved that both materials were highly reactive from the very beginning of interaction with SBF (significant decrease of Ca^{2+} and $(PO_4)^{3-}$ concentrations in the leachate). SEM/EDS images have shown that the surface of bovine HA-B was covered with a new hydroxyapatite (HAp) phase in the first two weeks of the test while synthetic HA–S was covered after two weeks of the immersion in SBF. At the end of the test, day 56, both materials were completely covered with well developed porous HAp phase in form of nano-plates. A calculation of the rate of HAp formation from the concentration of $(PO_4)^{3-}$ ions in SBF leachates confirmed that all removed ions were consumed for the formation of the HAp phase throughout the entire testing time for bovine HA–B and only during the second half of the testing time for synthetic HA–S.

INTRODUCTION

Bioactive materials based on calcium phosphates have been widely used in medicine, particularly in dental surgery. The materials may be in form of micro- or macro-porous granules, scaffolds, cements etc. After their implantation biochemical reactions occur at the interface between the implant and bone tissue which result in formation of a mechanically strong interconnection with a layer of precipitated hydroxyapatite - the so-called bioactive fixation [1-4]. The bioactive materials include glass, bioactive glass ceramics and ceramics based on calcium phosphates. The material most frequently used in calcium-phosphate ceramics is hydroxyapatite HA ($Ca_{10}(PO_4)_6(OH)_2$) because its chemical composition is similar to the mineral part of bone and teeth tissue. Another calcium-phosphate ceramics used in practice is tricalcium phosphate β-TCP ($Ca_3(PO_4)_2$) [1-4]. Much attention has been paid to the synthesis of calcium phosphates, particularly hydroxyapatite, while seeking preparation of a high-purity nano- to micro-crystalline product, which is stable in solutions with pH above 4.2. Basic methods of preparation of synthetic hydroxyapatites include chemical precipitation through aqueous solution [5-8], sol-gel method [9-11], mechanochemical process [8, 12, 13] or solid-state sintering process [14]. Other options include preparation of bovine hydroxyapatite from natural bovine bone by a sequence of thermal processes [15] or by annealing and sintering of bovine bone [16, 17]. An important feature of the prepared hydroxyapatites is their resorption and kinetics of solubility in water solutions. The processes can be described with several mechanisms [18], mainly a diffusion model (transport of mass) and reaction on the hydroxyapatite surface [19, 20]. Kinetics of the dissolution is affected primarily by pH and oversaturation of the solution.

Bioactivity of materials can be tested *in vivo* (in live organisms) or *in vitro* (by means of model body fluids). The tests result in formation of a biologically active hydroxyl-carbonate apatite layer on the surface of bioactive implants [1, 2]. Model solution used most frequently for *in vitro* testing is the so-called simulated body fluid (SBF) designed by Kokubo [21]. Ion composition of SBF is similar to the inorganic component of blood plasma and its pH is maintained by means of the TRIS buffer (tris-hydroxymethyl aminomethane) [22]. *In vitro* tests (monitoring kinetics of formation of the apatite phase in simulated body fluid) may be affected both by the material itself (its granulometry, porosity, firing temperature) and by the testing conditions (static or dynamic exposure of the material to SBF, pH value) [23-27]. Essential factors for incorporation of calcium-

phosphate-ceramics-based bioactive materials include not only the rate of intergrowing with the surrounding tissue but also the level of their transformation into a new form of hydroxyapatite phase (HAp).

The first objective of the submitted paper was to compare HAp growth kinetics on the surface of synthetic (HA–S) and bovine (HA–B) micro- and macro-porous granulated hydroxyapatites in the course of their long-term interaction with simulated body fluid under dynamic conditions. The measured increases of weight of the materials and relevant concentrations of phosphates in leachates were used to calculate the growth rate of the new HAp phase. The second objective was to monitor the level of resorption of the tested materials into the new phase of the hydroxyapatite (HAp).

EXPERIMENTAL PART

The micro- and macro-porous apatite materials used in the tests were designed for replacement of bone tissue and made by Lasak Ltd. and by Geistlich Pharma AG. In the former case (Lasak Ltd.) the material was synthetic hydroxyapatite (HA–S, $Ca_{10}(PO_4)_6(OH)_2$) in the form of white granules with the diameter of 1 - 2 mm. Porosity of the granules ranged from 60 to 70 %. In the latter case (Geistlich Pharma AG.) the tested bovine hydroxyapatite (HA–B, $Ca_{10}(PO_4)_6(OH)_2$) was prepared from a mineral component of bovine bone in the form of spongious bone granulate, with the granule size of 1-2 mm. The materials were identified as follows: HA–S 14d, HA–B 14d, HA–S 28d, HA–B 28d, HA–S 42d, HA–B 42d and HA–S 56d, HA–B 56d.

The model fluid used for *in vitro* testing has an ion composition is similar to the inorganic component of blood plasma; this is a frequently used one as designed by Kokubo [21-23]. The simulated body fluid (SBF) was prepared by mixing of solutions of the following reagents: KCl, NaCl, $NaHCO_3$, $MgSO_4.7H_2O$, $CaCl_2$, KH_2PO_4 in appropriate ratios. SBF was buffered with TRIS (Tris-hydroxymethyl aminomethane) and HCl to achieve pH = 7.45. Azide (NaN_3) was added to prevent bacteria growth in the solution [25, 26] during the long-term test.

The long-term interaction of the materials with SBF was monitored under dynamic conditions in order to simulate as close as possible the flow conditions of extracellular fluid in a human organism and the materials were continually exposed to "fresh" SBF. Both the materials were weighed into individual testing cells to fill ¼ of their volumes. Previous work [26] has shown that this filling is optimal for the monitoring of interaction of the material with the solution. The SBF is continually pumped by a peristaltic pump from a supply bottle into four testing cells (with volume 5.5 ml). The flow rate of the solution was approximately at 48 ml per day.

The cells with the tested material were placed in a thermostat set at 36.5 ± 0.5°C. Subsequently, SBF leachates were collected from each of the cells in accurately specified intervals to determine the concentrations of Ca^{2+} and $(PO_4)^{3-}$ ion and to measure the pH values. Every two weeks (on days 14, 28, 42 and 56) one cell was disconnected and the material was examined.

EXPERIMENTAL

The surface of the tested materials before and after the interaction was monitored with (SEM) Hitachi S-4700 electron microscope with EDS analyzer (NORAN D-6823) using the accelerating voltage of 15 kV. The material was coated with a layer of Au-Pd for 80 s.

Diffraction patterns were collected with a PANalytical X´Pert PRO diffractometer equipment with a conventional X-ray tube (CuKα radiation, 40 kV, 30 mA, point focus) and a position-sensitive PIXcel detector with an anti-scatter shield. X-ray patterns were measured in the 2θ range of 10 - 100°, with steps of 0.0131° and 200 s counting per step. Quantitative analysis was performed with the HighScorePlus software package (PANalytical, the Netherlands, version 2.2.5), Diffrac-Plus software package (Bruker AXS, Germany, version 8.0) and JCPDS PDF-2 database (International Centre for Diffraction Data, Newtown Square, PA, USA) release 54,2004 (in the Institute of Inorganic Chemistry of the Czech Academy of Science, Řež u Prahy). The specific surface of the materials before and after the interaction was determined using the BET method using ASAP 2020 analyzer by Micromeritic, using N_2; temperature 60 - 200°C, heating rate 10°C/min, time at temperature 600 - 2000 min.

The concentration of Ca^{2+} ions in the leachate was analyzed by atomic absorption spectrometry using VARIAN - Spectr AA 300. Atomization was performed in acetylene-N_2O flame. The wavelength used for absorbance measurements was 422.7 nm. The content of $(PO_4)^{3-}$ ions was analyzed on UV-VIS Spectrophotometer UV1601 at $\lambda = 830$ nm under ČSN 830540. Concentrations of both the ions were calculated using a calibration curve from the measured absorbance values. pH values in leachates were measured with inoLab pH-meter with a combined glass electrode at the laboratory temperature.

Calculation of the rate of formation of the new HAp phase on the surface of synthetic and bovine hydroxyapatite

Due to the use of the TRIS buffer in SBF, which can incorporate Ca^{2+} ions into its structure [26, 27], the calculation of the rate of formation of the new HAp phase on the surface of both the materials used values of $(PO_4)^{3-}$

concentrations. The rate of precipitation of the new HAp phase on the surface of HA–S, HA–B was calculated from the actual increase of weight (R_m, equation (3)) and from the decrease of the $(PO_4)^{3-}$ concentration in SBF leachates from the beginning of the interaction (R_c). It is assumed that all $(PO_4)^{3-}$ ions removed from SBF are used for the formation of HAp phase.

$$\Delta m' = [(m_t - m_0)\cdot 100]/m_0\ (\%) \quad (1)$$

$$\Delta S' = [(S_t - S_0)\cdot 100]/S_0\ (\%) \quad (2)$$

$$R_m = (m_t - m_0)/t\ (\mathrm{mg\cdot hour^{-1}}) \quad (3)$$

$$m_{c(t)} = (c_0 - c_t)\cdot (M_{HAp}/6\cdot M_{(PO4)3-})\cdot F\cdot \Delta t + m_{c(t-\Delta t)}\ (\mathrm{mg}) \quad (4)$$

$$A_{\mathrm{HA-S}} = m_{0\,\mathrm{HA-S}}\cdot S_{0\,\mathrm{HA-S}}\ (\mathrm{m^2}) \quad (5)$$

$$A_{\mathrm{HA-B}} = m_{0\,\mathrm{HA-B}}\cdot S_{0\,\mathrm{HA-B}}\ (\mathrm{m^2}) \quad (6)$$

where m_t, m_0 are the weights of the material at the time t and at the beginning of the interaction respectively, rm' is a change of the weight of the material at the time t in percentages, t is the time of the interaction of the material with SBF, S_t, S_0 are the specific surfaces of the material at the time t and at the beginning of the interaction respectively, rS' is a change of the specific surface of the material at the time t in percentages, rt is the time between two collections of SBF leachate samples, R_m is the rate of formation of the new HAp phase calculated from the increase of the material weight, c_t, c_0 are the concentrations of $(PO_4)^{3-}$ ions in SBF at the time t and at the beginning of the interaction respectively, $m_{c(t)}$, $m_{c(t-rt)}$ is the weight of the newly formed HAp calculated from the quantity of $(PO_4)^{3-}$ ions at the respective time, M_{HAp}, $M_{(PO4)3-}$ are the molar weights of HAp and $(PO_4)^{3-}$ respectively, F is the flow rate of SBF (48 ml.day^{-1}), R_c is calculated from tangent of the linear fit of $m_{c(t)}$ time dependence from Figure 4 (HA–S) or Figure 7 (HA–B), A is the original surface area of the material.

RESULTS AND DISCUSSION

Synthetic hydroxyapatite HA–S

Table 1 shows the weight of material HA–S before and after the interaction with SBF. The results indicate that the weight of material slowly grows with the growing time of interaction with SBF. By the end of the interaction the weight increased in total by 69.4 %.

Table 1. The weights of material HA–S before and after 14, 28, 42 and 56 days of interaction with SBF.

Material	Weight (g)		$\Delta m_{\mathrm{HA-S}}$ (g)	$\Delta m'_{\mathrm{HA-S}}$ (%)
	before interaction	after interaction		
HA–S 14d	0.500	0.612	+0.112	+22.4
HA-S 28d	0.500	0.698	+0.198	+39.6
HA-S 42d	0.500	0.761	+0.261	+52.2
HA-S 56d	0.500	0.847	+0.347	+69.4

Changes on the surface of the HA–S material after the interaction with SBF are visible in Figures 1b-e. Figure 1a shows the material before the interaction.

Figures 1b-e show the changes of HA–S morphology as a result of formation of a new hydroxyapatite phase (HAp) on its surface. Formation of the new phase on the surface of the original material is obvious as early as after 14 days of interaction with SBF (Figure 1b) and after 28 days of the interaction (Figure 1c) plates of nano-crystals of the new HAp phase can be observed. With the growing time of interaction the newly formed HAp phase becomes more developed (Figure 1d-e). Using a detailed image of a crack that developed due to drying (Figure 1f) we were able to determine the thickness of the new HAp phase (ca. 30 μm) after 56 days of interaction.

During the first 14 days of interaction with SBF there was an obvious decrease of the specific surface HA–S (Table 2). The trend was recorded throughout the entire time of interaction. Measurements of specific surface have confirmed that the newly developing HAp phase filled the macro- and micro-pores of HA–S and gradually covered the entire surface, as indicated by SEM images. We estimate that after approximately 28 days the original synthetic material HA–S no longer reacts with SBF but probably the newly developed HAp phase.

Table 2. The values of the specific surface of material HA–S before and after 14, 28, 42 and 56 days of interaction with SBF.

Material	Specific surface ($\mathrm{m^2\cdot g^{-1}}$)		$\Delta S_{\mathrm{HA-S}}$ ($\mathrm{m^2\ g^{-1}}$)	$\Delta S'_{\mathrm{HA-S}}$ (%)
	before interaction	after interaction		
HA–S 14d	72.1	64.3	–7.8	–10.8
HA–S 28d	72.1	57.9	–14.2	–19.7
HA–S 42d	72.1	54.7	–17.4	–24.1
HA–S 56d	72.1	50.9	–21.2	–29.4

Records from a powder X-ray diffraction analysis (XRD) of HA–S were the same before and after individual time intervals of interaction with SBF. This is due to the chemical, as well as physical similarity of the synthetic hydroxyapatite HA–S and the newly developed phase HAp.

Figures 2 a-c show concentrations of Ca^{2+} and $(PO_4)^{3-}$ ions and pH values in SBF leachates depending on the time of interaction with HA–S.

Concentrations of ions in leachates reflect changes in behavior of the synthetic material almost immediately. After 2 hours after of the exposition of HA–S in SBF a sharp decrease of concentrations was observed for calcium ion (from 98 to 28 mg·l^{-1}) and phosphate ion (from 93 to 17.5 mg·l^{-1}) which suggests that the material surface was highly active for the nucleation of the new phase. Analyses of leachates have confirmed that precipitation of the new HAp phase occurred from the very beginning of the exposure. After 7 days the interaction between HA–S and the solution stabilized.

The reason may be the fact that it was mainly the newly developed HAp phase that reacted with SBF, as it was also observed on SEM images. The pH values were in conformity with the resulting changes of concentrations of ions analyzed in the leachates. After two hours of interaction with the HA–S material, pH decreased from 7.6 to 7.27. The pH then settled at 7.7 ± 0.3 and oscillated around that value until the end of the test.

Figure 3 shows the rate of formation of the new HAp phase on the surface of HA–S, i.e. relationship of weight of the developed HAp according to the Equation (4) on the interaction time. It is obvious that the rate of formation of the new HAp phase was linear throughout the entire time of interaction and nearly the same in all testing cells.

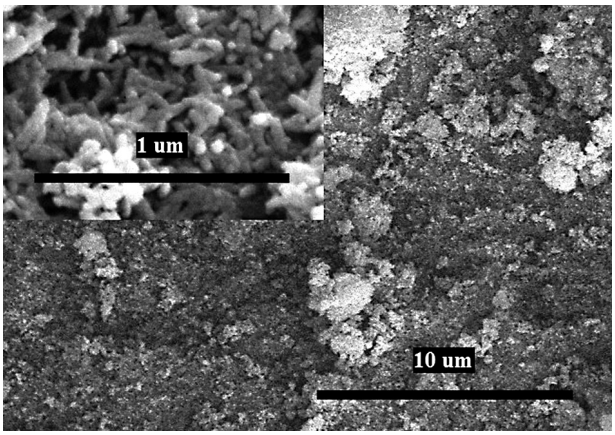

a) before interaction-origin

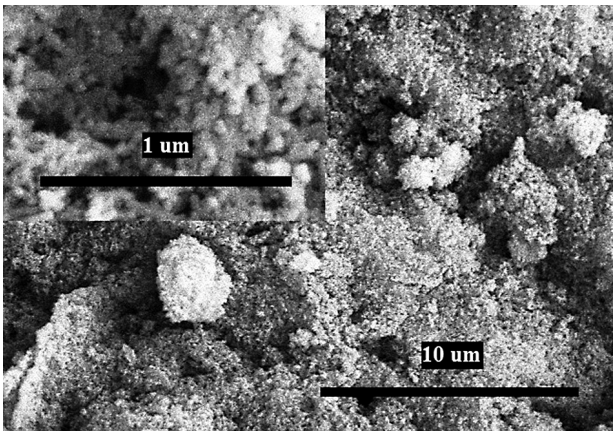

b) after 14 days

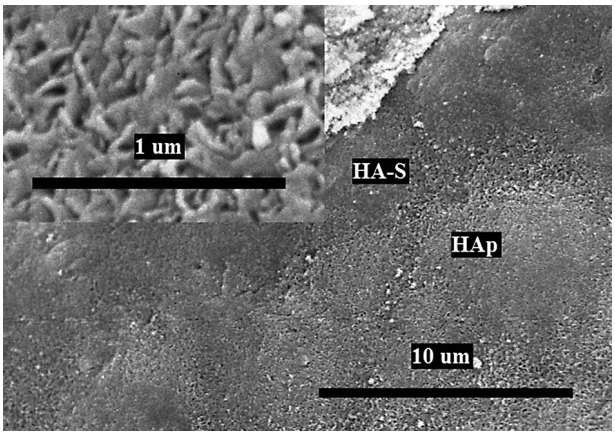

c) after 28 days

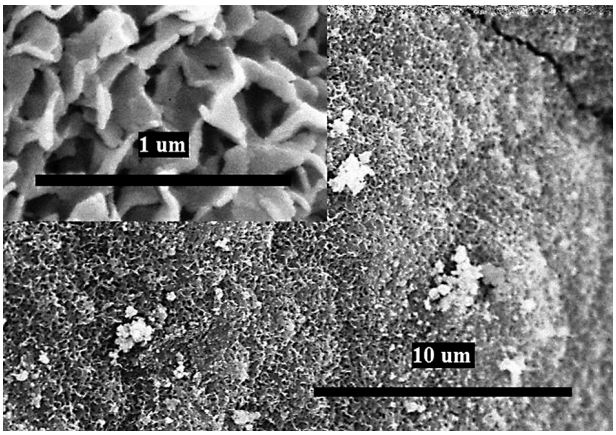

d) after 42 days

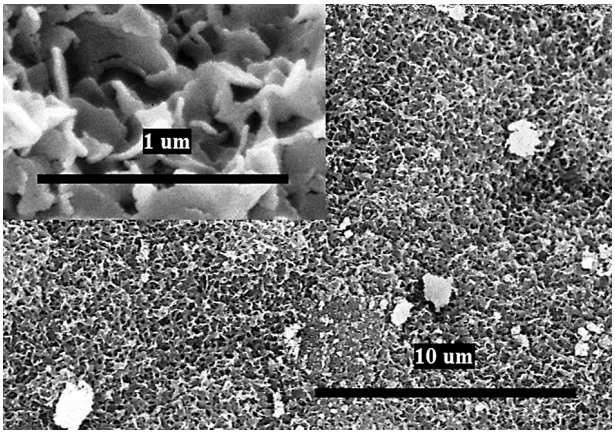

e) after 56 days

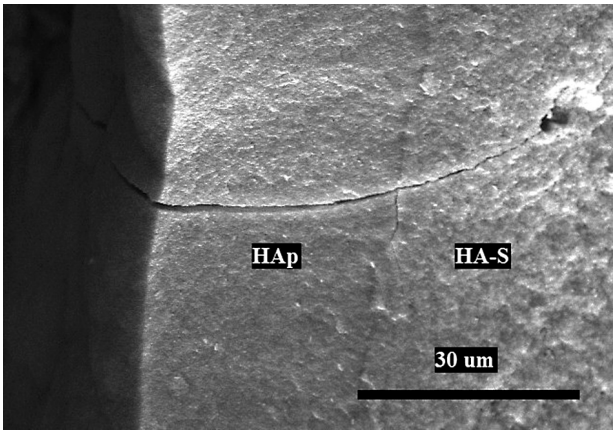

f) new HAp phase

Figure 1. SEM images of the material HA–S: a) before interaction-origin, b) after 14 days in SBF, c) after 28 days in SBF, d) after 42 days in SBF, e) after 56 days in SBF, f) detail of thickness of new HAp phase after 56 days in SBF.

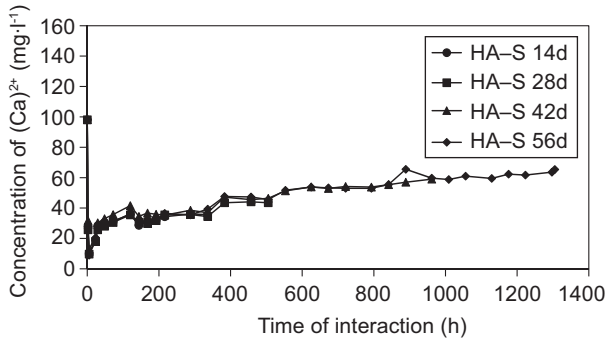

a) Ca^{2+}

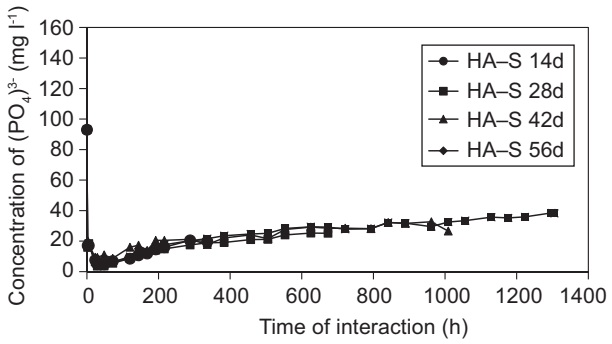

b) $(PO_4)^{3-}$

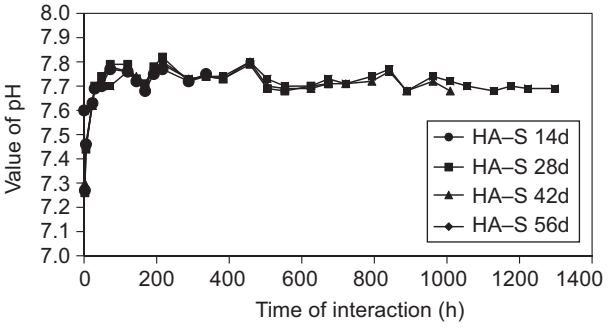

c) values of pH

Figure 2. Concentrations of a) Ca^{2+}, b) $(PO_4)^{3-}$ ions and c) values of pH in SBF during interaction with HA–S.

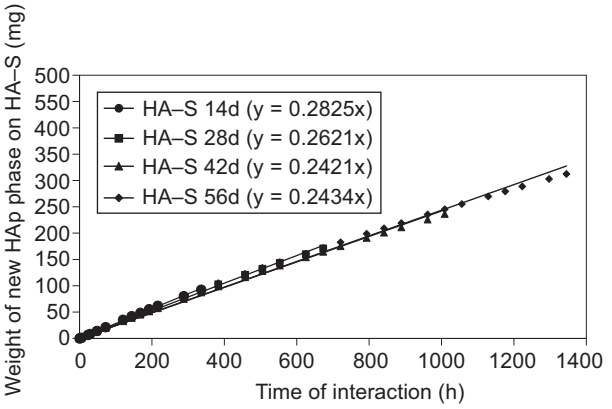

Figure 3. The weight of the new HAp phase on HA–S calculated from concentrations of $(PO_4)^{3-}$ ion during interaction with SBF.

Table 3 provides precipitation rates of the new HAp phase calculated from the growing weight of the material ($R_{m\,HA–S}$) and from the decrease of phosphate ion concentration in SBF ($R_{c\,HA–S}$) and their ratio ($R_{m\,HA–S}$/ $R_{c\,HA–S}$). The rate constants for the time periods were calculated using linear regression equations provided in (Figure 3).

Table 3. Rate of precipitation of the new HAp phase on the surface of HA–S after 14, 28, 42 and 56 days of interaction with SBF.

Material	$R_{m\,HA–S}$ (mg·hour^{-1})	$R_{c\,HA–S}$ (mg·hour^{-1})	$R_{m\,HA–S}/R_{c\,HA–S}$
HA–S 14d	0.332	0.282	1.177
HA–S 28d	0.294	0.262	1.122
HA–S 42d	0.258	0.242	1.066
HA–S 56d	0.258	0.243	1.061

Values shown in Table 3 clearly indicate that HA–S was reactive immediately after the beginning of the interaction with SBF. However, gradually, as the surface covered with the new phase, the rate of formation of the HAp phase slightly decreased. The ratio between the values $R_{m\,HA–S}$ and $R_{c\,HA–S}$ between day 14 and 28 was greater than 1. After 42 - 56 days the values of $R_{m\,HA–S}$ and $R_{c\,HA–S}$, obtained by two different methods of measurement ($R_{m\,HA–S}$ from weight of HA–S and $R_{c\,HA–S}$ from concentration of $(PO_4)^{3-}$ ion in SBF) stabilized and they were nearly identical (the ratio (R_m/R_c) was close to 1). The assumption that all $(PO_4)^{3-}$ ions removed from SBF were used to form HAp phase after day 42 has been confirmed.

Bovine hydroxyapatite HA–B

Also the weight of HA–B after the interaction with SBF (Table 4) increased with the interaction time. After 56 days of interaction the weight of HA–B increased in total by 76.5 %.

Table 4. The weights of material HA–B before and after 14, 28, 42 and 56 days of interaction with SBF.

Material	Weight (g)		$\Delta m_{HA–B}$ (g)	$\Delta m'_{HA–B}$ (%)
	before interaction	after interaction		
HA–B 14d	0.375	0.468	+0.093	+24.8
HA–B 28d	0.375	0.542	+0.167	+44.5
HA–B 42d	0.375	0.609	+0.234	+62.4
HA–B 56d	0.375	0.662	+0.287	+76.5

The original material before the interaction with SBF is in Figure 4a. Figures 4b-f show the surfaces of HA–B after specific periods of time of the interaction.

Figure 4b indicates that as early as during the first 14 days the surface of HA–B covered with the new phase made of nanocrystalline plates of hydroxyapatite (HAp). The phase filled macro and micro pores of HA–B and the nanocrystals gradually formed a continuous layer. A cracked layer made up of globules of aggregated nanocrystals, typical for the newly formed hydroxyapatite (HAp), is well visible when a smaller resolution is used (Figure 4f). The HA–B surface covered with the newly formed HAp phase in a shorter period of time (14 days) in comparison with the synthetic material HA–S, for which it took approximately 28 days. A comparison of SEM/EDS images of both the materials shows that the surface of synthetic HA–S started to cover with nanoplates of HAp on the day 14 of the interaction and on day 28 it was covered completely.

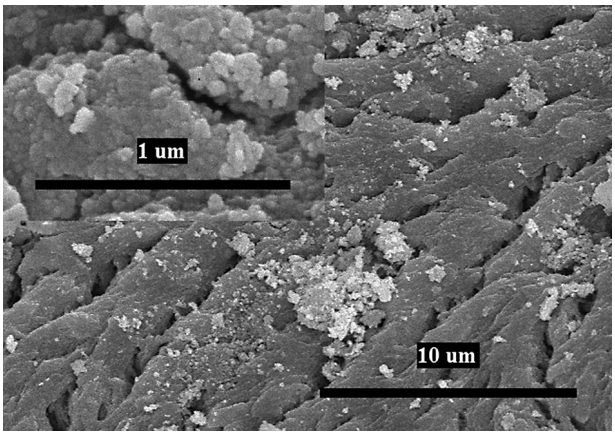

a) before interaction-origin

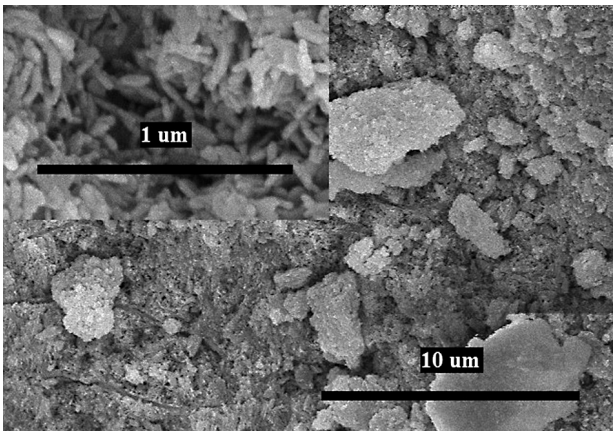

b) after 14 days

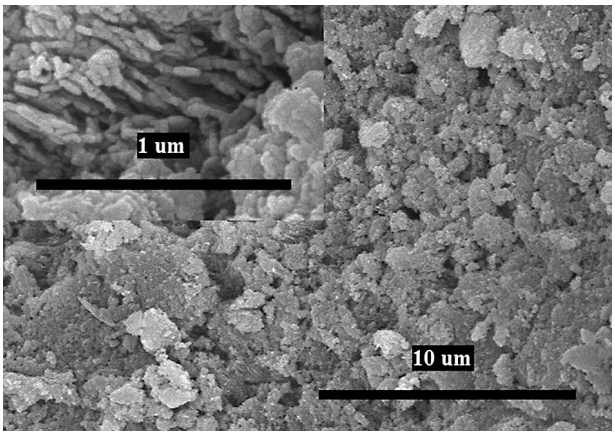

c) after 28 days

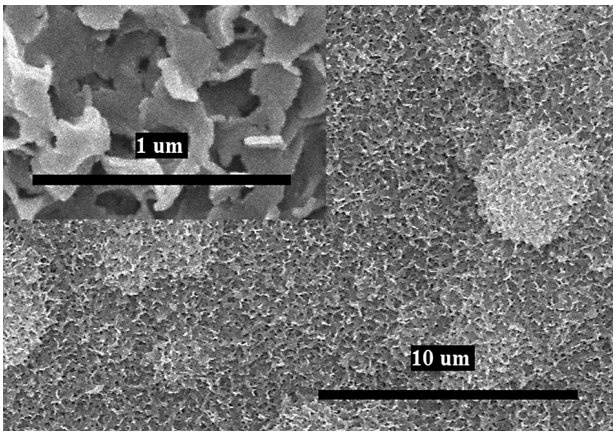

d) after 42 days

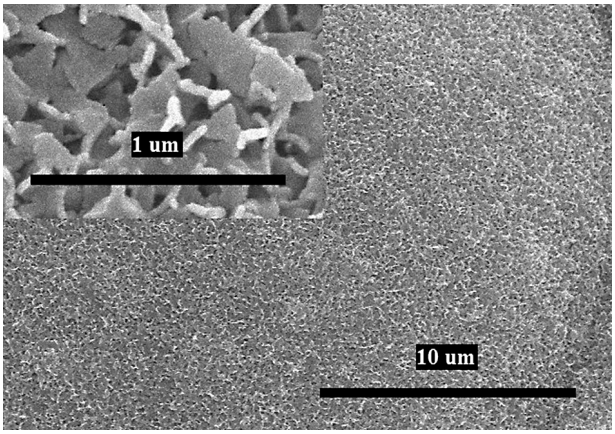

e) after 56 days

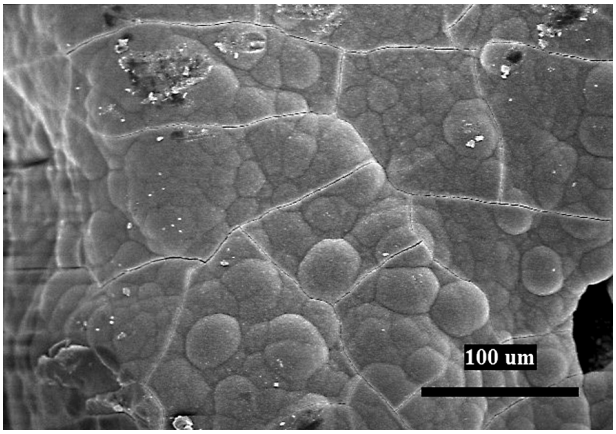

f) new HAp phase

Figure 4. SEM image of the material HA–B: a) before interaction- origin, b) after 14 days in SBF, c) after 28 days in SBF, d) after 42 days in SBF, e) after 56 days in SBF, f) surface of new HAp phase after 56 days in SBF.

After 14 days of exposure a decrease of the specific surface (Table 5) was observed. After 56 days the specific surface of bovine hydroxyapatite HA–B decreased from the original 94.4 $m^2.g^{-1}$ to 52.4 $m^2 \cdot g^{-1}$, i.e. to values similar to that of HA–S (50.9 $m^2 \cdot g^{-1}$).

Table 5. The values of specific surface of material HA–B before and after 14, 28, 42 and 56 days of interaction with SBF.

Material	Specific surface ($m^2 \cdot g^{-1}$) before interaction	Specific surface ($m^2 \cdot g^{-1}$) after interaction	ΔS_{HA-B} ($m^2\ g^{-1}$)	$\Delta S'_{HA-B}$ (%)
HA–B 14d	94.4	75.9	–18.5	–19.6
HA–B 28d	94.4	63.7	–30.6	–32.4
HA–B 42d	94.4	56.9	–37.4	–39.6
HA–B 56d	94.4	52.4	–42.0	–44.5

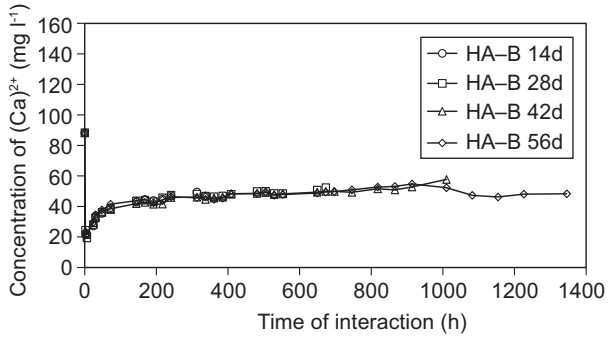

a) Ca^{2+}

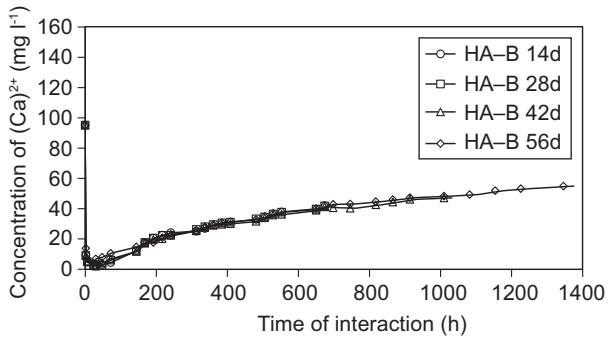

b) $(PO_4)^{3-}$

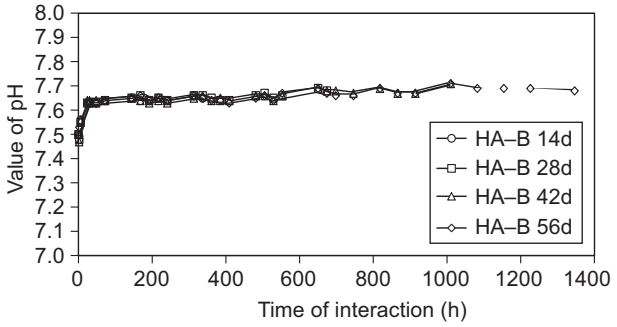

c) values of pH

Figure 5. Concentrations of a) Ca^{2+}, b) $(PO_4)^{3-}$ ions and c) values of pH in SBF during interaction with HA–B.

The XRD method did not succeed to differentiate between the original bovine hydroxyapatite HA–B and the newly formed HAp phase. The reason (equally as for the previous HA–S material) was their chemical and phase similarity (Ref. Code: 01-074-0566).

Figure 5 show concentrations of Ca^{2+} and $(PO_4)^{3-}$ ions and pH values in SBF leachates depending on the time of interaction with HA–B.

Two hours after the beginning of interaction a sharp drop of concentrations occurred for both the ions, which suggests an immediate reaction of the material with SBF. In the case of $(PO_4)^{3-}$ ion it dropped nearly to zero. After 7 days the concentration of Ca^{2+} stabilized, the concentration of $(PO_4)^{3-}$ after the initial dramatic decrease gradually grew and the trend persisted until the end of the experiment. Changes of concentrations of Ca^{2+} and $(PO_4)^{3-}$ ions with time in SBF for bovine hydroxyapatite HA–B were similar those found in case of synthetic hydroxyapatite HA–S. The pH values slightly increased after two hours of interaction and remained nearly constant until the end of the experiment.

Figure 6 shows the rate of formation of the new HAp phase on the surface of HA–B throughout the entire 56 days of interaction with SBF (according to the equation (4)). The rate of formation of the new HAp phase on the surface of HA–B was nearly identical in all the testing cells.

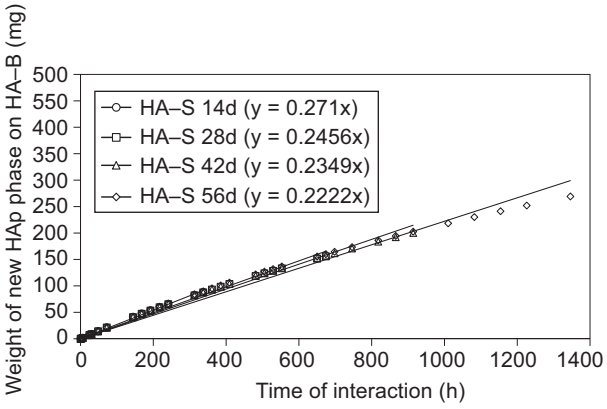

Figure 6. The weight of the new HAp phase on HA–B calculated from concentrations of $(PO_4)^{3-}$ ions during interaction with SBF.

Table 6 shows precipitation rates of the new HAp phase on the surface of HA–B calculated, equally as for the previous material, from the increased weight of HA–B ($R_{m\ HA-B}$) and from the decrease of $(PO_4)^{3-}$ ions concentration in SBF leachates ($R_{c\ HA-B}$) and their ratio ($R_{m\ HA-B}/R_{c\ HA-B}$). The rate constants for the time periods were calculated using linear regression equations provided in (Figure 6).

Values shown in Table 6 indicate that bovine hydroxyapatite HA–B is also highly reactive from the beginning of exposure to SBF and the rate of formation of the new HAp phase ($R_{m\ HA-B}$) slightly decreases with time.

Values of the rates ($R_{m\ HA–B}$ and $R_{c\ HA–B}$) for bovine HA–B were obtained by two different methods: the change of weight of HA–B and from concentration of $(PO_4)^{3-}$ ions in SBF. From the beginning of exposure these values were nearly the same. The assumption that all $(PO_4)^{3-}$ removed from SBF were used to form HAp has been confirmed.

Table 6. Rate of precipitation of the new HAp phase on the surface of HA–B after 14, 28, 42 and 56 days of interaction with SBF.

Material	$R_{m\ HA–B}$ (mg·hour^{-1})	$R_{c\ HA–B}$ (mg·hour^{-1})	$R_{m\ HA–B}/R_{c\ HA–B}$
HA–B 14d	0.279	0.271	1.029
HA–B 28d	0.248	0.246	1.008
HA–B 42d	0.232	0.232	1.000
HA–B 56d	0.213	0.222	0.959

Comparison of synthetic and bovine hydroxyapatite

For the comparison of relative coverage of HA–S and HA–B materials with the new HAp phase it is necessary to take into account their original weights and original specific surfaces according to equations (5) and (6). It is obvious that, due to the different initial weights and specific surfaces, the surfaces area of the materials were nearly the same ($A_{HA–S}$ = 36.1 m^2, $A_{HA–B}$ = 35.4 m^2). When comparing synthetic and bovine hydroxyapatites in terms of their changing weights, $\Delta m'$ (Tables 1 and 4), we can conclude that the trends found for both the materials were similar. In this comparison (Figure 7) bovine HA–B seemed slightly more reactive than synthetic HA–S. The weight of HA–B grew almost linearly from the beginning of exposure. For synthetic HA–S we observed a slight slowdown of formation of the new phase after the 28th day of exposure.

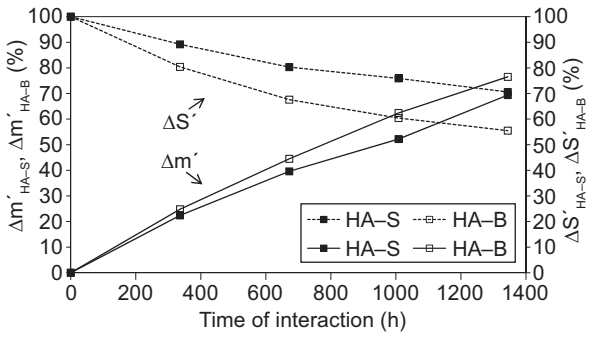

Figure 7. Comparison of the weight and the specific surface difference of material HA–S and HA–B during interaction with SBF.

A more significant difference between the tested materials was observed for the specific surface. The percentage change $\Delta S'$ of HA–S was smaller than that of HA–B (Tables 2 and 5). However, the trends of the $\Delta S'$ decrease were again the same for both the materials (Figure 7).

The assumption that all $(PO_4)^{3-}$ ions removed from the SBF are consumed for the formation of HAp (according to R_c calculation) was found correct for HA–S after day 42 and from the very beginning of the interaction for HA–B. It is probable that either non-stoichiometric HAp or amorphous calcium phosphate (ACP) develops on synthetic HA–S during the interval of 0 - 42 days. After day 42 the ratios R_m/R_c were nearly the same (value 1) for both materials. For clinical using could be interesting information that 0.5 g of synthetic HA–S and 0.375 g of bovine HA–B material provide the same surface area (A) and the bulk density (materials filled exactly ¼ of the testing cell volume). This study indicates that the both HA materials cause the formation of the Ca-P phase immediately after application. The newly formed phase has amorphous character (probably ACP) in the case of the synthetic HA–S. Gradually, HAp crystals are formed on the HA–S surface (28 days after interaction). The crystalline HAp was formed on the surface of the bovine HA–B from the beginning of the exposition and the crystals very quickly covered the original surface. The newly formed crystalline layer could reduce further remodelling of the bovine HA–B.

CONCLUSION

The SEM/EDS measurements have shown that granules of synthetic HA–S started covering with the newly formed HAp phase ca. 14 days later than granules of bovine HA–B. Both materials were completely covered with the new well developed HAp phase and also the rates of its formation were similar on the day 42 of the immersion in SBF. Therefore SBF further reacted probably only with the newly developed HAp phase on the surface of the both materials under our experimental conditions. Our model, which assumes that all $(PO_4)^{3-}$ ions removed from SBF precipitated on the tested material surface to form HAp, can be used for bovine HA–B throughout the entire time of interaction and for the synthetic HA–S after the 42th day of interaction. It is probable that, at the beginning of the exposure, an amorphous calcium phosphate phase (ACP) develops on the surface of synthetic HA–S instead of HAp phase. The tested materials were identical hydroxyapatites, in terms of their chemical composition, crystallinity and even with the same reaction surface area. In spite of different way of preparation, the weight and the specific surface, the granules of synthetic and bovine hydroxyapatites react very similar with SBF in second period of our experiment.

Acknowledgements

This work was supported by the Technology Agency for the Czech Republic within the project TE01020390 Center for development of modern metallic biomaterials for medicinal implants. We thank Dr. Petr Bezdička for XRD measurement and Ing. Miloslav Lhotka Ph.D. for BET measurement.

References

1. Cao W., Hench L.L.: Ceram. Inter. *22*, 493 (1996).
2. Best S.M., Porter A.E., Thian E.S., Huang J.: J. Eu. Ceram. Soc. *28*, 1319 (2008).
3. Dorozhkin S.V.: Materials *2*, 1975 (2009).
4. Dorozhkin S.V.: Acta Biomaterialia *6*, 4457 (2010).
5. El Hammari L., Merroun H., Coradin T., Cassaignon S., Laghzizil A., Saoiabi A.: Mater. Chem. Phys. *104*, 448 (2007).
6. Cao L-y., Zhang Ch-b., Huang J-f.: Ceram. Inter. *31*, 1041 (2005).
7. Kweh S.W.K., Khor K.A., Cheang P.: J. Mater. Proces. Tech. *89-90*, 373 (1999).
8. Mostafa N.Y.: Mater. Chem. Phys. *94*, 333 (2005).
9. Fathi M.H., Hanifi A.: Materials Letters *61*, 3978 (2007).
10. Bezzi G., Celotti G., Landi E., La Torretta T.M.G., Sopyan I., Tampieri A.: Mater. Chem. Phys. *78*, 816 (2003).
11. Wang F., Li M.S., Lu Y.P., Qi Y.X.: Materials Letters *59*, 916 (2005).
12. Rhee S.H.: Biomaterials *23*, 1147 (2002).
13. Yeong K.C.B., Wang J., Ng S.C.: Biomaterials *22*, 2705 (2001).
14. Pramanik S., Agarwal A.K., Rai K.N., Garg A.: Ceram. Inter. *33*, 419 (2007).
15. Ruksudjarit A., Pengpat K., Rujijanagul G., Tunkasiri T.: Cur. Ap. Phys. *8*, 270 (2008).
16. Ooi C.Y., Hamdi M., Ramesh S.: Ceram. Inter. *33*, 1171 (2007).
17. Herliansyah M.K., Hamdi M., Ide-Ektessabi A., Wildan M.W., Toque J.A.: Mater. Sci. Eng. *C29*, 1674 (2009).
18. Dorozhkin S.V.: Prog. Crys. Gro. Char. Mater. *45*, (2002).
19. Christoffersen J., Christoffersen M.R., Kjaergaard N.: J. Cryst. Gro. *43*, 501 (1978).
20. Christoffersen J., Christoffersen M.R.: J. Crysy. Gro. *53*, 42 (1981).
21. Kokubo T., Takadama H.: Biomaterials *27*, 2907 (2006).
22. Kokubo T., Kim H-M., Kawashita M.: Biomaterials *24*, 2161 (2003).
23. Kim H-M., Himeno T., Kokubo T., Nakamura T.: Biomaterials *26*, 4366 (2005).
24. Bohner M., Lemaitre J.: Biomaterials *30*, 2175 (2009).
25. Helebrant A., Jonášová L., Šanda L.: Ceram.-Sil. *46*, 9 (2002).
26. Horkavcová D., Zítková K., Rohanová D., Helebrant A., Cílová Z.: Ceram.-Sil. *54*, 398 (2010).
27. Rohanová D., Boccaccini A.R., Yunos D.M., Horkavcová D., Březovská I., Helebrant A.: Acta Biomaterialia *7*, 2623 (2011).

Práce **[7]**

El-Maghraby H.F., Gedeon O., Rohanová D., Greish Y.E.: Compressive strength and preliminary in vitro evaluation of gypsum and gypsum-polymer composites in protein-free SBF at 37ºC. Ceramics International 36; 1561-1569, 2010.

Podíl: 40%: návrh experimentu, zpracování výsledků, příprava publikace

Available online at www.sciencedirect.com
ScienceDirect
Ceramics International 36 (2010) 1561–1569
CERAMICS INTERNATIONAL
www.elsevier.com/locate/ceramint

Compressive strength and preliminary *in vitro* evaluation of gypsum and gypsum–polymer composites in protein-free SBF at 37 °C

H.F. El-Maghraby [a,1], O. Gedeon [a], D. Rohanova [a], Y.E. Greish [b,*]

[a] *Institute of Chemical Technology, ICT, Department of Glass and Ceramics, Technicka 5, Praha 6, 166 28, Czech Republic*
[b] *Department of Chemistry, UAE University, Maqam Campus, Al Ain, P.O. Box 17551, United Arab Emirates*

Received 12 October 2009; received in revised form 3 January 2010; accepted 5 February 2010
Available online 9 March 2010

Abstract

Gypsum is a bioresorbable material that has been used in many applications such as tissue regeneration. Mechanical properties of gypsum have limited its applications to non-load bearing sites. The current study aimed at studying the compressive strength and behaviour of gypsum–polymer composites in protein-free simulated body fluids (SBF). Polymers studied were poly(vinyl alcohol) (PVA) and its copolymers with vinyl acetate and itaconic acid in addition to vinyl acetate and vinyl chloride. Composites with the highest compressive strength results were chosen for the preliminary *in vitro* evaluation in protein-free SBF solutions. Changes in the concentrations of Ca^{2+} and PO_4^{3-} ions, weight loss and morphology of the solid samples were monitored after soaking them in SBF and 1.5 SBF solutions. Results showed resorption of gypsum, concurrently with deposition of apatite in all composites, including polymer-free gypsum. Mechanical integrities of all samples were maintained, suggesting their stabilities when used as bone cements.

Keywords: Gypsum; Hydroxyapatite; Biomimetic; Microstructure; Compressive strength

1. Introduction

Gypsum is considered a highly biocompatible material that is one of the simplest synthetic bone graft materials with the longest clinical history, spanning more than 100 years [1]. It is classified as a bioresorbable material, whose resorption products integrate with the different cycles in the human body. It has been successfully used to treat periodontal disease, endodontic lesions, alveolar bone loss, and maxillary sinus augmentation [1]. It has been used as a binder to facilitate healing and prevent loss of grafting materials, which is also attributed to its tissue compatibility [2]. Gypsum-containing biomaterials have also exhibited promise as grafts in a preclinical repair model of interabony periodontal defects, as well as in clinical reports for sinus augmentation and treatments of femoral shaft nonunions [3,4]. Plaster of Paris, which is considered a gypsum precursor, was previously shown to improve the setting reactions of a biodegradable calcium phosphate cement [5]. Due to their chemical composition and porous structure, these gypsum-containing cements combined both the resorbability and osteoconductivity [6]. Sato et al. further indicated the promising characteristics of gypsum after mixing it with apatite particles, based on the relatively fast absorption of gypsum without interfering with the process of bone healing [7]. In an attempt to use gypsum as a bone graft substitute for lumbar spinal fusion, however, gypsum showed unsuccessful results because of its rapid resorption [8]. Plaster of Paris was also added to a calcium phosphate cement, producing a biodegradable bone cement that was used for bone reconstruction [9]. The advantage of bioresorption of gypsum was utilized in a composite involving plaster of Paris and a nanocrystalline hydroxyapatite, that was successfully used for the delivery of antibiotics in bone infections [10].

Despite the advantage of bioresorption of gypsum that makes it an attractive candidate for certain applications, its relatively low mechanical properties have limited its scope of application as a bone replacement implant or even as a bone

* Corresponding author. Permanent address: Department of Ceramics, National Research Centre, Cairo, Egypt. Tel.: +971 50 2338203; fax: +971 3 7671291.
E-mail address: y.afifi@uaeu.ac.ae (Y.E. Greish).
[1] Permanent address: Department of Ceramics, National Research Centre, Cairo, Egypt.

0272-8842/$36.00
doi:10.1016/j.ceramint.2010.02.023

cement. Different classes of materials were mixed with gypsum in order to improve its mechanical properties. Blending gypsum with polymers has been considered one of the successful approaches to modulate the mechanical properties of gypsum [11–13]. The presence of certain functional groups on these polymers, such as hydroxyl and carboxyl groups, is mostly favoured. These were found to bind with the calcium sites along the set gypsum products. Polymers that do not have these groups are usually passive throughout the setting reaction of gypsum. However, the mechanical interlocking of these polymers with the set gypsum crystals improves the overall mechanical performance of the produced composites. For biomedical applications, polymers used with gypsum should be biocompatible to avoid rejection by the human immune system. Different polymers could be used in this regard, ranging from bioactive to bioinert, depending on the type and site of application. The current study investigated the formation of gypsum composites with poly(vinyl alcohol) (PVA) and its copolymers with different vinyl moieties. The bioactivity of PVA and its different copolymers was previously investigated and was attributed to the presence of certain functional groups along the neat polymer as well as its copolymers [14–17]. Both hydroxyl (–OH) and carboxylic (–COOH) groups were showed to help in the mineralization of polymers containing these groups, a process that is similar to the mineralization of collagen in nature [18]. Studies on the mineralization of polymers bearing these groups were carried out in solutions containing ions with type and concentrations similar to those existing in the human body, called simulated body fluids; SBF. The ability to induce formation of apatite coatings on composites containing these polymers indicates the strong potential of these composites to bind with natural bone if used as an implant or cement [19]. Although a conclusion of the suitability of a new biomaterial cannot be solely based on using these protein-free SBF solutions, it is still considered a valid approach to preliminary evaluate new biomaterials [19]. This has to be followed by detailed *in vitro* and *in vivo* studies. [20]. The bioactivity of the starting materials used in the current study has been previously established, both *in vitro* and *in vivo*. Gypsum was found to grow an apatite layer on its surface in SBF as well as *in vivo* [21]. In a recent study, PVA substrates coated with apatite showed enhanced an enhanced fibroblast cells adhesion and proliferation compared to uncoated PVA substrates [22]. The current study, therefore, investigates the performance of their combinations in SBF solutions. Composites containing optimum concentrations of the three investigated polymers were subjected to the SBF evaluation experiments. Selection of these optimum composites was made based on the mechanical properties of composites containing different proportions of each of the three polymers. Changes in the solution chemistry of these solutions as a result of the immersion of gypsum and its composites in SBF for up to 2 weeks were followed concurrently with the investigation of changes in the weights of the studied samples. Moreover, morphologies and phase composition of the immersed samples after different periods in the SBF solutions were monitored.

2. Materials and methods

Starting materials used in the current study included plaster of Paris ($CaSO_4 \cdot 1/2H_2O$) (BPB Formula Gmbh, Germany), poly(vinyl alcohol) (Aldrich); PI, poly(vinyl alcohol-*co*-vinyl acetate-*co*-itaconic acid) (Aldrich); PII, and poly(vinyl chloride-*co*-vinyl acetate-*co*-vinyl alcohol) (Aldrich); PIII. Analysis of the plaster starting material revealed a purity of 96% [23]. Composites were made by blending a powder mixture of the plaster of Paris and the solid powder with water. Powder-to-liquid ratio was decided based on a previously determined normal consistency of 46% of neat plaster [23]. Based on preliminary experiments, the following powder mixtures containing plaster of Paris and all polymers were investigated for their mechanical properties:

(a) Plaster of Paris + PI at percentages of 0.25, 0.5, 1.0, 2.0, 3.0, and 4.0 by weight.
(b) Plaster of Paris + PII at percentages of 0.2, 0.4, 0.6, 0.8, 1.0, 1.2, 1.4, 1.6, and 2.0 by weight.
(c) Plaster of Paris + PIII at percentages of 1, 2, 3, 4, 6, and 8 by weight.

Compressive strength measurements were carried out on cubic samples of both neat gypsum and gypsum–polymer composites with dimensions 2.5 cm × 2.5 cm × 2.5 cm. Samples cured at ambient conditions for 7 days were investigated for their compressive strength using a universal testing machine (FPZ100/1, HECKERT/THURINGER INDÜSTRIEWERKE, Germany) at a crosshead speed of 0.56×10^{-4} m/s. The mean value of five measurements for each sample was recorded. Composites with optimum compressive strengths were chosen for the SBF evaluation studies.

For the preliminary *in vitro* evaluation, two types of protein-free simulated body fluids (SBF and 1.5 SBF) were prepared as was previously described [24]. The composition of these solutions is given in Table 1. Two types of treatments were carried out for both neat gypsum and gypsum–polymer composites. In the first set of experiments, pre-weighed rectangular samples with dimensions 2.0 cm × 2.0 cm × 2.0 cm were immersed in 100 cm^3 SBF solution and kept at 37 °C for 2 weeks. Aliquot of 1.5 cm^3 was collected from each solution every day to be analyzed for Ca^{2+}, and PO_4^{3-} ions. Measurements of these ions were carried out in triplicates ($n = 3$), and the average was recorded. In the second set of experiments, the pre-weighed samples were soaked in SBF solution for a week, followed by soaking in 1.5 SBF for another week. At the end of each of the treatments, solid samples were collected, flushed with acetone, completely dried then weighed to determine weight change, if any, and to investigate its morphology changes as a result of immersion in SBF. Microstructural features of Au–Pd alloy-coated samples were investigated by scanning electron microscopy (SEM) (Hitachi, S-4700) equipped with an energy-dispersive X-ray (EDX) unit. Determinations of variations in the Ca^{2+}, and PO_4^{3-} ions were carried out on the collected aliquots by spectrophotometry and atomic absorption spectroscopy (AAS), respectively. Analysis of Ca^{2+} ions concentration was performed

Table 1
Ion concentrations of SBF and 1.5 SBF solutions compared with those of human blood plasma.

	Concentration (mM)							
	Na^+	K^+	Ca^{2+}	Mg^{2+}	HCO_3^-	Cl^-	HPO_4^{2-}	SO_4^{2-}
Blood Plasma	142.0	5.0	2.5	1.5	27.0	103.0	1.0	0.5
SBF	142.0	5.0	2.5	1.0	5.0	131.0	1.0	1.0
1.5 SBF	213.0	7.5	3.75	1.5	7.5	196.5	1.5	1.5

at $\lambda = 442$ nm by AAS using VARIAN-Spectr AA 300 using acetylene with N_2O gases. The KCl releasing buffer with concentration of 4000 ppm was added to each sample. Reproducibility of results was relatively 5–10%. On the other hand, analysis of PO_4^{3-} ions was performed using a SHIMADZU UV-1201 spectrophotometer at a wavelength of 830 nm. Error bars in time dependences represent maximum difference for 2 independent measurements. Changes in the pH of SBF solutions, in which samples were soaked for 2 weeks, were followed by measuring it on the sample surface by a pH-meter.

Phase composition of both neat gypsum and gypsum–polymer composites were also studied by X-ray powder diffraction (XRD) using an automated diffractometer (X'Pert PRO θ–θ), with a step size of 0.02°, counting time of 0.3 s/step and a scan range from 5° to 65° 2θ. A Cu Kα tube operated at 40 kV and 20 mA was used for X-rays generation. XRD patterns were manipulated and interpreted using the "High Score Plus" software package.

3. Results and discussion

Compressive strength results of all tested composites compared to polymer-free samples, after curing at ambient conditions for seven days, are shown in Fig. 1. Previous findings showed a progressive increase in the compressive strength of all samples with curing, achieving maximum values after seven days [23]. This was attributed to the completion of hydration of plaster of Paris and its conversion into gypsum as well as the full evaporation of the extra water that was added to improve the workability of the paste. In presence of polymers, all composites showed an overall improvement in their compressive strengths. Comparing composites to each other, the improvement followed the order: Gypsum–PI > Gypsum–PII > Gypsum–PIII. These differences may be explained in terms of the solubility of the original polymers, where PI is totally soluble, PII is slightly soluble, while PIII is insoluble in water. The presence of polymer in solution is thought to facilitate the reaction with the Ca^{2+} ions that are present in the medium during the process of dissolution of plaster and its re-precipitation as gypsum. The formation of calcium salt polymers containing –OH, –COOH, and –COOR groups is known to improve the mechanical properties of composites containing them [25]. On the other hand, the presence of –OH and –COOR groups along the completely insoluble PIII is still thought to be involved in the formation of salts with Ca^{2+} ions in solution through direct reaction with the –OH groups and the hydrolysis of the –COOR groups and the consequent formation of Ca-salts [26]. Due to the insolubility of PIII, the impact of these reactions on the compressive strengths of the obtained composites was not pronounced. Fig. 2 shows SEM micrographs of fractured surfaces of gypsum and its composites after curing for 7 days at ambient conditions. Gypsum is characterized by its high crystallinity and appears as long needles with an average aspect ratio of 7. Strength of polymer-free gypsum samples arises from the mechanical interlocking among the gypsum fibers within the sample, as shown in Fig. 2a. Adding a polymer to these fibers, as shown in Fig. 2b–d, seems to augment them through adsorption on their surfaces. This adsorption, as discussed above, takes place through chemical interaction between each of the polymers and the gypsum fibers. The overall augmented structure, therefore, explains the improvement in the mechanical properties of the composites compared to polymer-free gypsum samples. A closer look at the compressive strength results indicates the progressive enhancement of compressive strength of composites with increasing the polymer in all composites. However, it appears that the presence of excessive amounts of each of the polymers is not recommended as a decrease in the compressive strength values was noticed. Based on these findings, composites containing the optimum concentrations of these polymers were chosen for the preliminary *in vitro* evaluation in protein-free SBF solutions. Those compositions together with a summary of their optimum final setting times and compressive strength values are given in Table 3. An average setting time of 30 ± 2 min was found of all composites.

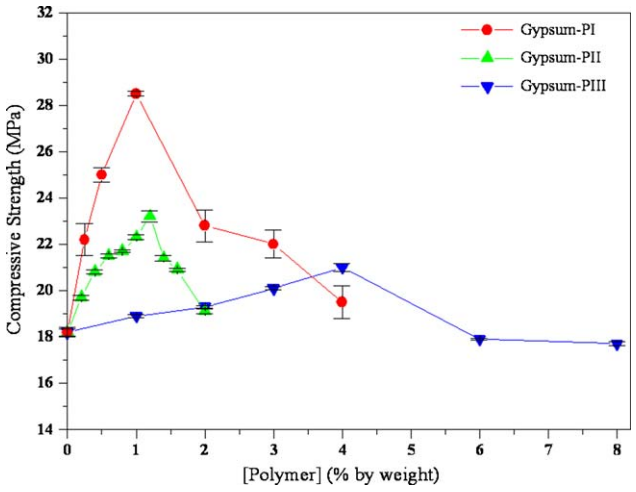

Fig. 1. Compressive strength of gypsum–polymer composites as a function of [polymer] in wt%.

Fig. 3a shows the variations in the concentrations of Ca^{2+} and PO_4^{3-} ions in SBF, as a result of soaking gypsum and its

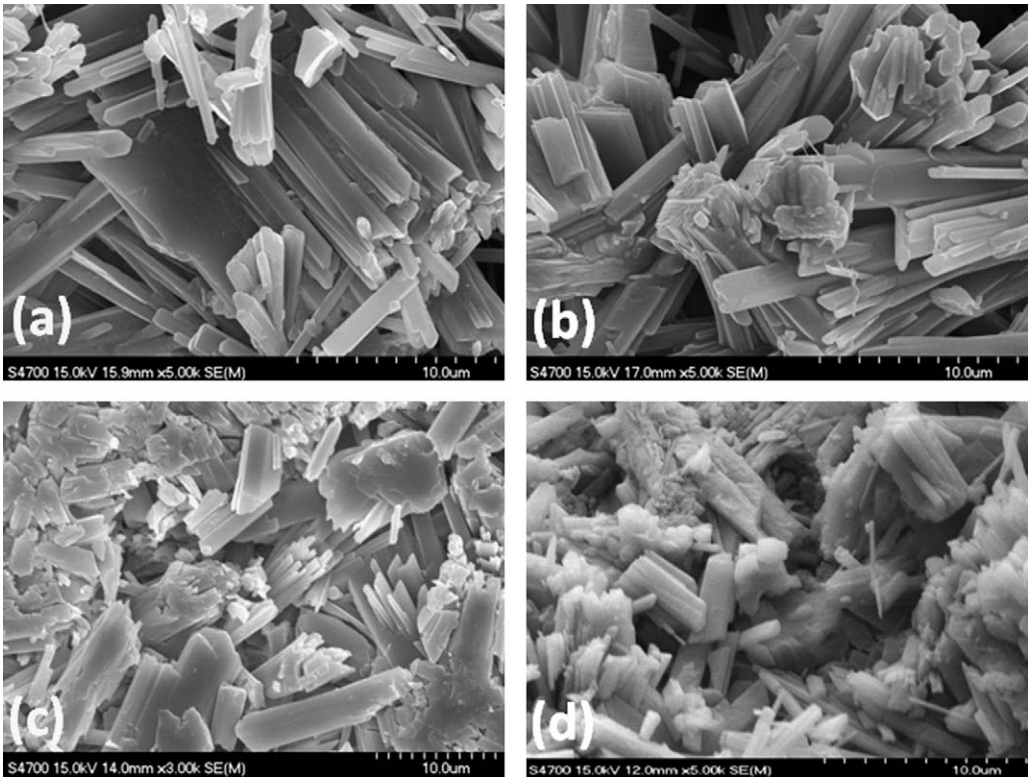

Fig. 2. Scanning electron micrographs of the fractured surfaces of (a) neat gypsum, (b) gypsum–PI, (c) gypsum–PII, and (d) gypsum–PIII composites after curing at ambient conditions for 7 days.

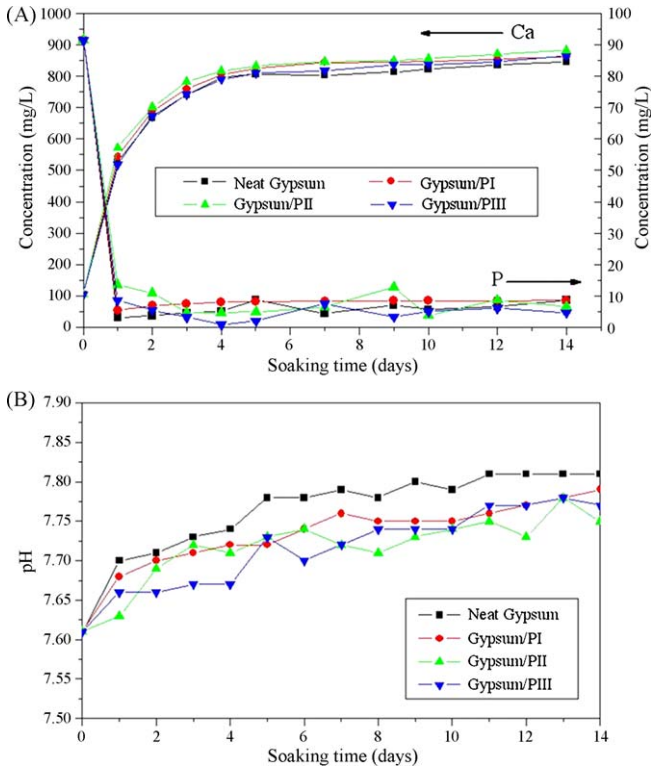

Fig. 3. (a) Total concentrations of Ca and P in SBF solutions after immersing gypsum and gypsum–polymer composites for different time periods. (b) Variations in the pH of SBF solutions as a result of immersing gypsum and gypsum–polymer composites for different time periods.

composites for up to 2 weeks. Concentrations were expressed as total Ca and P in these solutions. A pronounced increase in the concentration of calcium, and a concurrent decrease in the concentration of phosphate, was observed. Deposition of apatite on substrates containing certain functional groups, such as silicates and carboxylates, was previously observed [27]. This process mimics a similar process that takes place in nature, where mineralization of collagen takes place via attracting calcium and phosphate ions from the surrounding body fluids [28–29]. Formation of apatite nuclei is usually followed by growth of these nuclei into apatitic nanocrystals [29]. Mineralization of collagen is attributed to the presence of carboxylic and amino groups along their chains [28]. The currently investigated polymers contain (–COOH) groups along its structures as well as (–OH) and (–COOR) groups. The presence of these groups in the investigated composites are thus considered the sites on which apatite was deposited. Deposition of apatite takes place by consuming Ca^{2+} and PO_4^{3-} ions from solutions, which are known to be supersaturated with respect to apatite. Apatite deposition was thus expected to lead to a decrease in the concentrations of both ions from their solutions

Table 2
Weight loss (%) of gypsum and gypsum–polymer composites after immersion in SBF and 1.5 SBF solutions.

	Gypsum	Gypsum/PI	Gypsum/PII	Gypsum/PIII
SBF	2.9	4.2	4.3	2.4
1.5 SBF	22.9	15.7	15.8	14.3

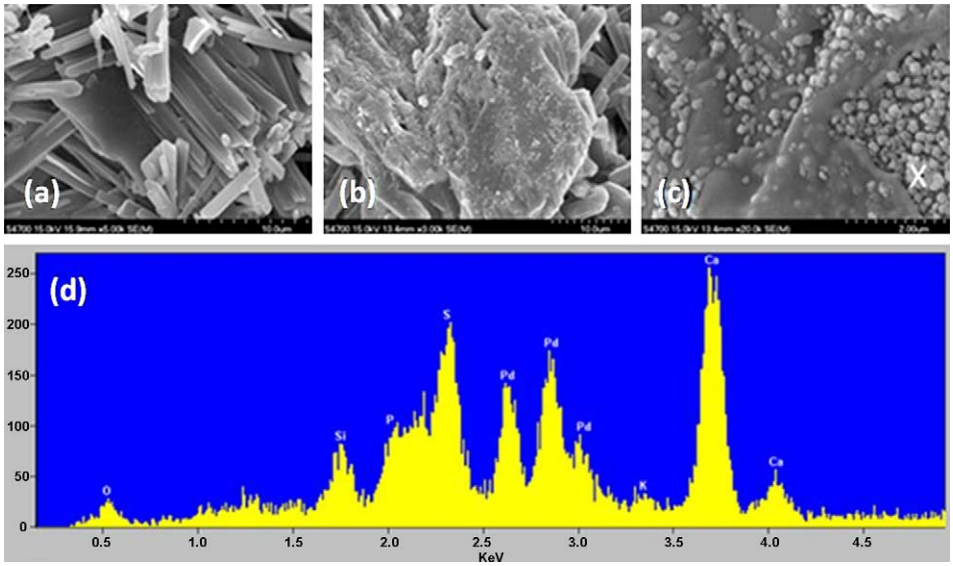

Fig. 4. Scanning electron micrographs of (a) neat gypsum, (b) gyspum after treatment in SBF followed by 1.5 SBF solutions for a week in each, (c) same as in (b) at a higher maginification. (d) Energy-dispersive X-ray analysis of the spot marked by (X) in micrograph (c).

[27]. On the contrary, an increase in the Ca^{2+} concentration in the tested solutions was observed. This is, therefore, attributed to the resorption of gypsum from the investigated composite samples. This trend indicates that the rate of gypsum resorption is higher than the rate of apatite deposition on all surfaces. This was also confirmed by measuring changes in the weight of these samples as a result of the SBF treatment for 2 weeks. Table 2 shows the weight loss observed in all samples, confirming the previous finding that the weight loss due to resorption of gypsum is more pronounced than the weight gain due to deposition of apatite. The rate of resorption, however, is shown to decrease after 4 days, and continued in the same fashion until the end of experiments. These findings were also confirmed by pH measurements where an increase in the solution pH was observed over time, as shown in Fig. 3b. The slow rate of gypsum resorption after 4 days was also reflected in a less pronounced change in the pH of the solutions, achieving a plateau of pH 7.7 $\pm$ 0.05 after 4 days in all samples. Despite the absence of polymers in the neat gypsum samples, similar trends were observed and were confirmed by SEM analysis. Fig. 4a–c shows SEM micrographs of a blank untreated polymer-free gypsum sample as well as polymer-free gypsum samples aged in SBF then 1.5 SBF for a week in each. Fig. 4b shows the formation of a coating on gypsum crystals causing them to agglomerate. Fig. 4c shows a higher magnification of the coating appearing as apatitic spherolites. An elemental analysis of these spherolites was carried out by EDX. The presence of Ca and P in these spherolites is evident, indicating the chemical composition of the coating. The presence of S in the EDX pattern may be attributed to the underlying highly crystalline gypsum crystals. The agglomeration of gypsum crystals as a result of soaking it in SBF and 1.5 SBF solutions may be attributed to the fusion of the gypsum crystals as they undergo degradation. The concurrent precipitation of apatite, therefore, enhanced the gelling of gypsum crystals together. Deposition of apatite on gypsum crystals may be attributed to the increase of $[Ca^{2+}]$ ions in SBF as a result of the resorption of gypsum. As mentioned before, this increase in a solution that is readily supersaturated with respect to apatite should lead to its deposition on the existing surfaces. The SEM/EDX results are thus in accord with those given in Fig. 3a and b for polymer-free gypsum samples. Among the functional groups, that were shown to help in the nucleation of apatite from SBF solutions, is the sulfonate ($–SO_3^-$) group [30]. Previous work by Chan et al. [21] also indicated the formation of apatite from SBF solutions on neat gypsum samples, which is, therefore, in accordance with our current findings, and indicates that sulphate ($–SO_4^-$) groups could also act as nucleating sites for apatite deposition.

Development of phase composition of all samples was followed by X-ray diffraction. Fig. 5 shows XRD patterns of polymer-free gypsum and gypsum composites containing the studied polymers. All patterns showed a complete conversion of plaster of Paris to gypsum, since no peaks of the former phase were detected. Due to the high crystallinity of the gypsum

Table 3
Setting time, and compressive strength values for gypsum and gypsum–polymer composites.

Type of composite	[Polymer] (%)	Setting time (min s)	Compressive strength[a] (MPa)
Neat gypsum	0.0	30 00	18.2 $\pm$ 1.2
Gypsum/PI	1.0	33 15	28.5 $\pm$ 0.1
Gypsum/PII	1.2	33 00	23.2 $\pm$ 0.3
Gypsum/PIII	4.0	27 15	21.0 $\pm$ 0.2

[a] Measurement taken after curing for 7 days at 37 °C.

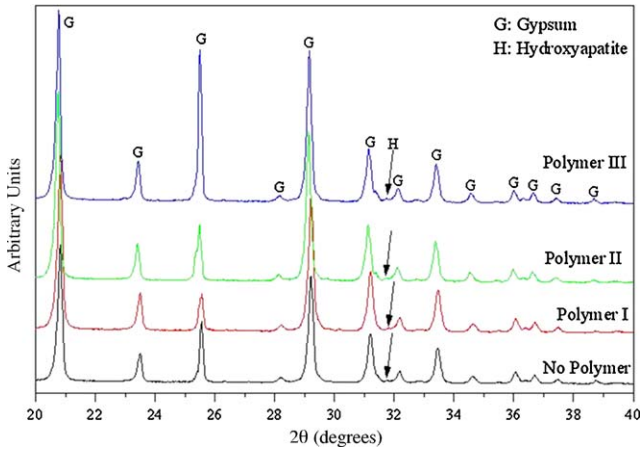

Fig. 5. Phase compositions of gypsum and gypsum–polymer composite solids after immersion I SBF and 1.5 SBF solutions for a week in each.

crystals, its characteristic peaks dominated all patterns, making it difficult to find an evidence for the formation of apatite deposits. However, a closer look at the patterns shows the presence of traces of the 2 1 1 peak of HAp at 2θ value of 31.8°. This peak was found in all samples, with relatively different intensities after treatment in SBF and 1.5 SBF solutions.

The extent of deposition of apatite on polymer-containing composites was variable, depending on the type and structure of the polymer as well as the immersion periods in SBF and 1.5 SBF. Fig. 6a–c shows SEM micrographs of gypsum composites containing the three polymers after 2 weeks of soaking in SBF solutions. The well-known spherolitic morphology of the apatite grown from SBF [31] can be observed in the three Micrographs in Fig. 6a–c and marked by X_1, X_2, and X_3. The elemental composition of these spherolites was also confirmed by EDX analysis, as shown in Fig. 6d for those grown on gypsum–PII composite. It is evident from the micrographs that the extent of apatite deposition was more pronounced in gypsum/PII composites compared to gypsum/PI composites. The presence of –OH groups, as those found along PI chains, are known to bind Ca^{2+} ions from solutions [22]. Therefore, it was expected to see more apatite deposition in gypsum/PI composites than what was actually shown in Fig. 6a. This could be attributed to the high solubility of PI (PVA) in water. The presence of PVA in solution is thought to result in less polymer surfaces that can grow apatite from solution on them. Despite these facts, apatite deposition took place, and was confirmed by EDX. This could be attributed to the deposition of apatite on the PVA thin films immobilized on the formed gypsum crystals, which takes place via bonding to the Ca^{2+} ions in solution that result from the conversion of plaster of Paris into gypsum. On the other hand, the presence of two (–COOH) groups and one (–$COOCH_3$) group in addition to the (–OH) group per monomer of PII rendered the polymer slightly soluble, thus increased the extent of apatite deposition on these active sites. In addition, those groups collectively participated and favoured a higher extent of apatite deposition than composites containing PVA (PI). The presence of apatite deposition on the gypsum composite containing PIII, which is insoluble in water, supports the assumption that both OH and ester groups along the polymer chains participated in the formation of apatite deposits. Additionally, the presence of a highly electronegative atom such as Cl in the polymer structure may also be considered a point of attraction to the positively charged Ca^{2+} ions from solution. Deposition of apatite on the ester (–$COOCH_3$) sites could be related to the local basic hydrolysis of these groups during the conversion of plaster of Paris into gypsum. Similar findings were observed during the treatment of a polyphosphazene, that contains ester groups along its chains, in SBF [26]. Apatite deposition on composites containing PIII, therefore, took place in a slightly different fashion where it

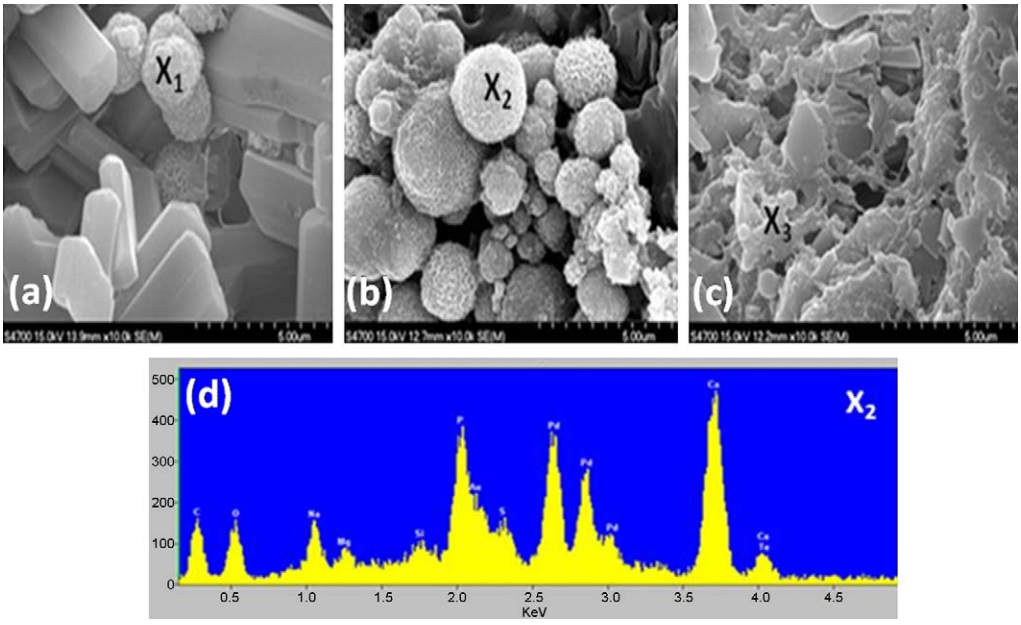

Fig. 6. Scanning electron micrographs of gypsum composites containing (a) polymer I, (b) polymer II, and (c) polymer III after immersion in SBF solutions for 2 weeks, (d) energy-dispersive X-ray analysis of the spot marked by (X) in micrograph (b).

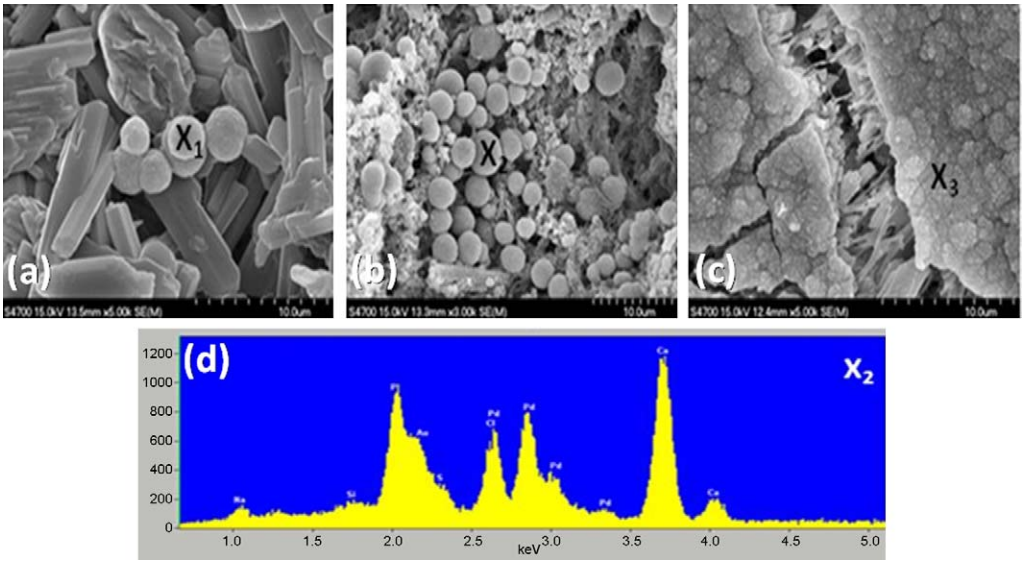

Fig. 7. Scanning electron micrographs of gypsum composites containing (a) polymer I, (b) polymer II, and (c) polymer III after immersion in SBF for 1 week, followed by 1.5 SBF for another week. (d) Energy-dispersive X-ray analysis of the spot marked by (X) in micrograph (b).

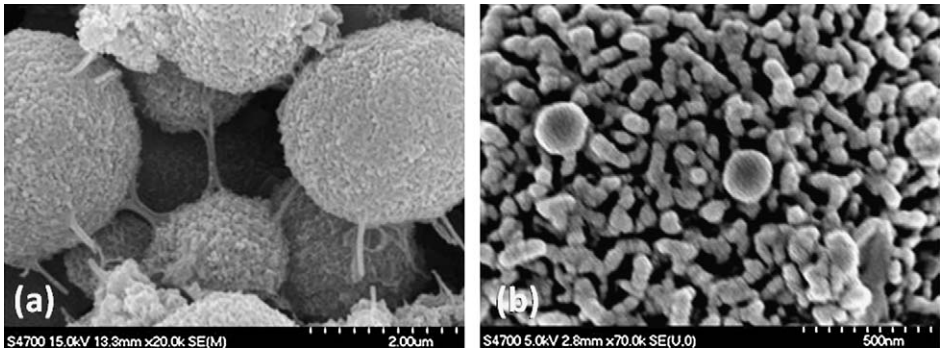

Fig. 8. Scanning electron micrographs of (a) apatite spherolites grown on a gypsum/polymer III composite, and (b) detailed ultrastructure of a spherolite grown on gypsum/polymer III composite.

appeared as continuous layers. Its composition was also confimed by EDX analysis to be apatitic in nature.

Biomimetically deposited apatite spherolites, on solid surfaces, are known to grow if soaked in a highly concentrated SBF solution, in this case called 1.5 SBF [27]. Fig. 7a–c shows SEM micrographs of gypsum–polymer composites after the second treatment in 1.5 SBF solutions for 1 week. Formation of more apatite deposites is evident in all composites compared to those treated in SBF solutions only. Comparing the three composites with each other, the least extent of apatite deposition was found in gypsum–PI composites, while gypsum–PIII composites were found to develop a continuous layer of apatite on their surfaces. Fig. 7d shows an EDX pattern of those spherolites grown on gypsum–PII composites, as an example, confirming the chemical composition of those spherolites to be apatitic in nature. Although apatite deposition on gypsum–PII composites did not take place in the form of layers, the extensive presence of apatite spherolites was reflected in higher intensity Ca and P EDX peaks with lower S peak. Detailed ultrastructure of apatite spherolites grown on gypsum–PIII composites is shown in Fig. 8. The average spherolite size is 2 μm, and each spherolite is made of nanoapatite crystallites with an average dimension of 200 nm. The presence of bridges between the apatite spherolites, shown in Fig. 8a, explains the formation of a continuous apatitic layer on gypsum–PIII composites where apatite spherolites are grown side-by-side on the polymer-coated gypsum crystals.

Taken together, these results clearly indicate the possibility of growing apatite with bone-like morphology on gypsum and its composites, suggesting their potential application as bone cements after being subjected to thorough *in vitro* and *in vivo* evaluations. Moreover, the presence of a bioresorbable gypsum phase in these composites is further expected to result in the formation of pores in a manner that can be synchronized with tissue integration within the set cement after implantation to facilitate the integration of these cements with the surrounding bone tissues after.

4. Summary

Compressive strength was measured for gypsum and its composites with PVA and its copolymers after curing at ambient conditions for 7 days. All Composites showed improved mechanical properties compared to polymer-free

gypsum samples. Composites with highest compressive strengths were further subjected to preliminary *in vitro* evaluation in protein-free SBF solutions. Deposition of apatite spherolites on gypsum–polymer composites was observed with the three different types of polymers used. Moreover, an evidence of the deposition of apatite on polymer-free gypsum samples was also given. Deposition of apatite was concurrent to the normal resorption of gypsum in all samples. Confirmation of the deposition of apatite on all samples was carried out using SEM and EDX techniques. Deposition of apatite on gypsum–polymer composites was attributed to the presence of functional groups along the polymer chains that are known to act as nucleating sites for apatite. Our previous studies showed the formation of chemical bonds between each of the used polymers and gypsum during the process of conversion of plaster of Paris into gypsum. Immobilization of the polymeric chains on gypsum, as a result of their chemical interaction, formed surfaces with nucleating sites for apatite deposition. A water-insoluble copolymer, was, therefore, found to have the greatest extent of apatite coating. On the other hand, the unprecedented deposition of apatite on polymer-free gypsum samples was related to the resorption of gypsum, that resulted in an increase of total [Ca^{2+}] ions in solution exceeding the supersaturating limit of apatite in these solutions. This was consequently followed by precipitation of gel-like apatitic layer on the gypsum crystals, leading to their augmentation, as was observed by the SEM micrographs of these samples and was also supported by their analysis by EDX. Deposition of apatite on the investigated samples indicates their high tendency to bond with bone if used as a bone cement for bone construction. Moreover, the presence of a resorbable fibrous ingredient; gypsum, will provide channels for tissue integration and a consequent enhanced bonding with the surrounding bone. Further *in vitro* and *in vivo* studies are, however, required to fully characterize these composites.

Acknowledgement

This work was a part of the project No 2A-1TP1/063, realized under financial support of the Ministry of industry and trade, Czech Republic. It was also a part of the research programme MSM 6046137302 Preparation and research of functional materials and material technologies using micro- and nanoscopic methods.

References

[1] B. Flautre, J. Lemâitre, C. Maynou, P. Van Landuyt, P. Hardouin, Influence of polymeric additives on the biological properties of brushite cements: an experimental study in rabbit, J. Biomed. Mater. Res. 66A (2003) 214–223.
[2] P. Maragos, N.F. Bissada, R. Wang, R.P. Cole, Comparison of three methods using calcium sulfate as a graft/barrier material for the treatment of class II mandibular molar furcation defects, Int. J. Periodont. Rest. Dent. 22 (2002) 493–501.
[3] C.K. Kim, H.Y. Kim, J.K. Chai, K.S. Cho, I.S. Moon, S.H. Choi, J.S. Sottosanti, U.M. Wikesjo, Periodontal repair in intrabony defects treated with a calcium sulfate implant and calcium sulfate barrier, J. Periodont. 69 (1998) 982–988.
[4] G.E. Pexcora, D. DeLeonardis, C.D. Rocca, R. Cornelini, C. Cortesini, Short-term healing following the use of calcium sulfate as a grafting material for sinus augmentation: a clinical report, Int. J. Oral Max Imp. 13 (1998) 866–873.
[5] M. Nilsson, E. Fernandez, S. Sarda, L. Lidgren, J.A. Planell, Bone-defect healing with calcium-sulfate particles and cement: an experimental study in rabbit, J. Biomed. Mater. Res. 68B (2002) 199–208.
[6] J. Lemâitre, E. Munting, A. Mirtchi, STOMATO 91 (1991) 1–5.
[7] S. Sato, T. Koshino, T. Saito, Osteogenic response of rabbit tibia to hydroxyapatite particle-plaster of paris mixture, Biomaterials 19 (1998) 1895–1900.
[8] P.A. Glazer, U.M. Spencer, R.N. Alkalay, J. Schwardt, In vivo evaluation of calcium sulfate as a bone graft substitute for lumbar spinal fusion, Spine J. 1 (2001) 395–401.
[9] H. Guo, J. Wei, C.S. Liu, Development of a degradable cement of calcium phosphate and calcium sulphate composite for bone reconstruction, Biomed. Mater. 1 (2006) 193–197.
[10] M.A. Rauschmann, T.A. Wichelhaus, V. Stirnal, E. Dingeldein, L. Zichner, R. Schnettler, V. Alt, Nanocrystalline hydroxyapatite and calcium sulphate as biodegradable composite carrier material for local delivery of antibiotics in bone infections, Biomaterials 26 (2005) 2677–2684.
[11] A. Çolak, Characteristics of aqcrylic latex-modified and partially epoxy-impregnated gypsum, Cem. Concr. Res. 31 (2001) 1539–1547.
[12] S. Eve, M. Gomina, J. Hamel, G. Orange, Investigation of the setting of polyamid fiber/latex filled plaster composites, J. Eur. Ceram. Soc. 26 (2006) 2541–2546.
[13] A. Çolak, Physical and mechanical properties of polymer–plaster composites, Mater. Lett. 60 (2006) 1977–1982.
[14] C.K. Chua, K.F. Leong, K.H. Tan, F.E. Wiria, C.M. Cheah, Development of tissue scaffolds using selective laser sintering of polyvinyl alcohol/hydroxyapatite biocomposite for craniofacial and joint defects, J. Mater. Sci. Mater. Med. 15 (2004) 1113–1121.
[15] N. Degirmenbasi, D.M. Kalyon, E. Birinci, Biocomposites of nanohydroxyapatite with collagen and poly(vinyl alcohol), Colloids Surf. B: Biointerfaces 48 (2006) 42–49.
[16] T. Taguchi, A. Kishida, M. Akashi, Apatiteformation on/in hydrogel matrices using an alternate soakingprocess: II. Effect of swelling ratios of poly(vinyl alcohol) hydrogel matrices on apatite formation, J. Biomater. Sci. Polym. Ed. 10 (1999) 331–339.
[17] F.E. Wiria, C.K. Chua, K.F. Leong, Z.Y. Quah, M. Chandrasekaran, M.W. Lee, Improved biocomposite development of poly(vinyl alcohol) and hydroxyapatite for tissue engineering scaffolds fabrication using selective laser sintering, J. Mater. Sci. Mater. Med. 19 (2008) 989–996.
[18] D. Zahn, O. Hochrein, A. Kawska, J. Brickmann, R. Kriep, Towards an atomistic understanding of apatite-collagen biomaterials: linking molecular simulation studies of complex-crystal- and composite-formation to experimental findings, J. Mater. Sci. 42 (2007), 8966-2973.
[19] T. Kokubo, H. Takadama, How useful is SBF in predicting *in vivo* bone bioactivity, Biomaterials 27 (2006) 2907–2915.
[20] M. Bohner, J. Lemaitre, Can bioactivity be tested in vitro with SBF solution? Biomaterials 30 (2009) 2175–2179.
[21] H. Chan, D. Mijares, J.L. Ricci, *In vitro* dissolution of calcium sulphate: evidence of bioactivity, Trans. 7th World Biomater. Congress, 2004, p. 627.
[22] T. Hayami, K. Matsumura, M. Kusunoki, H. Nishikawa, S. Hontsu, Imparting cell adhesion to poly(vinyl alcohol) hydrogel by coating with hydroxyapatite thin film, Mater. Lett. 61 (2007) 2667–2670.
[23] H.F. El-Maghraby, O. Gedeon, A.A. Khalil, Formation and Characterization of Poly(vinyl alcohol-co-vinyl acetate-co-itaconic acid)/Plaster Composites, Part I: Characterization of β-Hemihydrate Plaster, Review of Alexander Dubček University of Trenčin, Slovakia, vol. 1, no. 3, 2007, pp. 39–44, , ISSN 1337-6047.
[24] C. Ohtsuki, T. Kokubo, T. Yamamuro, Mechanism of apatite formation on $CaO–SiO_2–P_2O_5$ glasses in a simulated body fluid, J. Non-cryst. Solids 143 (1992) 84–92.
[25] Y.E. Greish, P.W. Brown, An evaluation of mechanical property and microstructural development in HAp-Ca polycarboxylate biocomposites prepared by hot pressing, J. Biomed. Mater. Res. Appl. Biomater. 53 (2000) 421–429.

[26] Y.E. Greish, J.D. Bender, S. Lakshmi, P.W. Brown, H.R. Allcock, C.T. Laurencin, Low temperature formation of hydroxyapatite-poly(alkyl oxybenzoate)phosphazene composites for biomedical applications, Biomaterials 26 (2005) 1–9.
[27] C. Ohtsuki, H. Kushitani, T. Kokubo, S. Kotani, T. Yamamura, Apatite formation on the surface of ceravital-type glass-ceramic in the body, J. Biomed. Mater. Res. 25 (1991) 1363–1370.
[28] Y.E. Greish, J.D. Bender, S. Lakshmi, P.W. Brown, H.R. Allcock, C.T. Laurencin, Formation of hydroxyapatite-polyphosphazene polymer composites at physiologic temperature, J. Biomed. Mater. Res. 77A (2006) 416–425.
[29] J.F. Shackelford, Bioceramics, Gordon & Breach Science, New York, 1999.
[30] I.B. Leonor, H.–M. Kim, F. Balas, M. Kawashita, R.L. Reis, T. Kokubo, T. Nakamura, J. Mater. Sci. Mater. Med. 18 (2007) 1923–1930.
[31] T. Kokubo, A/W glass-ceramic: processing and properties, in: L.L. Hench, J. Wilson (Eds.), An Introduction to Bioceramics, World Scientific Advanced, Singapore, 1993, pp. 75–88.

Práce **[8]**

Hlaváč J., Rohanová D., Helebrant A.: The effect of TRIS-buffer on the leaching behaviour of bioactive glass-ceramics. Ceramics- Silikáty 38 (3-4): 119-122, 1994.

Podíl: 70%: návrh a realizace experimentu, analýzy, zpracování výsledků, příprava publikace

THE EFFECT OF TRIS-BUFFER ON THE LEACHING BEHAVIOUR OF BIOACTIVE GLASS-CERAMICS

JAN HLAVÁČ, DANA ROHANOVÁ, ALEŠ HELEBRANT

Department of Glass and Ceramics, University of Chemical Technology 166 28 Praha 6, Czech Repulic

Received 13. 4. 1994

The leaching of bioactive glass-ceramics of the apatite-wollastonite type in water and in a simulated body fluid was studied using standard tests with granular specimens and exposures at 37 °C. The solutions were analyzed for Ca and SiO_2 and the evolution of both concentrations with time was examined in comparison with the CaO/SiO_2 ratio. A considerable increase in the rate of leaching was found in buffered solutions due to the effect of TRIS on the conditions for the deposition of a hydroxyapatite protective layer on the leached surface.

INTRODUCTION

Bioactive glasses and glass-ceramics can become attached to the bone tissue due to the formation of a joining layer of hydroxyapatite which results from a chemical reaction at the interface between the bone and the biomaterial. The blood plasma participates on the reaction mechanism as a transport medium and as a source of hydroxyapatite (HA) components – mainly calcium and phosphorus. The release of calcium ions into the body liquid by extraction from the biomaterial increases their concentration beyond the solubility limit and enables the precipitation and deposition of HA. For this reason the leaching behaviour of bioactive materials in a suitable simulated liquid has been studied in vitro by many authors (1–7).

During the leach tests, the changing pH values of the solution can affect the rate of the solid-liquid interaction. There are several possibilities how to eliminate that effect: 1) by periodical or continuous exchange ot the leachant, 2) using pH stat titration technique (8, 9) or 3) using suitable buffers. The last method is the most simple and most common but involves the possibility of affecting the leaching rate by the chemical reactivity of the buffer (10, 11).

TRIS, i.e. tris(hydroxymethyl)aminomethane, has been frequently used as a buffer in studies of the leaching of bioactive glasses and glass-ceramics in solutions simulating the composition of blood plasma (simulated body fluid – SBF). The effect of TRIS on Si and Ca release from a glass-ceramic material was studied in this work.

EXPERIMENTAL

Leaching tests were performed with specimens of bioactive glass-ceramics supplied by Lasak Co*. The material was composed af apatite, wollastonite, whitlockite and the residual glass phase. The standard granular specimens were prepared of 0.315–0.50 mm grain size, equivalent to a surface area of approx. 110 cm^2/g and exposed to the leaching attack of the simulated body fluid (SBF) having the following composition: 142,0 Na^+, 5.0 K^+, 1.5 Mg^{2+}, 2.5 Ca^{2+}, 148.0 Cl^-, 4.2 HCO_3^- and 1.0 HPO_4^{2-} (mmol/l). TRIS was added to the solution in the amount of 7,47 g/l and pH of the solution was adjusted by addition of HCl to 7.45 (room temperature) or 7.25 (37 °C). All of the leaching exposures were carried out at 37 °C. The so-

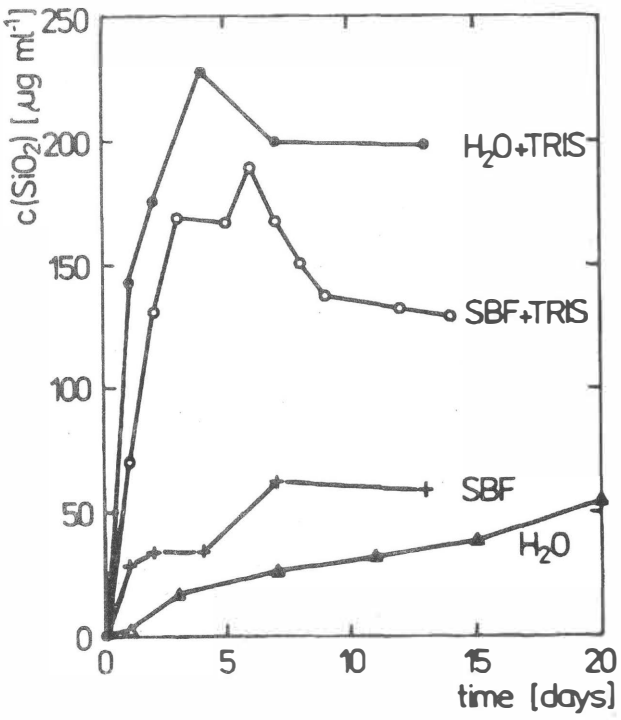

Fig. 1. SiO_2 concentration in the solution after leaching of the glass-ceramics in a buffered and a non-buffered SBF, and in distilled water.

*Lasak Co., producer of biomaterials, Prague 6, Papírenská 25

lutions were than analyzed using AAS for Ca and the silicon-molybdate photometric method for SiO_2.

Similar leaching experiments were performed in SBF without any buffer addition and in distilled water, again with or without the TRIS buffer. During all leaching exposures, the interaction of the specimens with the liquid occurred, under static conditions, with a surface to volume ratio of 1.1–1.5 cm^{-1}. Besides the concentration changes, pH was measured after leaching in the resulting solutions.

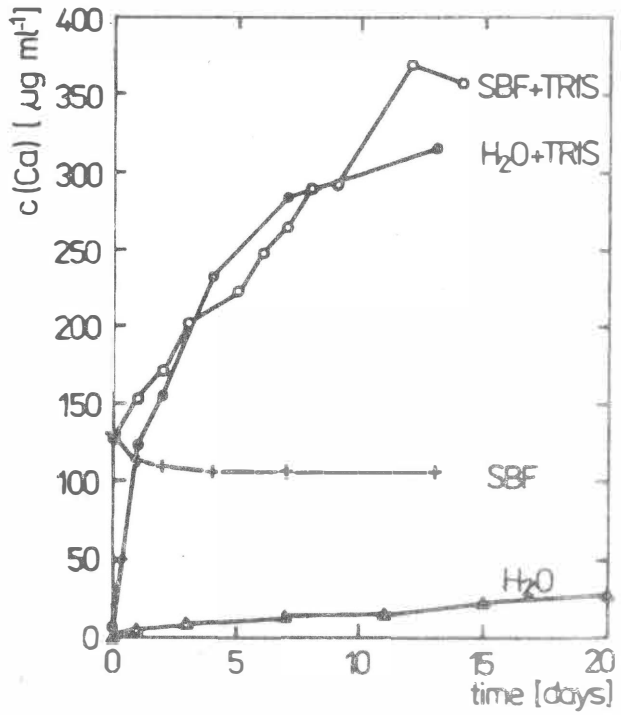

Fig. 2. Calcium concentration in the solution after leaching of the glass-ceramics in a buffered and a non-buffered SBF, and in distilled water.

RESULTS AND DISCUSSION

The silica concentrations in solution in terms of time are shown in Fig. 1. The results for distilled water depend very considerably on the presence of TRIS, the dissolution being more extensive in the buffered solution, although the pH was changing only within the range 7.45–8.1.

In the case of SBF, there was also a higher value of dissolved SiO_2 in the presence of TRIS, with an apparent trend to supersaturation. Both curves approached to a constant value which was higher about two times in the buffered solution.

The concentration change of Ca is shown in Fig. 2. The release of Ca into distilled water was higher by an order of magnitude in the presence of TRIS. Similarly, the release of Ca into buffered SBF was more extensive and high values of Ca concentration in the solution were attained continuously, whereas in non-buffered SBF a lower constant concentration level was established. The original value of pH = 7.45 was increased to 8.0 and 8.5 in buffered and non-buffered SBF solutions, respectively.

According to common experience, the changes in pH between 7.5 and 8.5 cannot be considered to be a direct cause of the differences shown above; moreover, they should act in the oposite direction. The following hypothetical explanation can be offered, based on a widely accepted mechanism of leaching which was confirmed to be valid also for the glass-ceramics studied in the present paper (13):

During interaction of silicate materials with aqueous solutions a leached layer is formed on the surface by selective extraction of cations which are transferred from the material into the solution by diffusion through this layer of gradually increasing thickness. This process can be accompanied by deposition of a secondary film on the reaction surface from the suspersaturated solution [12, 14]. The film then retards the diffusion as well as the surface dissolution of silica. The two compounds followed in this work (i.e. Ca and SiO_2) represent diffusing and dissolving species, respectively.

The following mechanism of TRIS involvement comes into consideration: TRIS is known as a compound forming complexes with various cations including Ca^2. In the case od interaction between the bioactive material and SBF, calcium ions released from the material are strongly bound into a soluble complex so that they are not available for deposition of a surface layer exhibiting a protective effect.

Several aspects should be considered in this connection: the ratio of CaO to SiO_2 in the solution after leaching, the solubility product for hydroxyapatite, and finally, the amount of CaO which can be bound into the complex with TRIS.

The CaO/SiO_2 weight ratio in the solution is shown in Fig. 3 where CaO is expressed as the change of its concentration in comparison with the actual one in the case of SBF. In non-buffered solutions, the CaO/SiO_2 value is low and remains at an approximately constant level. A considerable increase of the ratio occurs in buffered solutions. The values of CaO/SiO_2 indicate that congruent dissolution does not occur in the systems followed and that, consequently, depleted layers of different compositions are formed in different solutions. The permeability of these layers for diffusing species can also vary.

The following conclusions can be made from a comparison of the CaO/SiO_2 ratio with the concentration changes of Ca and SiO_2:

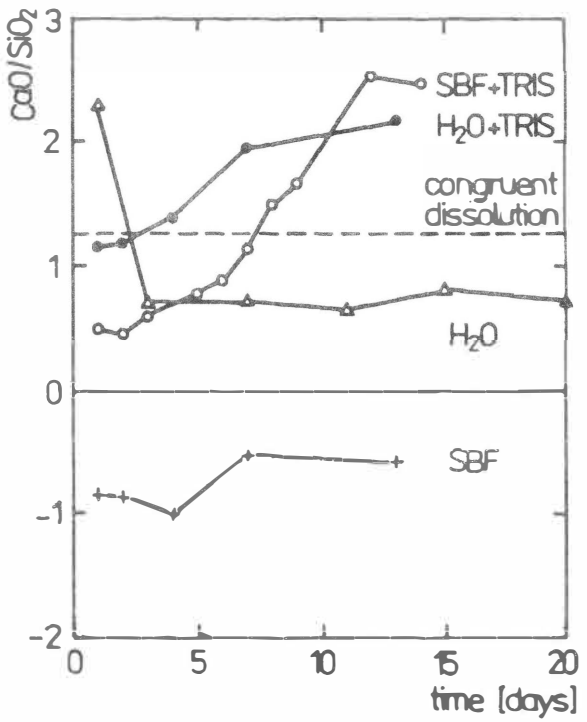

Fig. 3. The weight ratio of CaO to SiO_2 in the solutions after leaching (ΔCaO related to the original concentration in the solution).

a) In distilled water (without TRIS), CaO remains chemically bound in the surface as calcium phosphate or silicate (the silica concentration in the solution increases whereas CaO/SiO_2 remains constant and the Ca concentration does not show any great change – see Figs. 1–3).
b) In SBF without TRIS, the CaO/SiO_2 ratio has a negative, nearly constant value, probably as a result of the CaO consumed in HA formation. In agreement with this conclusion, the concentration of Ca decreases with time (see Fig. 2).
c) The increase in the CaO/SiO_2 ratio in terms of time in TRIS-buffered solutions (in both distilled water and SBF) corresponds with the continuous increase of Ca (Fig. 2) and with the increase in silica content to a supersaturated value followed by a decrease to the final saturated limit (Fig. 1). A steep increase in both concentrations at the beginning of the interaction indicates that calcium ions preferably enter the complex and are not available for HA layer formation which would otherwise suppress the leaching.

The deposition of hydroxyapatite layer on the reaction surface represents an important process influencing the leaching rate in a way associated with pH of the solution: The rate of growth of HA layer is a function of relative supersaturation $S = (I/K)^{1/18}$ [15] where I is the ion activity product and K the solubility product in respect to hydroxyapatite. Assuming that calcium in SBF is in the form of Ca^{2+} only and pK = 117.2 [16], then at 37 °C (pH = 7,3), pI = 94.38 and S = 18.5. At pH = 7.9 the supersaturation is twice as high (pI = 89.1 and S = 36.4). Unfortunately there is a lack of equilibrium data on the TRIS-calcium complex but assuming that 50% of calcium is bound in the complex, supersaturation decreases to approx. 66% (pI = 97.4 and S = 12.6). This means that relatively small changes of the solution pH result in a considerable change of suspersaturation and consequently, the HA layer growth is slower in the buffered solutions.

The results indicate that leaching of biomaterials in simulated liquids brings about some doubt concerning the reliability of leaching tests in vitro for conclusions to be made on the bioactivity of various materials in vivo. Moreover, the SBF used represents only the inorganic part of the blood plasma. In order to find out if albuminous compounds of the plasma can affect the leaching behaviour, experiments were carried out using the SBF enriched with albumin. The results shown in Fig. 4 indicate that the leaching behaviour of the material studied is very similar in both the SBF+TRIS and SBF+albumin solutions. Therefore a good prediction capability can be attributed to the

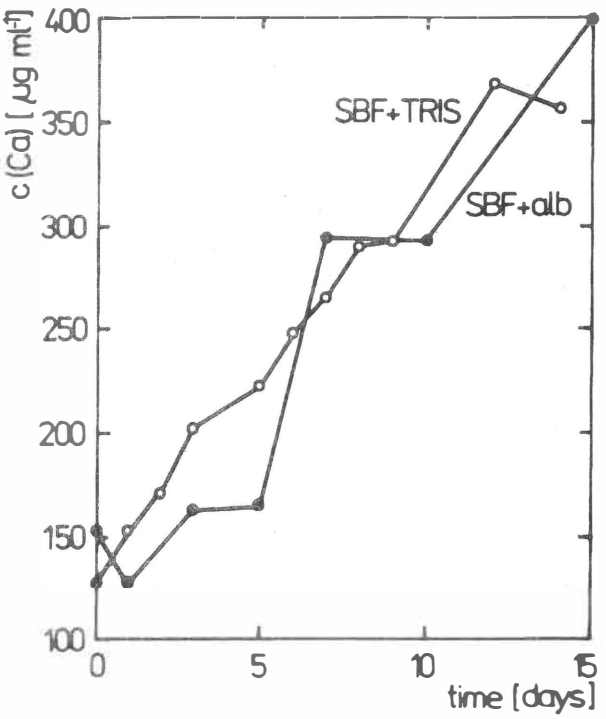

Fig. 4. Calcium ion concentration in the solution after leaching of the glass-ceramics in buffered SBF and in SBF + albumin.

tests described above, at least for the type of material examined in the present study.

CONCLUSIONS

The presence of TRIS-buffer in the solution can considerably increase the rate of leaching of bioactive glass-ceramics of the apatite-wollastonite type by aqueous solutions. The effect of TRIS is based on binding calcium ions into a soluble complex by a reaction competitive with HA formation. In this way, the buffer suppresses the deposition of a secondary film on the leached surface exhibiting a protective effect. At the same time, the buffer keeps the pH of the solution at a lower level which, owing to a strong dependence of supersaturation on pH, results in a reduced tendency of the solution to HA precipitation. Both effects act in the same direction, i.e. increase the intensity of leaching.

References

[1] Weinstein A. M., Klawitter J. J., Cook S. D.: J. Biomed. Mat. Res. *14*, 23 (1980).
[2] Klein C. P. A. T., Driessen A. A., deGroot K.: Biomaterials *5*, 157 (1984).
[3] Hench L. L. et al.: J. Biomed. Mat. Res. *23*, 685, (1989).
[4] Kokubo T.: J. Noncryst. Sol. *120*, 138, (1990): Biomaterials 12, 155 (1991).
[5] Kokubo T., Ito S., Huang Z. T.: Biomed. Mat. Res. *24*, 331 (1990).
[6] Anderson O. H.: The Bioactivity of Silicate Glass. PhD Thesis, Dep. Chem. Eng., Abo Akad. Univ., Finland 1990.
[7] Ducheyne P. et al.: Bioceramics, Vol. 4 p. 135. (Proceed. 4th Int. Symp. on Cer. in Med.), London 1991.
[8] Mc Grail B. P., Pederson L. R., Peterson D. A.: Ph. Chem. Gl. *27*, 59 (1986).
[9] Pederson L. R. et al.: Ph. Chem. Gl. *34*, 140 (1993).
[10] Klein C. P. A. T. et al.: Biomaterials *11*, 509 (1990).
[11] Anderson O. H., Yrjas K. P., Karlsson K. H.: Bioceramics, Vol. 4, p. 127 (Proceed. 4th Int. Symp. on Cer in Med.), London 1991.
[12] Ohura K. et al.: J. Biomed. Mat. Res. *25*, 357 (1991).
[13] Rohanová D.: PhD Thesis, Inst. Chem. Technol., Prague 1993.
[14] Helebrant A., Tošnerová B.: Glass Technol. *30*, 220 (1989).
[15] Mann S., Webb J., Williams R. J. P.: *Biomineralisation.* VCH Verlagsgesellschaft, Weinheim 1989.
[16] Driessens F. C. M.: *Mineral Aspects of Dentistry.* S. Karger, Basel 1982.

Submitted in English by the authors

VLIV PUFRU TRIS NA LOUŽENÍ BIOAKTIVNÍ SKLOKERAMIKY

JAN HLAVÁČ, DANA ROHANOVÁ, ALEŠ HELEBRANT

Ústav skla a keramiky, Vysoká škola chemicko-technologická Technická 5, 166 28 Praha 6

Bylo studováno loužení bioaktivní sklokeramiky apatit-wollastonitového typu ve vodě a v simulované tělní kapalině (SBF) za použití statických testů se standardní drtí, s expozicí na 37 °C. Ve výluzích byl pak stanoven obsah Ca^{2+} a SiO_2 a výpočtem poměr CaO/SiO_2.

Byl nalezen podstatný rozdíl mezi výsledky získanými v nepufrovaných roztocích a v roztocích obsahujících pufr TRIS (tris-hydroxymethyl-aminomethan). Z výsledků plyne, že přítomnost TRISu může podstatně zvýšit rychlost loužení sledované sklokeramiky ve vodných roztocích (viz obr. 1–4). Vliv TRISu je přičítán tomu, že váže vyloužený vápník do rozpustného komplexu a tím omezuje tvorbu hydroxyapatitového povlaku. Současně se udržuje pH pufrovaného roztoku na nižší hodnotě, což vzhledem k silné závislosti součinu rozpustnosti pro hydroxyapatit rovněž redukuje tendenci roztoku k precipitaci HA. Oba tyto efekty zvyšují rychlost loužení tím, že omezují tvorbu vrstvy, jež má z hlediska vyluhování a rozpouštění ochranný účinek.

Obr. 1. Koncentrace SiO_2 ve výluhu ze sklokeramiky v pufrovaném a nepufrovaném SBF, a v destilované vodě.

Obr. 2. Koncentrace vápníku ve výluhu v pufrovaném a nepufrovaném SBF, a v destil. vodě.

Obr. 3. Hmotností poměr $CaO:SiO_2$ ve výluhu (obsah CaO uveden jako rozdíl od původní koncentrace v roztoku).

Obr. 4. Koncentrace vápenatých iontů ve výluhu v pufrovaném SBF a v SBF s přídavkem albuminu.

Práce **[9]**

Rohanová D., Boccaccini A.R., Yunos D.M., Horkavcová D., Březovská I., Helebrant A.: TRIS buffer in simulated body fluid distorts the assessment of glass-ceramic scaffold bioactivity. Acta Biomaterialia 7; 2623-2630, 2011.

Podíl: 70%: návrh a realizace experimentu, zpracování výsledků, příprava publikace

Acta Biomaterialia 7 (2011) 2623–2630

Contents lists available at ScienceDirect

Acta Biomaterialia

journal homepage: www.elsevier.com/locate/actabiomat

TRIS buffer in simulated body fluid distorts the assessment of glass–ceramic scaffold bioactivity

Dana Rohanová [a,*], Aldo Roberto Boccaccini [b,c], Darmawati Mohamad Yunos [b], Diana Horkavcová [a], Iva Březovská [a], Aleš Helebrant [a]

[a] Department of Glass and Ceramics, Institute of Chemical Technology, Technická 5, 166 28 Prague 6, Czech Republic
[b] Department of Materials, Imperial College, London, Prince Consort Road, London SW7 2BP, UK
[c] Institute of Biomaterials, Department of Materials Science and Engineering, University of Erlangen–Nuremberg, 91058 Erlangen, Germany

ARTICLE INFO

Article history:
Received 21 December 2010
Received in revised form 15 February 2011
Accepted 16 February 2011
Available online 21 February 2011

Keywords:
Scaffold
Bioactive glass–ceramics
Simulated body fluid
Dissolution
TRIS buffer

ABSTRACT

The paper deals with the characterisation of the bioactive phenomena of glass–ceramic scaffold derived from Bioglass® (containing 77 wt.% of crystalline phases $Na_2O{\cdot}2CaO{\cdot}3SiO_2$ and $CaO{\cdot}SiO_2$ and 23 wt.% of residual glass phase) using simulated body fluid (SBF) buffered with tris-(hydroxymethyl) aminomethane (TRIS). A significant effect of the TRIS buffer on glass–ceramic scaffold dissolution in SBF was detected. To better understand the influence of the buffer, the glass–ceramic scaffold was exposed to a series of in vitro tests using different media as follows: (i) a fresh liquid flow of SBF containing tris (hydroxymethyl) aminomethane; (ii) SBF solution without TRIS buffer; (iii) TRIS buffer alone; and (iv) demineralised water. The in vitro tests were provided under static and dynamic arrangements. SBF buffered with TRIS dissolved both the crystalline and residual glass phases of the scaffold and a crystalline form of hydroxyapatite (HAp) developed on the scaffold surface. In contrast, when TRIS buffer was not present in the solutions only the residual glassy phase dissolved and an amorphous calcium phosphate (Ca–P) phase formed on the scaffold surface. It was confirmed that the TRIS buffer primarily dissolved the crystalline phase of the glass–ceramic, doubled the dissolving rate of the scaffold and moreover supported the formation of crystalline HAp. This significant effect of the buffer TRIS on bioactive glass–ceramic scaffold degradation in SBF has not been demonstrated previously and should be considered when analysing the results of SBF immersion bioactivity tests of such systems.

1. Introduction

In several bone tissue engineering strategies, bioactive materials in the form of highly porous structures, termed scaffolds, are required [1,2]. Scaffolds should not only meet the condition of bioactivity (ability to develop a firm bond with bone tissue), but also be resorbed sufficiently quickly in the body (i.e. become completely dissolved after the new bone tissue has formed) [3,4]. Since a new family of silicate glass–ceramic scaffolds has been proposed for bone tissue engineering [5], the present research was designed to investigate which of the phases (crystalline vs. residual glass) influences the bioactivity of the prepared glass–ceramic scaffold, and to what extent. In this context, the "bioactivity" of a material developed for bone replacement can be evaluated based on the ability of the material to form a hydroxyapatite (HAp) phase on its surface in contact with simulated body fluid (SBF) [6], which is considered to be related to the ability of the material to develop a strong bond with bone tissue [7].

Many authors have published results showing that the compound developing on the surfaces of glass–ceramic scaffolds upon immersion in SBF was weakly crystalline HAp but no publication has fully clarified the mechanism of its formation. In our previous work [5] we reported that the bioactivity of the scaffolds is partly affected by the presence of the crystalline phase $Na_2O{\cdot}2CaO{\cdot}3SiO_2$ and that this phase does not inhibit the apatite growth in SBF, but only slows it down. The mechanism of transformation of the crystalline phase into an amorphous one (Ca–P) was proposed by Hench [7] to be based on the well-known mechanism of HAp formation on amorphous Bioglass®. Moreover, the bioactivity of Bioglass® and of materials recrystallised from it was investigated by Clupper et al. [8] directly in tris-(hydroxymethyl) aminomethane (TRIS) buffer. The tests were performed on Bioglass® and glass–ceramics prepared from Bioglass® at 800, 900 and 1000 °C. It was found that a crystalline form of HAp developed on all forms of the material after as little as 24 h of exposure to the TRIS buffer under static conditions (at $S/V = 0.013\ cm^{-1}$). However, the function of the TRIS buffer in the formation of crystalline HAp was not discussed in detail by Clupper et al. [8]. The same authors [9] investigated bioactivity of the material in SBF (probably buffered with

* Corresponding author. Tel.: +420 22 0 44 4221.
E-mail address: dana.rohanova@vscht.cz (D. Rohanová).

1742-7061/$ - see front matter © 2011 Acta Materialia Inc. Published by Elsevier Ltd. All rights reserved.
doi:10.1016/j.actbio.2011.02.028

TRIS) using the ratio SA/V ~0.1 cm^{-1} and they found that a HAp crystalline phase developed on the glass–ceramic surface in all cases.

Crystallisation of hydroxycarbonated apatite, according to Filho et al. [10], seems to be in direct relation to the residual glass phase, which controls the rate of ion exchange and formation of Si–OH groups. The reaction rate (rate of HAp formation) for glass–ceramics made of 45S5 Bioglass® is seven times faster than for A/W (apatite–wollastonite) glass–ceramics. The findings are in agreement with the solubility products (K) of the individual crystalline phases. The apatite phase has one of the highest solubility products of the calcium phosphates (i.e. it is the least soluble one).

An investigation of glass–ceramic scaffolds by Vallet-Regí et al. [11] was oriented at studying the effects of P_2O_5 present in the matrix of the basic glass on the bioactivity of the material. The authors found that the presence of P_2O_5 in the glass plays no significant role in the bioactive behaviour. The difference in the mechanism of formation of carbonate HAp in glasses without phosphorus is associated with the fast formation of Si–OH (silanol) groups, which attract Ca ions from the solution and form an amorphous Ca–P phase. However, the time necessary for crystallisation of carbonate apatite (CHAp) is relatively long. In glasses containing phosphorus (P) the concentration of Si–OH groups is lower and the rate of formation of the amorphous phase is slower. However, phosphate nanocrystals present in the structure may serve as nucleation sites for the growth of CHAp crystals.

For two decades bioactivity tests have been conducted in SBF, as designed by Kokubo et al. [6]. However, in vitro tests to investigate structural changes on surfaces of glass, glass–ceramics and ceramics have been performed only in TRIS-buffered solutions. TRIS solution in combination with inorganic components of blood plasma (SBF + TRIS), which was used in the study conducted by Kokubo et al. [6], reproduces the in vivo changes in the structure of the material surface more accurately. The SBF solution test has been discussed in many papers and some controversy about its suitability exists [12,13].

Recently, a new variant of the ISO standard has been published [14], which is based on the Kokubo protocol [6]. Earlier studies conducted by some of the present authors [15] investigated the effects of TRIS buffer on the surface reactivity of glass–ceramics during in vitro tests (under static conditions), which were performed on a glass–ceramic material containing apatite, wollastonite and whitlockite phases. It was shown that the TRIS buffer forms a soluble complex with Ca^{2+} ions, which suppresses the deposition of a HAp layer on the material surface and thus reduces the potential protective effect of such a layer. The permeability of the layer for diffusing elements decreases with immersion time. In this context, the deposition of a HAp layer on the material surface represents a significant process influencing the rate of leaching of components from the material, which is closely associated with the pH of the solution. It is assumed that a relatively small decrease in the solution's pH will result in a significant change of supersaturation with respect to HAp and subsequently the HAp layer would grow slower from the solution [16].

It has become apparent that the test results are influenced not only by the solubility of the material tested, but also by the composition of the test solution and by the experimental conditions employed [16,17]. In vitro tests of bioactivity in SBF with TRIS buffer are mostly conducted under static conditions. Dynamic tests introduce an additional dimension into the in vitro testing of bioactivity of materials, i.e. by supplying fresh liquid to the sample they represent in vivo conditions more closely. Thus, dynamic testing conditions were chosen for this work. This guarantees stable concentrations of biogenic elements (Ca and P) and a stable pH of the test solution, and the sample is also exposed to a liquid flow (laminar flow). Low flow rates of a liquid around the material might well simulate the conditions in the human body.

2. Materials and methods

2.1. Materials

The scaffolds were prepared from 45S5 Bioglass® powder by the foam replica method following the procedure described in Ref. [5]. A slurry for the impregnation of polyurethane foams was prepared by mixing glass particles (<5 μm in size) with an aqueous solution of poly-DL-lactic acid. After drying, the porous precursor (the so-called "green body") was sintered at 1100 °C for 5 h. Partial crystallisation of the glass occurred upon heat treatment. Bioglass®-based glass–ceramic scaffolds fabricated by the foam replica technique exhibit one advantage for in vitro tests: after the thermal exposure to densify the struts, a main crystalline phase ($Na_2O{\cdot}2CaO{\cdot}3SiO_2$) and a minor phase ($CaO{\cdot}SiO_2$) usually develop, which in the ideal case (100% crystallisation) should consume all the CaO present in Bioglass®. The residual glass phase should therefore contain the entire quantity of P_2O_5. Thus calcium and phosphorus, as elements, could serve not only as indicators of the beginning of precipitation of the Ca–P phase (HAp) but also as "markers" of dissolution of the crystalline and glass phases in the test solutions. Under these conditions, the interpretation of results could be very simple. Another possible simplification of the dissolution behaviour of this system is the assumption that the content of the second crystalline phase ($CaO{\cdot}SiO_2$) is low and can be assumed to behave similarly to the main phase ($Na_2O{\cdot}2CaO{\cdot}3SiO_2$).

The specific surface area was measured by the BET method in nitrogen and a value of 1.6 $m^2\,g^{-1}$ was determined. Table 1 shows the composition of the starting 45S5 Bioglass® powder and of the main phases of the scaffolds investigated.

2.2. Solutions for in vitro tests

In this study the behaviour of the scaffold was investigated by exposing the materials to four types of water solutions: (i) solution containing inorganic components similar to blood plasma in combination with a buffer (SBF + TRIS), (ii) SBF solution without the TRIS buffer, (iii) the TRIS buffer solution alone and (iv) demineralised water.

The SBF buffered with TRIS and HCl is labelled as SBF + TRIS. The SBF without the TRIS buffer is labelled as SBF. The pH value was the one that developed after mixing all of the inorganic components of SBF. The tests were also conducted in the TRIS buffer and HCl alone (labelled as TRIS) and in demineralised water (labelled as H_2O).

The basic SBF + TRIS solution was prepared based on a formula found in the literature [16]. The solution was prepared from the following reagents: KCl, NaCl, $NaHCO_3$, $MgSO_4$, $CaCl_2$, KH_2PO_4. The TRIS buffer was completed with an admixture of HCl to achieve the required pH value at 37 °C. The pH value was set at 7.4–7.6 at 37 °C. The TRIS buffer concentration in the solution was 0.05 mol dm^{-3}. NaN_3 (1 g dm^{-3}) was added to the SBF solution to inhi-

Table 1
Compositions of Bioglass® and individual phases of the scaffold (wt.%).

Oxide	45S5 Bioglass® (100 wt.%)	$Na_2O{\cdot}2CaO{\cdot}SiO_2$ (77.4 wt.% of scaffold)[a]	Residual glass phase (22.6% of scaffold)
SiO_2	45.0	50.9	24.8
Na_2O	24.5	17.4	48.5
CaO	24.5	31.7	–
P_2O_5	6.0	–	26.5

[a] The crystalline phase $CaO{\cdot}SiO_2$ is included.

Table 2
Ion composition (mmol dm^{-3}) of SBF [17,18].

Na^+	K^+	Ca^{2+}	Mg^{2+}	Cl^-	HCO^{3-}	HPO_4^{2-}	SO_4^{2-}
142.0	5.0	2.5	1.0	131	5	1.0	1

bit possible bacteria formation. The ion composition of SBF (as SBF5 according to Müller and Müller [17] and Helebrant et al. [18]) is shown in Table 2.

2.3. Leachate analysis

2.3.1. Atomic absorption spectrophotometry

Concentrations of calcium in the leachate after glass–ceramics exposure were measured by means of atomic absorption spectrophotometry on a SpectrAA 880 spectrophotometer (VARIAN). To determine the quantity of calcium, the so-called releasing agent (KCl solution) was added into each sample. The flame used for atomisation was acetylene–N_2O. Ca concentrations were measured at $\lambda = 422.7$ nm, silicon concentrations were measured at $\lambda = 251.6$ nm and sodium concentrations at $\lambda = 589$ nm.

2.3.2. Spectrophotometry

The concentrations of $(PO_4)^{3-}$ ions were determined at $\lambda = 830$ nm (blue form) with a UV 1601 ultraviolet–visible spectrophotometer, in conformity with ČSN 83 05 40.

2.3.3. pH measurement

pH values of the solutions were measured after sample collection at ~32 °C (static test) and at the ambient temperature in the leachate from the dynamic test using an inoLab pH meter with a combined glass electrode.

2.4. Analysis of the scaffold material

2.4.1. Optical microscopy

The sample surface was analysed with a Jenapol optical microscope using the NIS-Element AR 3.0 image analysis software in a lateral incident light.

2.4.2. Scanning electron microscopy/energy-dispersive spectroscopy (SEM/EDS)

The surface morphology was examined by SEM (Hitachi S-4700) coupled with an EDS analyser (NORAN D-6823) and a silicon drifted detector using an acceleration potential of 15 kV. Samples were sputtered by Au/Pd.

2.4.3. X-ray powder diffraction analysis

Diffraction patterns were collected with a PANalytical ŕPert PRO diffractometer equipped with a conventional X-ray tube (Cu K_α radiation, 40 kV, 30 mA, point focus) and a position-sensitive PIXcel detector with an anti-scatter shield. X-ray patterns were measured in the 2Θ range of 10–100°, with steps of 0.0131° and 200 s counting per step. Qualitative analysis was performed with the HighScorePlus software package (PANalytical, the Netherlands, version 2.2.5), Diffrac-Plus software package (Bruker AXS, Germany, version 8.0) and JCPDS PDF-2 database (International Centre for Diffraction Data, Newtown Square, PA, USA) release 54, 2004 (in the Institute of Inorganic Chemistry of the Czech Academy of Science, Řež u Prahy).

2.5. In vitro test under dynamic conditions

Dynamic in vitro tests enable a better simulation of the conditions in a living organism [19]. The tested materials were supplied with a "fresh" test liquid at a flow rate (48 ml day^{-1}) simulating the flow of extracellular fluid in the bloodstream. A mass of 0.05 g of tested scaffold per one cell was used in the tests. The test was conducted for a period of 10 or 17 days. Samples of the leachate were collected after short periods of time (hours to days) to be analysed for Ca, Si, Na and $(PO_4)^{3-}$ ions. The pH was also measured in a cooled down leachate (at ambient temperature).

3. Results

3.1. Analyses of leachates

The concentration of calcium grew with time in the solutions containing the TRIS buffer (i.e. in SBF + TRIS and in the 0.05 mol dm^{-3} solution of TRIS only), indicating the dissolution of the calcium-containing phase ($Na_2O{\cdot}2CaO{\cdot}3SiO_2$ and $CaO{\cdot}SiO_2$) of the scaffold. In solutions without the TRIS buffer (SBF and demineralised water) the concentration of calcium in the leachate decreased or oscillated around zero (in H_2O), which confirms that the crystalline phase practically does not dissolve in solutions without the TRIS buffer (Fig. 1).

The variation of $(PO_4)^{3-}$ ion concentration with time was different in the individual solutions. As mentioned above, the entire content of phosphate oxide (P_2O_5) is in the residual glass phase of the scaffold material after thermal exposure. In the SBF + TRIS solution, the TRIS buffer solution and the H_2O, the dissolution of the residual glass phase was obvious, as the concentration of $(PO_4)^{3-}$ ions increased during the first 24 h of immersion. The experiment in the SBF + TRIS solution demonstrated the dissolution of the residual glass phase, though 12 h later the concentration of $(PO_4)^{3-}$ ions decreased significantly as the rate of Ca–P phase precipitation was higher than that of the dissolution of the residual glass phase. In the SBF-only solution, the Ca–P phase precipitation started immediately (Fig. 2).

It should be pointed out that silica is present in both the crystalline and residual glassy phases of the scaffold. The concentrations of silicon in the leachates indicate that two processes can occur in the solutions containing the TRIS buffer: the dissolution of the scaffold material and the precipitation of hydrated calcium silicate (CSH phase). After the initial period, when dissolution prevails, approximately comparable rates of dissolution and precipitation processes are achieved during longer interaction (Fig. 3).

It is also noted that sodium is contained in both the crystalline and residual glass phases of the scaffold. Sodium was analysed in leachates from solutions not involving SBF, i.e. in TRIS and in H_2O. In the TRIS solution the curve of the sodium (Na) concentration is similar to that of calcium (Ca). After a week of exposure of the sample, the leachate demonstrated a sudden decline in Na con-

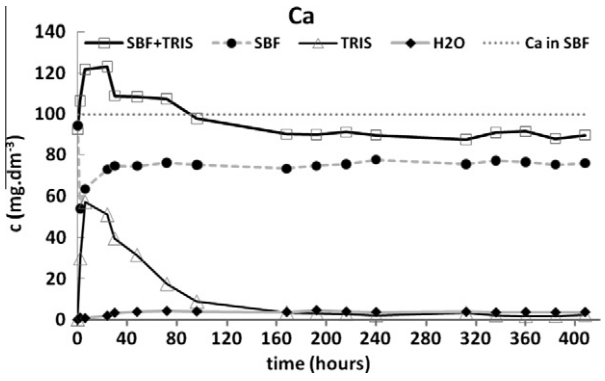

Fig. 1. Concentration of Ca in leachates from SBF + TRIS, SBF, TRIS and H2O under dynamic test conditions.

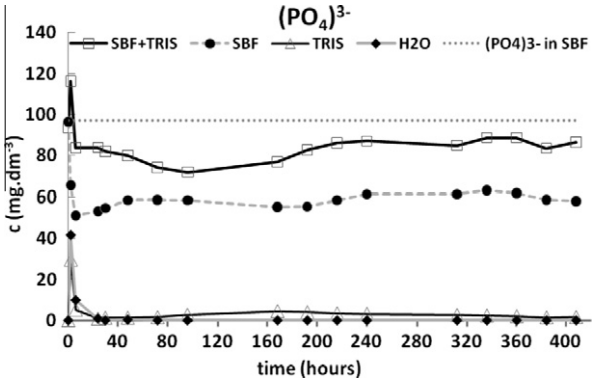

Fig. 2. Concentration of (PO4)3− ions in leachates from SBF + TRIS, SBF, TRIS and H2O under dynamic test conditions.

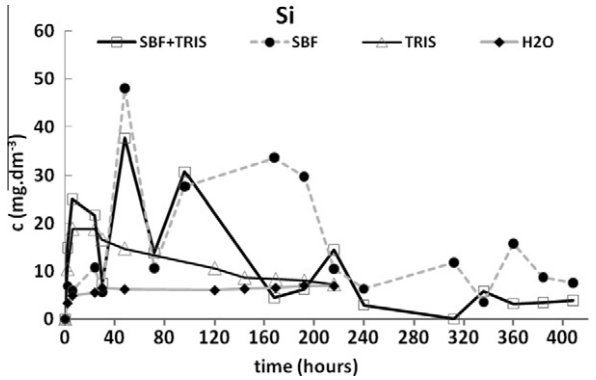

Fig. 3. Concentration of silicon ions in leachates from SBF + TRIS, SBF, TRIS and H2O under dynamic test conditions.

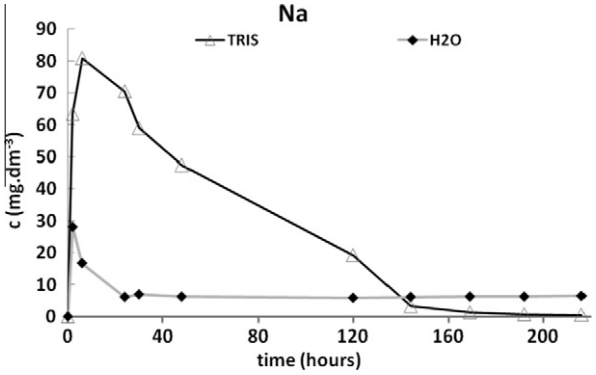

Fig. 4. Concentration of sodium ions in leachates from TRIS and H2O under dynamic test conditions.

centration, probably due to the reduced dissolution of the scaffold. In demineralised water the sodium concentration grew during the first hours of the test. However, after 24 h no more sodium was released into the demineralised water. It is probable that this trend is related to the dissolution of only the residual glass phase (Fig. 4).

In the in vitro tests under dynamic conditions (in SBF + TRIS and in TRIS), the TRIS buffer keeps the pH value close to the initial level. In solutions which do not contain any TRIS (SBF and H_2O) the pH value increases significantly due to the massive transport of sodium ions from the dissolving scaffold material. However, this did not accelerate scaffold dissolution (Fig. 5).

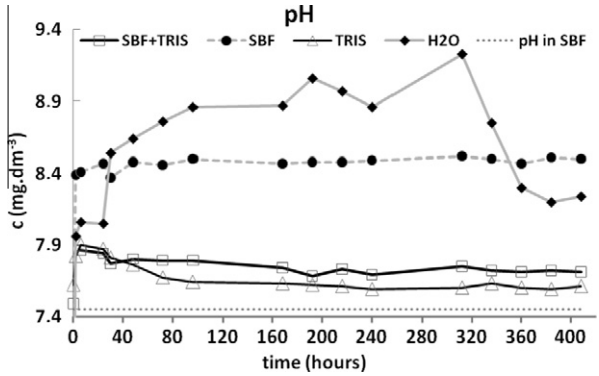

Fig. 5. Variation of pH value in SBF + TRIS, SBF, TRIS and H2O solutions under dynamic test conditions.

3.2. Weight variation of the scaffold samples

The significant reduction of material mass in the solutions containing TRIS buffer confirms the accelerated dissolution of scaffolds, in comparison with solutions without TRIS buffer. Based on the duration of the dynamic tests, it was observed that the sample weight in solutions containing TRIS decreased by 50 or even 75% of the original value. In demineralised water the weight of the scaffold material decreased by 21.1 wt.% in 17 days. About half of this reduction (i.e. 9.7 wt.%) was intercepted on a filter glass of the test cell. Over the course of the test, the material disintegrated. When exposed to water (H_2O), the main dissolved component was the residual glass phase, which in the glass–ceramic scaffold serves as a binder.

Following exposure of the scaffold to the SBF solution (without TRIS), the weight of the sample increased. After 9 days it increased by ~3.5 wt.% under static conditions, and under dynamic conditions it increased by 8.7 wt.% after 17 days. In this solution the scaffold did not dissolve so rapidly and, in contrast, the precipitation rate of the amorphous Ca–P phase was higher.

3.3. X-ray diffraction (XRD) analysis after the dynamic test

XRD analysis of the original material confirmed two crystalline phases in the scaffold: $Na_2O{\cdot}2CaO{\cdot}3SiO_2$ (combeite) and a small amount of $CaO{\cdot}SiO_2$ (Fig. 6a). After 17 days of exposure to the SBF + TRIS solution a new crystalline phase was found (HAp). Neither $Na_2O{\cdot}2CaO{\cdot}3SiO_2$ nor $CaO{\cdot}SiO_2$ was detected. They had probably completely dissolved (Fig. 6b). In contrast, after 17 days of exposure to the SBF solution without TRIS buffer, the original crystalline phases were detected and the crystalline HAp form was not found (Fig. 6c). In a sample exposed to TRIS solution only HAp was detected and no other crystalline phase was found (Fig. 6d). Samples exposed to demineralised water (H_2O) contained the original crystalline phases, $Na_2O{\cdot}2CaO{\cdot}3SiO_2$ and $CaO{\cdot}SiO_2$, as expected (Fig. 6e).

3.4. SEM/EDS characterisation after the dynamic in vitro test

The image of the original scaffold material (Fig. 7a) indicates the presence of two crystalline phases (tabular (combeite) and needle crystals ($CaO{\cdot}SiO_2$)), as confirmed by XRD analysis. Fig. 7b shows the scaffold after exposure to SBF + TRIS. The image exhibits a single globule formed of very small crystals of HAp. The image of the scaffold exposed to the solution without the TRIS buffer (SBF), in Fig. 7c, is completely different. In comparison with the HAp globule developed after the exposure to SBF + TRIS, this surface features multiple smaller spherical formations, and represents the amor-

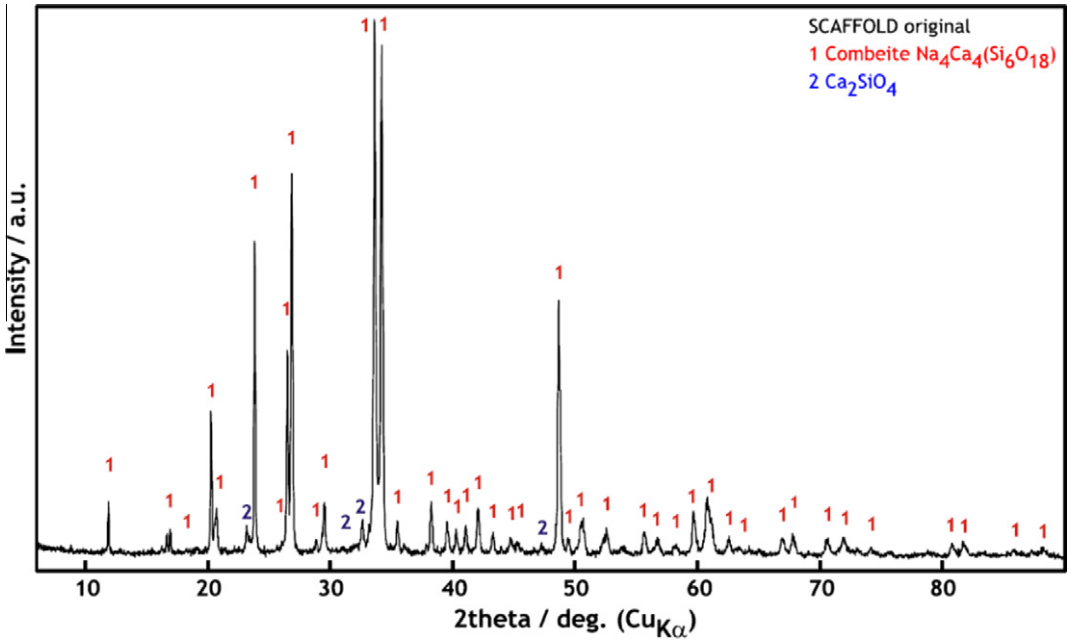

Fig. 6a. XRD of the original scaffold material, indicating the presence of two crystalline phases (combeite and $CaO{\cdot}SiO_2$).

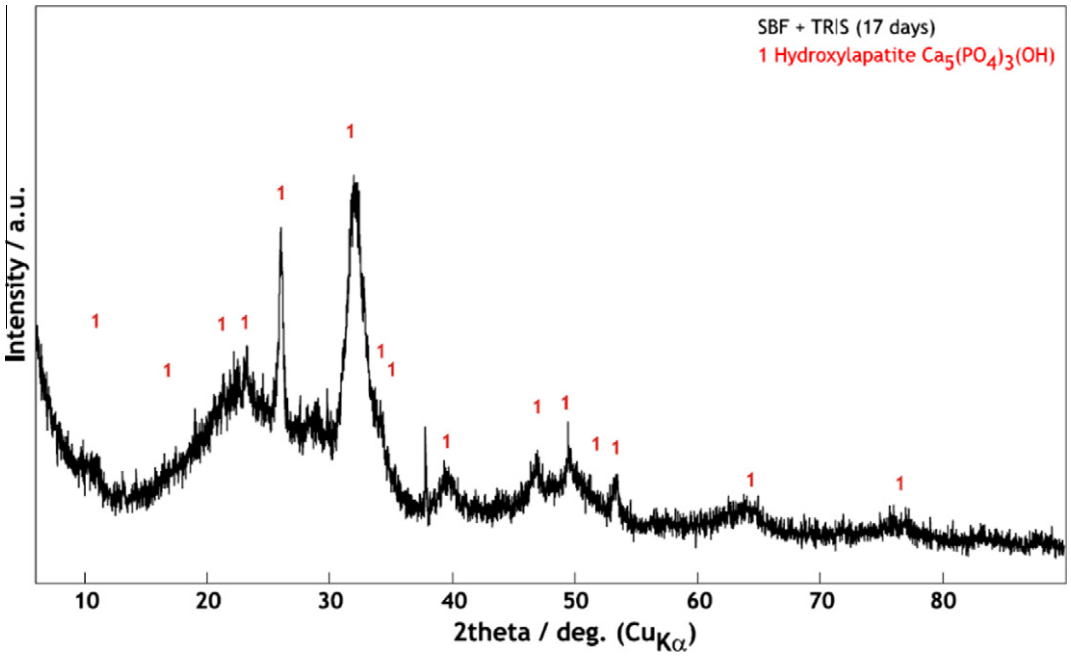

Fig. 6b. Scaffold after 17 days of exposure to the SBF + TRIS solution. The XRD pattern detected only the HAp phase.

phous (nanocrystalline) phase of calcium phosphate (as confirmed by XRD). The EDS analysis confirmed high concentrations of calcium and phosphorus. The original crystalline phases were selectively dissolved from the material exposed to the TRIS solution (Fig. 7d), which is in agreement with results of the leachate characterisation and XRD analysis. The EDS analysis also showed that the porous network consists mainly of silicon dioxide, probably in the form of an SiO_2 gel. Fig. 7e shows the scaffold structure after leaching in water, where the residual glass phase was partly dissolved, and the image shows both crystalline phases and probably a remnant of the glassy phase.

4. Discussion

Our dynamic tests have confirmed the effect of the TRIS buffer on dissolution behaviour of the Bioglass®-based glass–ceramics scaffold material. The scaffold is highly soluble in solutions containing TRIS and therefore even a very small quantity of the material in a test cell will disturb the metastable equilibrium of the test solution and induce precipitation of the HAp crystalline phase. It was found that in solutions containing the TRIS buffer (SBF + TRIS, TRIS) the primarily dissolving phases were the crystalline phases ($Na_2O{\cdot}2CaO{\cdot}3SiO_2$ and $CaO{\cdot}SiO_2$), but the residual glassy phase also

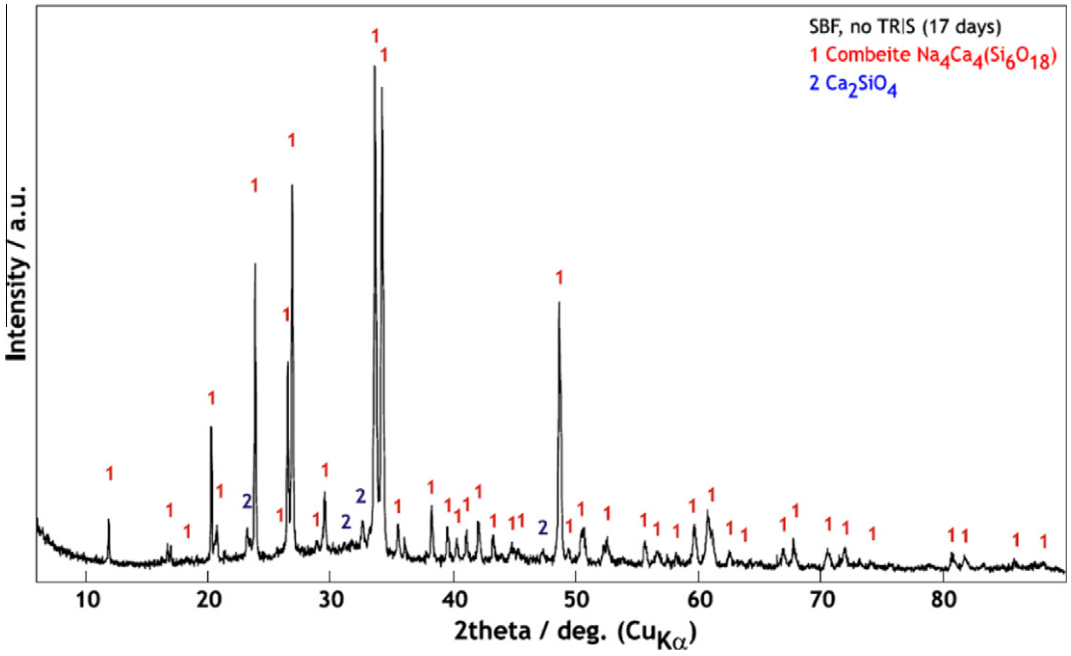

Fig. 6c. XRD pattern of a scaffold after 17 days of exposure to the SBF solution.

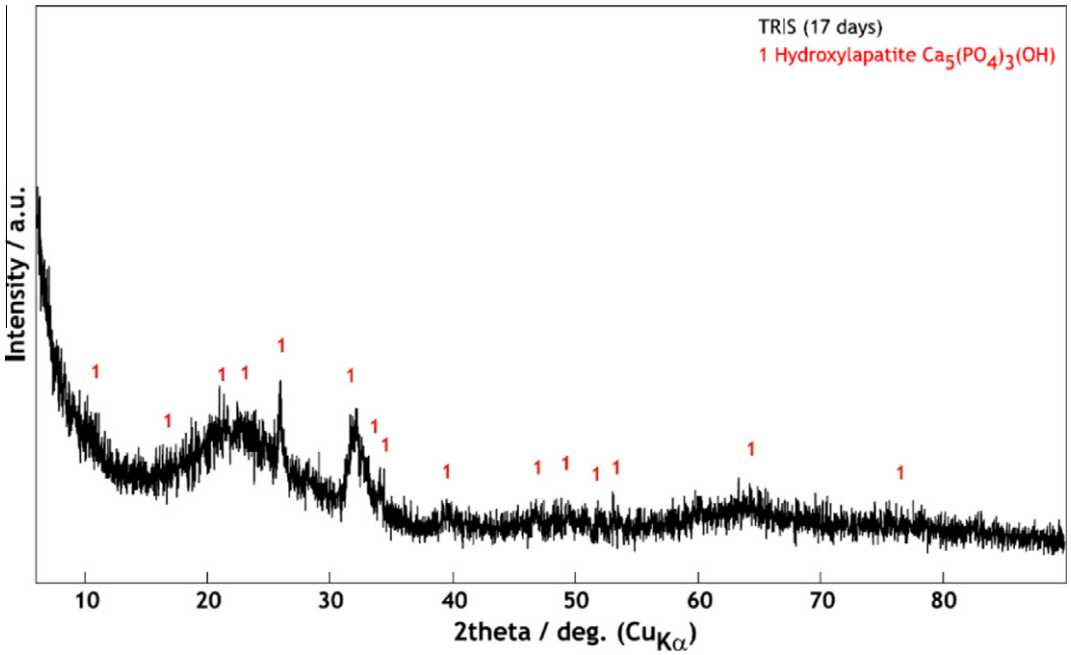

Fig. 6d. XRD pattern of a scaffold after 17 days of exposure to the TRIS solution indicate HAp phase.

partly dissolved. In the solutions which did not contain any TRIS buffer (SBF and H_2O) the only dissolving phase was the residual glassy phase. These findings were confirmed by XRD data and SEM/EDS measurements, and are in good agreement with the concentrations of elements found in the leachates after scaffold exposure to various solutions.

Further, it was found that the presence of the TRIS buffer in solutions doubles the dissolving rate of the material (in the TRIS buffer the scaffold material dissolved at a rate of 0.2 wt.% h^{-1}; in demineralised water it was 0.1 wt.% h^{-1}). This finding is in agreement with the results of our previous studies [20], which identified the same effect on dissolution of the crystalline form of β-tricalcium phosphate. The specific effect of the TRIS buffer will be discussed in a future publication.

5. Conclusions

1. The glass–ceramic scaffold material prepared by crystallisation of Bioglass® significantly dissolves in SBF + TRIS. It is obvious that bioactivity is associated mainly with the crystalline phase,

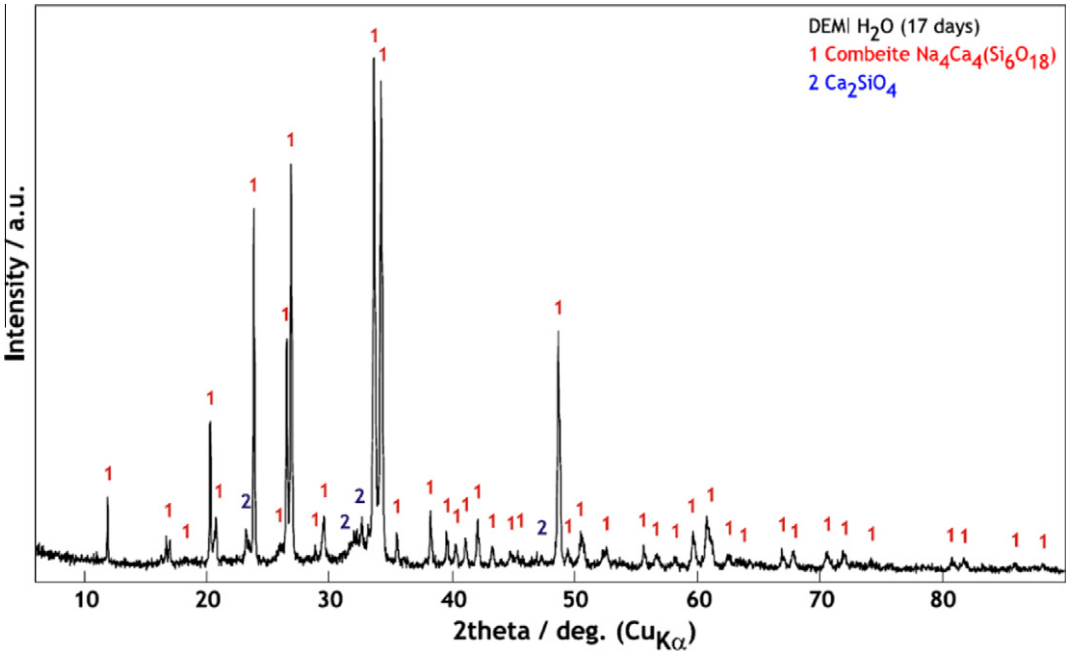

Fig. 6e. XRD pattern of a scaffold after 17 days of exposure to H_2O. The original crystalline phases of the scaffold remained.

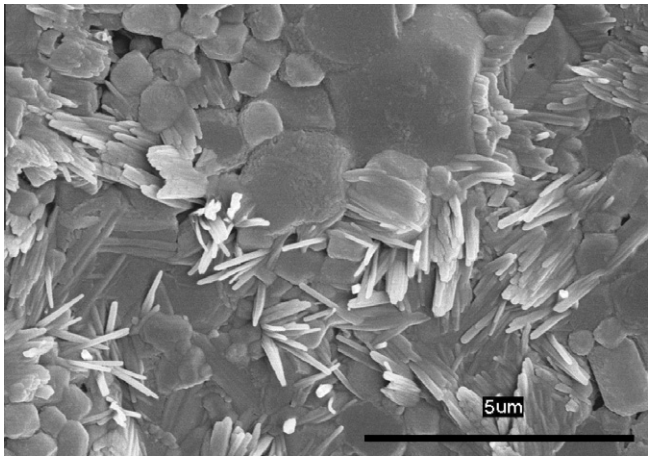

Fig. 7a. SEM image of the original glass–ceramic scaffold material. Two crystal phases are visible: tabular combeite and needle-like $CaO{\cdot}SiO_2$.

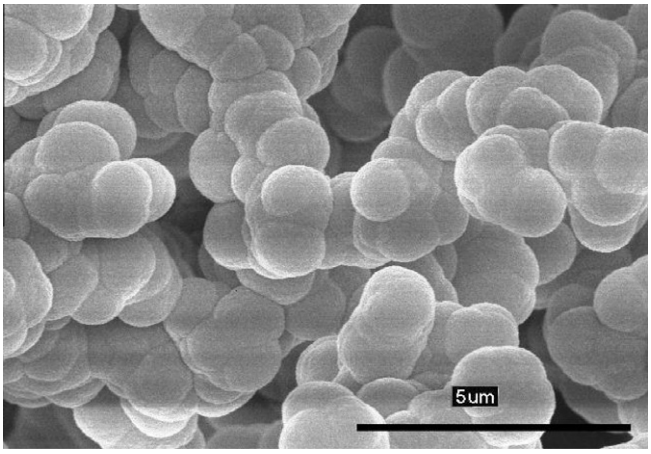

Fig. 7c. Globules of amorphous calcium phosphate phase formed after 17 days of scaffold exposure to SBF solution.

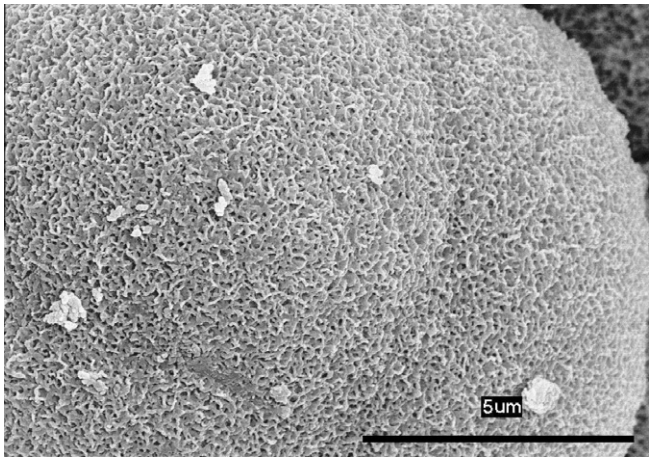

Fig. 7b. Large globule formed by small HAp crystals after 17 days of scaffold exposure to SBF + TRIS solution.

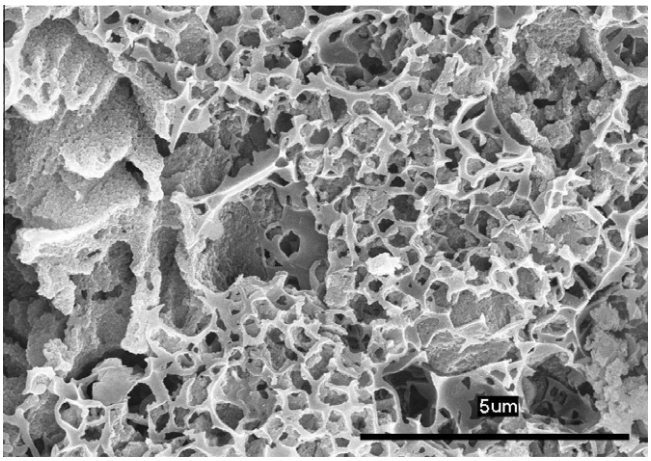

Fig. 7d. Scaffold residual phase (composed mainly by SiO_2) and newly formed HAp after 17 days of exposure to TRIS solution.

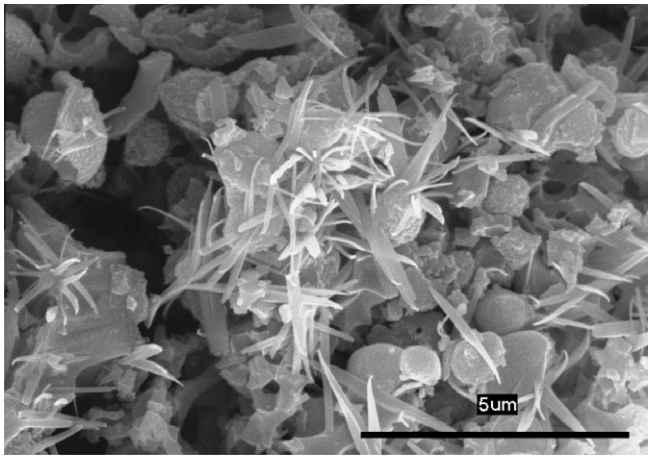

Fig. 7e. The original crystal phases of the scaffold survived after 17 days of exposure to H_2O.

which is readily soluble. The bioactivity of the scaffold is certainly affected by the crystalline high content (77 wt.%) in the material. This statement applies for solutions containing the TRIS buffer.

2. In solutions without TRIS (H_2O and SBF), the only dissolving phase is the residual glass phase.
3. The TRIS buffer, which has been used in standard bioactivity tests for two decades (Kokubo solution), strongly influences the test results. The dissolution of the scaffold in the presence of TRIS buffer is twice as fast as in solutions containing no TRIS. Moreover, the crystalline form of the newly developed apatite phase (HAp) was found only on samples exposed to solutions containing the TRIS buffer.

Acknowledgements

This study was prepared with the support of the research program MSM 6046137302. We thank Dr. Petr Bezdička of the Institute of Inorganic Chemistry of the Czech Academy of Science for careful XRD measurements and our colleague, Ms. Zuzana Cílová, PhD, for SEM/EDS measurements.

Appendix A. Figures with essential colour discrimination

Certain figures in this article, particularly Fig. 6, is difficult to interpret in black and white. The full colour images can be found in the on-line version, at doi:10.1016/j.actbio.2011.02.028.

References

[1] Temenoff JS, Lu L, Mikos AG. Bone tissue engineering using synthetic biodegradable polymer scaffolds. In: Davies JE editor. Bone engineering, Toronto: EM Squared Inc., 2000, p. 455–462.
[2] Bueno EM, Glowacki J. Cell-free and cell-based approaches for bone regeneration. Nat Rev Rheumat 2009;5:685–97.
[3] Khan Y, Yaszemski MJ, Mikos AG, Laurencin CT. Tissue engineering of bone: material and matrix considerations. J Bone Joint Surg Am 2008;90:36–42.
[4] Rezwan K, Chen QY, Blaker JJ, Boccaccini AR. Biodegradable and bioactive porous polymer/inorganic composite scaffolds for bone tissue engineering. Biomaterials 2006;27(18):3413–31.
[5] Chen QZ, Thompson ID, Boccaccini AR. 45S5 Bioglass (R)-derived glass-ceramic scaffolds for bone tissue engineering. Biomaterials 2006;27(11):2414–25.
[6] Kokubo T, Kushitani H, Sakka S, Kitsugi T, Yamamuro T. Solutions able to reproduce in vivo surface-structure changes in bioactive glass–ceramic A-W^3. J Biomed Mater Res 1990;24:721–34.
[7] Hench LL. Bioceramics. J Am Ceram Soc 1998;81(7):1705–28.
[8] Clupper DC, Mecholsky Jr JJ, LaTorre GP, Greenspan DC. Sintering temperature effects on the in vitro bioactive response of tape cast and sintered bioactive glass–ceramics in TRIS buffer. J Biomed Mater Res 2000;57:532–40.
[9] Clupper DC, Mecholsky Jr JJ, LaTorre GP, Greenspan DC. Bioactivity of tape and sintered bioactive glass–ceramic in simulated body fluid. Biomaterials 2002;23(12):2599–606.
[10] Filho PO, LaTorre GP, Hench LL. Effect of crystallization on apatite-layer formation of bioactive glass 45S5. J Biomed Mater Res 1996;30:509–14.
[11] Vallet-Regí M, Salinas AJ, Aros D. From the bioactive glasses to the star gels. J Mater Sci: Mater Med 2006;17:1011–7.
[12] Kokubo T, Takadama H. How useful is SBF in predicting in vivo bone bioactivity? Biomaterials 2006;27(15):2907–15.
[13] Bohner M, Lemaitre J. Can bioactivity be tested in vitro with SBF solution? Biomaterials 2009;30(12):2175–9.
[14] Implants for Surgery: in vitro evaluation for apatite-forming ability of implant materials. ISO Standard 23317: 2007.
[15] Hlaváč J, Rohanová D, Helebrant A. The effect of TRIS-buffer on the leaching behaviour of bioactive glass-ceramics. Ceramics – Silikáty 1994;3–4:119–22.
[16] De Aza PN, Guitian F, Merlos A, Lora-Tamayo E, De Aza S. Bioceramics–simulated body fluid interfaces pH and its influence of hydroxyapatite formation. J Mater Sci Mater Med 1996;7:399–402.
[17] Müller L, Müller FA. Preparation of SBF with different HCO_3 content and its influence on the composition of biomimetic apatites. Acta Biomater 2006;2:181–9.
[18] Helebrant A, Jonášová L, Šanda L. The influence of SBF composition on carbonated hydroxyapatite formation. Ceramics – Silikáty 2002;46(1):9–14.
[19] Strnad J, Protivínský J, Mazur D, Veltruská K, Helebrant StrnadZ, Šesták A, et al. Interaction of acid and alkali treated titanium with dynamic simulated body environment. J Thermal Anal Calorimetry 2004;76:17–31.
[20] Brázda L, Rohanová D, Březovská I, Helebrant A. Behaviour of β-TCP in water and SBF at 37°C under static and dynamic conditions. In: Plešingerová B, Sučík G, Kuffa T, Vadász T, Horkavcová D, Pikna Ľ editors. Preparation of ceramic materials. Herľany, 2007. p. 66–68.

Práce **[10]**

Rohanová D., Boccaccini A.R., Horkavcová D., Bozděchová P., Bezdička P., Častorálová M.: Is non-buffered DMEM solution a suitable medium for in vitro bioactivity test? Journal of Materials Chemistry B. 2; 5068-5076, 2014.

Podíl: 60%: návrh a realizace experimentu, zpracování výsledků, příprava publikace

Journal of Materials Chemistry B

PAPER

View Article Online
View Journal

Is non-buffered DMEM solution a suitable medium for *in vitro* bioactivity tests?

Cite this: DOI: 10.1039/c4tb00187g

Dana Rohanová,*[a] Aldo Roberto Boccaccini,[b] Diana Horkavcová,[a] Pavlína Bozděchová,[a] Petr Bezdička[c] and Markéta Častorálová[d]

Several laboratories had tested bioactivity of the materials in commercially available solution DMEM (Dulbecco's Modified Eagle's Medium) that is normally used for cultivation of cell cultures. The objective of this work was to find out whether it is possible to replace TRIS-buffered SBF currently used for bioactivity tests with the non-buffered DMEM solution. To understand the role of the organic part of the DMEM solution in the process of crystallization, we have prepared non-buffered solution simulating only its inorganic part (identified as I-solution). It was found that under static-dynamic test conditions calcite ($CaCO_3$) and the amorphous phase of calcium phosphate (ACP) formed on the surface of the glass-ceramic (45S5 bioactive glass based) scaffold exposed to both solutions. Additionally, halite (NaCl) formed at the beginning of exposure to DMEM. Hydroxyapatite phase was not detected on the surface in either non-buffered solution. Organic components contained in the DMEM solution failed to prevent formation of crystalline phases. The present results indicate that it is not recommendable to use DMEM for bioactivity tests of glass-ceramic materials due to its low concentration of Ca^{2+} ions, high concentration of HCO_3^- ions and the necessity to maintain sterile environment during the test.

Received 4th February 2014
Accepted 15th May 2014

DOI: 10.1039/c4tb00187g

www.rsc.org/MaterialsB

1. Introduction

The first tests usually performed on materials intended for substitution of hard tissues are bioactivity tests, *i.e.* tests monitoring the formation of a layer of biologically active hydroxyl carbonate apatite formed on the biomaterial surface.[1] Several preconditions need to be met for biomineralization (osseointegration) of the tested materials. The material must be dissolvable in blood serum (it must release Ca^{2+} ions or potentially also $(PO_4)^{3-}$, Na^+ and Si ions in a controlled manner); "fresh" solution (blood serum) is supplied to the proximity of the material and bone mineral hydroxyapatite (HAp) may crystallize on it due to local supersaturation. The so-called simulated body fluid (SBF) has been used for bioactivity tests for many years.[2] Unlike human blood serum, the original SBF[3] contains no organic components; it has a higher content of Cl^- ions and a lower content of HCO_3^- ions (4 mmol dm^{-3} *versus* 27 mmol dm^{-3} in real human serum). The pH of SBF is maintained at around 7.3 (at 37 °C) by using Tris ($NH_2C(CH_2OH)_3$), tris-[(hydroxymethyl)aminomethane]. In blood serum, the pH is partly buffered by hydrogen carbonate ions and by partial pressure of CO_2. The pH value is critical for the formation of HAp. According to de Aza *et al.*,[4] the ideal pH for precipitation and crystallization of HAp is in the alkaline region (pH = 7.5–8.0). However, during static and dynamic tests of dissolution of bioactive glasses, glass-ceramics and calcium-phosphate materials (*i.e.* easily dissolving ones), the pH values in Tris-buffered SBF do not remain in the neutral area. Several hours after the material is exposed to SBF the pH value increases towards the alkaline region. This pH increase results in formation of an ideal, but not realistic, environment for HAp formation. Some authors have questioned whether bioactivity of materials can be predicted based only on development of a HAp layer on their surface after exposure to SBF.[5,6] This is because SBF cannot simulate physiological conditions in a live organism completely but it only substitutes its analytical components (inorganic part of blood serum). Certainly it is justified to question if this information is sufficient for bioactivity assessment? Indeed for a first indication of potential bioactivity of biomaterials, it probably is. As we have found out in our previous work,[7] Tris buffer, which is a part of SBF, reacts with the tested material (in our case with 45S5 bioactive glass-derived glass-ceramic). We exposed the scaffold to a series of SBF solutions – Tris-buffered SBF, SBF without Tris, Tris alone and water. The Tris buffer supported dissolution of the crystalline phase of the glass-ceramic scaffold and it was the principal component for crystallization of the HAp phase. Moreover, Ca^{2+} ions bind with Tris

[a]Department of Glass and Ceramics, Faculty of Chemical Technology, Institute of Chemical Technology Prague, Technická 5, 166 28 Prague 6, Czech Republic. E-mail: dana.rohanova@vscht.cz

[b]Department of Materials Science and Engineering, Institute of Biomaterials, University of Erlangen-Nuremberg, 91058 Erlangen, Germany

[c]Institute of Inorganic Chemistry of the ASCR, v.v.i., 250 68 Husinec-Řež, Czech Republic

[d]Department of Biochemistry and Microbiology, Faculty of Food and Biochemical Technology, Institute of Chemical Technology Prague, Technická 3, 166 28 Prague, Czech Republic

buffer to form a soluble complex which had been described elsewhere[8,9] and which may distort the results of *in vitro* tests.

Other authors[3] have reported on preparation of SBF solutions whose concentrations of HCO_3^- are near to those in human blood serum (27 mmol dm^{-3}) and, apart from approaching the real biological environment, they also anticipated an increased buffering ability of the inorganic part of SBF alone. However, all revised or modified SBF solutions still contain Tris buffer (revised (r-SBF), corrected (c-SBF) and newly improved (n-SBF)). The authors of ref. 10 and 11 used a modified SBF27 solution (concentration of HCO_3^- was 27 mmol dm^{-3}) and demonstrated formation of carbonate hydroxyapatite (CHAp). In another investigation,[12] collagen spongious Ap-CaP whiskers and $CaSO_4$ doped with calcium hydrophosphate ($CaHPO_4$ monetite) were exposed to a solution of Tris-SBF-27 mmol dm^{-3}. All the mentioned materials induced formation of nanoporous apatite in the solution, with the exception of $CaSO_4$ alone, which crumbled in the solution into powder.

In a relevant investigation involving bioactive glasses, Cannillo *et al.*[13] exposed two types of glasses (BG45 and MG45) not only to SBF but also to commercial solutions HBSS+ and HBSS−, designed for growing tissue cultures. HBSS solutions were not buffered with Tris but they differed in the contents of Ca and Mg ions. SBF solution was the most reactive one and it induced formation of apatite on the surface of BG45 glass in a shorter time than other solutions. The microstructure of the crystallized apatite on the BG45 glass was identical both in HBSS+ and in SBF. However, the reactivity (in the sense of apatite formation) was higher in SBF and this was explained by the authors in the presence of a higher concentration of Ca ions in SBF (1.4 mmol dm^{-3} Ca^{2+} in HBSS+ compared to 2.5 mmol dm^{-3} in SBF). A magnesium phosphate phase developed on the surface of MG45 glass in SBF which means that also glass significantly dissolved in SBF and that SBF was in this case supersaturated with respect to magnesium phosphate.

In other published articles,[14–16] attempts to substitute SBF with the commercially available DMEM solution, which is primarily designed for growing and maintaining tissue cultures, have been reported. The solution is available in many variants – non-buffered or buffered with Tris, and with another buffer – HEPES ($C_8H_{18}N_2O_4S$), 4-(2-hydroxyethyl) piperazine-1-ethanesulfonic acid, (Sigma Aldrich, Invitrogen GIBCO USA). Apart from the inorganic part of blood serum, this solution also contains the organic component. For example, Theodorou *et al.*[17] have found that as early as after three days of immersion in DMEM solution, the amorphous apatite phase developed at certain locations on silicate glass (*Bioactive glass 45S5*) and the carbonated crystalline apatite (CHAp) phase was found on *58S* glass. It was discussed that development of the CHAp crystalline phase is inhibited by the organic part of DMEM solution and the authors explained it by the effect of the adsorption of proteins on an amorphous Ca–P layer.[17] However, it is not clear whether they used buffered or non-buffered DMEM solution which is critical for interpretation of the results. Miller *et al.*[18] studied the transformation of brushite into OCP (octacalcium phosphate) in various DMEM derived solutions. Solutions without organic phase did not have any SO_4^{2-} ions and solutions with organic phases as lactic acid and Tris buffer contained SO_4^{2-} ions. None of the solutions were able to maintain the pH at 7.4, even during the first 24 h. Brushite crystals were transformed into a biphasic mixture of OCP and CDHA (Ca-deficient HA), when soaked for 1 week in different biomineralization solutions at 37 °C. The authors also noticed that the extent of any hydrothermal transformation of DCPD into OCP and CDHA strongly depended on the overall dimensions or thicknesses (sizes) of the samples. Temizel *et al.*[19] used derived solutions of DMEM buffered with HEPES and solution marked as BM-3 non-buffered with HEPES. When HEPES was eliminated in BM-3, it became possible for the first time to completely convert the DCPD crystals to OCP in less than 72 h at 36.5 °C. The effect of the presence of HEPES could be due to the complexation of some of the Ca^{2+} ions of the solution by the HEPES buffer at the Ca/P molar ratio of 1.99 and could reduce the concentration of free Ca^{2+} ions available for the DCPD to OCP transformation. The experimental results showed that increasing the temperature from 55 °C to 60 °C in a 1 h stirred experiment increased the possibility of obtaining apatite-CaP mainly due to the high solubility of DCPD. The optimum temperature required to achieve a complete transformation to OCP crystals was 75–80 °C. Evidently, the type of used solution, buffering system and the arrangement of the test (*e.g.* S/V) and temperature are very important for the interpretation of obtained results.

The purpose of this research was to study the suitability of non-buffered DMEM solution for bioactivity testing, considering its reduced concentration of Ca^{2+} and high concentration of HCO_3^- ions, the fact that it contains organic components of blood serum and, unlike SBF, it is not buffered with Tris.

2. Materials and methods

2.1. Materials

The material used for testing was silicate glass-ceramic in the form of a highly porous structure (scaffold) prepared by the foam replica technology.[20] The initial material for preparation of a glass suspension was 45S5 bioactive glass (45S5 BG) powder with a mean particle size <5 μm. For scaffold preparation the polyurethane (PUR) foam was immersed into the prepared suspension, it was taken out 15 minutes later and the excessive suspension was squeezed out. The created porous precursors, the so-called *green bodies*, were left to dry for 12 hours at room temperature and were then subjected to thermal treatment consisting of firing at 400 °C per 1 hour to burn-out the PUR template and further sintering at 1100 °C for 5 hours.[20] The scaffold had an open porous structure with the pore size in the range of 510–720 μm and porosity of approximately 90%. The material contained crystalline and residual glass phases. Their contents before and after the crystallization, according to a previous publication,[20] are shown in Table 1.

2.2. Solutions for the *in vitro* test

The modified simulated body fluid with reduced concentration of Ca^{2+} ions and increased concentration of HCO_3^- ions to

44 mmol dm^{-3} (I-solution) was prepared by mixing solutions of the following reagents: KCl, NaCl, $NaHCO_3$, $MgCl_2 \cdot 6H_2O$, $CaCl_2$, Na_2SO_4 and KH_2PO_4 in respective ratios. Azide (NaN_3) was added to prevent bacterial growth in the solution.[7,21] I-solution was not buffered and the pH value was not adjusted.

Dulbecco's Modified Eagle's Medium (DMEM) is normally used to grow tissue culture and it simulates the environment of the human body because, in addition to inorganic ions, it also contains organic substances, such as amino acids, glucose and vitamins. A modified DMEM (mod-DMEM) was prepared for testing in this study by enriching the standard DMEM (D1145, Sigma-Aldrich) with fetal bovine serum (FBS, Invitrogen), vitamins (MEM, Invitrogen) and antibiotics (Sigma-Aldrich), A5955 Sigma Antibiotic Antimycotic solution (100×) stabilized with 10 000 units penicillin, 10 mg streptomycin and 25 μg amphotericin B per mL, sterile-filtered, BioReagent.

The reason for the FBS and vitamin addition was to enrich the organic part of the DMEM. Antibiotics protect prepared solution against degradation during the test. Table 2 presents the ion composition of I-solution and the inorganic part of mod-DMEM in comparison with blood plasma (BP), as published in the literature,[22] the Ca/P molar ratio is presented.

2.3. Static-dynamic conditions of the *in vitro* test

To prevent the effect of exhaustion of ions from the solutions, the so-called static-dynamic test was carried out in which, although the testing solutions did now flow continually around the sample as in dynamic tests, the solution was replaced on a daily basis (50 ml per day), *i.e.* every 24 hours. The scaffolds used for the static-dynamic arrangement of the *in vitro* test had an average weight in the range of 0.045–0.055 g, they were placed in platinum spirals and suspended in 50 ml plastic bottles filled with I-solution or mod-DMEM. The bottles with the samples were placed into a thermostat maintaining the temperature at 36.5 ± 0.5 °C. The interaction time was 15 days and two samples were collected in selected time intervals (after 1, 3, 7, 11 and 15 days), rinsed with demineralized water and left to dry at laboratory temperature. In order to maintain a sterile environment the replacement of the mod-DMEM solution was performed in a "flow box".

2.4. Analysis of the materials

2.4.1. Scanning electron microscopy/energy-dispersive spectroscopy (SEM/EDS). The surface of tested materials before and after the immersion tests was inspected with a Hitachi S-4700 scanning electron microscope (SEM) equipped with an EDS analyzer (NORAN D-6823) working at an accelerating voltage of 15 kV. The samples were powder coated with an Au–Pd layer during 80–100 s for SEM observations.

2.4.2. X-ray powder diffraction analysis. Samples were ground in an agate mortar in a suspension with cyclohexane. The suspension was then placed on a mylar film and fixed to a transmission sample holder. After solvent evaporation a thin layer of the prepared sample was covered with another mylar film. The diffraction patterns were collected using a PANalytical X'Pert PRO diffractometer equipped with a conventional X-ray tube ($Cu_{K\alpha}$ 40 kV, 30 mA, line focus) working in transmission mode. An elliptic focusing mirror with divergence slit 0.5°, an anti-scatter slit 0.5° and a soller slit of 0.02 rad were used in the primary beam. A fast linear position sensitive detector PIXcel with an anti-scatter shield and a soller slit of 0.02 rad was used in the diffracted beam. All patterns were collected in the range of 3 to 88 deg. 2 theta with the step of 0.013 deg and 600 s per step producing a scan of about 4.5 hours. Qualitative analysis was performed with a HighScorePlus software package (PANalytical, The Netherlands, version 3.0e), a Diffrac-Plus software package (Bruker AXS, Germany, version 8.0) and JCPDS-ICDD PDF-2 database.[23]

2.5. Leachate analysis

All tests and analyses were performed using two parallel series of samples.

2.5.1. Atomic absorption spectrophotometry. Concentrations of Ca^{2+} ions were analyzed in leachates from both types of solutions with a VARIAN-SpectrAA 300. The so-called release agent (KCl) was added to each sample to determine the quantity of Ca. The leachate was atomized in acetylene–N_2O flame. The wavelength used for absorbance measurements was 422.7 nm. Concentrations of Si were analyzed in leachates from both types of solutions with a VARIAN-SpectrAA 880. The leachates were atomized in acetylene–N_2O flame. The wavelength used for absorbance measurements was 251.6 nm.

2.5.2. Spectrophotometry. Concentrations of $(PO_4)^{3-}$ ions were analyzed in I-solution leachates with a UV-Vis spectrophotometer UV1601 at wavelength 830 nm (ČSN 830540). Ion concentrations were calculated using a calibration line method from the measured absorbance values.

2.5.3. Inductively coupled plasma-optical emission spectroscopy (ICP-OES). Concentrations of P in mod-DMEM leachates were measured by ICP-OES with a Perkin Elmer-Optima

Table 1 Composition of 45S5 BG, crystalline and glass phases[20]

Oxides	45S5 BG (100 wt%)	$Na_2Ca_2Si_3O_9$ (77.4 wt% scaffold)[a]	Residual glass phase (22.6 wt% scaffold)
SiO_2	45.0	50.9	24.8
Na_2O	24.5	17.4	48.5
CaO	24.5	31.7	—
P_2O_5	6.0	—	26.5

[a] The minority crystalline phases $CaO \cdot SiO_2$ and $NaCaPO_4$ (buchwaldite) are included.

Table 2 Ion composition (mmol dm^{-3}) of mod-DMEM, I-solution BP,[22] SBF[22] and Ca/P molar ratio

	Na^+	K^+	Ca^{2+}	Mg^{2+}	Cl^-	HCO_3^-	HPO_4^{2-}	SO_4^{2-}	Ca/P
mod-DMEM	154.5	5.4	1.8	0.8	118.5	44.0	0.9	0.8	1.97
I-solution	142.0	5.0	1.8	1.0	91.6	44.0	1.0	0.5	1.80
BP	142.0	5.0	2.5	1.5	103.0	27.0	1.0	0.5	2.50
SBF orig.	142.0	5.0	2.5	1.0	148.8	4.2	1.0	0.0	2.50

2000DV instrument. The solution was vaporized with a Gem-ConeTM nebulizer and the flow rate of the solution through the nebulizer was 2.2 ml min^{-1}. The produced fine aerosol was carried with an argon stream into a plasmatic burner (1300 W). The concentrations were measured at wavelengths 231.620, 214.917 and 178.221 nm.

2.5.4. pH measurement. pH values in I-solution and mod-DMEM leachates were measured with an inoLab pH-meter with a combined glass electrode at laboratory temperature.

3. Results

3.1. Interaction of scaffolds with mod-DMEM

3.1.1. Leachate analysis of mod-DMEM during interaction with the scaffold. Fig. 1a and b show concentrations of Ca^{2+} and $(PO_4)^{3-}$ and pH in mod-DMEM leachates after the scaffold exposure. The leachate analysis suggests that potential processes of scaffold dissolution and precipitation of new phases occurred at a stable rate practically throughout the entire duration of the experiment. Concentrations of $(PO_4)^{3-}$ ions after 7 days of interaction slightly increased which means that the process of scaffold dissolution started prevailing over the precipitation of new phases. ICP could not be used to determine concentrations of Si (which is a "marker" for scaffold dissolution) in mod-DMEM leachates, because of the high error of the measurement of the samples with low concentration of Si (1–10 mg dm^{-3}). The mod-DMEM solution was not buffered and the pH value increased from 7.45 to 8.90 soon after the beginning of the exposure and it oscillated at around pH 8.90 until the end of the test (Fig. 1b). The pH changes can be considered an indicator of ongoing processes of dissolution and precipitation during scaffold exposure to mod-DMEM.

3.1.2. X-ray powder diffraction analysis of scaffolds before and after interaction with mod-DMEM. Records from XRD powder diffraction analysis of the scaffold before and after 3, 7, 11 and 15 days of interaction with mod-DMEM are shown in Fig. 2.

XRD analysis before the exposure confirmed the presence of the main crystalline phase $Na_2O{\cdot}2CaO{\cdot}3SiO_2$ (combeite) and two minority structurally isomorphic phases $CaO{\cdot}SiO_2$ and $NaCaPO_4$ (buchwaldite) in the original scaffold (Fig. 2). Crystalline phases of NaCl (halite) and $CaCO_3$ (calcite) developed after three days of exposure (3D). The intensity of diffraction lines for the halite phase decreased with increasing interaction time (7–15D) and, in contrast, it increased for the calcite phase. The XRD diffractograms indicate the growth of a nanocrystalline phase (indicated in the diffractogram as a broad diffusion maximum) approximately from the 7th day of the test. It is probably a phase consisting of a mixture of nanocrystalline–amorphous calcium phosphate (ACP), which has been also discussed in the literature for immersion in SBF.[7] The intensity of the original crystalline phases of the scaffold remained practically unchanged which means that they did not dissolve in the mod-DMEM solution.

3.1.3. SEM/EDS characterization of scaffolds before and after interaction with mod-DMEM. Changes on the surface of the scaffolds after 3, 7, 11, 15 days of interaction with mod-DMEM can be seen in the SEM images (Fig. 3b–e) and EDS analyses (indicative measurement) are provided in Table 3. The original morphology of the scaffold surface is shown in Fig. 3a.

Fig. 3a shows the surface of the original scaffold with small tabular crystals of combeite and needle like crystals, likely corresponding to buchwaldite as well as to the structural isomorphic phase $CaO{\cdot}SiO_2$. The SEM/EDS analysis confirmed that as early as after three days (3D) the scaffold surface was

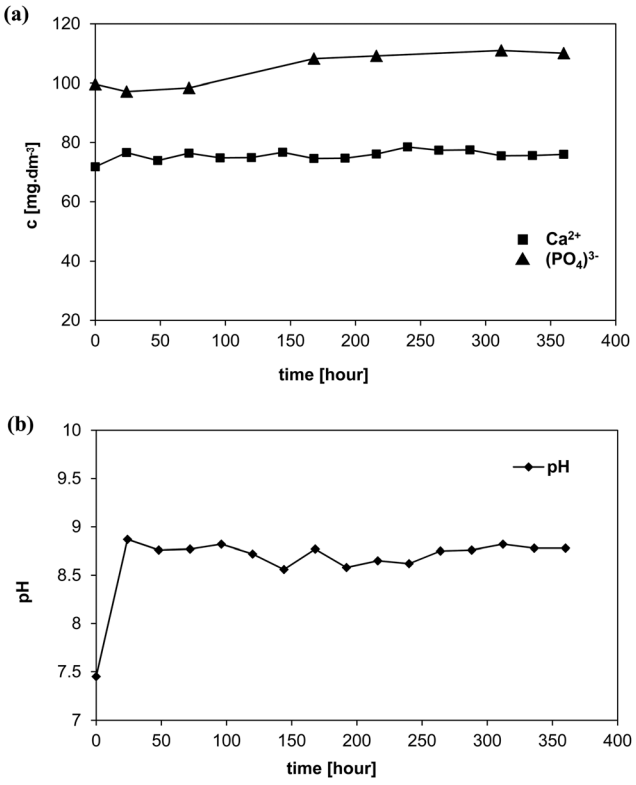

Fig. 1 Concentrations of (a) Ca^{2+} and $(PO_4)^{3-}$ ions and (b) values of pH in mod-DMEM during interaction with scaffolds.

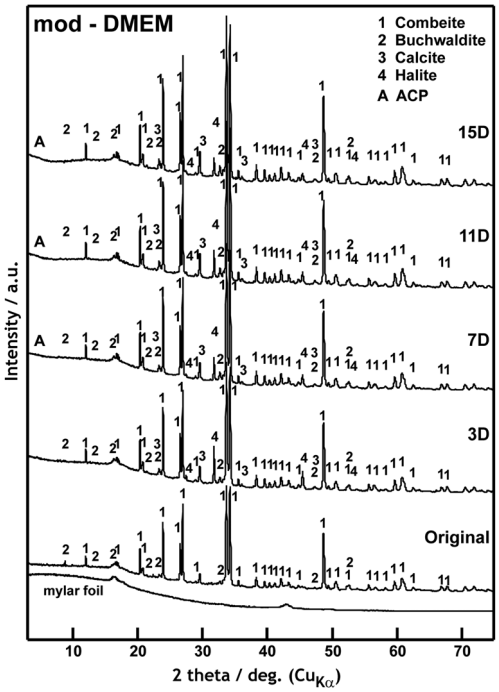

Fig. 2 XRD patterns of the scaffold before and after 3, 7, 11 and 15 days of interaction with mod-DMEM.

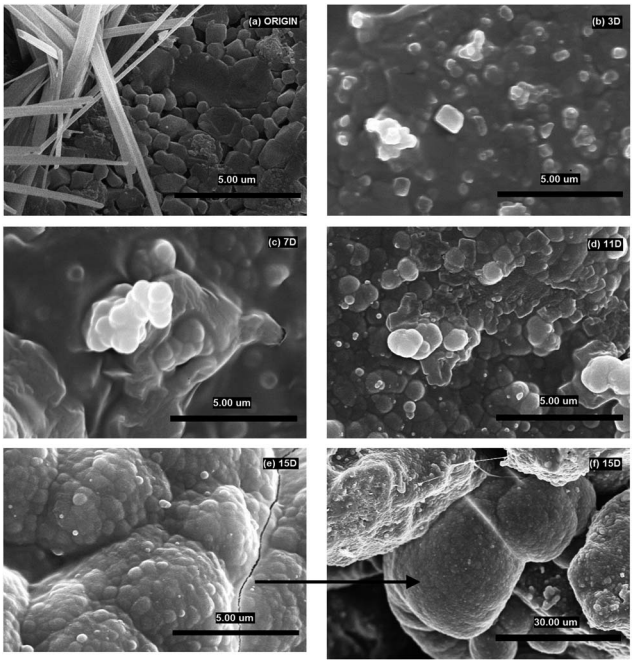

Fig. 3 SEM images of scaffolds (a) before (combeite – the small tabular crystals, buchwaldite and structurally isomorphic phase $CaO{\cdot}SiO_2$ – needle-like crystals) and after (b) 3, (c) 7, (d) 11, and (e and f) 15 days of interaction with mod-DMEM.

covered with ACP (amorphous calcium phosphate) (growing content of Ca and P) and NaCl (Table 3, Fig. 3b, white crystal, 1 μm in size), which is in agreement with the XRD analysis (Fig. 2). A phase with a high content of Ca developed after one week (7D) (by XRD diffraction detected as $CaCO_3$) and it can be seen in images from SEM/EDS as white 1 μm globules (Fig. 3c). After 11 days (11D) the phase with a high Ca content started prevailing and quantities of Na and Cl on the scaffold surface gradually decreased. The content of P remained unchanged after the third day of interaction. At the end of the test (15D) the scaffold surface was mostly covered with a phase having a high content of Ca (according to XRD – $CaCO_3$, Fig. 2) and with a cauliflower-like structure (Fig. 3e and f) and also ACP was detected on scaffold surfaces. The results of SEM/EDS measurements were therefore in good agreement with the XRD analysis.

3.2. Interaction of scaffolds with I-solution

3.2.1. Leachate analysis of I-solution during interaction with the scaffold. Analyses of the I-solution leachates showed that the scaffold significantly dissolved immediately after exposure to the medium, which was well-documented by the presence of Si in the leachates (Fig. 4a). 48 hours after the beginning of exposure the rates of scaffold dissolution and precipitation of the Ca–P phase stabilized, as documented by concentrations of Ca^{2+} and $(PO_4)^{3-}$ ions (Fig. 4b). The decrease of Ca^{2+} and $(PO_4)^{3-}$ concentrations indicates the precipitation of the Ca–P phase. The pH value of non-buffered I-solution was 8.50 at the beginning and, due to scaffold dissolution and formation of the new phase, it increased to 9.20 and remained around that value until the end of the test (Fig. 4c).

3.2.2. Si as a dissolution "marker". The concentrations of Si in I-solution leachates made it possible to calculate quantities of the dissolved scaffold. The calculation was also possible owing to the conditions of the static-dynamic test as it was possible to use the current concentration of Si in a known volume of leachate (every day precisely 50 ml) to calculate the quantity of leached SiO_2. The total quantity of leached SiO_2 was subsequently converted to the weight of the dissolved scaffold, based on an assumption that SiO_2 represents 45 weight% of the scaffold. The fact that the leached SiO_2 originated both from the crystalline and glass phases was neglected for reasons of simplification (the crystalline phase contains *ca.* 7× more SiO_2 than the residual glass phase). Thus assuming that the dissolution rates are identical for both scaffold phases our calculations indicate that 7.2 mg of SiO_2 leached in total from *ca.* 55 mg of the exposed sample. This means that *ca.* 16 mg of scaffold dissolved in 15 days of exposure to the I-solution, *i.e.* approximately 1/3 of the initial weight of the tested scaffold. If the dissolved phase had been only the residual glass phase it would have dissolved completely. We also tried to calculate quantities of dissolved Ca and P, however, due to their re-precipitation and formation of several different phases on the scaffold surface the calculation would be very complicated and indeed quantitatively inaccurate.

3.2.3. X-ray powder diffraction analysis of scaffolds before and after interaction with I-solution. Records from XRD powder diffraction analysis of the scaffold before and after 1, 3, 7, 11 and 15 days of interaction with I-solution are shown in Fig. 5.

Table 3 Chemical and crystalline composition of the original scaffold surface and the surface after its exposure to mod-DMEM [wt%] (by SEM/EDS)

Time [days]	O	Na	Mg	Si	P	Cl	K	Ca	Probable phases[a]
Origin	39.4	20.3	—	20.9	1.6	—	—	17.9	$Na_2Ca_2Si_3O_9$
3D	45.2	10.9	2.1	2.6	6.4	6.6	1.0	25.1	ACP, NaCl
3D – cube	49.3	14.0	2.6	—	—	7.9	0.8	19.6	NaCl
7D	37.3	9.8	1.3	5.8	3.7	7.3	0.7	34.2	NaCl, ACP, $CaCO_3$
11D	40.9	3.8	0.9	8.7	4.2	3.3	1.0	37.2	$CaCO_3$, ACP, NaCl
15D	45.5	2.4	1.5	3.5	5.5	1.5	0.3	39.9	$CaCO_3$, ACP

[a] Combeite: $Na_2Ca_2Si_3O_9$, halite: NaCl, calcite: $CaCO_3$, ACP: amorphous calcium phosphate.

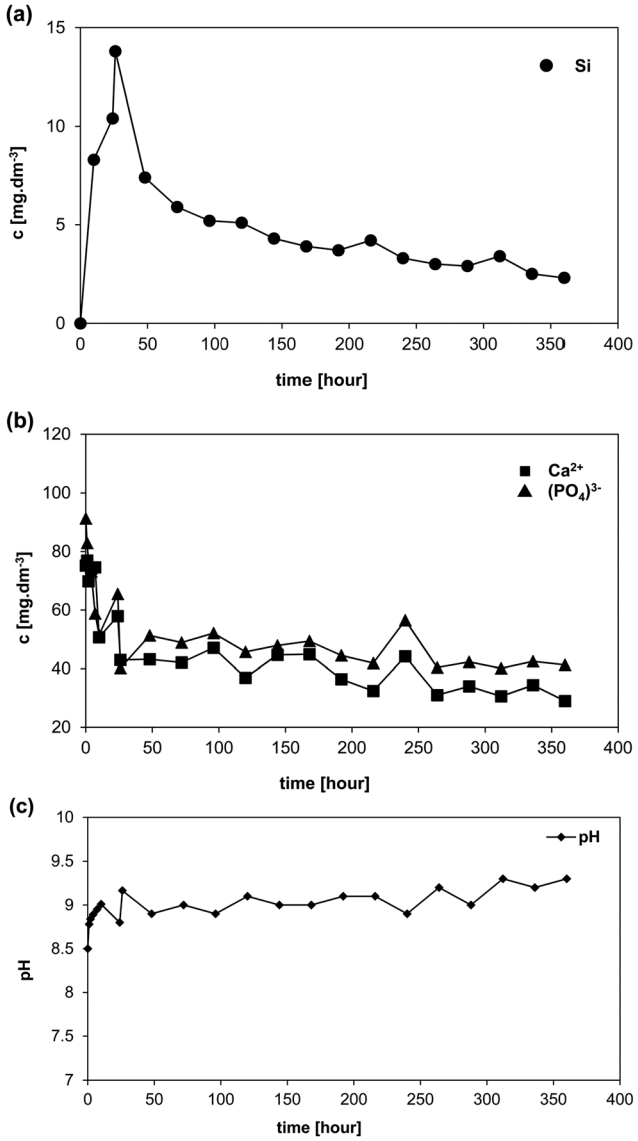

Fig. 4 Concentrations of (a) Si and (b) Ca^{2+} and $(PO_4)^{3-}$ ions and (c) values of pH in I-solution during interaction with scaffolds.

XRD diffraction confirmed formation of a calcite crystalline phase ($CaCO_3$) as early as after the first day (1D) of exposure to I-solution (Fig. 5). After three days of exposure (3D), an increase in the content of the amorphous phase ACP (Amorphous Calcium Phosphate) was recorded. No formation of the HAp phase was observed, not even after 15 days of exposure to I-solution. No halite (NaCl) was formed either, probably due to lower concentrations of Na^+ and Cl^- ions in the I-solution in comparison to mod-DMEM. The original phases of the scaffold are visible in the XRD patterns until the end of the test (0–15D). We assume that the main dissolved phase of glass-ceramic was the residual glass phase of the scaffold.

3.2.4. SEM characterization of scaffolds before and after interaction with I-solution. Changes on the scaffold surface after 1, 3, 7, 11, 15 days of interaction with I-solution are shown in Fig. 6b–f. The scaffold surface before the interaction is shown in Fig. 6a.

Fig. 6b–f and results of EDS analyses in Table 4 confirm conclusions from XRD analysis. Well-developed globules of $CaCO_3$ (Fig. 6b) with the diameter of *ca.* 1 μm were visible from

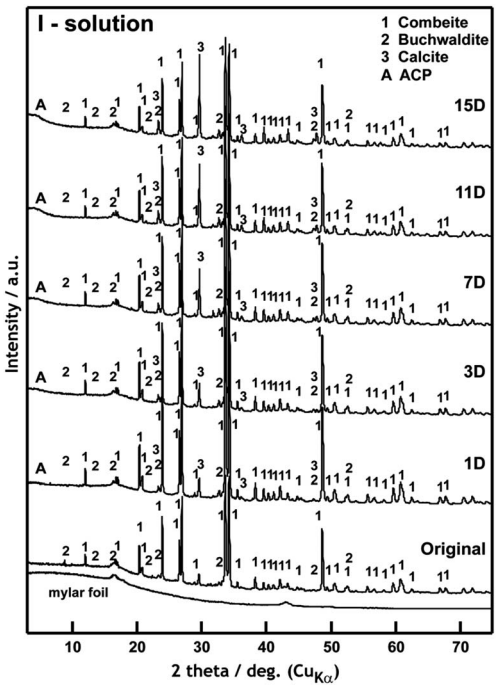

Fig. 5 XRD patterns of scaffolds before and after 1, 3, 7, 11 and 15 days of interaction with I-solution.

the very beginning of the interaction (1D). It was the same phase that developed on the scaffold surface exposed to mod-DMEM. Apart from the growth and agglomeration of the globules (3D) (Fig. 6c), there was a significant growth of the ACP phase (7–15D) (Fig 6d), which has been also detected for immersion in SBF.[7] NaCl was not detected, neither with XRD nor with SEM/EDS. $CaCO_3$ globules covered by the ACP phase formed in I-solution looked like hydroxyapatite at the first sight but XRD analysis failed to confirm the presence of the HAp crystalline phase.

4. Discussion

Analyses of leachates from 45S5 BG-based glass-ceramic scaffolds immersed in non-buffered mod-DMEM and non-buffered I-solutions showed that pH values in those systems (because of enormous dissolution of the tested scaffold) increased far into the alkaline area (up to pH 9). We assume that at such pH values the residual glass phase, which functions as a "binding agent" in the glass-ceramic material, will significantly dissolve. This fact has been confirmed by practical experience from the test as the glass-ceramic material in non-buffered I-solution (but also in mod-DMEM) disintegrated. XRD measurements after 15 days of exposure in both cases confirmed the presence of the original crystalline phases of the scaffold. The results indicate therefore that the high concentration of HCO_3^- ions (DMEM contains approx. 160% HCO_3^- (s) of that in human plasma) coupled with CO_2 (g) from air does not have sufficient buffering capacity in the tested solutions. The DMEM solution fails to contain sufficient quantity of Ca^{2+} ions (only 70% of that in human serum) and the Ca/P molar ratio is near 2 in contrast to human plasma (2.5). Such an environment is not supersaturated with respect to HAp but, it is preferentially supersaturated with respect to the amorphous calcium phosphate phase and $CaCO_3$.

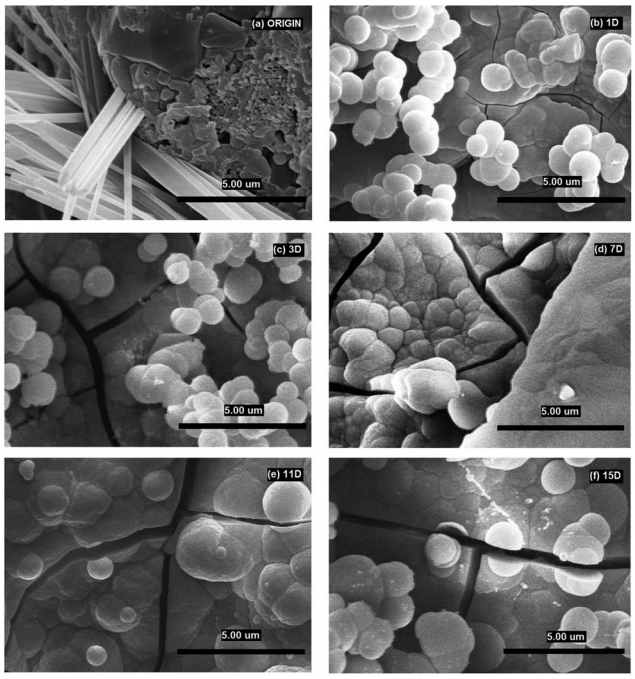

Fig. 6 SEM images of scaffolds (a) before (combeite – the small tabular crystals, buchwaldite and structurally isomorphic phase $CaO \cdot SiO_2$ – needle-like crystals) and after (b) 1, (c) 3, (d) 7, (e) 11 and (f) 15 days of interaction with I-solution. The fractures in the newly developed layers were caused by drying of samples.

Table 4 Chemical and crystalline composition of the original scaffold surface and the surface after the interaction with I-solution [wt%] (SEM/EDS)

Time [day]	O	Na	Mg	Si	P	Ca	Probable phase[a]
Origin	43.5	22.8		17.1	0	16.6	$Na_2Ca_2Si_3O_9$
1D	44.2	4.9	2.0	8.2	5.2	35.4	$Na_2Ca_2Si_3O_9$, ACP, $CaCO_3$
3D	36.1	1.6	—	2.0	4.4	56.0	ACP, $CaCO_3$
7D	49.8	2.5	2.8	3.1	6.9	34.9	ACP, $CaCO_3$
11D	45.5	2.6	2.7	—	7.0	42.2	ACP, $CaCO_3$
15D	41.6	2.6	3.5	3.0	5.5	43.7	ACP, $CaCO_3$

[a] Combeite: $Na_2Ca_2Si_3O_9$, calcite: $CaCO_3$, ACP: amorphous calcium phosphate.

After being exposed to both investigated solutions the newly formed crystalline phase on the surface of scaffolds was mainly calcite ($CaCO_3$) (shaped into globules). In our previous study,[7] we discussed that a visually identical phase that formed in SBF without Tris buffer was amorphous ACP, and even after conducting XRD analysis we were not able to prove the presence of $CaCO_3$ after the scaffold exposure to SBF without Tris. The quantity of $CaCO_3$ was very low and the most intense lines for $CaCO_3$ overlapped with diffraction lines of the main crystalline phase of the as-fabricated scaffold; *i.e.* combeite. However, we have to take into account, that solution SBF without Tris from our previous experiment had the concentration of HCO_3^- ions more than 10-times lower opposite to I-solution or mod-DMEM used here. Based on the findings described above it is possible to expand our knowledge on the *in vitro* behavior of these particular 45S5 BG-derived scaffolds. In this study we found that the amorphous phase containing Ca and P (ACP) precipitated in both tested solutions on the scaffold surface, as it was anticipated on the grounds of consumed Ca and P in the non-buffered I-solution leachates. In both cases the phase was detected owing to the increased quantity of phosphorus on the sample surface as detected by EDS. The presence of ACP was also confirmed by the XRD results (the share of the amorphous phase increased with the time of scaffold exposure to the solutions). The ACP phase is probably in the form of nanospheres covering the $CaCO_3$ globules. Later, the amorphous phase can transform into OCP crystals.[24] As also shown in our recent study,[25] crystallization of $CaCO_3$ on the glass-ceramic surface in the non-buffered DMEM derived solution with concentration of HCO_3^- ions near to those of human plasma (27 mM dm^{-3}) will prevail. Moreover, ACP was also found in 27-SBF solution (without buffer Tris).[25]

We have not found evidence that the organic part of non-buffered mod-DMEM suppresses crystallization of phases, as calcite crystallized on the scaffold surface in both solutions. Another phase, halite, crystallized at the beginning of the immersion in mod-DMEM owing to higher concentrations of

Na^+ and Cl^- ions (not only in comparison with I-solution but also with blood serum) and the presence of Na^+ ions released from the tested glass-ceramic scaffold. It has to be noticed that halite is not the residue of mod-DMEM or I-solution. The same treatment was applied on each glass-ceramic scaffold taken out from testing solutions (see Section 2.3.). The transmission geometry of the XRD measurement enabled finding the NaCl phase covered later by the precipitated $CaCO_3$ phase. Probably, halite crystals served as advantageous sites for $CaCO_3$ and ACP nucleation.

The presence of the organic components in mod-DMEM solution affects the rate of glass-ceramic dissolution; it is possible that the tested scaffold dissolved more slowly in mod-DMEM compared to I-solution: we estimated this based on small changes of Ca and P concentrations in the mod-DMEM leachates.

After completion of the test in I-solution the inert Pt spirals, in which the scaffold samples were suspended, were covered with a very thin layer. XRD analysis of the precipitate showed that the layer consisted mainly of the NaCl phase and Ca-defective carbonate apatite (CDHA). This phenomenon had no influence on the conclusions of the present experiments but it should be discussed in the context of establishing a suitable setup and experimental conditions of bioactivity tests which is the matter of current work.

5. Conclusions

1. Non-buffered mod-DMEM solution is not the ideal environment for the formation of a hydroxyapatite phase in bioactivity tests of glass-ceramic material.
2. Exposure to non-buffered mod-DMEM and non-buffered I-solutions resulted in crystallization of calcite and precipitation of amorphous calcium phosphate (ACP) on the scaffold surface.
3. The organic part of mod-DMEM does not suppress crystallization of calcite, halite or precipitation of ACP; probably it suppresses the glass-ceramic dissolution.
4. Considering the general goal of monitoring the growth of hydroxyapatite phase (HAp) on the surface of materials as one of the important factors determining the so-called "bioactivity", a highly critical question remains to be answered related to the selection of the suitable buffering system to be commonly used for SBF and to the determination of appropriate *in vitro* test conditions.

Acknowledgements

This work was supported by the Technology Agency of the Czech Republic within the project TE01020390 Center for development of modern metallic biomaterials for medicinal implants. The authors would like to express their thanks for SEM/EDS analyses to Ing. Zuzana Zlámalová Cílová, PhD, from the Department of Glass and Ceramics of the Institute of Chemical Technology in Prague. The authors would also like to thank Prof. Ing Jan Hlaváč, DrSc., professor emeritus, for his inspiring comments.

References

1 W. Cao and L. L. Hench, Bioactive materials, *Ceram. Int.*, 1996, **22**(6), 493–507.
2 ISO 23317, *Implants for surgery – In vitro evaluation for apatite-forming ability of implant materials*, 1st edn, 2007.
3 T. Kokubo and H. Takadama, How useful is SBF in predicting in vivo bone bioactivity?, *Biomaterials*, 2006, **27**, 2907–2915.
4 P. N. De Aza, F. Guitan, A. Merlos, E. Lora-Tamayo and S. De Aza, Bioceramics-simulated body fluid interfaces: pH and its influence of hydroxyapatite formation, *J. Mater. Sci.: Mater. Med.*, 1996, **7**, 399–402.
5 H. Pan, X. Zhao, B. W. Darvell and W. W. Lu, Apatite-formation ability – predictor of "bioactivity"?, *Acta Biomater.*, 2010, **6**, 4181–4188.
6 M. Bohner and J. Lemaitre, Can bioactivity be tested in vitro with SBF solution?, *Biomaterials*, 2009, **30**, 2175–2179.
7 D. Rohanová, A. R. Boccaccini, D. M. Yunos, D. Horkavcová, I. Březovská and A. Helebrant, Tris buffer in simulated body fluid distorts the assessment of glass-ceramic scaffold bioactivity, *Acta Biomater.*, 2011, **7**, 2623–2630.
8 J. Hlaváč, D. Rohanová and A. Helebrant, The effect of Tris-buffer on the leaching behavior of bioactive glass-ceramics, *Ceram.-Silik.*, 1994, **38**, 119–122.
9 I. N. Bastos, G. M. Platt, M. C. Andrade and G. D. Soares, Theoretical study of Tris and bistris effects on simulated body fluids, *J. Mol. Liq.*, 2008, **139**(1–3), 121–130.
10 E. Z. Kurmaev, R. G. Wilks, R. Filby, A. Moewes, L. Müller and F. A. Müller, Characterization of chemically treated titanium using soft X-ray fluorescence, *Mater. Sci. Eng., C*, 2009, **29**(1), 136–139.
11 L. Müller and F. Müller, Preparation of SBF with different HCO_3^- content ant its influence on the composition of biomimetic apatites, *Acta Biomater.*, 2006, **2**, 181–189.
12 S. Jalota, S. B. Bhaduri and A. C. Tas, Using a synthetic body fluid (SBF) solution of 27 mmol dm^{-3} HCO_3^- to make bone substitutes more osteointegrative, *Mater. Sci. Eng., C*, 2008, **28**, 129–140.
13 V. Cannillo, F. Pierli, I. Ronchetti, C. Siligardi and D. Zaffe, Chemical durability and microstructural analysis of glasses soaked in water and in biological fluids, *Ceram. Int.*, 2009, **35**, 2853–2869.
14 S. Mandel and A. C. Tas, Brushite ($CaHPO_4 \cdot 2H_2O$) to octacalcium phosphate ($Ca_8(HPO_4)_2(PO_4)_4 \cdot 5H_2O$) transformation in DMEM solutions at 36.5 °C, *Mater. Sci. Eng., C*, 2010, **30**, 245–254.
15 J. Faure, A. Balamurugan, H. Benhayoune, P. Torres, G. Balissier and J. M. F. Ferreira, Morphological and chemical characterisation of biomimetic bone like apatite formation on alkali treated Ti6Al4V titanium alloy, *Mater. Sci. Eng., C*, 2009, **29**, 1252–1257.
16 V. Aina, G. Malavasi, A. Fiorio Pla, L. Munaron and C. Morterra, Zinc-containing bioactive glasses: surface reactivity and behaviour towards endothelial cells, *Acta Biomater.*, 2009, **5**, 1211–1222.

17 G. Theodorou, O. M. Goudouri, E. Kontonasaki, X. Chatzistavrou, L. Papadopoulou, N. Kantiranis and K. M. Paraskevopoulos, Comparative bioactivity study of 45S56 and 58S bioglasses in organic and inorganic environment, *Bioceramics edit. Kim Sukyoung*, 2009, **22**, 391–394.

18 M. A. Miller, R. M. Kendal, K. J. Manoj, P. R. Larson, A. S. Madden and A. C. Tas, Testing of Brushite ($CaHPO_4 \cdot 2H_2O$) in Synthetic Biomineralization Solutions and *In Situ* Crystallization of Brushite Micro-Granules, *J. Am. Ceram. Soc.*, 2012, **95**(7), 2178–2188.

19 N. Temizel, G. Girisken and A. C. Tas, Accelerated transformation of brushite to octacalcium phosphate in new biomineralization media between 36.5 °C and 80 °C, *Mater. Sci. Eng., C*, 2011, **31**, 1138–1143.

20 Q. Z. Chen, L. D. Thompson and A. R. Boccaccini, 45S5 Bioglass-derived glass-ceramic scaffolds for bone tissue engineering, *Biomaterials*, 2006, **27**, 2414–2425.

21 A. Helebrant, L. Jonášová and L. Šanda, The influence of simulated body fluid composition on carbonated hydroxyapatite formation, *Ceram.-Silik.*, 2002, **46**(1), 9–14.

22 X. Lu and Y. Leng, Theoretical analysis of calcium phosphate precipitation in simulated body fluid, *Biomaterials*, 2005, **26**(10), 1097–1108.

23 JCPDS-ICDD PDF-2 database, International Centre for Diffraction Data, Newtown Square, PA, U.S.A. release 54, 2004.

24 A. C. Tas, X-ray-amorphous calcium phosphate (ACP) synthesis in a simple biomineralization medium, *J. Mater. Chem. B*, 2013, **1**, 4511–4520.

25 D. Rohanová, D. Horkavcová, A. R. Boccaccini, I. Březovská, P. Bozděchová, P. Bezdička, M. Častorálová and A. Helebrant, Interakce sklokeramického "scaffoldu" připraveného ze skla Bioglass® se simulovanými tělnými tekutinami, *Sklář a keramik, C*, 2011, **61**, 125–128.

Práce **[11]**

Rohanová D., Horkavcová D., Paidere L., Boccaccini A.R., Bozděchová P., Bezdička P.: Interaction of HEPES buffer with glass-ceramic scaffold: Can HEPES replace TRIS in SBF? Journal of Biomedical Materials Research Part B, DOI:10.1002/jbm.b.33818, 2017 in print.

Podíl: 60%: návrh experimentu, zpracování výsledků, příprava publikace

Society For Biomaterials

Interaction of HEPES buffer with glass-ceramic scaffold: Can HEPES replace TRIS in SBF?

Dana Rohanová,[1] Diana Horkavcová,[1] Laine Paidere,[2] Aldo Roberto Boccaccini,[2] Pavlína Bozděchová,[1] Petr Bezdička[3]

[1]Department of Glass and Ceramics, Faculty of Chemical Technology, University of Chemistry and Technology Prague, Technická 5, 166 28 Prague 6, Czech Republic
[2]Department of Materials Science and Engineering, Institute of Biomaterials, University of Erlangen-Nuremberg, 91058 Erlangen, Germany
[3]Institute of Inorganic Chemistry of the ASCR, v.v.i., 250 68 Husinec- Řež, Czech Republic

Received 30 June 2016; revised 25 October 2016; accepted 8 November 2016
Published online 00 Month 2016 in Wiley Online Library (wileyonlinelibrary.com). DOI: 10.1002/jbm.b.33818

Abstract: An international standard (ISO: 23317:2014) exists for the *in vitro* testing of inorganic biomaterials in simulated body fluid (SBF). This standard uses TRIS buffer to maintain neutral pH in SBF, but in our previous paper, we showed that the interaction of a tested glass-ceramic material with TRIS can produce false-positive results. In this study, we evaluated whether the HEPES buffer, which also belongs to the group of Good's buffers, would be more suitable for SBF. We compared its suitability in two media: SBF with HEPES and demineralized water with HEPES. The tested scaffold (45S5 bioactive glass-based) was exposed to the media under a static-dynamic arrangement (solutions were replaced on a daily basis) for 15 days. Leachate samples were collected daily for the analysis of Ca^{2+} ions and Si (AAS), $(PO_4)^{3-}$ ions (UV-VIS), and to measure pH. The glass-ceramic scaffold was analyzed by SEM/EDS, XRD, and WD-XRF before and after 0.3, 1, 3, 7, 11, and 15 days of exposure. Our results confirmed the rapid selective dissolution of the glass-ceramic crystalline phase (*Combeite*) containing Ca^{2+} ions due to the presence of HEPES, hydroxyapatite supersaturation being reached within 24 h in both solutions. These new results suggest that, like TRIS, HEPES buffer is not suitable for the *in vitro* testing of highly reactive inorganic biomaterials (glass, glass-ceramics). The ISO standard for such tests requires revision, but HEPES is not a viable alternative to TRIS buffer. © 2016 Wiley Periodicals, Inc. J Biomed Mater Res Part B: Appl Biomater 00B: 000–000, 2016.

Key Words: *in vitro* test, simulated body fluid, HEPES buffer, glass-ceramic scaffold, biomaterial

How to cite this article: Rohanová D, Horkavcová D, Paidere L, Boccaccini AR, Bozděchová P, Bezdička P 2016. Interaction of HEPES buffer with glass-ceramic scaffold: Can HEPES replace TRIS in SBF?. J Biomed Mater Res Part B 2015:00B:000–000.

INTRODUCTION

Recently, much work has focused on the development of inorganic materials for use in bone tissue engineering, such as glass[1,2] and glass-ceramic scaffolds.[3,4] For such a material to be classified as "bioactive," it should first pass an *in vitro* test in simulated body fluid (SBF), which models the inorganic part of blood plasma. *In vitro* testing not only gives indicative results for comparing the dissolution reactions of different samples under specific conditions, but also aids understanding of the behavior of a tested biomaterial during the important first hours after exposure to solutions similar to blood plasma. In the future, it may help in the development of new inorganic biomaterials. Thus, an inert buffer in SBF is necessary to maintain conditions close to those in blood plasma. In accordance with ISO standard 23317, neutral pH in SBF is usually maintained using TRIS buffer.[5] While Bohner and Lemaitre[6] considered the appropriateness of using protein-free SBF, as designed by Kokubo and Takadama,[7] we are focused on the search for a suitable buffer for SBF. As we reported recently,[8] TRIS buffer used with a highly reactive glass-ceramic scaffold accelerates the dissolution of the glass-ceramic crystalline phase (*Combeite*) and leads to the formation of hydroxyapatite (HAp). Subsequently, we showed that non-buffered SBF alone is equally unable to maintain neutral pH during the *in vitro* testing of a soluble inorganic material, with pH either increasing or decreasing due to material dissolution.[8–10] Consequently, other alternatives to TRIS buffer are being sought for *in vitro* testing.

One alternative is HEPES buffer, which has been widely used in biochemistry and microbiology laboratories. Similar to TRIS buffer, HEPES buffer (*4-(2-Hydroxyethyl)piperazine)-1-ethanesulfonic acid*) belongs to the group known as "Good's" buffers.[11] HEPES buffer is a standard part of one series of the

Correspondence to: D. Rohanová (e-mail: dana.rohanova@vscht.cz)
Contract grant sponsor: The Technology Agency of the Czech Republic within project TE01020390, *Centre for development of modern metallic biomaterials for medicinal implants*

TABLE I. Composition of 45S5 Bioglass®, Crystalline and Glass Phases of Scaffolds Used in this Study[8]

Oxides	45S5 Bioglass® (100 wt %)	$Na_2Ca_2Si_3O_9$ (77.4 wt % scaffold[a])	Residual glass phase (22.6 wt % scaffold)
SiO_2	45.0	50.9	24.8
Na_2O	24.5	17.4	48.5
CaO	24.5	31.7	–
P_2O_5	6.0	-	26.5

[a] Minority phases $CaO{\cdot}SiO_2$ and Buchwaldite ($NaCaPO_4$) are included.

commercially produced Eagle's minimal essential medium (MEM) and Dulbecco's modified Eagle's medium (DMEM) solutions. These solutions are primarily used for the cultivation and incubation of cell cultures for biochemical, pharmacological, and toxicological studies. Despite this, Lelong and Rebel[12] expressed skepticism about the use of HEPES buffer in biochemical studies: "The HEPES presence may strongly jeopardize some studies linked to the ability of this compound to interfere with numerous pharmacological parameters." Moreover, Stellwagen et al.[13] confirmed that DNA-buffer (HEPES) interactions are very common, especially in neutral pH, amino-based buffers.

As Tas[14] pointed out in his review, MEM and DMEM solutions are used with HEPES buffer for *in vitro* bioactivity tests. For the *in vitro* testing of fluorine-doped bioactive glass, Shah et al.[15] prepared a non-buffered MEM solution with Earle's Salts (A-MEM) and three kinds of MEM media with HEPES buffer. Their results showed that fluoroapatite (a bioactivity indicator) preferentially formed in the non-buffered A-MEM medium. Fluorine-doped bioactive glass dissolved earlier (as was apparent from Si release) in MEM with HEPES buffer than in A-MEM. The authors concluded that media composition must be taken into account when interpreting dissolution results or cell behavior studies.[15] Dezfuli et al.[16] confirmed the effect of HEPES buffer on the dissolution of a magnesium-based material in DMEM. HEPES presence caused the local pH to increase on the sintered Mg and, thus, led to greater degradation of the tested material. The higher degradation rate at the surface formed cracks that led to further dissolution of the Mg. On this basis, HEPES buffer used in DMEM results in a corrosive environment.

Kim et al.[17] described the stability of SBF with HEPES buffer and a concentration of HCO_3^- ions that corresponded quite closely to blood plasma. Their prepared "revised" SBF solution (R-SBF) was stable, with no spontaneous precipitation of HAp observed for 4 weeks. In Oyane et al.'s follow-up works[18,19] SBF stability was tested with HEPES buffer and half of the normal concentration of HCO_3^- ions in blood plasma; in this case, solution stability extended to 8 weeks. Lu and Leng[20] used the aforementioned solutions for theoretical calculations of the driving force and nucleation rate of calcium phosphate (Ca-P) precipitation in SBF with TRIS buffer. However, the authors did not consider the possibility that TRIS or HEPES buffer might interact with the tested inorganic material.

In this study, we investigate the interaction of HEPES buffer with a glass-ceramic scaffold during *in vitro* testing to determine whether it could replace TRIS buffer in maintaining a neutral pH in SBF during such tests. The glass-ceramic scaffold was prepared by the foam replica method using 45S5 Bioglass®.[21] Crystallization of the 45S5 Bioglass® occurred upon heat treatment. A 45S5 Bioglass®-derived glass-ceramic scaffold was chosen because it has certain advantages for *in vitro* testing: the main crystalline phase ($Na_2O{\cdot}2CaO{\cdot}3SiO_2$) and one of the minor phases ($CaO{\cdot}SiO_2$) contain all the CaO present in 45S5 Bioglass® while the residual glass phase contains the entire amount of P_2O_5. Thus, Ca and P can serve not only as indicators of the beginning of precipitation, but also as "markers" of crystalline and glass phase dissolution in the testing solutions.

The *in vitro* testing of the scaffold was carried out under static-dynamic conditions (solutions were replaced every 24 h) in the presence of HEPES buffer in two solutions: simulated body fluid (SBF + HEPES) and demineralized water (D + HEPES). The material was assessed using XRD, XRF, and SEM/EDS. The interaction of the glass-ceramic scaffold with demi water (Demi H_2O) and non-buffered SBF (SBF) was discussed in our previous article.[8] In this article, we focus on the interaction of HEPES buffer with a glass-ceramic scaffold, demonstrating the effects of immersion for up to 15 days. Our results contribute to a deeper understanding of the dissolution mechanism of a highly reactive silicate glass-ceramic scaffold.

MATERIALS AND METHODS

Materials

The material used for the testing was silicate glass-ceramic in the form of a highly porous structure (scaffold) prepared by the well-known foam replica technology.[21] The initial material for the glass suspension was commercially prepared 45S5 Bioglass® powder with a mean particle size of <2 μm. To prepare the scaffold, polyurethane (PUR) foam was immersed into the suspension. After 1 min, the foam was removed and wrung to remove excess suspension. Then, the foam was dried for 30 s and the whole process repeated. The porous precursor, so-called *green body*, was left to dry for 24 h at 60°C

TABLE II. Ion Composition (mmol·dm^{-3}) of the Investigated Solutions

Solution	HEPES	Na^+	K^+	Ca^{2+}	Mg^{2+}	Cl^-	HCO_3^-	HPO_4^{2-}	SO_4^{2-}
SBF+HEPES	37.5	142.0	5.0	2.5	1.5	125.8	4.2	1.0	1.0
D+HEPES	37.5	[a]16,9	0	0	0	0	0	0	0
I-solution [23]	0	142.0	5.0	1.8	1.5	103.0	44.0	1.0	0.5

[a] Na^+ ions were added to the HEPES buffer in the form of NaOH in order to achieve the neutral pH.

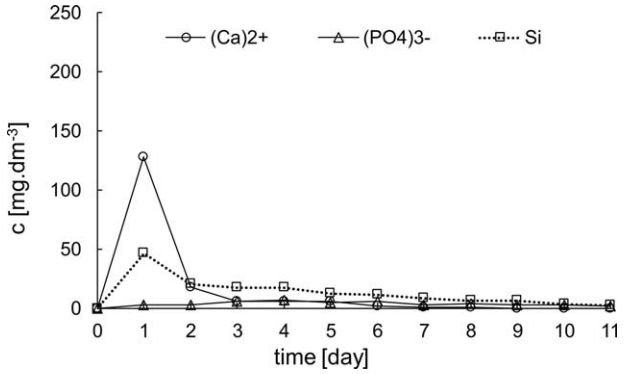

FIGURE 1. Concentrations of Ca^{2+}, $(PO_4)^{3-}$ ions and Si in D + HEPES during interaction with scaffold

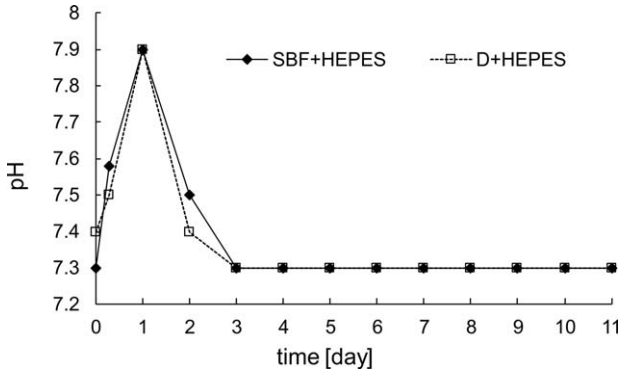

FIGURE 3. pH values in D + HEPES and SBF + HEPES during interaction with scaffold (static-dynamic conditions)

before being subjected to thermal treatment that consisted of firing at 400°C/1 h, burning-out the PUR template and sintering at 1050°C for 2 h. The scaffold exhibited an open porous structure with a pore size in the range of 510–720 μm and a porosity of approximately 90%. Samples containing the crystalline and residual glass phases were prepared with a dimension of 0.5 × 0.5 × 1 cm. Their compositions before and after crystallization[8] are shown in Table I.

Solutions for the *in vitro* tests

The interaction of HEPES buffer ((4-(2-Hydroxyethyl) piperazine)-1-ethanesulfonic acid); $C_8H_{18}N_2O_4S$) with the glass-ceramic scaffold was studied in protein-free SBF with HEPES buffer (**SBF + HEPES)** and in demineralized water with HEPES buffer (**D + HEPES**). The protein-free SBF solution was prepared according to ISO: 23317:2014[5] from the following reagents: KCl, NaCl, $NaHCO_3$, $MgSO_4{\cdot}7H_2O$, $CaCl_2$ and KH_2PO_4 (Table II). The buffer concentration in both solutions (SBF + HEPES and D + HEPES) was 0.0375 mol·dm^{-3} (determined experimentally). To prevent bacterial growth in the solutions, azide (NaN_3) was added to the SBF. The pH value of both solutions was adjusted with 1 *M* solution of NaOH to pH = 7.3 ± 0.1. To prevent changes in the resulting concentration of Na^+ ions in SBF + HEPES, NaCl addition was lower than in Kokubo and Takadama's solution. Because this work follows up our previous article,[8] for comparison purposes, the same chemical composition was used for the protein-free SBF.

Static-dynamic conditions of *in vitro* testing

To prevent ion exhaustion, the so-called static-dynamic *in vitro* test, in which the solutions were replaced every 24 h, was carried out The scaffold samples used for the static-dynamic *in vitro* test weighed 0.050 ± 0.005 g. They were placed in platinum spirals and suspended in plastic bottles filled with 50 mL of the testing solution. The sample bottles were put into a biological thermostat at a temperature of 36.5 ± 0.5°C. To measure pH and analyze Ca^{2+}, $(PO_4)^{3-}$ and Si concentrations, leachate samples were collected daily. Two samples were gently rinsed three times with demineralized water, left to dry at laboratory temperature and collected for WD-XRF, XRD, and SEM/EDS measurements before and after 0.3, 1, 3, 7, 11, and 15 days. The D + HEPES test had to be terminated as early as after 11 days due to enormous sample dissolution and disintegration.

Leachate analysis

All tests and analyses were performed on two parallel series of samples. The diagrams do not show the deviations for the individual curves as they were very small and would have made the diagrams less transparent. The indicated curves represent the average of two parallel measurements.

Atomic absorption spectrophotometry

The concentrations of Ca^{2+} ions were analyzed by a VARIAN-SpectrAA 300. The leachates were atomized with an

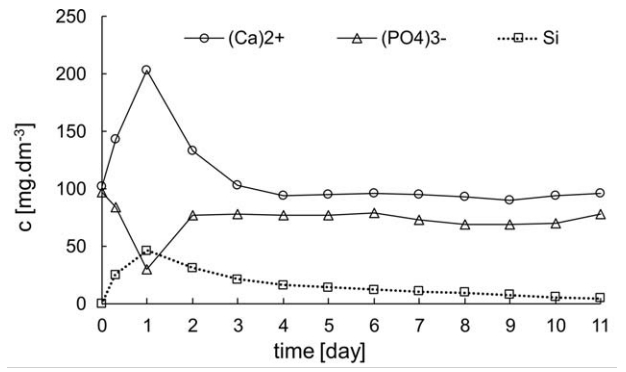

FIGURE 2. Concentrations of Ca^{2+}, $(PO_4)^{3-}$ ions and Si in SBF + HEPES during interaction with scaffold

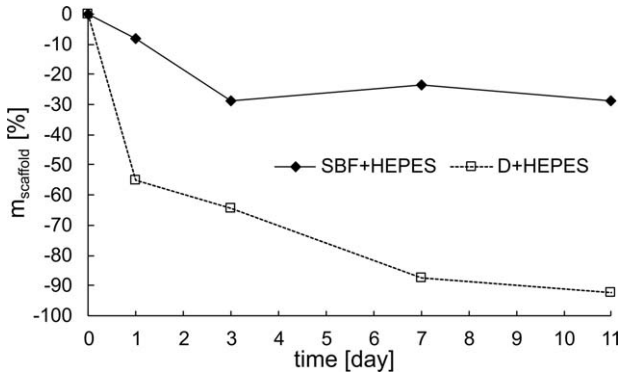

FIGURE 4. Change of scaffold weight in SBF + HEPES and D + HEPES during experiment

TABLE III. Chemical Composition of Original Scaffold Before and After Exposure to D + HEPES [wt %] (WD-XRF), Normalized to 100%.

Time [days]	Na_2O	MgO	SiO_2	P_2O_5	SO_3	Cl	K_2O	CaO	CaO/P_2O_5 ratio[a]
ORIGIN	24.5	0	43.7	5.4	0	0	0	26.3	4.87
0.3	14.4	0	56.5	7.7	0.1	0	0	21.1	2.74
1	5,9	0	63.7	12.8	0.1	0	0	17.3	1.36
3	1.0	0	65.0	16.3	0.2	0	0	17.1	1.05
7	0.5	0	63.4	18.5	0.1	0.1	0	14.4	0.78
11	1.2	0	54.8	23.6	1.8	0.2	0	18.0	0.76
15									Not analyzed[b]

[a] Hydroxyapatite - $Ca_{10}(PO_4)_6(OH)_2$: theoretical CaO/P_2O_5 ratio = 1.32
[b] low amount of sample

acetylene-N_2O flame. The wavelength used for the absorbance measurements was 422.7 nm.

The concentrations of Si were analyzed by a VARIAN-SpectrAA 880. The leachates were atomized with an acetylene-N_2O flame. The wavelength used for the absorbance measurements was 251.6 nm.

Spectrophotometry

The concentrations of $(PO_4)^{3-}$ ions were analyzed by a UV-1601 UV–VIS spectrophotometer at a wavelength of 830 nm (ČSN 830540).

pH measurement. The pH values were measured by an inoLab pH-meter with a combined glass electrode at 33 ± 2°C.

Analysis of the materials

Scanning electron microscopy/energy-dispersive spectroscopy. Before and after every test, the sample surfaces were inspected by an Hitachi S-4700 scanning electron microscope (SEM) equipped with an energy-dispersive spectroscopy (EDS) analyzer (NORAN D-6823) working at an accelerating voltage of 15 kV. The samples were powder coated with an Au-Pd layer for 80–100 s for SEM observation.

X-ray powder diffraction analysis. The samples were ground in an agate mortar in a suspension with cyclohexane. The suspension was then put on a mylar film and placed into a transmission sample holder. After solvent evaporation, a thin layer of the prepared sample was covered with another mylar film. Diffraction patterns were collected using a PANalytical XPert PRO diffractometer equipped with a conventional X-ray tube ($Cu_{K\alpha}$ 40 kV, 30 mA, line focus) working in transmission mode. An elliptical focusing mirror with a 0.5° divergence slit, 0.5°anti-scatter slit and 0.02 rad Soller slit were used in the primary beam. A PIXcel fast linear position sensitive detector with an anti-scatter shield and a 0.02 rad Soller slit was used in the diffracted beam. All patterns were collected in the range of 3°–88° 2 theta; at steps of 0.013° with 600 s per step, the measurement took approximately 4.5 h. Qualitative analysis was performed using HighScorePlus software (PANalytical, the Netherlands, version 4.5.0), Diffrac-Plus software (Bruker AXS, Germany, version 8.0) and the JCPDS-ICDD PDF-2 database.[22]

WD-XRF

XRF analysis was carried out using a PerformX (Thermo Scientific) sequential wavelength dispersive X-ray spectrometer equipped with an X-ray lamp with a 4GN Rh anode and a 50 μm thick Be end-window. The intensities of the spectral lines of the elements were measured for 6 or 12 s in vacuum using OXAS software. The obtained intensities were processed by UNIQUANT 5 software without the need to measure standards. The analyzed powder samples were compressed into binder-free 5 mm thick tablets with a diameter of 40 mm. The measuring time for each sample was approximately 15 min.

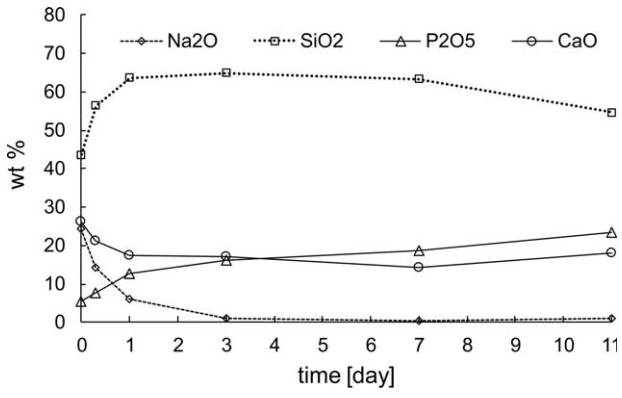

FIGURE 5. Ratios of scaffold components (% of oxides) in D + HEPES (WD-XRF)

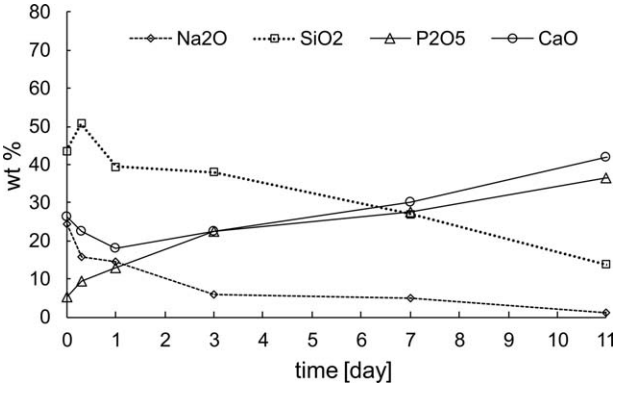

FIGURE 6. Changes of oxide representation [wt %] (up to 100% of the material) in glass-ceramic scaffold during interaction with SBF + HEPES (WD-XRF)

TABLE IV. Chemical Composition of Original Scaffold Before and After Exposure to SBF + HEPES [wt %] (WD-XRF), Normalized to 100%.

Time [days]	Na_2O	MgO	SiO_2	P_2O_5	SO_3	Cl	K_2O	CaO	CaO/P_2O_5 ratio[a]
ORIGIN	24.5	0	43.7	5.4	0	0	0	26.3	4.87
0.3	15.7	0.3	50.8	9.4	0.1	0	0	22.5	2.39
1	14.4	0.5	39.5	13.1	5.6	8.4	0.4	18.0	1.37
3	6.1	0.7	38.0	22.6	3.9	5.6	0.3	22.5	1.00
7	4.9	1.0	27.1	27.6	3.9	4.8	0.3	30.2	1.09
11	1.2	1.2	13.8	36.5	0.3	0.4	0.1	41.9	1.15
15	4.7	1.3	14.4	32.0	2.8	3.8	0.2	40.5	1.27

[a] Hydroxyapatite - $Ca_{10}(PO_4)_6(OH)_2$: theoretical CaO/P_2O_5 ratio = **1.32**

RESULTS

Scaffold dissolution—leachate analysis

The tested solutions were exchanged daily (static-dynamic conditions) to maintain both the pH value and the Ca^{2+} and $(PO_4)^{3-}$ concentrations at their original levels during the experiment. The obtained curves represent the average of the two parallel experiments. The ion concentrations in the leachates reflect the processes of material dissolution (in D + HEPES, the concentrations of Si and Ca^{2+}) and of the precipitation of a new phase [in SBF + HEPES, the concentrations of Ca^{2+} and $(PO_4)^{3-}$]. As early as the first day there was an extreme increase in the concentrations of Ca^{2+} and Si ions in both leachates (Figures 1 and 2). Within three days, the Ca^{2+} concentration in the SBF + HEPES leachates returned to approximately its original value (in D + HEPES to 0). After 1 week of exposure, scaffold dissolution slowed down significantly, as indicated by the Si concentrations in both solutions. The major decrease in $(PO_4)^{3-}$ ions identified on the first day, together with their stable low concentration until the end of the test, confirmed that the precipitation of the Ca-P phase occurred throughout the entire experiment in SBF + HEPES.

The pH value in the leachates reflects the process of scaffold dissolution (Figure 3). Due to the enormous release of Na^+ and Ca^{2+} ions at the beginning of the test, the pH value rapidly increased. The pH value in both solutions (D + HEPES and SBF + HEPES) stabilized around 7.3 after the third day due to daily solution replacement and the fact that scaffold dissolution, and thus the release of Na^+ and Ca^{2+} ions, slowed down.

Although the weights of the glass-ceramic scaffold samples were very low and, thus, the resulting values may be influenced by errors, significant sample weight loss is clear. Massive dissolution was recorded as early as after the first day of exposure, by which time up to 55% of the scaffold had dissolved into the D + HEPES solution. By day 11, >90% had dissolved, and by the end of day 11, the scaffold had completely dissolved. The formation of a new phase, later identified as the HAp phase, did not have a significant effect on weight (Figure 4). As with D + HEPES, it is obvious that the change in scaffold weight in SBF + HEPES involved scaffold dissolution and a significant increase in new phases (HAp and NaCl, as determined by XRD and WD-XRF). In D + HEPES, scaffold weight decreased by 14 wt % after 8 h while SBF + HEPES was only 8 wt % after 24 h. Although after 3, 7, and 11 days, the scaffold had lost 30% of its initial weight, by the end of the test it had only lost ca. 18 wt % (Figure 4). Collectively, these results confirm the formation of the HAp phase in SBF + HEPES.

The WD-XRF results of analyses of the residual scaffold material were in agreement with those of the leachate analyses (Table III, Figure 5). At the beginning of the exposure, there was a significant release of CaO and Na_2O, as shown by the decrease in their content. The increase in SiO_2 after the first day of exposure is only ostensible as it represents the ratios of scaffold components at a given time. Although the D + HEPES solution did not contain the inorganic part of blood plasma, the precipitation of Ca-P is obvious from both the increasing ratio of P_2O_5 and slower release of CaO

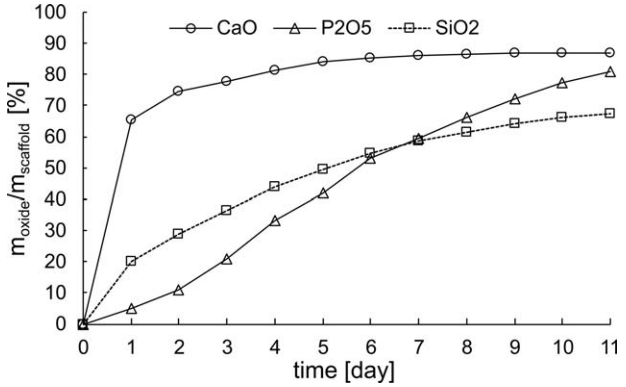

FIGURE 7. Cumulative dissolution of scaffold components (oxides) in D + HEPES (% of weight loss) showing that the scaffold dissolved incongruently

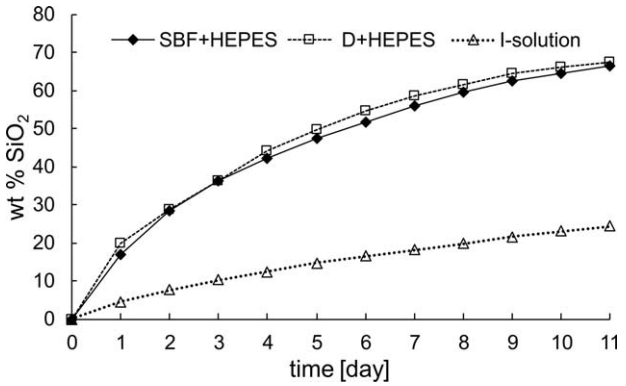

FIGURE 8. Cumulative dissolution of SiO_2 in SBF + HEPES, D + HEPES and non-buffered I-solution [23] as calculated from material balance of leached Si (see Note 1)

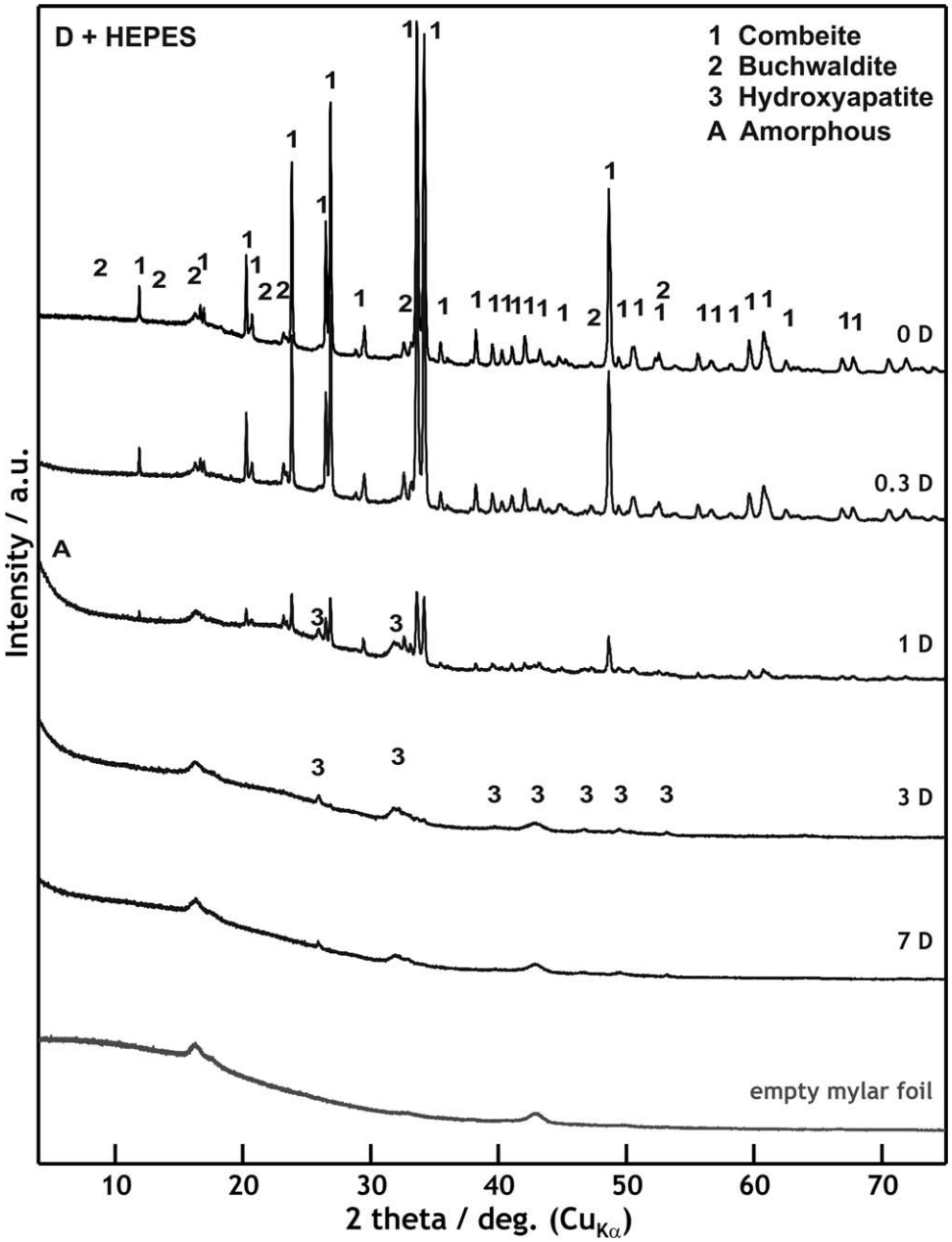

FIGURE 9. XRD patterns of scaffold samples before and after 0.3, 1, 3 and 7 days of interaction with D + HEPES. The small amount of scaffold remaining after 11 days of immersion consisted almost entirely of an amorphous phase (not shown in the diffractogram)

within the very first hours of the test. In combination with the alkaline environment, the biogenic components released from the scaffold created the ideal conditions for HAp precipitation. After day 11 of the test, the Ca-P phase represented up to 40% of the residual material.

After 8 h, the dissolution of the glass-ceramic scaffold in SBF + HEPES was obvious from the reduced content of Na_2O and CaO (Figure 6). The slight increase of SiO_2 in the scaffold was only relative and associated with enormous leaching of the alkaline components at the beginning of exposure. Virtually none of the phosphorous in the residual glass phase was released from the scaffold because the Ca-P phase utilized the phosphorus present in the solution. By the end of the test, the Ca-P phase represented ca. 80% of the analyzed material. WD-XRF also indicated a slight increase in chlorine concentration; namely, the formation of NaCl after the first day. Moreover, as the exposure time increased, small concentrations of Mg, K, and S (from 0.1 to 3 wt %), which also precipitated from the SBF solution, appeared in the scaffold (Table IV). However, for simplicity's sake, these elements are not indicated in the diagram.

DISCUSSION

With regards to our previous article[8] on the effect of TRIS buffer on the dissolution of a tested scaffold, we should briefly point out the mechanism of scaffold dissolution in demineralized

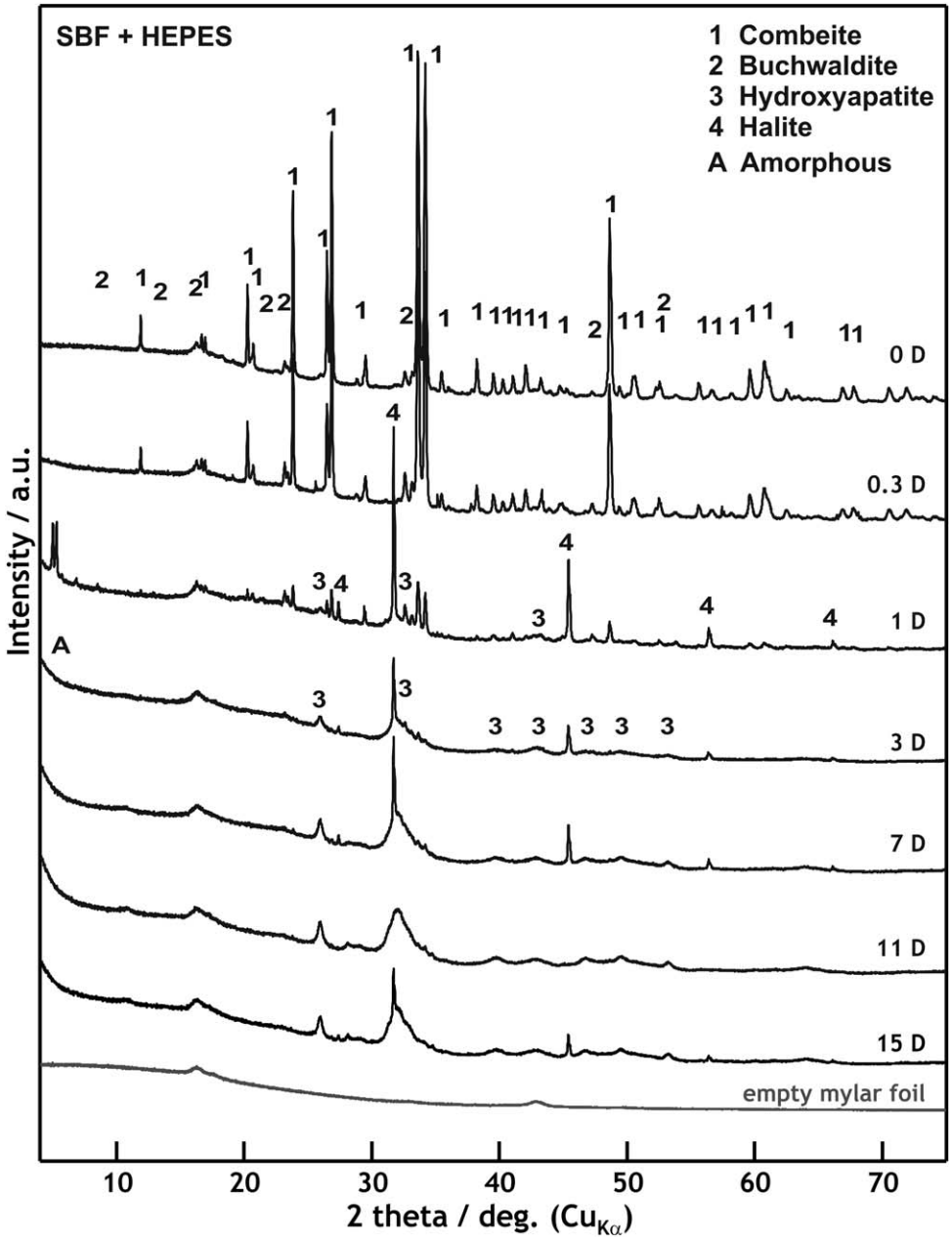

FIGURE 10. XRD patterns of scaffold before and after 0.3, 1, 3, 7, 11 and 15 days of interaction with SBF + HEPES

water (Demi H_2O) and in non-buffered SBF solution (SBF). In that study, water (Demi H_2O) caused the preferential dissolution of the remaining glass part of the scaffold, as evidenced by an increase in the concentration of $(PO_4)^{3-}$ ions. In the non-buffered SBF solution,[8] as in non-buffered I-solution,[23] there was no significant increase of Ca^{2+} ions in the leachates; XRD identified the *Combeite* phase in the scaffold even after 2 weeks of exposure. In other words, whenever TRIS was not present, the *Combeite* phase was only slightly dissolved.

The tests in this study have shown that the mechanism by which HEPES buffer interacts with a glass-ceramics scaffold is very similar to TRIS buffer[8]; namely, both of them promote *Combeite* dissolution. Nearly three quarters of the total quantity of CaO was released within 24 h of exposure to D + HEPES. SiO_2 and P_2O_5 were released more slowly during the first days of exposure, but by the end of day 11, nearly 90% of CaO and P_2O_5, and 70% of SiO_2, had been released from the material into D + HEPES. Leachate analyses confirmed our assumption of the preferential dissolution of the *Combeite*, which contains all of the CaO, in the presence of HEPES buffer. The development of the P_2O_5 concentration in the leachate indicated that the residual glass phase, containing nearly all of the P_2O_5, started to dissolve significantly on the third day of exposure. Thus, analyses of both the leachates and the glass-ceramic scaffold have shown that, as early as within the first hours of exposure,

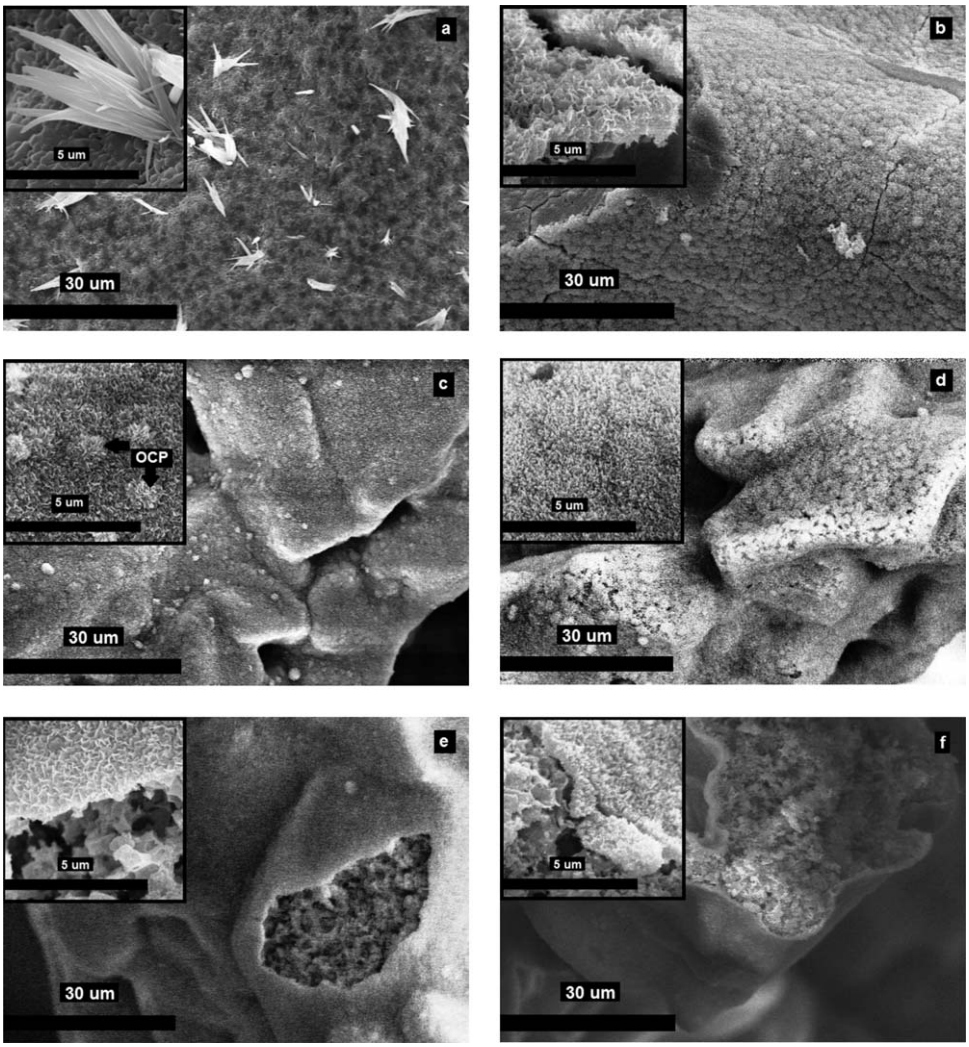

FIGURE 11. SEM images at two different magnifications of glass-ceramic scaffold: a) before exposure (combeite = the small tabular crystals; buchwaldite and structurally isomorphic $CaO.SiO_2$ phases = the needle-like crystals); b-f) after 0.3, 1, 3, 7 and 11 days of interaction with D + HEPES, respectively

the scaffold dissolved significantly in the presence of the HEPES buffer. The dissolution process is incongruent; most alkaline ions (Na^+ and Ca^{2+}) are released from the material during the first day of exposure (Figure 7)

When scaffold dissolution in the HEPES solutions (D + HEPES and SBF + HEPES) is compared with dissolution in similar buffer-free solutions [the so-called I-solution (see details in Rohanová et al.,[23] Figure 4)], it is obvious that the HEPES buffer significantly accelerated the dissolution of the glass-ceramic scaffold (Figure 8). Scaffold dissolution in the non-buffered I-solution occurred at a stable rate, four times slower than in the solutions containing HEPES buffer. Rather surprisingly, the presence of the inorganic part of blood plasma (here identified as SBF) did not influence the interaction of the HEPES buffer with the glass-ceramic scaffold. The scaffold dissolved at the same rate and by the same mechanism in both solutions (SBF + HEPES and D + HEPES). It is interesting to note that even the newly formed HAp layer on the scaffold surface failed to effectively prevent its dissolution, the rate of Si dissolution being the same in both solutions (Figure 8).

Note 1: Cumulative dissolution of SiO_2 calculation:

$$c_{\mathrm{Si}}\left[\mathrm{mg}\cdot\mathrm{dm}^{-3}\right]\ \text{by AAS} \tag{1}$$

$$c_{\mathrm{SiO_2}} = \mathrm{MW_{Si}}/\mathrm{MW_{SiO_2}} \times c_{\mathrm{Si}}\left[\mathrm{mg}\cdot\mathrm{dm}^{-3}\right];\ V = 1\,\mathrm{dm}^3 \tag{2}$$

$$m_{\mathrm{SiO_2}}\mathrm{solution} = (c_{\mathrm{SiO_2}}/V) \times \mathrm{df}[\mathrm{mg}];\quad \text{if } V_{\mathrm{leachant}} = 0.05\,\mathrm{dm}^3;\ \mathrm{df} = 0.05/1 \tag{3}$$

$$w_{\mathrm{iSiO_2}} = m_{\mathrm{iSiO_2}}\mathrm{solution}/m_{\mathrm{SiO_2}}\mathrm{scaffold} \tag{4}$$

$$\sum \mathrm{wt}\,\%_{\mathrm{SiO_2}} = \sum_i (w_{i\mathrm{SiO_2}}) \times 100\%;\ i = <\ 0-11\ > \tag{5}$$

where c_{Si} and $c\mathrm{SiO_2}$ are the concentrations [$\mathrm{mg}\cdot\mathrm{dm}^{-3}$], V is the volume [dm^3], $m\mathrm{SiO_2}$ is the weight of the SiO_2 in the leachant or glass-ceramic material, and $\sum$wt $\%\mathrm{SiO_2}$ is the cumulative mass [%] for each of the 11 days.

As the D + HEPES solution provided information about scaffold dissolution, it was possible to compare the dissolution

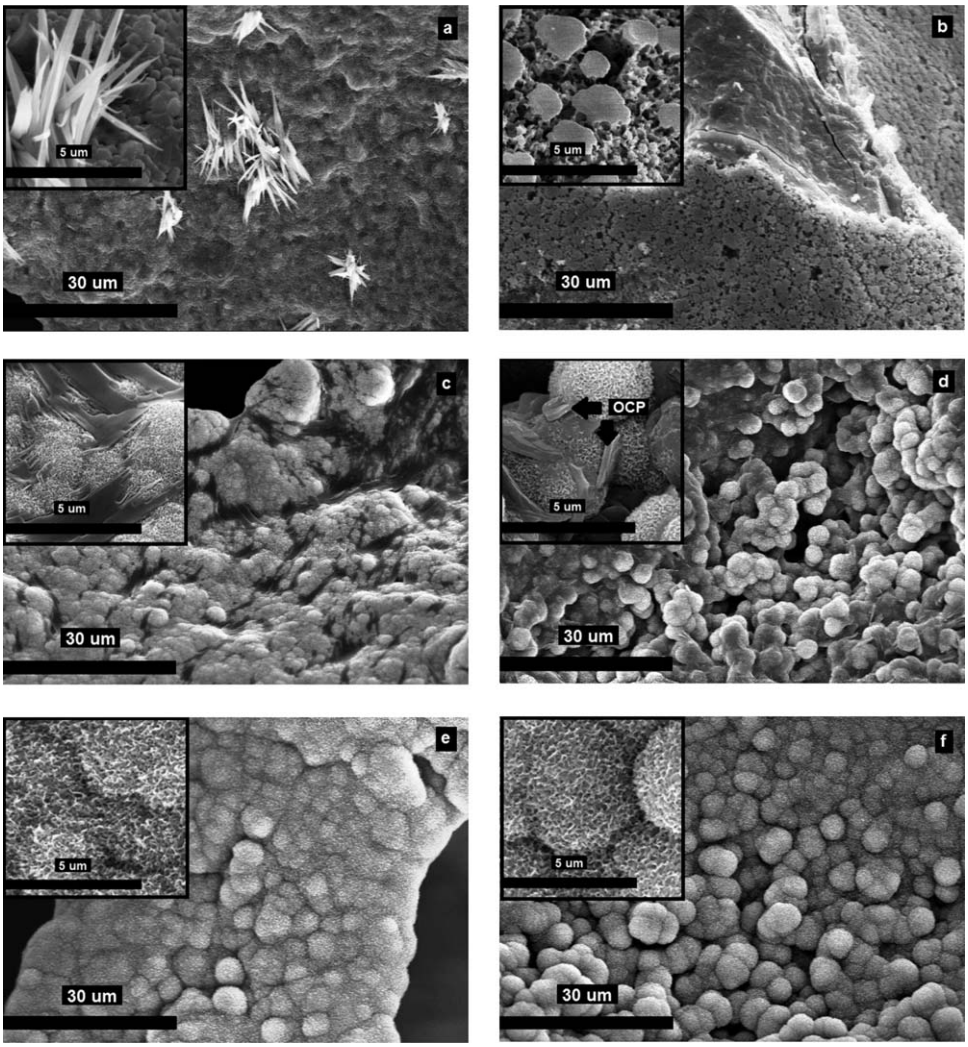

FIGURE 12. SEM images at two different magnifications of glass-ceramic scaffold: a) before exposure (combeite = the small tabular crystals; buchwaldite and structurally isomorphic $CaO.SiO_2$ phases = the needle-like crystals); b-f) after 0.3, 1, 3, 7 and 11 days of interaction with SBF + HEPES, respectively

rates and weight changes during the tests and, thereby, to confirm that:

- on day 1 of interaction, the crystalline phase of the scaffold (*Combeite*) completely dissolved in the presence of the HEPES buffer
- from day 3 of the test, the Ca-P phase formed at a stable rate (0.7 $mg.day^{-1}$) in SBF+HEPES
- based on the material balance and changes in calcium and phosphorus concentrations, approximately 45 mg of the new Ca-P (calculated as HAp) phase developed under the static-dynamic conditions of the test in SBF+HEPES, which is in perfect agreement with the leachate analyses and the identified weight changes.

Newly formed phases on the scaffold surface

As with our work on TRIS buffer,[8] the original crystalline phases of the scaffold, the main *Combeite* phase ($Na_2O{\cdot}2CaO{\cdot}3SiO_2$) and the minor $CaO{\cdot}SiO_2$ and *Buchwaldite* ($NaCaPO_4$) phases, were only detected during the first day of exposure. Even in the absence of the inorganic part of blood plasma, hydroxyapatite (HAp) developed on the scaffold surface (Figure 9). Apart from crystalline HAp, an increase in the XRD amorphous phase (residual SiO_2 phase and partly precipitated non-stoichiometric Ca-P phase, as confirmed by WD-XRF) was observed from the very first day of exposure.

XRD analysis also confirmed a significant decrease in the crystalline phases of the glass-ceramic scaffold within 24 h of interaction with SBF + HEPES. After day 1 of exposure, XRD identified the formation of HAp and halite (NaCl), which is in agreement with the WD-XRF results. XRD also showed that from day 3 of exposure the amorphous phase mainly consisted of the residual silica network (SiO_2); again this was confirmed by WD-XRF (Figure 10).

The interaction of the glass-ceramic scaffold with D + HEPES was documented by SEM/EDS images of both the original scaffold [Figure 11(a)] and the material after exposure [Figure 11(b-f)]. On the surface, a newly

developed layer of crystalline nano plates corresponding to HAp is clearly visible, together with "roses" that probably represent octacalcium phosphate (OCP)[24] [Figure 11(c)]. Under the thin crust, some residual original material, consisting solely of SiO_2 can be seen.

The original surface of the glass-ceramic scaffold [Figure 12(a)] was visibly disrupted as early as after 8 h in SBF + HEPES [Figure 12(b)]. After day 1, the surface "healed up" with the newly formed HAp and NaCl phases. Within 3 days, globules of the HAp phase covered the scaffold surface [Figure 12(d)]. After 7 days, the scaffold surface was completely covered with a HAp layer. The detail in Figure 12(d) shows the layer growth mechanism; the perpendicular-oriented crystals (probably OCP, but not confirmed by XRD) were gradually covered with HAp nano-crystals.

It is important to note that crystalline hydroxyapatite was only formed in the presence of the TRIS[8] and HEPES buffers, and not in that of the non-buffered solutions (SBF[8] and I-solution,[23] see details in Rohanová et al.[23] Figures 5 and 6). Moreover, HAp was observed in the D + HEPES and D + TRIS[8] solutions without the presence of biogenic components (Ca and P). However, biogenic elements were released from the scaffold in such quantities that the leachates became supersaturated with HAp. Thus, the "bioactivity" (HAp formation) of the glass-ceramic scaffold was undoubtedly activated by the TRIS or HEPES buffer.

CONCLUSION

We have shown that, far from being inert, HEPES buffer interacts with the tested glass-ceramic material under the conditions of *in vitro* testing carried out in accordance with ISO 23317:2014. As in our previous work with TRIS buffer, HEPES buffer significantly increases the dissolution of the material, meaning that neither is suitable for such tests. These findings strongly suggest that the ISO norm requires some revision. Our future work will be focused on the behavior of other buffers (TES, BES, MOPS) in order to better understand the mechanism of interaction between Good's buffers and glass-ceramic materials in SBF.

ACKNOWLEDGMENT

The authors would like to express their thanks to Ing. Zuzana Zlámalová Cílová, PhD. (Department of Glass and Ceramics, UCT Prague) for SEM/EDS analyses and to Ing. Simona Randáková (Central Laboratories, UCT Prague) for WD-XRF analyses.

REFERENCES

1. Varila L, Fagerlund S, Lehtonen T, Tuominen J, Hupa L. Surface reaction of bioactive glasses in buffered solutions. J Eur Ceram Soc 2012;32:2757–2763.
2. Zhang D, Hupa M, Hupa L. In situ pH within particle beds of bioactive glasses. Acta Biomater 2008;4:1498–1505.
3. Qutachi O, Vetsch JR, Gill D, Cox H, Scurr DJ, Hofmann S, Müller R, Quirk RA, Shakesheff KM Rahman ChV. Injectable and porous PLGA microspheres that form highly porous scaffolds at body temperature. Acta Biomater 2014;10: 5090–5098.
4. Chew KK, Low KL, Zein SHS, McPhail DS, Gerhardt LCh, Roether JA, Boccaccini AR. Reinforcement of calcium phosphate cement with multi-walled carbon nanotubes and bovine serum albumin for injectable bone substitute applications. J Mech Behav Biomed Mater 2011;4:331–339.
5. International standard ISO 23317: Implants for surgery - In vitro evaluation for apatite-forming ability of implant materials; Third edition 2014.
6. Bohner M, Lemaitre J. Can bioactivity be tested in vitro with SBF solution? Biomaterials 2009;30:2175–2179.
7. Kokubo T, Takadama H. How useful is SBF in predicting in vivo bone bioactivity? Biomaterials 2006;27:2907–2915.
8. Rohanová D, Boccaccini AR, Yunos DM, Horkavcová D, Březovská I, Helebrant A. Tris buffer in simulated body fluids distorts the assessment of glass-ceramic scaffold bioactivity, Acta Biomater 2011;7:2623–2630.
9. Fagerlund S, Hupa L, Hupa M. Dissolution patterns of biocompatible glasses in 2-amino-2-hydroxymethyl-propane-1,3-diol (Tris) buffer. Acta Biomater 2013;9:5400–5410.
10. Rohanová D, Horkavcová D, Boccaccini AR, Helebrant A. Assessment of in vitro testing approaches for bioactive inorganic materials. J Non-Crystal Sol A 2016;432:53–59.
11. Good NE, Winget GD, Winter W, Connolly TN, Izawa S, Singh RMM. Hydrogen Ion Buffers for Biological Research. Biochemistry 1966;5(2):467–477.
12. Lelong IH, Rebel G. pH drift of "physiological Buffers" and culture media used for cell incubation during in vitro studies. J Pharm Toxic Met 1988;39:203–210.
13. Stellwagen NC, Bossi A, Gelfi C, Righetti PG. DNA and buffers: Are there any noninteracting, neutral pH buffers? Analyt Biochem 2000;287:167–175.
14. Tas AC. The use of physiological solutions or media in calcium phosphate synthesis and processing. Acta Biomater 2014;10:1771–1792.
15. Shah FA, Brauer DS, Wilson RM, Hill RG, Hing KA. Influence of cell culture medium composition on *in vitro* dissolution behaviour of a fluoride-containing bioactive glass. J Biomed Mater Res A 2014;102:647–654.
16. Dezfuli SN, Huan Z, Mol JMC, Leeflang MA, Chang J, Zhou J. Influence of HEPES buffer on the local pH and formation of surface layer during *in vitro* degradation tests of magnesium in DMEM. Prog Natur Sci Mater Inter 2014;24:531–538.
17. Kim HM, Miyazaki T, Kokubo T, Nakamura T. Revised simulated body fluid. Key Eng Mater Trans Tech Publ 2001;192-195:47–50.
18. Oyane A, Kim HM, Furuya T, Kokubo T, Miyazaji T, Nakamura T. Preparation and assessment of revised simulated body fluids. J Biomed Mater Res A 2003;65:188–195.
19. Oyane A, Onuma K, Ito A, Kim HM, Kokubo T, Nakamura T. Formation and growth of clusters in conventional and new kinds of simulated body fluids. J Biomed Mater Res A 2003;64:339–348.
20. Lu X, Leng Y. Theoretical analysis of calcium phosphate precipitation in simulated body fluid. Biomaterials 2005;26:1097–1108.
21. Chen QZ, Thompson LD, Boccaccini AR. 45S5 Bioglass-derived glass-ceramic scaffolds for bone tissue engineering. Biomaterials 2006;27:2414–2425.
22. JCPDS-ICDD PDF-4 database. International Centre for Diffraction Data, Newtown Square, PA, USA release 54; 2016.
23. Rohanová D, Boccaccini AR, Horkavcová D, Bozděchová P, Bezdička P, Častorálová M. Is non-buffered DMEM solution a suitable medium for in vitro bioactivity tests? J Mater Chem B 2014;2:5068–5076.
24. Barrère F, Layrolle P, Van Blitterswijk CA, De Groot K. Biomimetic coatings on titanium: a crystal growth study of octacalcium phosphate. J Mater Sci: Mater Med 2001;12:529–534.

Práce **[12]**

Rohanová D., Horkavcová D., Helebrant A., Boccaccini A.R.: Assessment of *in vitro* testing approaches for bioactive inorganic materials. Journal of Non-Crystalline Solids 432; 53-59, 2016.

Podíl: 70%: návrh experimentů, zpracování výsledků, příprava publikace

Journal of Non-Crystalline Solids 432 (2016) 53–59

Contents lists available at ScienceDirect

Journal of Non-Crystalline Solids

journal homepage: www.elsevier.com/ locate/ jnoncrysol

Assessment of *in vitro* testing approaches for bioactive inorganic materials

Dana Rohanová [a,*], Diana Horkavcová [a], Aleš Helebrant [a], Aldo Roberto Boccaccini [b]

[a] Department of Glass and Ceramics, Faculty of Chemical Technology, University of Chemistry and Technology Prague, Technická 5, 166 28 Prague 6, Czech Republic
[b] Department of Materials Science and Engineering, Institute of Biomaterials, University of Erlangen-Nuremberg, 91058 Erlangen, Germany

ARTICLE INFO

Article history:
Received 31 October 2014
Received in revised form 18 February 2015
Accepted 15 March 2015
Available online 31 March 2015

Keywords:
Biomaterial;
In vitro test;
Hydroxyapatite;
SBF;
Dynamic arrangement

ABSTRACT

This paper deals with non-standard *in vitro* testing of bioactive inorganic materials shaped as granules or scaffolds. The ISO 23317 standard describes the *in vitro* test arrangement of bulk bioactive materials under static conditions. However, this norm has not dealt with bioactive materials shaped as granules (with large surface area) that are commonly used in clinical practice. We found that in the case of highly reactive (bioactive) materials, the biogenic elements were exhausted from simulated body fluid (SBF) solution very quickly (within hours) under static conditions. In such exhausted SBF solution the formation of Ca–P layer (hydroxyapatite — HAp) was stopped in agreement with the decrease of Ca and P concentrations. On the contrary, highly soluble materials (glass-ceramic scaffold) induced the formation of a new mineral layer also on the walls of the PE container used. For a non-standard shape of the tested materials the usage of dynamic or static–dynamic *in vitro* test arrangement was confirmed to be a better option to test bioactivity. However, also for this type of arrangement it is essential to determine the S/V or S/F ratios (the surface area/volume or flow of SBF solution) very precisely. For detailed understanding of the interaction between the tested material and SBF it is important to analyze the leachates (monitoring Ca^{2+}, $(PO_4)^{3-}$ and minor element concentrations) and to monitor the pH value. An expected result of the *in vitro* test (according ISO standard) is the formation of HAp on the surfaces of tested samples in SBF. However, the formation of hydroxyapatite may not be the proof of their potential bioactivity necessarily (*e.g.* due to the use of TRIS buffer).

1. Introduction

In vitro testing seems to be an ideal method to quickly test the chemical stability of newly developed materials in a solution similar to human blood serum. Such materials must be capable of creating a firm bond with bone tissue. Kokubo et al. prepared ISO standard 23317:2014(E) [1]: "Implants for surgery — *In vitro* evaluation for apatite-forming ability of implant materials". While this standard describes the chemical composition of an SBF solution in detail, certain critical aspects of *in vitro* tests need to be resolved in the near future:

1. SBF
   To simulate the conditions in living organisms, it is very important to use a solution that contains the inorganic part of blood serum. The ISO standard prescribes an acellular and protein free solution; namely, simulated body fluid buffered with TRIS tris-(hydroxymethyl) aminomethane [1]. However, we found [2] that, for example, TRIS buffer used in SBF supports the dissolution of the crystalline phase of glass-ceramics and the crystallization of HAp on its surface, thereby leading to false positive *in vitro* test results. Bohner and Lemaitre [3] similarly note that "*the use of SBF for bioactivity testing leads to the positive and false negative results*".
2. Limitations to the bulk compact shape of an inorganic sample
   The description of the form and dimensions of test samples given in the ISO standard is limited to compact samples with a defined S_a/V ratio (sample surface area/ SBF volume). Rules for materials in the form of the grit, scaffolds and granules (with a large surface area) used in ordinary clinical practice (*e.g.* HA, TCP, glass-ceramics) are missing.
3. Arrangement of *in vitro* test
   The ISO standard only covers the static arrangement of an *in vitro* test, in which a limited volume of solution (SBF) is used and not changed during the test. Under such static conditions, the biogenic elements (Ca or P) of SBF can be quickly exhausted. However, inside a real living organism, SBF is never exhausted. Therefore, to more closely resemble the conditions in an *in vivo* environment, the dynamic arrangement of an *in vitro* test has been used [4–7].
4. HAp formation
   The ISO standard [1] requires that the *in vitro* test results in the formation of hydroxyapatite on the surface of tested material. However, this may not be the sole indicator of the behavior of the material in the human body [8]. Ion release may be the other appropriate indicator of the reactivity of a tested material.

* Corresponding author.
E-mail address: dana.rohanova@vscht.cz (D. Rohanová).

http://dx.doi.org/10.1016/j.jnoncrysol.2015.03.016
0022-3093/

5. The term “bioactivity”
   It has been used in a major part of the published works, in which the material is tested only *in vitro*, probably because of the convenience of the single word expression. In fact the term “bioactivity” should be used only in connection with *in vivo* tests [9]. When discussing results of *in vitro* tests, as carried out in the present study, the term “reactivity” appears as more appropriate.

In this work, under various conditions, we perform *in vitro* tests on silicate glass-ceramic scaffolds derived from 45S5 glass and calcium phosphates (HA, β-TCP), and interpret results in relation to the aforedescribed issues.

2. Experimental procedures

2.1. Materials

2.1.1. Glass-ceramic material

The silicate material used for testing was the a glass-ceramic (45S5 bioactive glass based) in the form of a highly porous structure (scaffold) prepared by the foam replica technology [10]. The material contained crystalline and residual glass phases as shown in Table 1.

2.1.2. Calcium phosphate materials

The tested materials (white granules, 1–2 mm) were prepared by Lasak Ltd., Prague, Czech Republic. The first material – resorbable β-tricalcium phosphate (Poresorb®-TCP, β-$Ca_3(PO_4)_2$), called TCP with the specific weight 2900–3100 $kg \cdot m^{-3}$ – contained macro (100–200 μm) and micro (1–5 μm) pores. The second material was micro and macro porous hydroxyapatite (OSSABASE®-HA, $Ca_{10}(PO_4)_6(OH)_2$) called HA [11].

2.2. Solutions for the in vitro test

Modified simulated body fluids used for the tests are in Table 2.

2.3. Arrangements of the tests

The arrangements of the *in vitro* tests are presented in Table 3.

2.4. Analysis of the materials

2.4.1. Scanning electron microscopy/energy-dispersive spectroscopy (SEM/EDS)

The surface of tested materials before and after the tests was inspected with a Hitachi S-4700 scanning electron microscope (SEM) equipped with an EDS analyzer (NORAN D-6823) working at an accelerating voltage of 15 kV. The tested materials were powder coated with an Au–Pd layer during 80–100 s for SEM observations.

2.4.2. X-ray powder diffraction analysis (XRD)

The tested materials were ground in an agate mortar in a suspension with cyclohexane. The suspension was then placed on a mylar film and fixed to a transmission sample holder. After solvent evaporation a thin layer of the prepared sample was covered with another mylar film. The diffraction patterns were collected using a PANalytical X'Pert PRO diffractometer equipment with a conventional X-ray tube ($Cu_{K\alpha}$ 40 kV, 30 mA, line focus) working in the transmission mode. An elliptic focusing mirror with divergence slit 0.5°, an anti-scatter slit 0.5° and a soller slit of 0.02 rad were used for the primary beam. A fast linear position sensitive detector PIXcel with an anti-scatter shield and a soller slit of 0.02 rad was used for the diffracted beam. All patterns were collected in the range of 3 to 88° 2 theta with the step of 0.013° and 200 or 600 s per step producing a scan of about 4.5 h. Qualitative analysis was performed with a HighScorePlus software package (PANalytical, the Netherlands, version 2.2.5 or 3.0 e), a Diffrac-Plus software package (Bruker AXS, Germany, version 8.0) and JCPDS-ICDD PDF-2 database.

Table 1
Compositions of 45S5 bioactive glass and individual phases of the 45S5 bioactive glass based scaffold (wt.%) [10].

Oxide	45S5 (100 wt.%)	$Na_2O \cdot 2CaO \cdot SiO_2$ (77.4 wt.% of scaffold)[a]	Residual glass phase (22.6% of scaffold)
SiO_2	45.0	50.9	24.8
Na_2O	24.5	17.4	48.5
CaO	24.5	31.7	–
P_2O_5	6.0	–	26.5

[a] The minority crystalline phases $CaO \cdot SiO_2$ and $NaCaPO_4$ (buchwaldite) are included.

2.5. Solution analysis

All tests and analyses were measured using two parallel series of samples.

2.5.1. Atomic absorption spectrophotometry (AAS)

The concentration of Ca^{2+} ions in the leachate from all types of solutions was analyzed with a VARIAN-Spectr AA 300. The so-called release agent (KCl) was added to each sample to determine the quantity of Ca. Atomization was performed in acetylene-N_2O flame. The wavelength used for absorbance measurements was 422.7 nm.

2.5.2. Spectrophotometry

The concentration of $(PO_4)^{3-}$ ions (except mod-DMEM) was analyzed with a UV–VIS Spectrophotometer UV1601 at $\lambda = 830$ nm (ČSN 830540). Ion concentrations were calculated using a calibration line method from the measured absorbance values.

2.5.3. Inductively coupled plasma-optical emission spectroscopy (ICP-OES)

The concentration of P in mod-DMEM leachates was measured by ICP-OES with a PerkinElmer-Optima 2000DV instrument. The leachate was vaporized with a Gem-ConeTM nebulizer and the flow rate of the leachate through the nebulizer was 2.2 $ml \cdot min^{-1}$. The produced fine aerosol was carried with an argon stream into a plasmatic burner (1300 W). The concentrations were measured at wavelengths 231.620, 214.917 and 178.221 nm.

2.5.4. pH measurement

The pH in all types of leachates was measured with an inoLab pH-meter with a combined glass electrode at the laboratory temperature (dynamic test) and at 36 ± 1 °C (static and static–dynamic test).

3. Results and discussion

3.1. Solutions for the in vitro tests

The effort to define a relation between *in vitro* and *in vivo* tests has resulted in development of testing solutions which simulate human cellular fluid. To determine the ability to form apatite on the surface of glass or glass-ceramics, some authors [12–14], have used TRIS buffer alone, which is well known from biological laboratories. A turning point in the development of solutions simulating *in vivo* conditions were the solutions prepared by Kokubo et al. [15] and also by other authors [16]. In the mentioned studies, in addition to TRIS buffer (pH = 7.25 at 36.5 °C), the simulated solutions also contained ions in concentrations close to the inorganic part of blood plasma, however the concentration of HCO_3^- was only 4.2 $mmol \cdot l^{-1}$ instead of 27 $mmol \cdot l^{-1}$. Höland, Völksch et al. [16] explained the apatite phase formation on the A-W glass-ceramics by reaction of the material and by the effect of ions from the simulated solution. In 2001 Helebrant et al. [17] and later Müller and Müller [18] tested a series of SBF solutions with gradually increasing concentrations of HCO_3^- ions, up to the value close to blood plasma. They found that carbonate hydroxyapatite

Table 2
Ion composition (mmol·dm^{-3}) of modified solutions, SBF orig. and blood plasma (BP) [2,9,23,28].

Solution	Na^+	K^+	Ca^{2+}	Mg^{2+}	Cl^-	HCO_3^-	HPO_4^{2-}	SO_4^{2-}	TRIS	Ca/P
SBF-T	142.0	5.0	2.5	1.0	131.0	5.0	1.0	1.0	–	2.5
SBF+T	142.0	5.0	2.5	1.0	131.0	5.0	1.0	1.0	50.0	2.5
mod-DMEM	154.5	5.4	1.8	0.8	118.5	44.0	0.9	0.8	–	2.0
I-solution	142.0	5.0	1.8	1.0	91.6	44.0	1.0	0.5	–	1.8
SBF 27	142.0	5.0	2.5	1.0	110.0	27.0	1.0	0.5	50.0	2.5
SBF orig.	142.0	5.0	2.5	1.0	148.8	4.2	1.0	0.5	50.0	2.5
BP	142.0	5.0	2.5	1.0	103.0	27.0	1.0	0.5	–	2.5

developed on the surface of tested materials but the thickness and crystallinity of the layers differed, which indicated an important role of HCO_3^- ions in nucleation and formation of the apatite layer. Moreover Oyane et al. [19] tested a series of SBF solutions (r-SBF, i-SBF, m-SBF) with ion concentration equal to or closer to those of blood plasma. The m-SBF solution was evaluated as the most stable one and "*optimal for in vitro bioactivity assessment of artificial materials*". Further, Kim et al. [20] presented the revised SBF (R-SBF), in which they increased the concentration of HCO_3^- ions to the level present in blood plasma. TRIS or HEPES buffers were used in all solutions to maintain pH, however, it is likely that, TRIS and HEPES buffers are unable to maintain neutral pH in the SBF solution in the course of *in vitro* tests [2,21]. TRIS supports dissolution of the crystalline phase of glass-ceramics and it also supports crystallization of HAp alone [2]. The use of various simulated solutions naturally clearly influences the results of *in vitro* tests, as stated by Varila et al. [22]. The results showed that "*dissolution and layer formation on glasses in different buffer solutions vary significantly and results obtained in different buffer solutions cannot be directly compared*" [22]. It was also found that even non-buffered DMEM solution containing an organic phase, is not the right solution for *in vitro* tests [23]. In addition to the necessity of having an sterile environment during the test execution, DMEM solution has a low concentration of Ca^{2+} ions and, on the contrary, a too high concentration of HCO_3^- ions, which leads to precipitation of $CaCO_3$ instead of apatite [23].

3.1.1. In vitro test of glass-ceramic scaffold in various solutions

The results of this study show the *in vitro* tests of the glass-ceramic scaffold (Table 1) in SBF solutions with TRIS (SBF+T) and without TRIS (SBF-T), in mod-DMEM and in the simulated inorganic part of DMEM (I-solution) (Table 2).

The arrangement of the tests in SBF solution with TRIS (SBF+T) and without TRIS (SBF-T) was dynamic using a liquid flow rate F = 48 ml·day^{-1}. The tests with mod-DMEM and I-solution were arranged as static–dynamic with daily replenishment of liquid (V = 50 ml) (Table 3). In all the cases the weight of the samples was 0.05 g ± 0.005 g. At the beginning of the interaction the scaffold in SBF+T significantly dissolved, (Fig. 1). On the other hand, in the solution without buffer (SBF-T) the rate of Ca–P phase formation from the beginning of interaction was higher than that of scaffold dissolution. This was also reflected by the concentrations of $(PO_4)^{3-}$ ions. The pH value increased even when TRIS buffer was used. In mod-DMEM solution (Fig. 1) the Ca^{2+} concentration at the beginning of the interaction slightly increased; in I-solution (without organic phase) the process of precipitation of a new phase clearly prevailed (removal of Ca^{2+} ions). The increase of the pH was associated with the solubility of the tested materials in the simulated solution and the high pH then accelerated dissolution of the residual glass phase. An analysis of the surfaces with XRD has confirmed [2] that crystalline HAp (Fig. 2a) developed in SBF+T, while in the solution without TRIS buffer (SBF-T) the developed phase was amorphous calcium phosphate (Fig. 2b). This phase was not detectable with XRD and its formation was confirmed by SEM/EDS. After 15 days of exposure to mod-DMEM and I-solution visually different phases of ACP (amorphous calcium phosphate) and $CaCO_3$ developed on the surface. The differences between the precipitates developed in different solutions are well visible on SEM/EDS images (Fig. 2c and d).

3.2. Testing conditions

3.2.1. Static test — determination of the S/V ratio

Results of *in vitro* tests are significantly influenced not only by the size but also by the quality of the material surface and by the ratio of the surface area of material to the volume of testing solution (S_a/V). The standard ISO 23317:2014(E) [1] recommends samples in form of disks (d = 10 mm, v = 2 mm) or prisms sized ca. 10 × 10 × 2 mm. For solid samples and static tests the standard recommends the following ratios: S/V = 10 mm^{-1} or 0.1 cm^{-1}.

Vallet-Regí et al. [24] used pressed disks made of glass particles having sizes from 32 to 63 μm. The S/V ratio was 0.07 cm^{-1}. However, it is possible to expect that during interaction of glass particles with SBF (additionally buffered with TRIS) the specific surface (SS) of the tablets will increase many times immediately at the beginning of the interaction with SBF.

When testing samples in the form of grit or scaffolds a potentially inappropriate S_a/V ratio may lead to several situations. One of them is an enormous increase of pH as discussed by Greenspan et al. [25]. In case of highly reactive systems, such as bioactive glasses and glass-ceramics, the size of particles is linked to the rate of their dissolution in SBF [25]. Zhang et al. [26] found out that "the formation of layers (Si, Si + CaP or CaP) on particles strongly depended on the particle size, glass composition and local environment around the particles".

3.2.2. Duration of static tests

The ISO standard [1] recommends tests lasting up to 28 days. Analyses of leachates after exposure of TCP and HA materials (0.5 g of sample, 100 ml SBF 27, static conditions, Tables 2 and 3), have shown that concentrations of biogenic ions (Ca^{2+} and $(PO_4)^{3-}$) immediately decreased after placement of samples into SBF 27 and from the third day of exposure the concentration does not change significantly (Fig. 3). The values indicated the end of interaction between the tested material and simulated fluid solution, which means that the solution was no more supersaturated in HAp. A similar conclusion is published in [22] and [27]. Therefore tests under static conditions which are longer than one week are not recommended.

Table 3
Arrangements of *in vitro* test.

Method	Solution volume/hours	Exchange of solution	Flow of solution	Solution	Material	Citation
Static	100 ml/336	No	No	SBF 27	HA, TCP granules	None
Dynamic	48 ml/24	Continuously	Yes	SBF+T, SBF-T	Glass-ceramic, scaffold, HA granules	[2]
Static–dynamic	50 ml/24	Daily	No	I-solution, mod-DMEM	Glass-ceramic scaffold	[23]

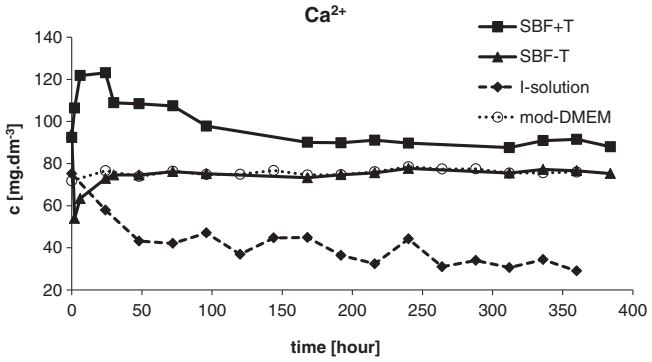

Fig. 1. Concentration of Ca^{2+} ions in SBF+T, SBF-T solutions during dynamic and I-solution, mod-DMEM during static–dynamic *in vitro* tests of glass-ceramic scaffold.

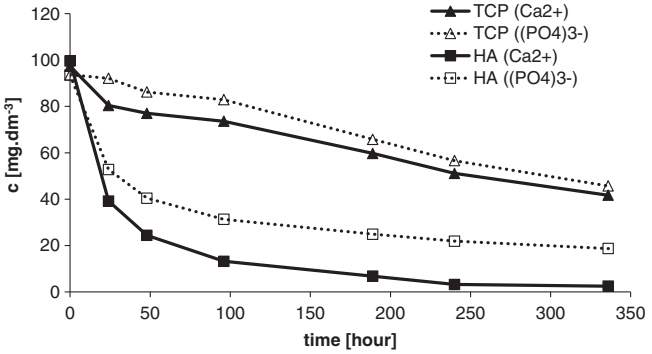

Fig. 3. Concentration of Ca^{2+} and $(PO_4)^{3-}$ ions in 100 ml of SBF 27 during static *in vitro* tests of 0.5 g TCP and 0.5 g HA.

3.2.3. Dynamic tests

No ISO standard exists so far for this type of tests. Zhang et al. noticed [5], "*when testing bioactive glasses to fulfill particular medical needs, the fluid circulation should be carefully adjusted to imitate the conditions in the final application*". Rámila and Vallet-Regí [4] describe *e.g.* a dynamic test with a *flow of big volume of fresh SBF* (1440 ml·day^{-1}), which is one of the possibilities keeping constant the pH value of SBF and to avoid the high supersaturation in tests of highly soluble materials.

Zhang et al. [5] exposed samples of bioactive glasses in a flow chamber using the SBF flow rate of 33 ml·min^{-1}; it means that there was a respectable volume of 47520 ml per day. Another type of a dynamic test is the one with *circulation of a large volume of SBF* (F = 2.8 ml·s^{-1}, V = 3000 ml) without replenishment [6]. In this case there is the possibility of supersaturation and there is also the issue of keeping the set-up the pH value which, however, was not monitored in the quoted work.

The third type of tests has been used by our laboratory and it is a dynamic test *with a flow of a very small volume of fresh SBF solution* [7]. Real values of the flow rate around the implants have not been published yet, but in the case of a small volume of solution in the testing cell (5.5 ml) the rate of replenishment of the solution has been estimated at 48 ml·day^{-1}.

A modification of the last mentioned variant is the so-called static–dynamic test in which the solution (50 ml) is replaced with fresh SBF every day. The advantage of the test consists in the fact that it does not require any sophisticated apparatus, which is necessary for the dynamic tests, exchanging samples in daily intervals is very convenient and it is also possible to monitor the development of a layer on the material surface or to interrupt the test for a few days.

It is apparent that dynamic or static–dynamic arrangements of the tests were more suitable for simulation of real conditions in a living organism in comparison to static tests. The optimum arrangement of dynamic tests was somewhere between the mentioned variants.

3.2.3.1. Optimization of quantity of tested material for dynamic test. In preliminary studies it was considered that the test arrangement with fresh flowing SBF solution would resolve the problem of insufficient buffering ability of TRIS. The first experiment under dynamic arrangement was focused on highly reactive glass-ceramic scaffold. Even in the case of a relatively small quantity of tested material (0.2 or 0.5 g) in a flow testing

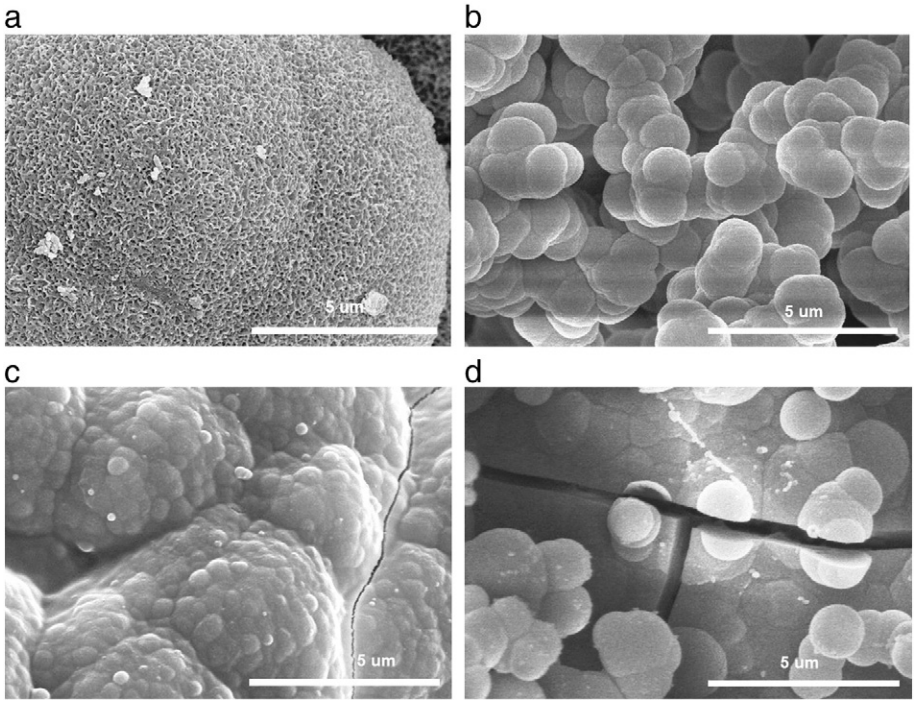

Fig. 2. (SEM) Surface of glass-ceramic scaffold after interaction with solutions: a) SBF+T, b) SBF-T, c) mod-DMEM and d) I-solution for 2 weeks.

cell, several minutes after the test the pH of the solution (SBF+T) enormously increased (glass-ceramic scaffold) or decreased (HA) (Fig. 4a). The growth of the pH was closely associated with the release of alkali ions (Ca^{2+}, Na^{+}) into the leachate (*i.e.* solubility of scaffold), while the decrease of pH, Ca^{2+} and $(PO_4)^{3-}$ ions documented the precipitation of Ca–P phase in the course of HA exposure (Fig. 4b).

Next experiment was arranged with a smaller quantity of tested scaffold. The crystalline phase of 45S5 bioactive glass based scaffold [10] contains practically all calcium while phosphorus is contained in the residual minor glass phase, which is a key for the interpretation of the results of the solution analyses. In case of a higher quantity of scaffold in the flow cell (0.2 g) it is obvious that released Na^{+} and Ca^{2+} ions (Fig. 5a) lead to an immediate increase of the pH (Fig. 5b) and, at the same time, precipitation of HAp phase (confirmed by XRD). If the sample weight is only 0.05 g then the pH of the solution is not maintained either, however the analysis indicates that the residual glass phase dissolves immediately after the beginning of exposure, which is confirmed by the increase of the concentration of $(PO_4)^{3-}$ (Fig. 5a). It was interesting to find out that the pH values in the second half of the test became similar for both tested samples. After a few days (between the 4th–6th day) of testing the scaffolds partly dissolved and the SBF+T solution further reacted with the newly created HAp layer on the scaffold surfaces.

3.2.3.2. Supersaturation of SBF solution. As revealed by the experiments, for a smaller sample of 45S5 bioactive glass based glass-ceramic scaffold (0.05–0.1 g in 5.5 ml volume cell with the flow rate of 48 ml·day^{-1}) the SBF+T solution was not significantly supersaturated in the test cell. However a lager sample in the cell (0.25 g) resulted in supersaturation of the solution even under dynamic test conditions. The strong

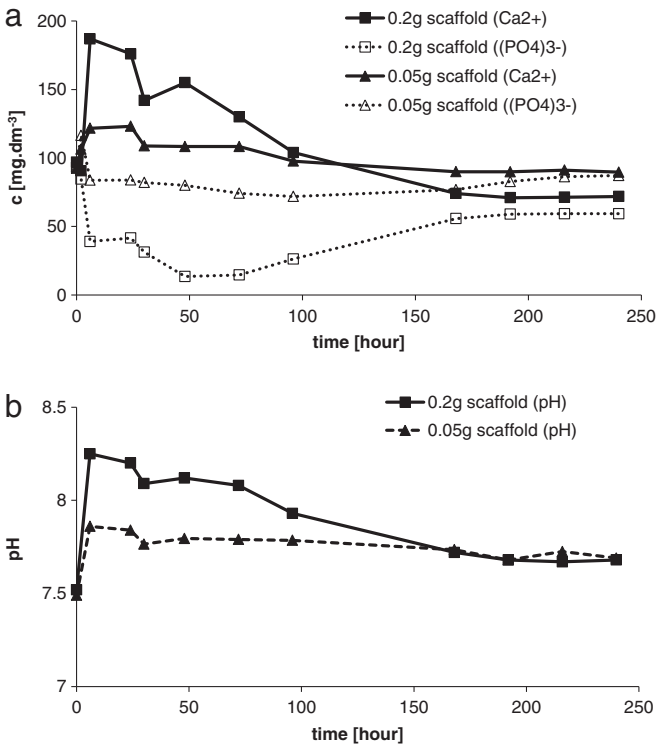

Fig. 5. a: Concentration of Ca^{2+} and $(PO_4)^{3-}$ ions in SBF+T during dynamic *in vitro* tests of 0.2 g and 0.05 g glass-ceramic scaffold. b: Values of pH in SBF+T during dynamic *in vitro* tests of 0.2 g and 0.05 g glass-ceramic scaffold.

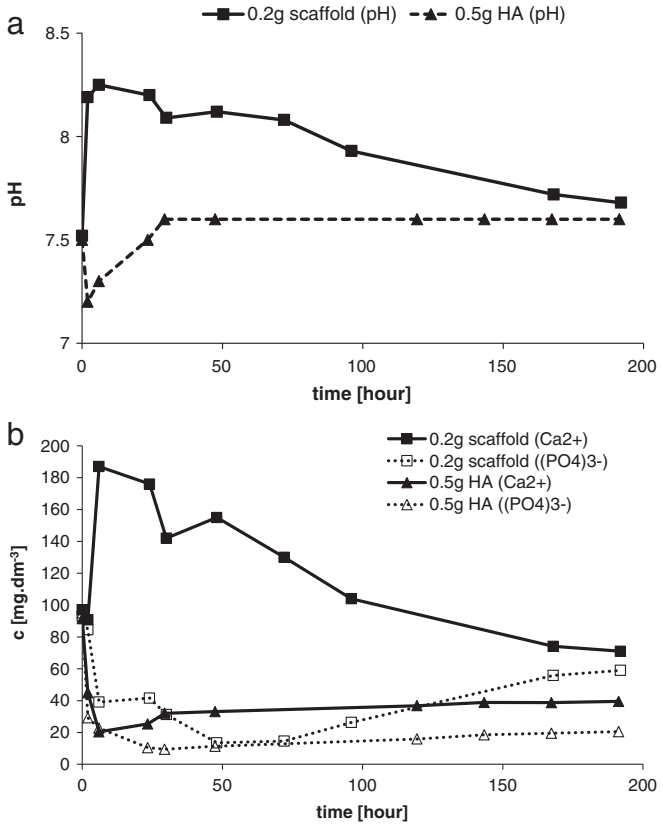

Fig. 4. a: Values of pH in SBF+T during dynamic *in vitro* tests of 0.5 g HA and 0.2 g glass-ceramic scaffold. b: Concentration of Ca^{2+} and $(PO_4)^{3-}$ ions in SBF+T during dynamic *in vitro* tests of 0.5 g HA and 0.2 g glass-ceramic scaffold. Values over 100 mg·dm^{-3} indicate that the rate of dissolving prevails.

supersaturation of the solution caused precipitation of several crystalline phases and growth of layers even on the surface of the inert polyethylene (PE) container. The container walls (the surface area was 16.6 cm^2) were covered with a deposit of 0.022 g of precipitate during 10 days. The thickness of the deposited layer was 8.5 μm. The rate of layer growth was calculated to be $5.5.10^{-6}$ g·cm^{-2}·h^{-1}. X-ray diffraction analysis (XRD) confirmed the crystalline phases NaCl (large transparent plates) and HAp (small globules). The precipitated layer also included an amorphous phase, which contained silicon from dissolution of the scaffold.

Precipitation of NaCl and development of CDHA (Ca defective carbonate apatite) were detected also on inert Pt spirals used to attach the tested scaffold during static–dynamic tests in I-solution [23]. The high solubility of glass-ceramic scaffold caused an increase in the concentration of Na^{+} ions in close proximity of Pt spirals and the I-solution became initially supersaturated in halite (NaCl). After Na^{+} and Cl^{-} ions were removed by precipitation of halite the solution in close proximity of the spirals was supersaturated in CDHA (this was confirmed by SEM/EDS and XRD) (Fig. 6). However, the I-solution in the remaining volume was not primarily supersaturated to CDHA. Due to the low concentration of Ca^{2+} ions and high concentration of HCO_3^{-} ions (44 mmol·dm^{-3}) the solution was supersaturated in $CaCO_3$ which precipitated on the glass-ceramic scaffold. Preferred precipitation of NaCl was observed also during other tests on glass-ceramic scaffold for which SBF 27mod solution was used with an increased content of HCO_3^{-} ions (27 mmol·dm^{-3}) and reduced quantity of Ca^{2+} ions [28].

3.3. Evaluation of the obtained results

The results of the above-mentioned *in vitro* tests demonstrate that the analysis of the solution (monitoring of the concentration of Ca^{2+} and $(PO_4)^{3-}$ ions and pH) is useful to reveal the reactivity of the tested materials immediately after beginning of exposure. It is accepted that the principal methods for evaluation of surfaces are XRD and SEM/EDS

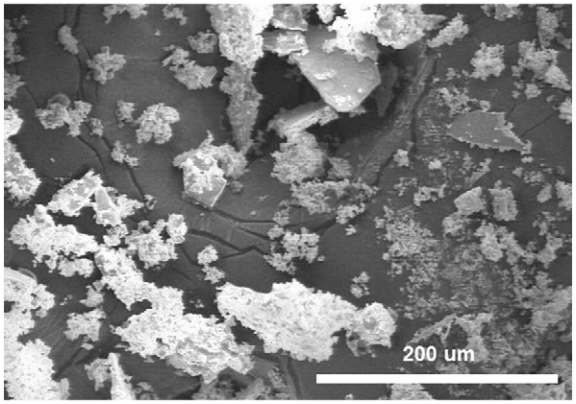

Fig. 6. Layers from Pt spiral: dark gray cracked layer — NaCl, white crystals — CDHA (confirmed by XRD), static–dynamic conditions.

and, *e.g.* for comparison of similar materials, also BET and FTIR (in the case of an amorphous phase). Without carrying out XRD analysis it is possible to confuse ACP (Fig. 2b and d) or $CaCO_3$ (Fig. 2c) with HAp. Recently Tas [29] had summarized in detail the use of various physiological solutions for *in vitro* tests and he stated that all studies using the physiological solutions or TRIS-buffered SBF have reported the formation of X-ray amorphous CaP nanopowders instead of Ap-CaP or stochimetric HAp.

Based on previous findings investigating *in vitro* behavior of inorganic materials we need to answer the following question: *Is it really necessary to create crystalline hydroxyapatite on the surface of a material to determine its bioactivity?* Our findings about interaction of TRIS buffer with the tested glass-ceramic scaffold confirms the fact that evaluation of reactivity of a particular material based on HAp detected on its surface provides only partial information on the actual surface reactivity. In our opinion it is more effective to focus on a suitable arrangement of the *in vitro* test for the given material so that relevant information (development of the concentrations and pH) can be obtained about its reactivity in the inorganic part of human serum, particularly in the early stages of the interaction (related *e.g.* to 1 ml of the employed solution or 1 cm^2 of material). A very important and completely neglected area is in fact the release of other elements from the tested glass or glass-ceramic material (Si, Na…), as well as the release of minor elements (*e.g.* in the case of ion-doped materials) [30]. Moreover, for each material it is necessary to determine limit instantaneous concentrations and maximum concentrations of elements released into the simulated solution and such concentrations shall be correlated to values, which are acceptable to cells.

4. Conclusions

The results have shown that hydroxyapatite formation on the surface of the tested biomaterials should not be the sole aim of a reactivity test. We suggest that the key to understanding the behavior of the biomaterial in SBF is to monitor the changes in pH and in the concentrations of Ca, P, Si as well as the minor elements released from the tested material. Furthermore, the dynamic (static–dynamic) arrangement of such *in vitro* testing should be used. Moreover, it is necessary to update the ISO 23317 standard for bioactive materials in the granule or scaffold form. In the context of the theme of the present paper, recently (February 2015), members of the Technical Committee 4 (TC04) of the International Commission on Glass (ICG) published a new method (modified ISO standard) for testing bioactive glasses, particularly those of high surface area [31], based on a round robin study, which is recommended to enable comparison of results from different laboratories in the future.

Acknowledgment

This work was supported by the Technology Agency of the Czech Republic within the project TE01020390 Center for development of modern metallic biomaterials for medicinal implants. The authors would like to express their thanks for SEM/EDS analyses to Ing. Zuzana Zlámalová Cílová, PhD., and to our students Iva Březovská, Pavlína Bozděchová, Klára Zítková, Lenka Kuncová and Jitka Kulhavá from the Department of Glass and Ceramics of the University of Chemistry and Technology Prague.

References

[1] International standard ISO 23317, Implants for surgery — in vitro evaluation for apatite-forming ability of implant materials, Third edition, 06-15-2014. (Geneva, Switzerland).
[2] D. Rohanová, A.R. Boccaccini, D.M. Yunos, D. Horkavcová, I. Březovská, A. Helebrant, TRIS buffer in simulated body fluid distorts the assessment of glass-ceramic scaffold bioactivity, Acta Biomater. 7 (2011) 2623–2630.
[3] M. Bohner, J. Lemaitre, Can bioactivity be tested in vitro with SBF solution? Biomaterials 30 (2009) 2175–2179.
[4] A. Rámila, M. Vallet-Regí, Static and dynamic in vitro study of a sol–gel glass bioactivity, Biomaterials 22 (2001) 2301–2306.
[5] D. Zhang, M. Hupa, H.T. Aro, L. Hupa, Influence of fluid circulation on in vitro reactivity of bioactive glass particles, Mater. Chem. Phys. 111 (2008) 497–502.
[6] P. Siriphanon, Y. Kameshima, A. Yasumori, K. Okada, S. Hayashi, Comparative study of the formation of hydroxyapatite in simulated body fluid under static and flowing systems, J. Biomed. Mater. Res. 60 (2002) 175–185.
[7] J. Strnad, J. Protivínský, D. Mazur, K. Veltruská, Z. Strnad, A. Helebrant, J. Šesták, Interaction of acid and alkali treated Titanium with dynamic simulated body environment, J. Therm. Anal. Calorim. 76 (2004) 17–31.
[8] H. Pan, X. Zhao, B.W. Darvell, W.W. Lu, Apatite-formation ability — Predictor of "bioactivity"? Acta Biomater. 6 (2010) 4181–4188.
[9] T. Kokubo, H. Takadama, How useful is SBF in predicting in vivo bone bioactivity? Biomaterials 27 (2006) 2907–2915.
[10] Q.Z. Chen, L.D. Thompson, A.R. Boccaccini, 45S5 Bioglass-derived glass-ceramic scaffolds for bone tissue engineering, Biomaterials 27 (2006) 2414–2425.
[11] D. Horkavcová, K. Zítková, D. Rohanová, A. Helebrant, Z. Cílová, The resorption of β-TCP and HA materials under conditions similar to those in living organisms, Ceramics-Silikáty 54 (4) (2010) 398–404.
[12] M. Ogino, L.L. Hench, Formation of calcium phosphate films on silicate glasses, J. Non-Cryst. Solids 38 & 39 (1980) 673–678.
[13] M. Ogino, F. Ohuchi, L.L. Hench, Compositional dependence of the formation of calcium phosphate films on bioglass, J. Biomed. Mater. Res. 14 (1980) 55–64.
[14] T. Fujiu, M. Ogino, Difference of bond bonding behavior among surface active glasses and sintered apatite, J. Biomed. Mater. Res. 18 (1984) 845–859.
[15] T. Kokubo, H. Kushitani, S. Sakka, T. Kitsugi, T. Yamamoto, Solutions able to reproduce *in vivo* surface-structure changes in bioactive glass-ceramic A-W[3], J. Biomed. Mater. Res. 24 (1990) 721–734.
[16] W. Höland, G. Völksch, K. Naumann, G. Carl, W. Götz, Characterization of bone–glass ceramic interface, in: W. Bonfield, G.W. Hastings, K.E. Tanner (Eds.),Proc. of the 4th Int. Symp. on Ceramics in Medicine, London, UK, Sept., Bioceramics, 4, 1991, pp. 171–178.
[17] A. Helebrant, L. Jonášová, L. Šanda, The influence of Simulated body fluid composition on carbonated hydroxyapatite formation, Ceramics-Silikáty 46 (1) (2001) 9–14.
[18] L. Müller, F.A. Müller, Preparation of SBF with different HCO_3^- content and its influence on the composition of biomimetic apatites, Acta Biomater. 2 (2006) 181–189.
[19] A. Oyane, H.-M. Kim, T. Furuya, T. Kokubo, T. Miyazaki, T. Nakamura, Preparation and assessment of revised simulated body fluids, J. Biomed. Mater. Res. 65 (A) (2003) 188–195.
[20] H.-M. Kim, T. Miyazaki, T. Kokubo, T. Nakamura, Revised simulated body fluid, Key Eng. Mater. 192–195 (2001) 47–50.
[21] P. Bozděchová, Interaction of glass-ceramic scaffold with simulated body fluid, [MSc. thesis], University of Chemistry and Technology Prague, 2013.
[22] L. Varila, S. Fagerlund, T. Lehtonen, J. Tuominen, L. Hupa, Surface reaction of bioactive glasses in buffered solutions, J. Eur. Ceram. Soc. 32 (2012) 2757–2763.
[23] D. Rohanová, A.R. Boccaccini, D. Horkavcová, P. Bozděchová, P. Bezdička, M. Častorálová, Is non-buffered DMEM solution a suitable medium for in vitro bioactivity tests? J. Mater. Chem. B 2 (2014) 5068–5076.
[24] M. Vallet-Regí, A. Rámila, New bioactive glass and changes in porosity during the growth of a carbonate hydroxyapatite layer on glass surfaces, Chem. Mater. 12 (2000) 961–965.
[25] D.C. Greenspan, J.P. Zhong, G.P. LaTorre, Effect of surface area to volume ratio on in vitro surface reactions of bioactive glass particulates, in: Ö.H. Andersson, A. Yli-Urpo (Eds.), Bioceramics, 7, 1994, pp. 55–60.
[26] D. Zhang, M. Hupa, L. Hupa, In situ pH within particle beds of bioactive glasses, Acta Biomater. 4 (2008) 1498–1505.
[27] R. Horváthová, D. Rohanová, A. Helebrant, The calcium phosphate formation on Ti alloy by precalcification process under static conditions, Ceramics-Silikáty 50 (3) (2006) 153–158.
[28] D. Rohanová, D. Horkavcová, A.R. Boccaccini, I. Březovská, P. Bozděchová, P. Bezdička, M. Častorálová, A. Helebrant, Interaction of glass-ceramic "scaffold"

prepared from Bioglass® with simulated body fluids, Sklář a keramik C 61 (2011) 125–128.
[29] A. Cuneyt Tas, The use of physiological solutions or media in calcium phosphate synthesis and processing, Acta Biomater. 10 (2014) 1771–1792.
[30] J. Massera, M. Vassallo-Breillot, B. Törngren, B. Glorieux, L. Hupa, Effect of CeO_2 doping on thermal, optical, structural and in vitro properties of a phosphate based bioactive glass, J. Non-Cryst. Solids 402 (2014) 28–35.
[31] A.L.B. Macon, T.B. Kim, E.M. Valliant, K. Goetschius, R.K. Brow, D.E. Daz, A. Hoppe, A.R. Boccaccini, I.Y. Kim, Ch. Ohtsuki, T. Kokubo, A. Osaka, M. Vallet-Regí, D. Arcos, L. Fraile, A.S. Salinas, A.V. Teixeira, Y. Vueva, R.M. Almeida, M. Miola, Ch. Vitale-Brovarone, E. Verné, W. Höland, J.R. Jones, A unified in vitro evaluation for apatite-forming ability of bioactive glasses and their variants, J. Mater Sci: Mater Med. 26 (115) (2015) 1–10.